CRANFIELD INSTITUTE OF TECHNOLOGY

COLLEGE OF AERONAUTICS

Ph.D. Thesis

Academic Year: 1992-93

A.N. Bercin

High Frequency Vibration Analysis of Plate Structures

Supervisor: Dr. R.S. Langley

March 1993

A thesis submitted for the degree of
Doctor of Philosophy

" *Of knowledge it is only A little that is communicated To you*"

Qur'an (17/85)

to my brother

ABSTRACT

Noise and vibration are important design issues for many types of vehicles such as ships, cars, and aeroplanes. Structure borne sound, which may be of relatively high frequency, usually emanates from an engine or some other type of localised source and propagates through the vehicle. Excessive vibration levels, and thus structural damage, may occur while structural acoustic interactions may lead to unacceptable interior noise.

In the analysis of energy transmission between plate structures, it is common practice to consider only bending modes (or waves) of the structure. However if the concern is with high frequency vibration analysis, then due allowance may need to be made for the presence of in-plane shear and longitudinal modes.

Due to the infeasibility of the industry standard technique, the Finite Element Method, at high frequencies, almost all of the studies that have investigated the importance of in-plane energy transmission have used Statistical Energy Analysis (SEA).

In this study an existing dynamic stiffness method is extended to include in-plane effects, and used as a benchmark against which SEA is assessed. Additionally the Wave Intensity Analysis (WIA) technique, which is an improved form of SEA, is extended to in-plane vibrations, and used to identify some of the reasons for the poor performance of SEA in certain applications. All three methods are applied to a wide range of plate structures within the frequency range of 600 Hz to 20 kHz. While the response levels as predicted by the WIA are generally quite close to exact results, it has been found that although all of the requirements which are usually postulated for the successful application of SEA are fulfilled, SEA severely underpredicts the energy transmission in large structures because of the diffuse wave field assumption. It is also shown that the exclusion of in-plane modes may lead to sizeable errors in energy predictions unless the structure is very simple.

ACKNOWLEDGEMENTS

I wish to express my sincere gratitude to Dr. R.S. Langley for his invaluable advice, patience, and encouragement throughout the course of this research programme.

My thanks are also due to Prof. C.L. Kirk for his good humour and guidance.

I am also grateful to my colleague Stewart McWilliam for providing me with a copy of SEA software.

Finally, my very special thanks to my parents who are eagerly looking forward to the day of my return from a country some 3000 miles away.

NOTATION

The notation used in this Thesis is as defined in the main text.

CONTENTS

1 INTRODUCTION.

1.1 GENERAL INTRODUCTION.

Noise and vibration are important design issues for many types of vehicles, such as ships, cars, and aeroplanes. Structure borne sound, which may be of relatively high frequency, usually emanates from an engine or some other type of localised source and propagates through the vehicle. Excessive vibration levels, and thus structural damage, may occur, while structural acoustic interactions may lead to unacceptable interior noise levels.

The exact analysis of the vibration of a system with many degrees of freedom is generally difficult, and the associated calculations are laborious. Broadly speaking, conventional vibration analysis of structures has centred on the low frequency range encompassing the first few natural frequencies. Much literature exists on the standard analytical and numerical techniques, such as Finite Element Method (FEM), and the Boundary Element Method (BEM). These methods are concerned with determining the first few natural frequencies, and the associated mode shapes. For low frequency excitation these modes tend to dominate the displacements and stress levels within the structure.

The most commonly used vibration analysis technique is perhaps the finite element method. The method is dependent for its success on skilful modelling procedures and efficient numerical techniques [1]. There are two basic steps in the finite element modelling of a structure:

(i). A built-up structure which is composed of various inter-connected structural members, such as beams, shells and plates of different geometry, needs to be broken down into components or "elements" whose behaviour may readily be obtainable. The properties of such elements are normally derived approximately on the basis of variational principles.

(ii). The original system is rebuilt or "assembled" from the constituent elements so that its global behaviour may be analysed.

The ability of FEM to model a wide range of structures makes it an attractive design tool for the approximate vibration analysis of complex systems in the low frequency regimes.

However, if the concern is the vibration analysis of structures at high frequencies, then the analysis becomes rather complicated because of the following characteristics of high frequency vibration:-

(i). The structural wave length is rather short which causes the modes to become more sensitive to design and fabrication details of the structure [2]: the mode shapes will generally display a rapid spatial variation.

(ii). A large number of modes will contribute to the vibrational response of the structure as the higher resonant frequencies tend to be relatively closely spaced on the frequency axis.

Even though in principle the FEM may be used at high frequencies, because of the following reasons it often becomes impracticable, if not impossible, to apply FEM successfully:-

(i). In order to obtain accurate results the system needs to be discritized into elements of smaller and smaller size. This process involves substantial data preparation and large systems of simultaneous equations [3].

(ii). Even if the previous problem is overcome successfully, the output information will reach to such an extent that may prohibit the interpretation of the results [4]: in a complicated model there would be many parameters. The sensitivity studies of these parameters will yield enormous computer output.

(iii). The calculation of a large number of resonant modes can be costly or even computationally infeasible.

(iv). During the modelling and discretization process slight differences between the real and idealised material properties, boundary conditions and structural dimensions may occur. Due to these differences, the theoretical mode shapes and natural frequencies may be shifted relative to the real mode shapes and natural frequencies; these two factors may lead to errors in displacements at discrete positions and frequencies [5,6].

In order to resolve the problems which are encountered by deterministic methods at high frequencies, a vibration engineer often resorts to statistical techniques. These methods relinquish the detailed knowledge of the modal behaviour in favour of the spatial mean square response which is averaged over broad frequency bands to include many resonant modes of the structure so that the effects of the system details on the model disappear [4].

The classical example of this type of method is the Statistical Energy Analysis (SEA) which is said to be an *ad hoc* extension of the exact results of two coupled single degree of freedom oscillators under broad band excitation. A more detailed discussion of SEA will be given in later sections; therefore no further comments will be made here.

One particular case in which high frequency vibration can and does occur, is the jet airliner. Here the vibration tends to be lowest at the nose of the aircraft and is progressively more severe moving towards the tail. The major source of the excitation is the turbulent boundary layer, which can contain frequency components up to 10 kHz [7]. The fuselage structure typically consists of stiffened panels, which, to a first approximation may be considered to be locally flat, as shown in Fig. 1.1.

Marine structures may also be subjected to high frequency excitation arising from turbulent wakes or engine vibrations. Again, to a first approximation the structure may be represented by an assembly of flat panels as shown in Fig. 1.2 [8,9].

The aim of the present work is to study in detail various aspects of the high frequency vibration of structures which are composed of flat plate elements. An understanding of this type of structure should allow a range of real engineering structures to be analysed and also serve as a basis for the study of more advanced structural configurations. Before outlining the full scope of the present work, previous work on the analysis of plate structures is reviewed in the following sections.

1.2 PREVIOUS WORK ON VIBRATION OF PLATE STRUCTURES: RIGOROUS METHODS.

1.2.1 FINITE ELEMENT METHOD.

The reasons why the FEM is hard to implement at high frequencies are given in the previous section. To eliminate at least some the shortcomings, especially the necessity for massive spatial discretization, several researchers proposed improved versions of FEM.

A recent work in this vein is that of Cuschieri [10]. In this method, which is referred as Mobility Power Flow (MPF) analysis, the structure is modelled by a set of coupled substructures, and forces and moments are introduced at the junctions between the substructures. At every junction forces and moments are treated as structural mobility functions. The input energy and coupling power to and from the excited structure to the other connected substructures are expressed in terms of input and structural transfer mobilities, and expressions are then written for the energy flowing between the elements of a structure in terms these mobilities. Thus, the method uses coupling power as the linking parameter between the substructures. In this respect the MPF method resembles SEA in which energy flow is written in terms of a parameter known as the coupling loss factor (see section 3.2.1).

Using the MPF technique Cuschieri [10] has obtained improved results in comparison to FEM and SEA for flexural vibrations of two finite plates joined along a common edge forming an L-shape, within the frequency range of 0 to 1000 Hz.

However, since the method is still based on the FEM, it suffers from being dependent upon the details and model, and therefore the use of MPF method is confined to mid range frequencies [11]. Moreover, the necessity of calculating the mobility functions may make the method difficult to apply on some types of structure [12].

1.2.2 DYNAMIC STIFFNESS METHOD.

The dynamic stiffness method is similar to FEM with the exception that the properties of each element are derived *exactly*.

In the case of plate-like structures, the method allows for arbitrary boundary conditions at the plate edges parallel to y axis (see Fig. 2.1), and to put it in a form amenable to "exact" analysis, it assumes that two opposite edges (x direction of Fig. 2.1) of the plate are simply supported. Having two opposite edges simply supported enables an individual plate to be reduced from a two-dimensional to a one dimensional element characterised by a stiffness matrix. It is well known [13] that if the boundary conditions at two opposite edges of the plate correspond to simple supports then the mode shapes of vibration in the y direction of Fig. 2.1 are proportional to $\sin(n\pi y/b)$.

Rather than modelling a structure as a global system, the methods treats each component of the structure individually in its local co-ordinates and assembles stiffness matrices for each plate to form the complete dynamic stiffness matrix of the structure. Treating the elements separately makes it possible to analyse a structure that consists of arbitrary number of elements, and transformation from local to global co-ordinates allows the plates to be connected at any orientation.

Hence the basic problem is then to determine the stiffness matrix which relates the amplitudes of the edge forces and moments to the amplitudes of the corresponding edge displacements and rotations for a single plate. Once this stiffness matrix is known, the equations of equilibrium of a junction enable a series of simultaneous equations relating the displacements and rotations of all plate junctions to be constructed.

Indeed, the dynamic stiffness method is very similar conceptually to the FEM. It does however have the following advantages:-

(i). The dynamic stiffness method requires less discretization, as the structure is broken down into its substructures at the natural boundaries and no further substructuring is needed to model the system.

(ii). In the dynamic stiffness method there are only eight degrees of freedom for a plate; four for each edge: out-of-plane, rotation, and two for the in-plane displacements. Note that these degrees of freedom relate to a specific lateral shape function $\sin(n\pi y/b)$.

(iii). Related to the two previous points, the dynamic stiffness method has the advantage of requiring a much smaller assembled stiffness matrix when compared with the FEM. Thus, it is possible to carry out calculations on a small computer.

(iv). The difficulties that restrict the use of the FEM at high frequencies do not create any problem for the dynamic stiffness method, since the accuracy of the results is not dependent on mesh refinement.

(v). The results of the dynamic stiffness method are strictly "exact" for the class of problems described above. This is a very useful feature as it allows the method to be employed as a "bench-mark" to compare the accuracy of approximate methods.

It may be argued that having boundary conditions at the two opposite edges of the plate as simply supported prohibits the applicability of this method; however it has been shown [6] that the type of constraint at the transverse edges of the plate have little influence on the energy transmission at high frequencies when there are many resonant modes.

Early applications of the dynamic stiffness method is due to Wittrick and Williams [14–16]. They applied the method for buckling and flexural

vibration analysis of stiffened plates. Another example of literature within this group is the work of Langley [17].

Langley [17] investigated the free and forced out-of-plane response of a row of connected rectangular plates, and derived expressions for the mean energy flow and mean energy stored in the individual panels.

Although the method is well established for flexural vibrations, no literature has been found concerning the in-plane of modes a plate structure.

1.2.3 OTHER METHODS.

In addition to the foregoing methods, several other techniques have been successfully applied to obtain the natural frequencies and mode shapes of stiffened/unstiffened plates. These include the Rayleigh-Ritz method [18], the transfer matrix method [19,20], the finite difference method [21], and the finite strip method [22]. Although these methods are within the field of interest of this study, because of the limitation of the range of structures that can be modelled (for example in the transfer matrix method only a linear array of plates can be modelled), or unsuitability for high frequency vibration, they are not considered here in any detail.

In what follows two other methods, namely statistical energy analysis and wave intensity analysis, that are well suited for the class of problems considered here, yet different in the method of approaches of previous two methods will be briefly reviewed. A more detailed description of these methods may be found in chapters 3 and 4 respectively.

1.3 PREVIOUS WORK ON VIBRATION OF PLATE STRUCTURES: ENERGY FLOW METHODS.

1.3.1 STATISTICAL ENERGY ANALYSIS.

Statistical Energy Analysis (SEA) is a technique for estimating the vibrational and acoustic response of complex dynamic systems. SEA was

first applied to a structural vibration problem by Lyon and Maidanik [23].

SEA generally considers the response of structures which have many modes excited in a certain frequency band. The approach is thus usually applied to high frequency vibrations. The approach has two distinctive features when compared to deterministic analysis methods, such as the FEM. Firstly, the use of energy and power as the system variables, and secondly the statistical description of the system itself. In order to express the analysis in a form which is amenable for engineering applications several assumptions are made in the derivation of the SEA equations. These assumptions and the parameters involved in the SEA approach are described briefly in chapter three and will not be detailed here.

Various authors have considered the underlying basis for SEA and tried to improve the accuracy of the method. Broadly speaking previous studies are directed towards four key issues: coupling loss factors, coupling strength, accuracy and limitations, and in-plane energy transmission.

In the following sections, the studies on these issues which are related to plate structures (directly or indirectly) will be reviewed.

Coupling Loss Factor.

The "coupling loss factor" governs the energy which flows between two components (or more generally "subsystems") of an engineering structure. This is a key parameter, which must be determined for each "junction" before SEA can be applied to a given problem. Existing work on coupling loss factors for plate structures is reviewed in what follows.

The coupling loss factor may generally be expressed in terms of the elastic wave transmission coefficients of a structural joint. Lyon and Eichler [24] and Hwang and Pi [25] studying the same system have obtained the transmission coefficients for a plate junction formed by rigidly attaching a semi infinite plate to an infinite plate. In the calculations only bending waves were considered. The latter assumed that the flex-

ural wave length may reach the order of the plate thickness: Mindlin's thick plate theory was applied, thus accounting for the effects of transverse shear deformation and rotatory inertia.

Gibbs and Gilford [26] calculated theoretically the coupling loss factors of cross, T, and L junctions of plates considering transmission between bending, longitudinal, and transverse waves and verified their results experimentally within the frequency range of 400 Hz. to 12.5 kHz. Wohle *et al.* [27] studied similar types of junctions for a diffuse wave field and determined coupling loss factors for a junction with flexible coupling.

Using the FEM Simmons [6] calculated the coupling loss factors for various types of junction, and suggested that if the coupling loss factors are calculated by the FEM, then this parameter may be used in the statistical energy analysis of systems with junctions of the same type. This leads to the possibility of analysing systems which are difficult to analyse with either the FEM or SEA.

For the case of a junction formed by plates which meet at a beam Cremer *et al.* [28] have presented the flexural wave transmission coefficients for a rectangular stiffener attached symmetrically to two plates. For the more general case of a junction composed of an arbitrary number of plates which are coupled directly or via a beam of any cross section, the transmission coefficients have been calculated by Langley and Heron [29]. In this analysis it is possible to take into consideration shear deformation, rotary inertia and warping effects as well as the offsets between the plate attachment lines and the shear axis of the stiffener.

Several attempts to obtain the coupling loss factors experimentally have also been made. Bies and Hamid [30] calculated coupling loss factor and plate loss factor under broad band random excitation, and using a matrix iteration procedure to predict loss factors, obtained good theoretical results compared to experimental ones.

Coupling Strength.

Standard SEA power flow relationships are generally thought to be valid under the assumption that the subsystems are weakly coupled. When the coupling strength is increased, alterations are needed to the fundamental SEA equations [31]. Therefore, a number of authors have tried to obtain more general relationships which are valid for any arbitrary coupling strength.

Smith [32] examined the effect of the strength of the coupling between the subsystems and, using the reciprocity principle, obtained the symmetry relations that need to be satisfied by the coupling loss factors. Keane and Price [31] investigated the response of two multi modal subsystems which are coupled at a single point, and showed that provided such a system is excited by rain-on-the roof type of forces, the standard SEA power flow relations holds regardless of the coupling strength. However the proportionality constants of power flow equations should be redefined. Similar work in this vein is that of Langley [33] who obtained a general form of the fundamental SEA equation for conservative coupling of any type. It is also shown that the results are not only applicable for rain-on-the roof type of excitation, but also point loading. In a later work by the same author [34] these results are used to obtain the coupling loss factors in terms of the system Green functions. A similar method which uses system Green functions is proposed by Keane [35]: the method was employed in calculating exactly the energy flows between many multi-coupled, multi-modal subsystems.

Dimitriadis and Pierce [36] derived power flow equations for two strongly coupled plates under the assumption that the driving forces are spatially uncorrelated and that power transmitted by the in-plane waves is negligible; thus they considered only flexural waves.

Mace [37] has investigated the energy flow between point coupled subsystems by using a wave approach. He has shown that due to the re-radiation of power by the finite subsystems the mean energy flow from an infinite to a finite subsystem is less than SEA; yet the mean energy flow from a finite to an infinite subsystem is greater than two infinite

subsystems because of the re-injection of the power by the finite subsystem. It has seen that while re-radiation effects are largest for strong coupling, re-injection effects are bigger for weak coupling.

Accuracy and Limitations.

In the study by Keane and Price [38] of two axially vibrating coupled rods, it was shown that the energy flow approaches to a steady value when there are around seven resonant modes in each rod and thus it can be concluded that this is the minimum number of resonant modes needed to obtain a reliable response estimate from SEA.

Guyader *et al.* [39] have shown that in general SEA overpredicts the energy transmission between two concrete plates forming an L-shaped structure. The method used to yield a reliable response estimate was referred to as the energy influence coefficient method. In this method the coupling of the substructures is represented in terms of generalised influence coefficients which relate one of the substructures average energy to the spectral density of the force applied on another substructure. They compared the amount of energy transmitted (due to flexural waves only) to the indirectly excited plate, and found that even though at low frequencies SEA predicts the energy transmission reasonably well when the plates are identical, it overpredicts by as much as 5 dB if the plates are different. At high frequencies the SEA results get progressively better; yet it still overestimates by around 2.5 dB.

The modal overlap factor, $M = \eta\omega n(\omega)$, (see chapter 3 for the definition of the variables) is a measure of the average separation between frequencies in relation to the average modal bandwidth. By considering randomly excited coupled beams, Davies and Wahab [40] showed that semi-infinite theory results are in better agreement with the practical case of finite beams if the modal overlap is above a certain value. They concluded that if the modal overlap factor, M, is greater than unity then the semi-infinite results would give reasonable approximations to the finite case. However if this parameter is less than one, semi-infinite theory overestimates the coupling loss factor.

Fahy and Mohammed [41] in their recent work on the uncertainty of SEA predictions of various structures, as a result of predictions based on the diffuse wave field assumption concluded that, for the case of coupled plates, to get unbiased results the plates should not be excited close to the junction as it leads to sizeable error in the average power flow and coupling loss factor, and also confirmed the view of Davies and Wahab [40] on the modal overlap factor.

Mace [42] studied the statistics of energy flow between two subsystems, and showed that for weak coupling the energy flow is the largest for the ensemble members that are resonant when they are uncoupled.

Coupling that occurs through the modes of the subsystems with natural frequencies outside the current frequency band of interest is termed as non-resonant coupling. In the majority of the practical cases, the contribution of non-resonant modes of the subsystems in the energy transmission is negligible compared to the resonant modes. On the other hand, if the coupling modes are widely spaced in frequency, are highly damped or are weakly excited by the power source, due allowance must be made for the non-resonant coupling path [43]. Craik *et al.* [44] have shown that at low frequencies when there are few modes; only the modal properties of the receiving subsystem affect the coupling between two subsystems. They have used the statistics of mobility to give the limits to the coupling loss factor, and obtained expressions for the errors that may occur at low frequencies.

In-Plane Energy Transmission.

It is well known that a vibrating flat plate may exhibit three types of mode (or wave), namely bending, longitudinal, and shear. Of these three modes, bending is referred to as the out-of-plane mode and longitudinal and shear, when grouped together, as the in-plane modes.

Even though it is usually the out-of-plane modes of a structure that are more strongly excited by a source of vibrational energy, a pure bending wave impinging at a junction induces in-plane longitudinal and shear waves as well as other flexural waves in the connected plates. The

in-plane waves are partly transformed into flexural waves at the other junctions, and less attenuated with distance in comparison with flexural waves since they have high wave speed [43]. Thus the in-plane waves, acting as energy carriers over long distances, contribute significantly to the energy levels at remote parts of the structure.

Until recently, the majority of the SEA (or deterministic) studies of energy transmission in plate type structures were based on the assumption that the main component of the energy transfer is due to flexural waves and the contribution of in-plane waves may be neglected. A typical example of the application of the deterministic method considering out-of-plane motion only is that of Nilsson [8]. The case studied was a scale model of a ship structure. As the calculations agreed with experiment, inclusion of in-plane modes did not seem to be necessary.

A similar conclusion is also reached by Gibbs and Gilford [26]. In their analysis of a T-junction they have shown that neglecting the in-plane modes makes only 2 dB difference to the response. However, they cautioned that the results of SEA at low frequencies are unreliable, as the modal density of the components are quite low. Similar work along the same line of thought is due to Landmann *et al.* [45]. In their study of low frequency vibration analysis of an aircraft fuselage, they considered bending and in-plane coupling of a frame and stringer stiffened structure. Although the SEA model indicated good agreement near the source of excitation, it over predicted at the points away from the drive point within the frequency range of 100 to 400 Hz. Thus they concluded that the inclusion of in-plane modes leads to overcoupling between the subsystems, and therefore they should not be included.

The main justification for not including in-plane motion in an SEA analysis has generally been that "bending only" theoretical results yielded satisfactory agreement with experimental results [46]. Furthermore, in an experiment usually one can only measure the vibration amplitudes of the out-of plane modes directly and the observation of in-plane motion is quite difficult since the local strains and accelerations of bending modes are generally higher than that of in-plane modes [43].

Besides, consideration of only bending vibrations vastly simplifies the analysis, especially if the structure is rather complicated.

Even though this simplification is justified in many instances, it may not always be so. In the literature examples of works which are in favour of the inclusion of in-plane modes also exist. For instance in the investigation of Gibbs and Craven [47] on the performance of a T junction, it has been shown that once a flexural wave impinging on a junction is converted into an in-plane wave it can travel through several junctions before converting back to a bending wave. Thus it may not be appropriate to neglect the contribution of in-plane waves in an SEA model. In the work performed by Tratch [9], in which the case was similar to that of Nilsson [8], a ship foundation and hull were modelled as an assembly of flat plates. Experiments were carried out on a scaled model structure (see Fig. 1.3.a) and the results were compared with SEA predictions including and excluding the in-plane modes. As can be seen in Fig. 1.3.b the bending only model underestimates the vibration transmission from plate number 1 to 7 by as much as 10 dB at the highest frequency of 20 kHz; yet the inclusion of in-plane modes improves the agreement significantly.

Powell and Manning [43] studied three coupled beams forming an H-shape with unequal leg lengths and showed that SEA predicts an energy level 20 dB less than that of an exact analysis at 10 kHz. They concluded that since in-plane modes are less subject to transmission, dissipation, radiation and reflection losses than are bending mode types, they become the dominant path of energy transmission. They have also noticed that the addition of in-plane modes may result in an overprediction in the transmitted energy. The suspected cause was overcoupling between the modes in the low frequency regime where the in-plane modal density is low, in line with the conclusion of Landmann *et al.* [45]. However they did not consider this phenomenon as a disadvantage, as an overprediction is a conservative result for design purposes.

Indeed, as Lyon [48] notes in his article, in which he summarises the work of Tratch [9], there exists a situation in which some of the re-

searchers believe that in-plane motions are important, some say they are not and a third group is neutral on this issue.

In short, the overall ideas that have been expressed on this issue so far can be listed as follows:

(i). An analysis based solely on the flexural modes of the structure is a reasonable approach in most circumstances [8,36,26,45].

(ii). Including the in-plane modes in an SEA model can significantly change the results in comparison to those that are obtained by using only the bending modes [9,48,43].

(iii). Including the in-plane modes in an SEA model can result in much better agreement between theory and experiment [9,48].

1.3.2 WAVE INTENSITY ANALYSIS.

A fundamental conjecture, which is common in the wave analysis of room acoustics, is that a wave disturbance impinging on the boundaries of a structure after many reflections and sufficient time becomes diffuse. This implies that the wave intensity per unit angle of incidence is constant for all wave heading angles [49]. In the modal point of view a direct corollary of this diffuse wave field assumption is that there is "equipartition" of modal energy, which means that all the modes of a system have the same kinetic energy level.

The meaning of the term "equipartition" can be interpreted in a manner similar to that used in thermodynamics [4]. In thermodynamics heat diffuses in the system from hotter to cooler regions until equilibrium is established in the system. Making the analogy between temperature and mean modal energy, SEA adopts the vastly simplifying diffuse field assumption to analyse high frequency structural vibrations. Although it is a perfectly valid assumption for a system to have the same temperature at steady state, the validity of SEA's equipartition assumption may be criticised, as it is known to be not satisfied at all circumstances [5].

Recently Langley [50] has developed an extended version of SEA known as Wave Intensity Analysis (WIA). The method follows closely the steps of conventional wave approach to SEA save that the wave field is not assumed to be diffuse. Rather the directional dependence of the wave field is represented in terms of shape functions. From a modal point of view, the energy of a mode depends upon the direction of the underlying wave components. The shape functions of the random wave field are taken as a finite Fourier series (see chapter 4), and a set of linear equations which relate the input energies to the dissipated and transmitted energies of the subsystems are derived. The coefficients of the linear equations are expressed in terms of wave transmission and reflection coefficients between the subsystems, and the resulting matrix is solved to yield the energies of each subsystem.

In reference [50] the method was applied to the flexural vibrations of three and four plates coupled in a row, and improved results were obtained compared to those of SEA. Although in principle the method is applicable to the same range of structures as SEA, it has not been applied to any other case other than those mentioned before. Therefore the method needs to be further developed and validated by applying it to different cases.

1.4 SCOPE OF THE PRESENT WORK.

Having reviewed previous work on the high frequency vibration analysis of plate structures, a number of unresolved questions can be listed as follows:-

(i). Although it has been shown that the dynamic stiffness method may be used as a deterministic approach to the high frequency vibration analysis of a certain class of plate structures, in its present form it is restricted to only flexural vibration analysis. The method therefore needs to be extended to include in-plane longitudinal and shear degrees of freedom.

(ii). In situations which favour the application of SEA both in terms of feasibility and usefulness, one has to rely on whatever re-

sults SEA has yielded. There is generally no other "exact" method available to validate the SEA results, and the "right" answer is usually unknown.

(iii). Even though all of the usual requirements for the successful implementation of SEA have been satisfied, the method is known to give poor results in some applications. The reasons why SEA produces such poor results require further investigation.

(iv). As mentioned previously almost all of the studies which have investigated the importance of in-plane energy transmission have used SEA without a validating "exact" analysis. This raises the questions: **a)** The inclusion of in-plane motion may shift the SEA results in the "right" direction, but is this a true physical model of what is really happening? **b)** How important is in-plane energy transmission in realistic situations?

The present study is a response to these issues. The three major goals of the work are:-

(i). The extension of the exact dynamic stiffness technique to include in-plane effects.

(ii). The extension of the Wave Intensity Analysis (WIA) method to in-plane vibrations, and use of this method to identify some of the reasons for the poor performance of SEA in certain applications.

(iii). A systematic assessment of effect of in-plane vibrations.

1.5 LAYOUT OF THESIS.

In chapter 2 the standard dynamic stiffness method is extended to deal with the case of in-plane vibrations. This allows exact results for the high frequency vibrations of a large class of plate structures to be obtained.

Chapter 3 contains a brief summary of the SEA approach and details are given concerning the application of SEA to plate structures. This serves as a necessary introduction to chapter 4 which concerns the Wave Intensity Analysis Method. An existing WIA formulation is extended to include in-plane vibrations, and the technique is illustrated by application to an L-shaped plate structure.

In chapter 5 all three methods are applied to a wide range of plate structures, such as plate assemblies coupled in a row by either stringers or simple supports, closed section plate assemblies, and plates coupled in L, T and cross junctions. The results of SEA and WIA are compared with exact dynamic stiffness analysis. A thorough investigation of the importance of in-plane energy transmission is performed.

Finally, in chapter 6 the present study is recapitulated. Conclusions are drawn and recommendations for future work are made.

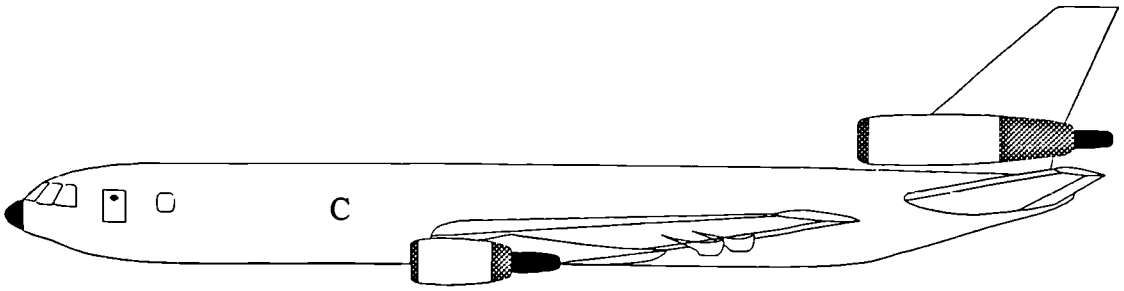

a)

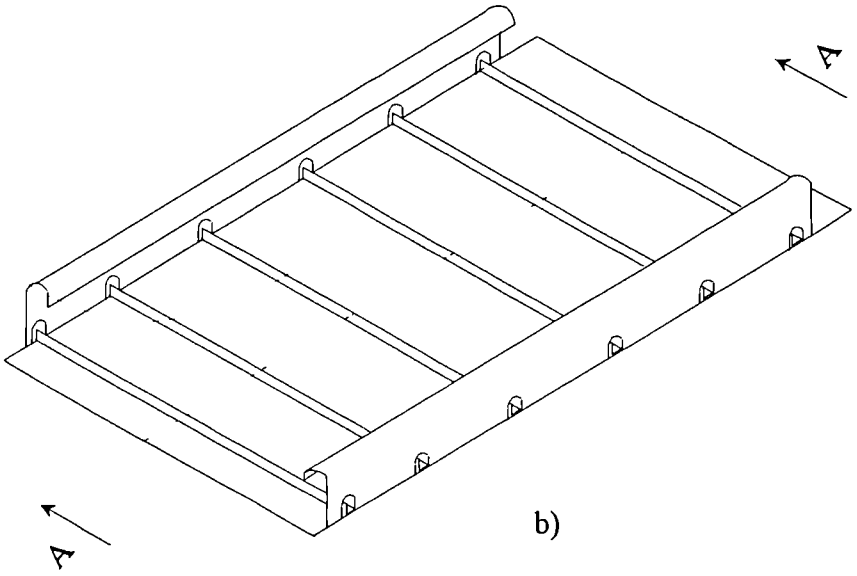

b)

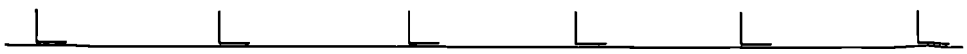

Section A - A

Fig. 1.1

a) Typical Aircraft

b) Details of a Section through Aircaft Structure
(Marked with C on the Aircaft)

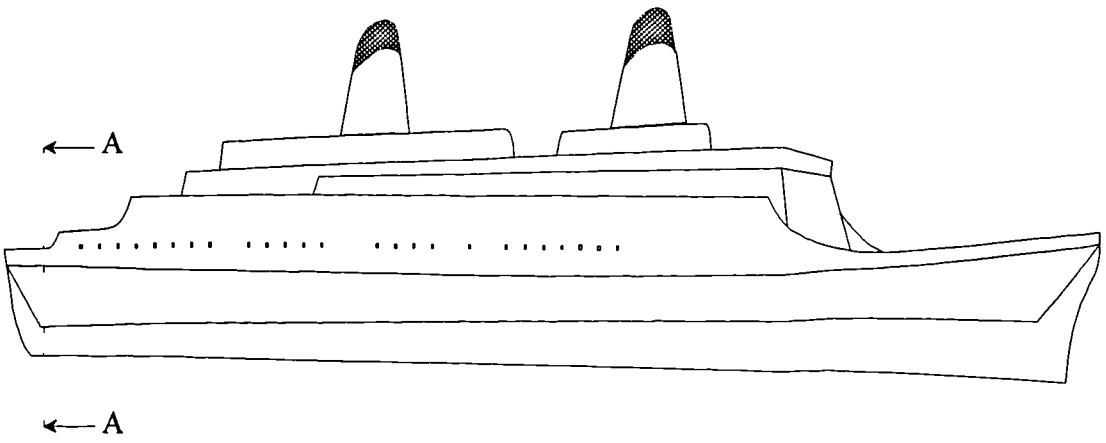

a)

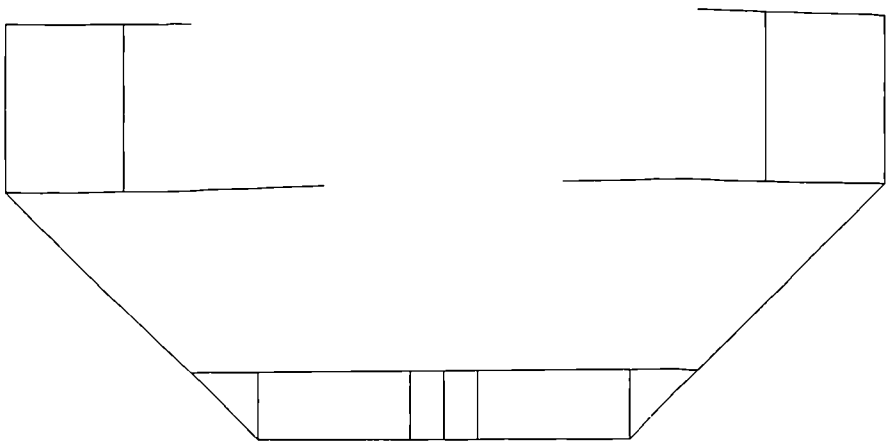

Section A - A

b)

Fig. 1.2 a) General View of a Ship
b) Simplified Cross Section Through the Ship Structure

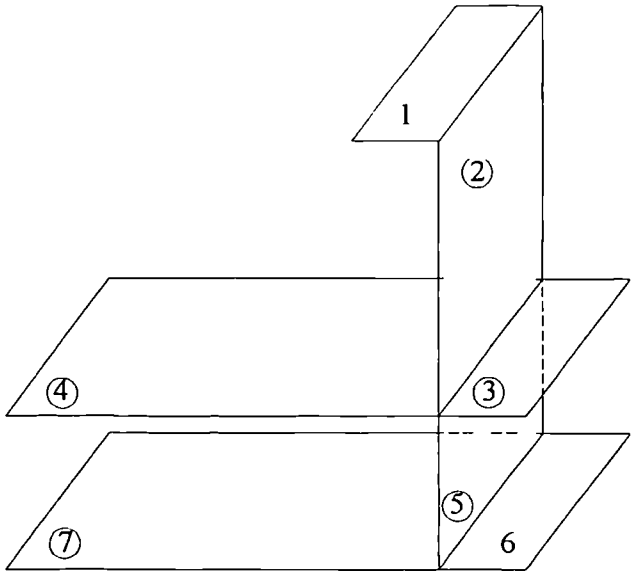

a)

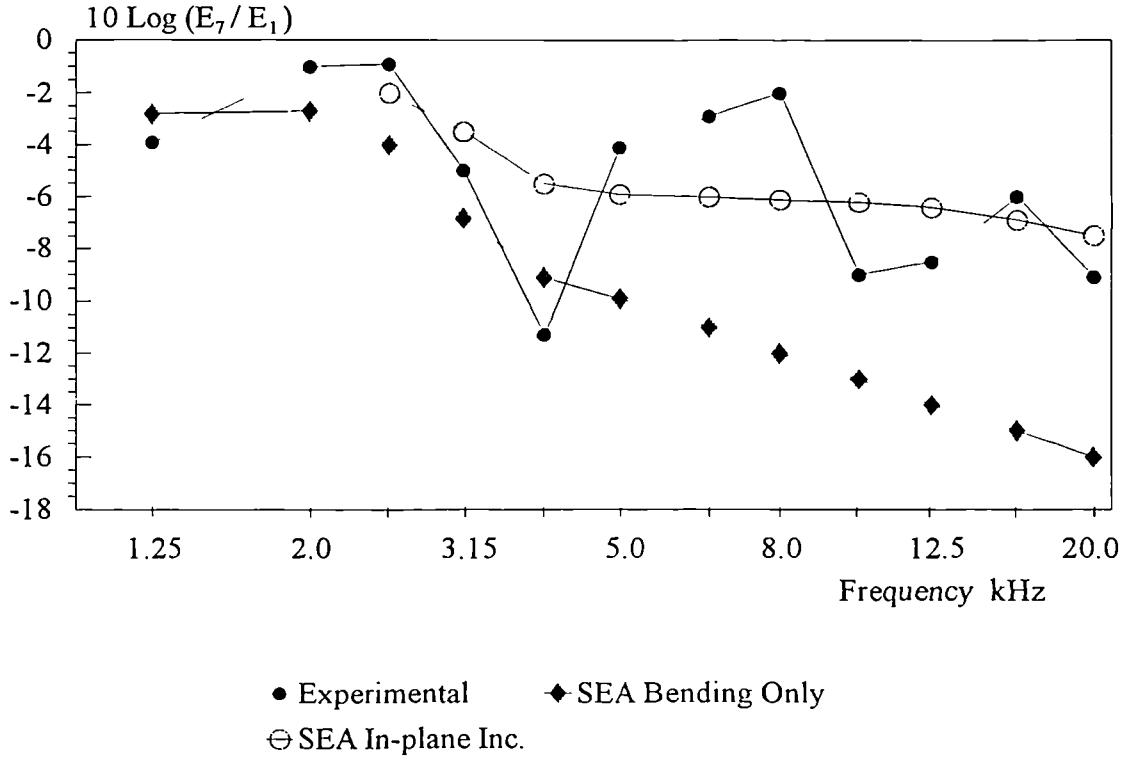

Fig. 1.3 Tracth's
a) Scaled Model of Ship Foundation & Hull.
b) SEA Predictions and Measured Data.

2 DYNAMIC STIFFNESS METHOD.

2.1 INTRODUCTION.

The method of approach of dynamic stiffness technique has been described in section 1.2.2. In what follows the expressions for bending moment, lateral and in-plane shear forces, and in-plane tension force will be derived from governing differential equations. Then assuming suitable deflection shapes the displacement expressions which are associated with these forces and moment will be obtained so that the differential equations may be solved to yield the dynamic stiffness matrix of a particular plate.

2.2 DYNAMIC STIFFNESS MATRICES IN LOCAL CO-ORDINATES.

A typical structure which consists of several panels and beams is depicted in Fig. 2.1. The common edge where the plates and beam meet has the same length for both plates and the beam. It is assumed that:

a) The plates are homogenous
b) Isotropic
c) Elastic and of uniform thickness.

The analysis can then be based on the standard theory of thin plates provided that the plate thickness, h, is not comparable to the wave number [28], k, i.e. $kh<1$: this is the appropriate condition for negligible shear deformation and rotational inertia. In the following derivations the standard theory will be used throughout.

During vibration the edges of the j'th plate are subjected to systems of edge forces and moment as shown in Fig. 2.2.b, whose magnitudes per unit length are

$$\left\{S_{1j}, M_{1j}, T_{1j}, N_{1j}, S_{2j}, M_{2j}, T_{2j}, N_{2j}\right\} \tag{2.1}$$

Here S is lateral shear force, M is moment about an edge, T is an in-plane shear force, and N is an in-plane tension/compression. The suffixes 1 and 2 refer to the transverse edges of the plate, while j identifies the plate under consideration.

The displacements corresponding respectively to these edge forces are

$$\{w_{1j}, \theta_{1j}, v_{1j}, u_{1j}, w_{2j}, \theta_{2j}, v_{2j}, u_{2j}\} \tag{2.2}$$

where θ represents a rotation about the edge and w, v, u represent translational displacements as shown in Fig. 2.2.a.

It is clear that the complete system of edge forces and displacements shown in Fig. 2.2.b can be divided into two uncoupled systems. The first S_{1j}, M_{1j}, S_{2j}, and M_{2j}, the second T_{1j}, N_{1j}, T_{2j}, and N_{2j} which are known as the out-of-plane and in-plane systems respectively. The first set correspond to the displacements w_{1j}, θ_{1j}, w_{2j}, θ_{2j}, the latter to v_{1j}, u_{1j},v_{2j}, u_{2j}.

One may therefore define the column vectors $\mathbf{d}_j^{o}$ and $\mathbf{d}_j^{in}$ of the edge displacements by the equations

$$\mathbf{F}_j^{o} = \{S_{1j}, M_{1j}, S_{2j}, M_{2j}\}, \qquad \mathbf{d}_j^{o} = \{w_{1j}, \theta_{1j}, w_{2j}, \theta_{2j}\} \tag{2.3),(2.4}$$

$$\mathbf{F}_j^{in} = \{T_{1j}, N_{1j}, T_{2j}, N_{2j}\}, \qquad \mathbf{d}_j^{in} = \{v_{1j}, u_{1j}, v_{2j}, u_{2j}\} \tag{2.5),(2.6}$$

and introduce 4x4 dynamic stiffness matrices $\mathbf{P}_j^{o}$, and $\mathbf{P}_j^{in}$ by the equations

$$\mathbf{F}_j^{o} = \mathbf{P}_j^{o}\mathbf{d}_j^{o}, \qquad \mathbf{F}_j^{in} = \mathbf{P}_j^{in}\mathbf{d}_j^{in} \tag{2.7),(2.8}$$

the superscripts " o" and " in" in the above matrices denote out-of-plane and in-plane respectively, and j represents the plate number in a structure. Since out-of-plane and in-plane forces are not coupled, it is convenient to establish the dynamic stiffness matrices separately in two phases and then combine them into a comprehensive matrix.

2.2.1 OUT-OF-PLANE STIFFNESS MATRIX.

Considering an individual panel of length L and width b (Fig. 2.1) and taking the local co-ordinates, x in the longitudinal direction and y in the transverse direction, the equation governing the out-of-plane response of an isotropic thin plate for free vibrations is [13]

$$D_j \nabla^4 w + \rho_j h_j \ddot{w} = 0 \qquad j=1,2... \tag{2.9}$$

where, ∇^4 is the biharmonic differential operator (i.e. $\nabla^4 = \nabla^2\nabla^2$, $\nabla^2 = \partial^2/\partial x^2 + \partial^2/\partial y^2$ in rectangular co-ordinates), w is the out-of-plane displacement, ρ_j is the mass per unit volume, h_j is the thickness and D_j is the bending rigidity of plate given by

$$D_j = \frac{E_j h_j^{\,3}}{12(1-\nu_j^{\,2})} \tag{2.10}$$

where E_j denotes the modulus of elasticity and ν_j the Poisson ratio for the material.

To model the internal losses a material loss factor, η_j, may be introduced. Then one can replace all the occurrences of Young's modulus in the analysis by the complex modulus $E_j(1+i\eta_j)$, where $i = \sqrt{-1}$.

The plates are simply-supported along the longitudinal edges. Hence for a simply-supported edge, the boundary conditions are: zero out-of-plane displacement and bending moment, that is at y=0 and y=b (Fig. 2.1):

$$w = 0 \qquad \text{and} \qquad \frac{\partial^2 w}{\partial y^2} + \nu \frac{\partial^2 w}{\partial x^2} = 0 \tag{2.11}$$

The out-of-plane deflection can be written as

$$w(x,y,t) = \sum_n W_n(x,t) \sin\left(\frac{n\pi y}{b}\right) \qquad n=1, 2, \ldots \tag{2.12}$$

where the subscript n is used to denote the fact that for each value of n there is a different function y that satisfies the differential equation and the particular boundary conditions, yet it will be omitted later for simplicity.

The deflection function (2.12) exactly satisfies the governing field equation (2.9) and the simply supported boundary conditions (2.11) along y=0 and y=b. Substituting expression (2.12) into equation (2.9) yields

$$\left[D_j W_n^{\mathrm{iv}} - 2k_n^2 D_j W_n'' + D_j k_n^4 W_n + \rho_j h_j \ddot{W}_n\right]\sin(k_n y) = 0 \qquad (2.13)$$

where each prime indicates one differentiation with respect to x and $k_n = (n\pi / b)$. Multiplication of both sides of equation (2.13) by $\sin(k_m y)$ and integration over y from 0 to b produces

$$D_j W_n^{\mathrm{iv}} - 2k_n^2 D_j W_n'' + D_j k_n^4 W_n + \rho_j h_j \ddot{W}_n = 0 \qquad (2.14)$$

Here m has been changed to n and use has been made of the orthogonality relation

$$\frac{2}{b}\int_0^b \sin\left(\frac{m\pi y}{b}\right)\sin\left(\frac{n\pi y}{b}\right)\mathrm{d}y = \begin{cases} 0 & \text{if } n \neq m, \\ 1 & \text{if } n = m. \end{cases} \qquad (2.15)$$

The problem is then essentially one dimensional. Assuming a harmonic response, the out-of-plane displacement of plate j has an x dependency in the form:

$$W_n(x,t) = \exp(rx + i\omega t) \qquad (2.16)$$

Using the displacement function (2.16), equation (2.14) may be rewritten as

$$r^4 - 2k_n^2 r^2 + \left(k_n^4 - \frac{\rho_j h_j \omega^2}{D_j}\right) = 0 \qquad (2.17)$$

Equation (2.17) is a fourth-order linear, homogeneous, ordinary differential equation. Its characteristic equation for an exponential function solution is the biquadratic. The solution of equation (2.17) gives

$$W_n(x) = \sum_{m=1}^{4} A_{nm} \exp(r_{nm} x) \tag{2.18}$$

Here A_{nm} terms are integration constants, r_{nm}, namely, $+r_n$, $-r_n$, $+\bar{r}_n$, and $-\bar{r}_n$ terms are four roots of equation (2.17), where

$$r_n = +(k_n^2 + k_B^2)^{1/2} \tag{2.19}$$

$$\bar{r}_n = +(k_n^2 - k_B^2)^{1/2} \tag{2.20}$$

and k_B is given by

$$k_B^4 = \frac{\rho_j h_j \omega^2}{D_j} \tag{2.21}$$

Note that $\bar{r}_n$ is imaginary for any given ω whenever $\hat{n} \geq n$, where

$$\hat{n} = \frac{b}{\pi} k_B^{1/2} \tag{2.22}$$

However, that would not bring any extra difficulty in calculations, as all the quantities are already complex if the structural damping is introduced.

Using expression (2.18) the out-of-plane response of a plate can be written as

$$w(x, y, t) = \sum_{m=1}^{4} A_{nm} \exp(r_{nm} x) \sin(k_n y) \exp(i\omega t) \tag{2.23}$$

The final form of the displacement given by eqn (2.23) may be used to express the displacement w_j and rotation θ_j of the plate edge in terms of

the integration constants. To avoid confusion, first two roots of equation (2.17) are renamed as r_1 and latter two as r_2

$$\begin{bmatrix} w_{1j} \\ \theta_{1j} \\ w_{2j} \\ \theta_{2j} \end{bmatrix} = \begin{bmatrix} 1 & 1 & 1 & 1 \\ r_1 & -r_1 & r_2 & -r_2 \\ e^{r_1 b} & e^{-r_1 b} & e^{r_2 b} & e^{-r_2 b} \\ r_1 e^{r_1 b} & -r_1 e^{-r_1 b} & r_2 e^{r_2 b} & -r_2 e^{-r_2 b} \end{bmatrix} \begin{bmatrix} A_1 \\ A_2 \\ A_3 \\ A_4 \end{bmatrix} \tag{2.24}$$

where w_{1j}, θ_{1j} and w_{2j}, θ_{2j} the displacements and rotations at x=0 and x=b respectively, as shown in Fig. 2.2.a. At this stage the suffix n is dropped for convenience, although it should be noted that all of the following equations relate to a prescribed value of n.

For the ease of reference in later sections, the above equation is rewritten in matrix form as

$$\mathbf{d}_j^o = \mathbf{R}_j \mathbf{A}_j \tag{2.25}$$

Before proceeding any further, it should be noted that exponential entries of the equation (2.24) may numerically overflow when the matrix is computed in its original form, because real part of r_m can, sometimes, be large and positive. To avoid this numerical difficulty the constant A_m may be replaced by $A'_m = A_m \exp(r_m b)$ in which case the first column of the above matrix becomes

$$\begin{bmatrix} e^{r_1 b} & r_1 e^{-r_1 b} & 1 & r_1 \end{bmatrix}^{\mathrm{T}} \tag{2.26}$$

Other entries of the matrix may be modified in a similar manner. To provide consistency throughout the calculations all occurrences of A_m can also be scaled using the above procedure. However this scaling procedure imposes restriction on the selection of the position of point force: this issue will be discussed in section 5.3.1.

The tractions which are shown in Fig. 2.2.b, namely, effective shear force, S_j, and bending moment, M_j, per unit length that are related to out-of-plane displacement are formulated as [13]

$$S_j = -D_j\left(\frac{\partial^3 w}{\partial x^3} + (2-\nu_j)\frac{\partial^3 w}{\partial x \partial y^2}\right) \tag{2.27}$$

$$M_j = D_j\left(\frac{\partial^2 w}{\partial x^2} + \nu_j \frac{\partial^2 w}{\partial y^2}\right) \tag{2.28}$$

In equation (2.27) allowance has been made for the Kirchhoff edge effect. Using equation (2.23), equation (2.27) and (2.28) may be written in terms of amplitudes A_m.

$$\begin{bmatrix} S_{1j} \\ M_{1j} \\ S_{2j} \\ M_{2j} \end{bmatrix} = D_j \begin{bmatrix} a_{11} & a_{12} & a_{13} & a_{14} \\ a_{21} & a_{22} & a_{23} & a_{33} \\ a_{31} & a_{32} & a_{33} & a_{34} \\ a_{41} & a_{42} & a_{43} & a_{44} \end{bmatrix} \begin{bmatrix} A_1 \\ A_2 \\ A_3 \\ A_4 \end{bmatrix} \tag{2.29}$$

The above expression may be put in matrix form as

$$\mathbf{F}_j^{\circ} = \hat{\mathbf{R}}_j^{\circ} \mathbf{A}_j \tag{2.30}$$

If equation (2.30) is combined with equation (2.25), the constants $\mathbf{A}_j$ may be eliminated and the edge tractions are then written in terms of edge displacements as

$$\mathbf{F}_j^{\circ} = \mathbf{P}_j^{\circ} \mathbf{d}_j^{\circ} \tag{2.31}$$

where $\mathbf{P}_j^{\circ}$ is given by

$$\mathbf{P}_j^{\circ} = \hat{\mathbf{R}}_j^{\circ} \mathbf{R}_j^{-1} \tag{2.32}$$

and $(\mathbf{F}_j^o)^T = (S_{1j}, M_{1j}, S_{2j}, M_{2j})$, $(\mathbf{d}_j^o)^T = (w_{1j}, \theta_{1j}, w_{2j}, \theta_{2j})$ and $\mathbf{P}_j^o$ is the 4x4 out-of-plane dynamic stiffness matrix of plate j. Superscript " o" denotes the out-of-plane.

2.2.2 IN-PLANE STIFFNESS MATRIX.

The in plane field equations along the longitudinal direction, u, and transverse direction, v, are coupled to each other, hence, they should be solved simultaneously. The differential equations which govern the in-plane deflections of the j'th plate for free vibration can be expressed as [13]

$$B_j(1+\gamma_j)\frac{\partial^2 u}{\partial x^2} + B_j\frac{\partial^2 v}{\partial y^2} + B_j\gamma_j\frac{\partial^2 v}{\partial x\,\partial y} - \rho_j\ddot{u} = 0 \qquad (2.33)$$

$$B_j(1+\gamma_j)\frac{\partial^2 v}{\partial y^2} + B_j\frac{\partial^2 u}{\partial x^2} + B_j\gamma_j\frac{\partial^2 u}{\partial x\,\partial y} - \rho_j\ddot{v} = 0 \qquad (2.34)$$

where B_j and γ_j are given by

$$B_j = \frac{E_j}{2(1+\nu_j)} \qquad \gamma_j = \frac{1+\nu_j}{1-\nu_j}$$

As the plate is simply-supported at y=0 and y=b, there is no displacement along the longitudinal direction at these two edges; therefore u can be expanded as a Fourier sine series. However the plate is free to move in the transverse direction at the simply-supported edges; thus v can be expanded as a Fourier cosine series. That is to say:

$$u(x,y,t) = \sum_n U_n(x,t)\sin\left(\frac{n\pi y}{b}\right) \qquad n=1,2,\ldots \qquad (2.35)$$

$$v(x,y,t)=\sum_n V_n(x,t)\cos\left(\frac{n\pi y}{b}\right) \qquad n=1,2,\ldots \qquad (2.36)$$

Substituting equations (2.35) and (2.36) into (2.33) and (2.34), reduces the field equations, related to the in-plane motion of plate j, to one dimensional differential equations in terms of spatial variable x, in the form

$$B_j(1+\gamma_j)U_n''-B_jk_n^2U_n-B_j\gamma_jk_nV_n'-\rho_j\ddot{U}_n=0 \qquad (2.37)$$

and

$$-k_n^2B_j(1+\gamma_j)V_n+B_jV_n''+B_j\gamma_jk_nU_n'-\rho_j\ddot{V}_n=0 \qquad (2.38)$$

It is now assumed that the in-plane displacements have exponential x dependency in the form

$$U_n(x,t)=U_{n0}\exp(\lambda x+i\omega t) \qquad (2.39)$$

$$V_n(x,t)=V_{n0}\exp(\lambda x+i\omega t) \qquad (2.40)$$

Inserting equations (2.39) and (2.40) into expressions (2.37) and (2.38) leads to the simultaneous equations in terms U_{n0} and V_{n0}

$$\begin{bmatrix} B_j(1+\gamma_j)\lambda^2-B_jk_n^2+\rho_j\omega^2 & -B_j\gamma_j\lambda \\ B_j\gamma_j\lambda & -k_n^2B_j(1+\gamma_j)+B_j\lambda^2+\rho_j\omega^2 \end{bmatrix}\begin{bmatrix} U_{n0} \\ V_{n0} \end{bmatrix}=\begin{bmatrix} 0 \\ 0 \end{bmatrix} \qquad (2.41)$$

When the above equation is solved for λ the four roots are:

$$\lambda^2=k_n^2-k_L^2 \qquad \lambda_{1,2}=\pm\sqrt{k_n^2-k_L^2} \qquad (2.42)$$

$$\lambda^2=k_n^2-k_T^2 \qquad \lambda_{3,4}=\pm\sqrt{k_n^2-k_T^2} \qquad (2.43)$$

where k_L and k_T are given by

$$k_L^2 = \frac{\rho_j \omega^2 (1 - \nu_j^2)}{E_j} \tag{2.44}$$

$$k_T^2 = \frac{2\rho_j \omega^2 (1 + \nu_j)}{E_j} \tag{2.45}$$

Equations (2.42) and (2.43) each yield two roots which are either real or complex. Renaming first and latter two roots that are obtained from equations (2.42) and (2.43) as λ_1, $-\lambda_1$, and λ_2, $-\lambda_2$ respectively, then V_n and U_n may be rewritten as

$$\begin{bmatrix} V_n \\ U_n \end{bmatrix} = \begin{bmatrix} k_n & k_n \\ \lambda_1 & -\lambda_1 \end{bmatrix} \begin{bmatrix} C_1 e^{\lambda_1 x} \\ C_2 e^{\lambda_1 x} \end{bmatrix} + \begin{bmatrix} \lambda_2 & -\lambda_2 \\ k_n & k_n \end{bmatrix} \begin{bmatrix} C_3 e^{\lambda_2 x} \\ C_4 e^{\lambda_2 x} \end{bmatrix} e^{i\omega t} \tag{2.46}$$

where C_m, m=1,...,4 are the amplitudes.

The general solution for the in-plane displacements can be written as

$$v(x,y,t) = \left\{ \begin{bmatrix} k_n & k_n \end{bmatrix} \begin{bmatrix} C_1 e^{\lambda_1 x} \\ C_2 e^{\lambda_1 x} \end{bmatrix} + \begin{bmatrix} \lambda_2 & -\lambda_2 \end{bmatrix} \begin{bmatrix} C_3 e^{\lambda_2 x} \\ C_1 e^{-\lambda_2 x} \end{bmatrix} \right\} \cos(k_n y) \exp(i\omega t) \tag{2.47}$$

$$u(x,y,t) = \left\{ \begin{bmatrix} \lambda_1 & -\lambda_1 \end{bmatrix} \begin{bmatrix} C_1 e^{\lambda_1 x} \\ C_2 e^{-\lambda_1 x} \end{bmatrix} + \begin{bmatrix} k_n & k_n \end{bmatrix} \begin{bmatrix} C_3 e^{\lambda_2 x} \\ C_1 e^{\lambda_2 x} \end{bmatrix} \right\} \sin(k_n y) \exp(i\omega t) \tag{2.48}$$

The in-plane edge displacements v_j, and u_j (see Fig. 2.2.a) can be expressed in terms of the amplitudes C_m, using the general form of in-plane displacements given by equations (2.47) and (2.48) as

$$\begin{bmatrix} v_1 \\ u_1 \\ v_2 \\ u_2 \end{bmatrix} = \begin{bmatrix} k_n & k_n & \lambda_2 & -\lambda_2 \\ \lambda_1 & -\lambda_1 & k_n & k_n \\ k_n e^{\lambda_1 b} & k_n e^{\lambda_1 b} & \lambda_2 e^{\lambda_2 b} & -\lambda_2 e^{\lambda_2 b} \\ \lambda_1 e^{\lambda_1 b} & -\lambda_1 e^{\lambda_1 b} & k_n e^{\lambda_2 b} & k_n e^{\lambda_2 b} \end{bmatrix} \begin{bmatrix} C_1 \\ C_2 \\ C_3 \\ C_4 \end{bmatrix} \tag{2.49}$$

Equation (2.49) may be rewritten in the matrix form as

$$\mathbf{d}_j^{\text{in}} = \mathbf{Q}_j \mathbf{C}_j \tag{2.50}$$

The forces, N_j, and T_j, which are related to in-plane displacements are given by the formulae

$$N_j = B_j(1+\gamma_j)\left(\frac{\partial u}{\partial x} + \nu_j \frac{\partial v}{\partial y}\right) \tag{2.51}$$

$$T_j = B_j\left(\frac{\partial u}{\partial y} + \frac{\partial v}{\partial x}\right) \tag{2.52}$$

Using the final form of in-plane displacement expressions (2.47) and (2.48) and traction equations (2.51) and (2.52), the in-plane edge tractions of panel j may be represented in terms of C_m, after necessary manipulations, in the form

$$\begin{bmatrix} T_{1j} \\ N_{1j} \\ T_{2j} \\ N_{2j} \end{bmatrix} = E_j \begin{bmatrix} c_{11} & c_{12} & c_{13} & c_{14} \\ c_{21} & c_{22} & c_{23} & c_{24} \\ c_{31} & c_{32} & c_{33} & c_{34} \\ c_{41} & c_{42} & c_{43} & c_{44} \end{bmatrix} \begin{bmatrix} C_1 \\ C_2 \\ C_3 \\ C_4 \end{bmatrix} \tag{2.53}$$

Equation (2.53) may be rewritten in matrix form as

$$\mathbf{F}_j^{\text{in}} = \hat{\mathbf{Q}}_j^{\text{in}} \mathbf{C}_j \tag{2.54}$$

In order to eliminate constants C_m from equation (2.54) the in-plane displacement matrix which is given by equation (2.50) may be inverted and when the result is substituted into equation (2.54), an expression which relates the edge tractions N_j, and T_j, to the deflections u_j, and v_j, can be obtained.

$$\mathbf{F}_j^{in} = \mathbf{P}_j^{in}\mathbf{d}_j^{in} \tag{2.55}$$

$\mathbf{P}_j^{in}$ is given by

$$\mathbf{P}_j^{in} = \hat{\mathbf{Q}}_j^{in}\mathbf{Q}_j^{-1} \tag{2.56}$$

where $(\mathbf{F}_j^{in})^T = (T_{1j}, N_{1j}, T_{2j}, N_{2j})$, $(\mathbf{d}_j^{in})^T = (v_{1j}, u_{1j}, v_{2j}, u_{2j})$ and $\mathbf{P}_j^{in}$ is the 4x4 in-plane dynamic stiffness matrix of the plate j, *superscript "in" means* the variables are in the in-plane direction.

2.2.3 COMPLETE STIFFNESS MATRIX OF A SINGLE PLATE.

Having determined the out-of-plane and in-plane dynamic stiffness matrices of a plate, it is a simple matter to construct the complete stiffness matrix, $\mathbf{K}_{cj}$, of a single plate in local co-ordinates. To achieve this, all one needs is to get the appropriate out-of-plane and in-plane stiffness terms, given in the previous two sections, and insert them into the relevant places of complete dynamic stiffness matrix. Before forming the complete stiffness matrix of a single plate, to avoid confusion in this process and to show clearly which entry of in-plane and out-of-plane stiffness matrices fits into which part of complete stiffness matrix, each four by four matrix $\mathbf{P}_j^{in}$ and $\mathbf{P}_j^{o}$ of equations (2.55) and (2.31), respectively, is partitioned into two by two sub matrices, leading to the expressions

$$\begin{bmatrix} T_{1j} \\ N_{1j} \\ T_{2j} \\ N_{2j} \end{bmatrix} = \left[\begin{array}{c|c} \mathbf{P}_{1j}^{in} & \mathbf{P}_{2j}^{in} \\ \hline \mathbf{P}_{3j}^{in} & \mathbf{P}_{3j}^{in} \end{array}\right] \begin{bmatrix} v_{1j} \\ u_{1j} \\ v_{2j} \\ u_{2j} \end{bmatrix} \tag{2.57}$$

and

$$\begin{bmatrix} M_{1j} \\ S_{1j} \\ M_{2j} \\ S_{2j} \end{bmatrix} = \left[\begin{array}{c|c} \mathbf{P}^{o}_{1j} & \mathbf{P}^{o}_{2j} \\ \hline \mathbf{P}^{o}_{3j} & \mathbf{P}^{o}_{4j} \end{array}\right] \begin{bmatrix} w_{1j} \\ \theta_{1j} \\ w_{2j} \\ \theta_{2j} \end{bmatrix} \tag{2.58}$$

Hence, the relationship between edge tractions and edge displacements for plate j can be written as

$$\begin{bmatrix} T_{1j} \\ N_{1j} \\ S_{1j} \\ M_{1j} \\ T_{2j} \\ N_{2j} \\ S_{2j} \\ M_{2j} \end{bmatrix} = \left[\begin{array}{c|c|c|c} \mathbf{P}^{in}_{1j} & \mathbf{0} & \mathbf{P}^{in}_{2j} & \mathbf{0} \\ \hline \mathbf{0} & \mathbf{P}^{o}_{1j} & \mathbf{0} & \mathbf{P}^{o}_{2j} \\ \hline \mathbf{P}^{in}_{3j} & \mathbf{0} & \mathbf{P}^{in}_{4j} & \mathbf{0} \\ \hline \mathbf{0} & \mathbf{P}^{o}_{3j} & \mathbf{0} & \mathbf{P}^{o}_{4j} \end{array}\right] \begin{bmatrix} v_{1j} \\ u_{1j} \\ w_{1j} \\ \theta_{1j} \\ v_{2j} \\ u_{2j} \\ w_{2j} \\ \theta_{2j} \end{bmatrix} \tag{2.59}$$

an eight by eight matrix composed of two by two sub-matrices. The location of zeros in the above matrix is a consequence of the fact that there is no coupling between in-plane edge forces and out-plane displacements, and vice versa. It follows from the theory of reciprocity [28] that the matrix of equation (2.59) is symmetric. Therefore

$$\mathbf{P}^{in}_{3j} = \mathbf{P}^{in}_{2j} \qquad \text{and} \qquad \mathbf{P}^{o}_{3j} = \mathbf{P}^{o}_{2j} \tag{2.60}$$

In abbreviated form equation (2.59) may be rewritten as

$$\mathbf{F}_{cj} = \mathbf{K}_{cj}\mathbf{d}_{cj} \tag{2.61}$$

where $\mathbf{F}_{cj}$ is the complete force vector, $\mathbf{K}_{cj}$ is the complete dynamic stiffness matrix, $\mathbf{d}_{cj}$ is the complete set of displacements for plate j. The term

"*complete*" is used here to show that the vectors and stiffness matrix contain a complete set of degrees of freedom of the sub-system. It is emphasised that equation (2.61) relates to a specific value of n. Considering the total number of Fourier terms, n, the equation (2.61) will take the form:-

$$\mathbf{F}_{cj} = \sum_{n} \mathbf{K}_{cjn}\mathbf{d}_{cjn} \qquad (2.61.a)$$

2.2.4 DYNAMIC STIFFNESS MATRIX OF A STRINGER.

The previous section has considered the dynamic stiffness matrix of a single plate (labelled j). In what follows the dynamic stiffness matrix of a stringer is developed; this allows the situation in which two plates are coupled via a stringer to be modelled, as explained in section 2.4.

The stiffeners which are often used in aircraft structures may be considered as open "thin-walled" beams. Assuming the stiffener is attached to the panel along a line in the transverse direction, and simply-supported at both ends, the dynamic stiffness matrix of a stringer of any cross section may be derived using a method developed by Langley [51]. In this approach cross sectional distortion of stiffeners during vibration is neglected for simplicity. However it is stated [52] that internal degrees of freedom of the beam should be taken into account in dynamic modelling as the resonance frequency of internal vibration is directly proportional to n.

The cross section of a typical stringer is depicted in Fig. 2.3, where point S is the shear centre, P is the attachment point to the panel and is taken to lie in the same vertical plane as S, and C is the centroid of the beam. The offsets c_0, c_1, c_2 between S, P and C are the various distances as shown in the figure. The rotation of the stiffener is represented by θ, and the translational displacements of shear centre, attachment point, and centroid are (u_0, v_0, w_0), (u, v, w), (u_c, v_c, w_c) respectively.

The forces and moments developed at the points S and C are shown in Fig. 2.4, where E and G are the moduli of elasticity and rigidity, ρ is the density per unit length, A is the cross sectional area of the beam, I_1, I_2, are second moments of area, with respect to neutral axes, along the z and y directions respectively, I_{12} is the product moment of inertia, Γ, and J are the torsional constants. Finally, a dash represents derivative with respect to the x co-ordinate.

Normally, the area of contact between the plate and stiffener is small in comparison to the area of panel. The stiffener acts along the width of the panel, effectively as a discontinuity in the plate moment and force distributions. The forces and moments acting on the stringer are exactly the same in magnitude as the forces and moments acting on the plate, yet in opposite direction to those of the plate.

An exaggerated view of the supporting stiffener in both undisplaced and displaced position is shown in Fig. 2.3. In order to facilitate later comparisons between the stiffener and plate deflections, the beam equations will be expressed only at the point of attachment, P. Since P is the point of contact between the stringer and the plate, the displacement and slope of the point P are the same as denoted by the plate deflection, w, and slope θ. Also the deflections u and v of the stringer in the x and y direction respectively would be the same as that of the plate at the contact point.

Referring to Fig. 2.3, the motions at the points S and C are generally different from those at P. However, by using subscripts "0" and "c" for motions at the points S and C respectively and unscripted variables for point P, the following linear relations may be derived when the slope θ is assumed to be small.

$$w_0 = w, \qquad u_c = u, \qquad v_0 = v + c_0\theta \qquad (2.62),(2.63),(2.64)$$

$$w_c = w + c_2\theta, \qquad v_c = v - c_1\theta \qquad (2.65),(2.66)$$

When the stringer is deformed, the elastic forces of the stringer may be combined into resultant vertical and horizontal forces through the shear

centre, S, of the cross section and a resultant moment about S. The inertial forces of the stringer, however, are more conveniently summed into similar resultants through and about the centroid, C. In addition, there are forces and moments transmitted from the panel to the stiffener at the attachment point, P, which is immediately beneath the shear centre. This location is the line of action of the stringer forces and moments.

Considering the equilibrium of forces and moments, the foregoing forces and moment may be expressed as

$$EAc_2v''' + EAc_1w''' - EAu'' + \rho A\ddot{u} - \rho Ac_1\ddot{w}' - \rho Ac_2\ddot{v}' = G \tag{2.67}$$

$$EI_2(v + c_0\theta)^{iv} + EI_{12}w^{iv} + \rho A(\ddot{v} - c_1\ddot{\theta}) = H \tag{2.68}$$

$$EI_1w^{iv} + EI_{12}(v + c_0\theta)^{iv} + \rho A(\ddot{w} + c_2\ddot{\theta}) = Q \tag{2.69}$$

$$E\Gamma\theta^{iv} - GJ\theta'' + \rho I_p\ddot{\theta} + c_0H - \rho A(c_0 + c_1)\ddot{v}_c + \rho Ac_2\ddot{w}_c = M \tag{2.70}$$

By substituting equation (2.68) into (2.70) H may be eliminated.

Since the stringer is simply-supported at the ends, the displacements u, v, w may be expanded in a Fourier series using the same approach as in section 2.2.1 and 2.2.2. Hence, for the present co-ordinate system shown in Fig. 2.4 displacements can be expressed as

$$u(x,y,t) = U_n(y)\cos(k_nx)\exp(i\omega t) \tag{2.71}$$

$$v(x,y,t) = V_n(y)\sin(k_nx)\exp(i\omega t) \tag{2.72}$$

$$w(x,y,t) = W_n(y)\sin(k_nx)\exp(i\omega t) \tag{2.73}$$

Differentiating the above equations with respect to x and inserting into equations (2.67), (2.68), (2.69), and (2.70), the forces and moment which act at the attachment point of the stiffener may be written in terms of the displacements in the form

$$\begin{bmatrix} G \\ H \\ Q \\ M \end{bmatrix} = \begin{bmatrix} d_{11} & d_{12} & d_{13} & d_{14} \\ & d_{22} & d_{23} & d_{24} \\ & sym. & d_{33} & d_{34} \\ & & & d_{44} \end{bmatrix} \begin{bmatrix} u \\ v \\ w \\ \theta \end{bmatrix} \tag{2.74}$$

where,

$$d_{11} = EAk_n^2 - \rho A\omega^2, \qquad d_{12} = -EAc_2k_n^3 + \rho A\omega^2 k_n, \tag{2.75),(2.76}$$

$$d_{13} = -EAc_1k_n^3 + \rho Ac_1k_n\omega^2, \qquad d_{14} = 0, \tag{2.77),(2.78}$$

$$d_{22} = (EI_2 + EAc_2^2)k_n^4 - \rho A(1 + c_2^2k_n^2)\omega^2, \tag{2.79}$$

$$d_{23} = (EI_{12} + EAc_1c_2)k_n^4 - \rho Ac_1c_2k_n^2\omega^2, \tag{2.80}$$

$$d_{24} = EI_2c_0k_n^4 + \rho Ac_1\omega^2 \tag{2.81}$$

$$d_{33} = (EI_1 + EAc_1^2)k_n^4 - \rho A(1 + c_1^2k_n^2)\omega^2 \tag{2.82}$$

$$d_{34} = EI_{12}c_0k_n^4 - \rho Ac_2\omega^2 \tag{2.83}$$

$$d_{44} = (E\Gamma + EI_2c_0^2)k_n^4 + GJk_n^2 - (\rho I_p + \rho Ac_1^2 + \rho Ac_2^2)\omega^2 \tag{2.84}$$

The symmetric matrix given in equation (2.74) constitutes the dynamic stiffness matrix of a stiffener. When the plates are elastically supported, this matrix may be used to implement the effect of stringers.

2.3 TRANSFORMATION TO GLOBAL CO-ORDINATES.

The stiffness matrices derived in the previous sections used a system of local co-ordinates as the in-plane, and bending components originally chosen for this system. A different co-ordinate system is used for every element to ease computation. In fact it is a simple matter to transform

the co-ordinates of the displacement and force components to any other co-ordinate system. Clearly it is necessary to do so before an assembly of the structure can be attempted, because the axes to which the displacement and force vectors at the two ends of an element are related should be chosen in such a way that when the two elements are connected together during the process of assembling, the displacement and the force at node-2 of left-hand element in Fig. 2.5.b are related to the same axes as the displacement and force vectors at node-1 of the right-hand element in the same figure.

In the case of structures having junctions lying on a straight line, as in Fig. 2.7.b and 2.7.c, this requirement amounts simply to the fact that the traction and deflection vectors at both ends of the sub-structure must be related to the same global axes. In the case of orthogonally (or at any angle) connected elements (see Fig. 2.7.a) it may be considered that the element makes an angle θ from the junction as shown in Fig. 2.5.a; the requirement means that the reference axes of the element are obtained by rotating the global axes by an angle θ.

The common global axes system will be denoted by x^g, y^g, z^g, and local system x, y, z as before. Initially, it will be more convenient to specify the element nodes by their global co-ordinates and to establish from these the local co-ordinates, thus requiring an inverse transformation.

The two systems of co-ordinates are shown in Fig. 2.6. By assuming that the local co-ordinate system (x, y, z) can be obtained by rotating (x^g, y^g, z^g) system about y^g axis by an angle θ as shown in Fig. 2.6.a, the transformation of the displacements and forces of a node from the global to local is accomplished by a matrix Λ giving

$$\begin{bmatrix} v_{ej} \\ u_{ej} \\ w_{ej} \\ \theta_{ej} \end{bmatrix} = \Lambda_j \begin{bmatrix} v^g_{ej} \\ u^g_{ej} \\ w^g_{ej} \\ \theta^g_{ej} \end{bmatrix} \qquad \begin{bmatrix} T_{ej} \\ N_{ej} \\ S_{ej} \\ M_{ej} \end{bmatrix} = \Lambda_j \begin{bmatrix} T^g_{ej} \\ N^g_{ej} \\ S^g_{ej} \\ M^g_{ej} \end{bmatrix} \qquad (2.85),(2.86)$$

where subscript e denotes the edge of the plate j and it is either 1 or 2, and superscript g represents the global nature of the variable.

Using Fig. 2.6.b the entries of Λ_j may be written as

$$\Lambda_j = \begin{bmatrix} 1 & 0 & 0 & 0 \\ 0 & \cos\theta & \sin\theta & 0 \\ 0 & -\sin\theta & \cos\theta & 0 \\ 0 & 0 & 0 & 1 \end{bmatrix} \tag{2.87}$$

For the whole set of forces on the edges of an element, one may therefore write

$$\mathbf{d}_{cj} = \mathbf{T}\mathbf{d}^{g}_{cj} \tag{2.88}$$

By the rules of orthogonal transformation the stiffness matrix of an element in the global co-ordinates becomes

$$\mathbf{K}^{g}_{cj} = \mathbf{T}^{T}\mathbf{K}_{cj}\mathbf{T} \tag{2.89}$$

where $\mathbf{K}_{cj}$ represents 8x8 dynamic stiffness matrix of the plate j, and $\mathbf{T}$ is the transformation matrix. In both of the above equations, (2.88) and (2.89), $\mathbf{T}$ is given by

$$\mathbf{T} = \begin{bmatrix} \Lambda & \mathbf{0} \\ \mathbf{0} & \Lambda \end{bmatrix} \tag{2.90}$$

a diagonal matrix built up of Λ matrices.

Finally, the tractions of the plate j in global co-ordinates may be expressed as

$$\mathbf{F}^{g}_{cj} = \mathbf{K}^{g}_{cj}\mathbf{d}^{g}_{cj} \tag{2.91}$$

2.4 ASSEMBLY AND SOLUTION OF EQUATIONS.

Once the element characteristics, namely, the element stiffness matrices and element vectors are found in a common global co-ordinate system, the next step is to construct the overall system equations for the structure under consideration.

The procedure of assembling the element matrices and vectors is based on the requirement of "compatibility" at the element nodes. This means that at the nodes where elements are connected, the values of the unknown nodal degrees of freedom, v, u, w, θ, are the same for all the elements joining at that node. As the conditions of overall equilibrium have already been satisfied within an element all that is necessary is to establish equilibrium conditions at the nodes of the structure. The resulting equations will contain the displacements as unknowns, and once these have been solved the structural problem is determined.

Representing the nodal displacement, $\mathbf{d}$, and forces, $\mathbf{F}$, as

$$\mathbf{d} = \begin{bmatrix} \mathbf{d}_1 \\ \vdots \\ \mathbf{d}_n \end{bmatrix} \qquad \mathbf{F} = \begin{bmatrix} \mathbf{F}_1 \\ \vdots \\ \mathbf{F}_n \end{bmatrix} \qquad (2.92),(2.93)$$

for the whole structure in which all elements participate, standard finite element techniques [1] may be used to analyse a structure which consists of any number of plate and stiffener elements. It should be noted that from this section onwards even though the subscript "g" is omitted for simplicity, all the variables correspond to global co-ordinates unless otherwise stated.

If now the equilibrium conditions of a typical node, i, are to be established, each component of $\mathbf{F}_i$ has, in turn, to be equated to the sum of the component forces contributed by the elements meeting at the node. In this analysis node (junction) is defined as a x=constant line as shown in Fig. 2.5, rather than a point contrary to the definition of node in standard finite element literature, where two plates and a stringer meet.

In this respect, there are three types of junctions considered throughout this research. These are:

(i). Two directly coupled plate elements at an angle as illustrated in Fig. 2.7.a, in which case force components which contains the element forces and discrete forces acting on the particular junction may be written in the form

$$\mathbf{F}_i = \sum_{s=1}^{2} \mathbf{F}_i^s = \mathbf{F}_i^1 + \mathbf{F}_i^2 + \mathbf{f}_i \tag{2.94}$$

where $\mathbf{F}_i^1$ is the force contributing to node i by element 1 of node i, $\mathbf{F}_i^2$ by element 2 of node i, and $\mathbf{f}_i$ is the nodal force vector which contains the details of the external forces applied in a particular direction. The detailed derivation of the force vector is given in section 2.6.

Substituting from the definition (2.93) the forces contributing to node i are

$$\mathbf{F}_i = \left(\mathbf{K}_i^1 + \mathbf{K}_i^2\right)\mathbf{d}_i + \mathbf{f}_i \tag{2.95}$$

For the sake of simplicity subscript j is also removed, because a node replaces an edge, and displacements are the same for both of the adjacent plates at a node i.

(ii). Two directly coupled coplanar plates via a simple support (see Fig. 2.7.b). Simple supports restrain any movement in u, v, w direction, yet allow rotation, θ. In this sense, two orthogonally directly coupled plates are akin to two coplanar simply supported plates, provide that in-plane effects are neglected. Therefore, the force vector may be obtained from equation (2.95) by making necessary alterations, for any constraints that are imposed, on the vector $\mathbf{d}_i$ which contains the degrees of freedom of each node.

(iii). Elastically supported plates, that is to say, row of flat plates that are connected together over a beam, rather than a simple support, as

shown in Fig. 2.7.c. The stiffener allows for translational as well as rotational motions of coupled plates.

For this case assembly of forces at the junctions becomes

$$\mathbf{F}_i = \left(\mathbf{K}_i^1 + \mathbf{K}_i^2 + \mathbf{K}_i^b\right)\mathbf{d}_i + \mathbf{f}_i \tag{2.96}$$

where $\mathbf{K}_i^b$ is the stiffness matrix of stringer, formed by using the appropriate values of equations (2.75)-(2.84).

In determining the structure dynamic stiffness matrix for this case, use is made of the fact that corresponding element displacement components at a common structure node must be equal. Clearly the process of writing equilibrium equations (or, more correctly, equations of motions) for each node is equivalent to adding corresponding element (plate and beam) stiffness components to yield the structure dynamic stiffness component.

Equations (2.95) and (2.96) may be solved using the standard finite element techniques to obtain the response vector **d**, which contains the relevant information about the displacements of all the nodes of the structure considered.

2.5 PLATE VIBRATIONAL ENERGIES.

After determining the response of the structure at each node, suitable expressions for the average plate vibrational energies need to be derived with the aim of relating them to the transmitted vibration energy throughout the structure. In order to compare the results of dynamic stiffness method with the predictions of Statistical Energy Analysis (SEA) temporal and spatial averages of plate vibrational energies need to be calculated as the examination of such relations are central to SEA, (see chapter 3). In what follows the kinetic energy of plate j is derived for a prescribed value of n.

In SEA it is assumed that the response of a dynamic system is mainly due to the responses of the modes which are resonant in a particular frequency band and interactions of non-resonant modes are negligible (see

section 3.2.2); it then follows that computation of the kinetic energy of each sub-structure would be enough to determine the vibrational energies of the complete structure, since for the resonant condition kinetic and potential energies may be assumed equal when time averaged. Thus the total energy of subsystem j may be expressed as

$$\left\langle E_j^{\text{total}} \right\rangle = 2\left\langle T_j \right\rangle \tag{2.97}$$

The time average kinetic energy per unit area of the plate j due to the out-of-plane component of displacement is given by the expression

$$\left\langle T_j^{\circ} \right\rangle = \left\langle \frac{1}{2A_j} \rho_j h_j \int_0^L \int_0^b \left(\frac{\partial w}{\partial t} \right)^2 \mathrm{d}y\, \mathrm{d}x \right\rangle \tag{2.98}$$

where T_j is the kinetic energy, A_j is the area of the plate j, and angle brackets represents the temporal average.

By substituting the assumed harmonic displacement function (2.23) with equation (2.25) into equation (2.98) it is possible, after differentiating with respect to time, to express bending component of kinetic energy in the following form

$$\left\langle T_j^{\circ} \right\rangle = \frac{\omega^2}{2A_j} \left[\mathbf{R}_j {}^{1}\mathbf{d}_j^{\circ} \right]^{\mathrm{T}} \mathbf{m}_j^{\circ} \left[\mathbf{R}_j \mathbf{d}_j^{\circ} \right]^{*} \tag{2.99}$$

where an asterix denotes complex conjugate and $\mathbf{m}_j^{\circ}$ is the bending mass matrix given as

$$\mathbf{m}_j^{\circ} = \rho_j h_j \int_0^L \int_0^b \left(\mathbf{p}_j^{\circ} \right)^{\mathrm{T}} \left(\mathbf{p}_j^{\circ} \right)^{*} \mathrm{d}y\, \mathrm{d}x \tag{2.100}$$

$\mathbf{p}_j^{\circ}$ is given by the vector

$$\mathbf{p}_j^{\circ} = \left[\mathrm{e}^{r_1 x} \quad \mathrm{e}^{-r_1 x} \quad \mathrm{e}^{r_2 x} \quad \mathrm{e}^{-r_2 x} \right] \tag{2.101}$$

In the same fashion, the time average kinetic energy per unit area of the in-plane displacement may be expressed as

$$\left\langle T_J^{\text{in}} \right\rangle = \left\langle \frac{1}{2A_J} \rho_J h_J \int_0^L \int_0^b \left[\left(\frac{\partial v}{\partial t} \right)^2 + \left(\frac{\partial u}{\partial t} \right)^2 \right] \mathrm{d}y \, \mathrm{d}x \right\rangle \tag{2.102}$$

Inserting the in-plane displacement functions (2.47) and (2.48) together with equation (2.50) into equation (2.102) in-plane kinetic energy expression may be put into the form

$$\left\langle T_J^{\text{in}} \right\rangle = \frac{\omega^2}{2A_J} \left[\mathbf{Q}_J {}^1\mathbf{d}_J^{\text{in}} \right]^{\text{T}} \mathbf{m}_J^{\text{in}} \left[\mathbf{Q}_J \mathbf{d}_J^{\text{in}} \right]^* \tag{2.103}$$

where $\mathbf{m}_J^{\text{in}}$ is the in-plane mass matrix given as

$$\mathbf{m}_J^{\text{in}} = \rho_J h_J \int_0^L \int_0^b \left[\left(\mathbf{p}_{1J}^{\text{in}} \right)^{\text{T}} \left(\mathbf{p}_{1J}^{\text{in}} \right)^* + \left(\mathbf{p}_{2J}^{\text{in}} \right)^{\text{T}} \left(\mathbf{p}_{2J}^{\text{in}} \right)^* \right] \mathrm{d}y \, \mathrm{d}x \tag{2.104}$$

$\mathbf{p}_{1J}^{\text{in}}$ and $\mathbf{p}_{2J}^{\text{in}}$ are the matrix forms of equations (2.47) and (2.48) respectively rewritten in the form,

$$\mathbf{p}_{1J}^{\text{in}} = \left[k_n \mathrm{e}^{\lambda_1 x} \quad k_n \mathrm{e}^{\lambda_1 x} \quad \lambda_2 \mathrm{e}^{\lambda_2 x} \quad \lambda_2 \mathrm{e}^{\lambda_2 x} \right] \tag{2.105}$$

$$\mathbf{p}_{2J}^{\text{in}} = \left[\lambda_1 \mathrm{e}^{\lambda_1 x} \quad -\lambda_1 \mathrm{e}^{-\lambda_1 x} \quad k_n \mathrm{e}^{\lambda_2 x} \quad -k_n \mathrm{e}^{\lambda_2 x} \right] \tag{2.106}$$

Finally, if ω_1 and ω_2 are the first and last frequency of the frequency range of interest, which is wide enough to contain a few resonant modes, the mean value of out-of-plane and in-plane kinetic energies may be obtained by integrating over the frequency band.

$$\left\langle T_J^{\text{o}} \right\rangle_{\text{av}} = \frac{1}{(\omega_2 - \omega_1)} \int_{\omega_1}^{\omega_2} \left\langle T_J^{\text{o}} \right\rangle d\omega \tag{2.107}$$

$$\left\langle T_j^{in} \right\rangle_{av} = \frac{1}{(\omega_2 - \omega_1)} \int_{\omega_1}^{\omega_2} \left\langle T_j^{in} \right\rangle d\omega \tag{2.108}$$

In obtaining the kinetic energies of the section 5.2 by using the expressions (2.107) and (2.108), the convergence checks revealed that around 25 increments in a given one-third octave frequency band suffice to yield converged results. The technique used for doing these numerical integrations in the computer program is the Simpson's Rule.

2.6 IMPLEMENTATION OF FORCED VIBRATION.

In almost all practical situations it is the force which is perpendicular to the plate that causes the vibration, therefore in this section only the response due to a force in the out-of-plane direction will be considered.

The spatial dependence of the response of a finite plate to a concentrated force that varies harmonically in time, and is applied at some arbitrary location $x=x_p$ and $y=y_p$, where $0<x_p<L$ and $0<y_p<b$ as shown in Fig. 2.8.a, is determined by modifying the governing homogenous equation (2.9) of flexural vibrations

$$D_j \nabla^4 w + \rho_j h_j \ddot{w} = F_{jp} \delta(x - x_p) \delta(y - y_p) \tag{2.109}$$

where F_{jp} is the magnitude of the applied force on plate j. The force acts in the same direction as the positive displacement.

Multiplying the right-hand side of equation (2.109), as was done for the left-hand side during the derivation of necessary equations in section 2.2, and integrating along y yields

$$\left[\frac{2}{b} \sin(k_n y_p)\right] F_{jp} \delta(x - x_p) \tag{2.110}$$

With the solution of the free vibration available, the response due to any prescribed excitation can be readily found. The effect of this discrete loading is to produce a discontinuity in the out-of-plane shear at the line

of application. Therefore, in order to implement the x dependency of excitation, the plate, on which the concentrated force is applied, can be artificially split into two plates with length x_p and $(L\ x_p)$ as illustrated in Fig. 2.8.b. Now, at distance x_p from the edge of the plate another node has been introduced into the structure, this means that the effect of the point force may be directly taken into account during the assembly procedure of the stiffness matrix via the vector $\mathbf{f}_i$ of equations (2.95) and (2.96).

2.6.1 AVERAGING POINT FORCES.

SEA is generally concerned with "rain-on-the roof" type excitation, this type of loading is known to excite all the modes of the system equally, thus leading to the equipartition of energy between the modes of a component [5]. Even though the dynamic stiffness method of this section can not incorporate rain-on-the roof type of excitation directly, the response to such loading can be simulated in this analysis by exciting the component with point loads over various locations. It is shown [33] that when these point loads are averaged over point load locations a response similar to that of rain-on-the roof excitation may be obtained. Energy transmission between the subsystems is weakly dependent, especially at high frequencies, on the position of point load locations as the multi point excitation has an averaging effect [53].

A resonance occurs whenever the excitation frequency, ω, equals one of the corresponding natural frequencies, unless the location of the point of excitation is such that the corresponding $\sin(n\pi y_p/b)$ also vanishes. Therefore, bearing in mind that from some of the point load locations there will not be any contribution to the excitation, the number of excitation points needs to be carefully decided within the capacity of the computer.

Consequently, when the total energies are averaged over all the point load locations it would give a fair representation of the mean energy over each plate at a discrete frequency. By repeating the above calculations over a number of frequencies within a frequency range, a quantity which is directly comparable with SEA may be attained. Hence, com-

parison of this quantity with standard SEA computations for energy ratio will check the appropriateness of the SEA model and predictions.

It is, once again, emphasised that previously given energy expressions correspond to *n*th lateral shape function. The complete response is obtained by summing the results over *n*: the way of determining maximum number of *n* is explained in section 5.1.

2.7 EXTENSION TO THE CASES OF A "T" OR CROSS JUNCTION.

With the solution of the two plate junction available, the solutions to "T" and cross junction problems can be obtained in the same manner as in section 2.2. When considering the case of "T" or cross junction (see Fig. 2.9.a and 2.9.b) all one needs to do is transfer all the plate elements to the same common global co-ordinates, then add the dynamic stiffness matrices together at this particular junction.

Assuming the plates are transferred to the same axis system equation (2.95), which accomplishes the assembly of stiffness matrices, these may be rewritten as follows:

$$\mathbf{F}_l = \left(\mathbf{K}_l^1 + \mathbf{K}_l^2 + \mathbf{K}_l^3\right)\mathbf{d}_l \tag{2.111}$$

$$\mathbf{F}_l = \left(\mathbf{K}_l^1 + \mathbf{K}_l^2 + \mathbf{K}_l^3 + \mathbf{K}_l^4\right)\mathbf{d}_l \tag{2.112}$$

for "T" and cross junction respectively.

As a matter of fact, at a junction there could be as many plates as necessary, since this analysis considers elements of a built up structure individually. However, in the later sections, for practical purposes, a maximum of four plates at a junction will be analysed.

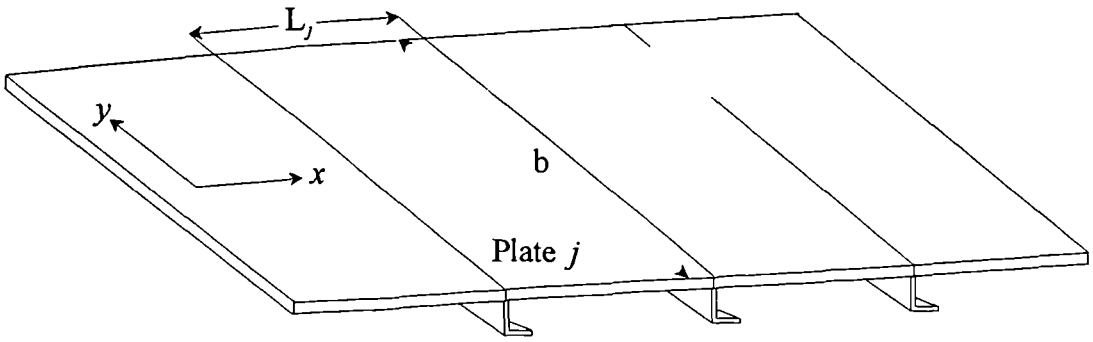

Fig. 2.1 A typical row of flat plates.

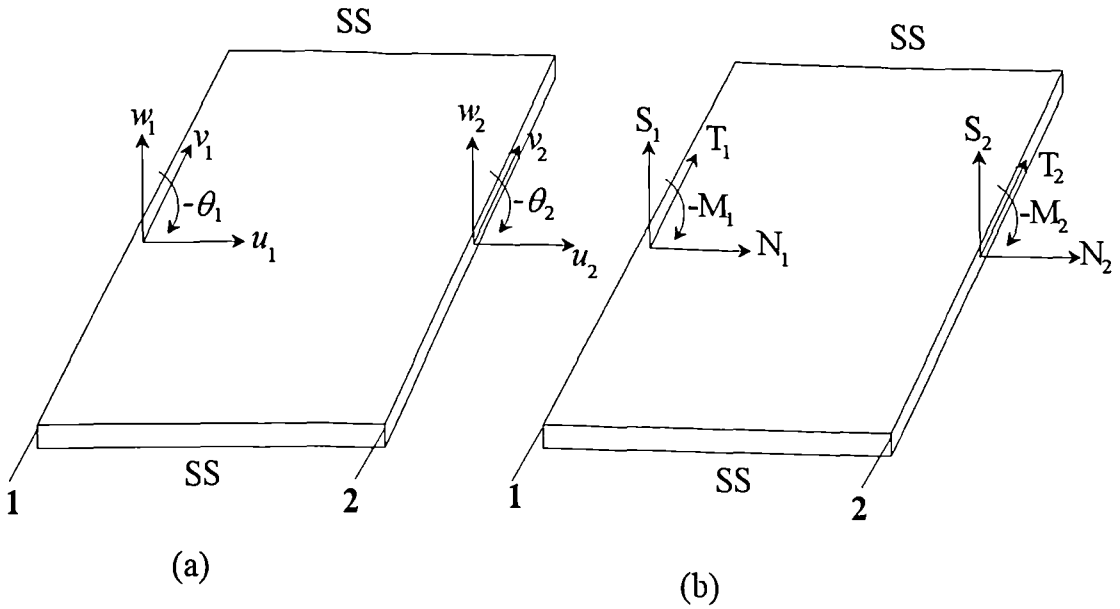

Fig. 2.2 Free body diagram of a plate;
(a) Deflections and rotations,
(b) Forces and moments.

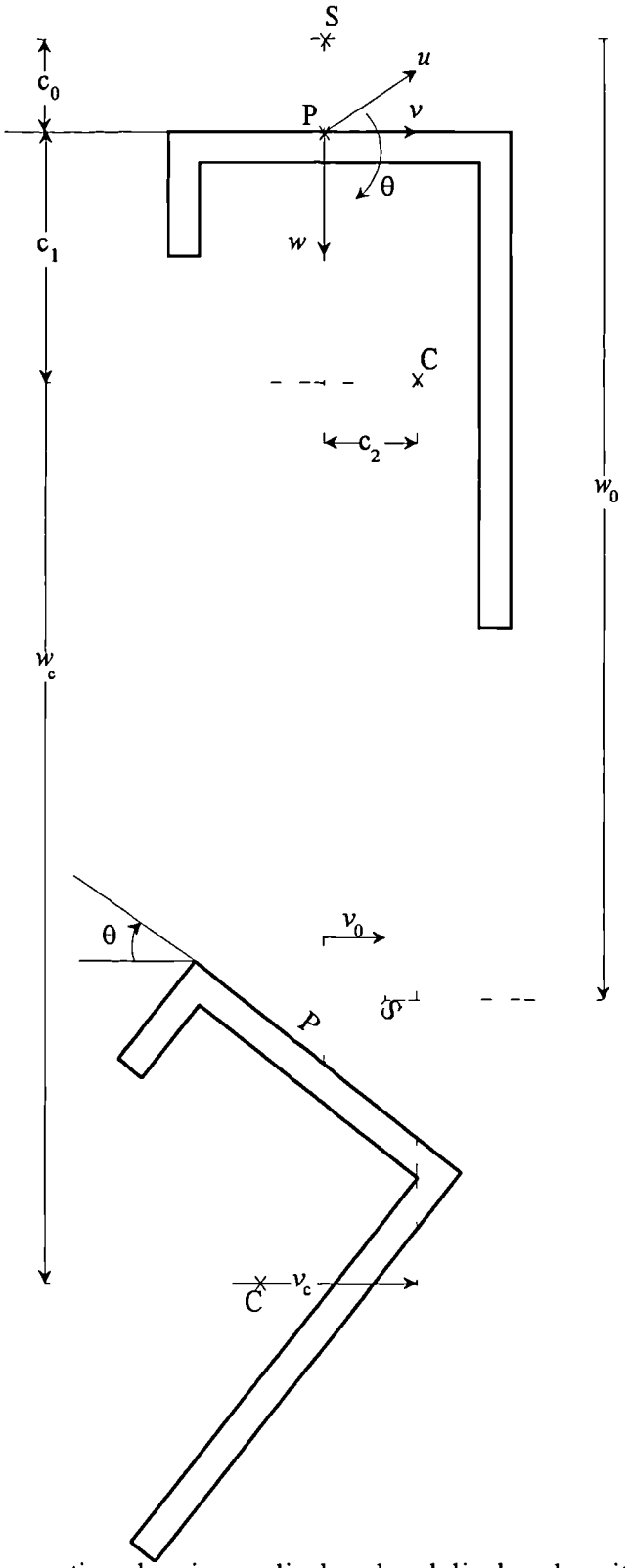

Fig. 2.3 Stringer cross section showing undisplaced and displaced positions

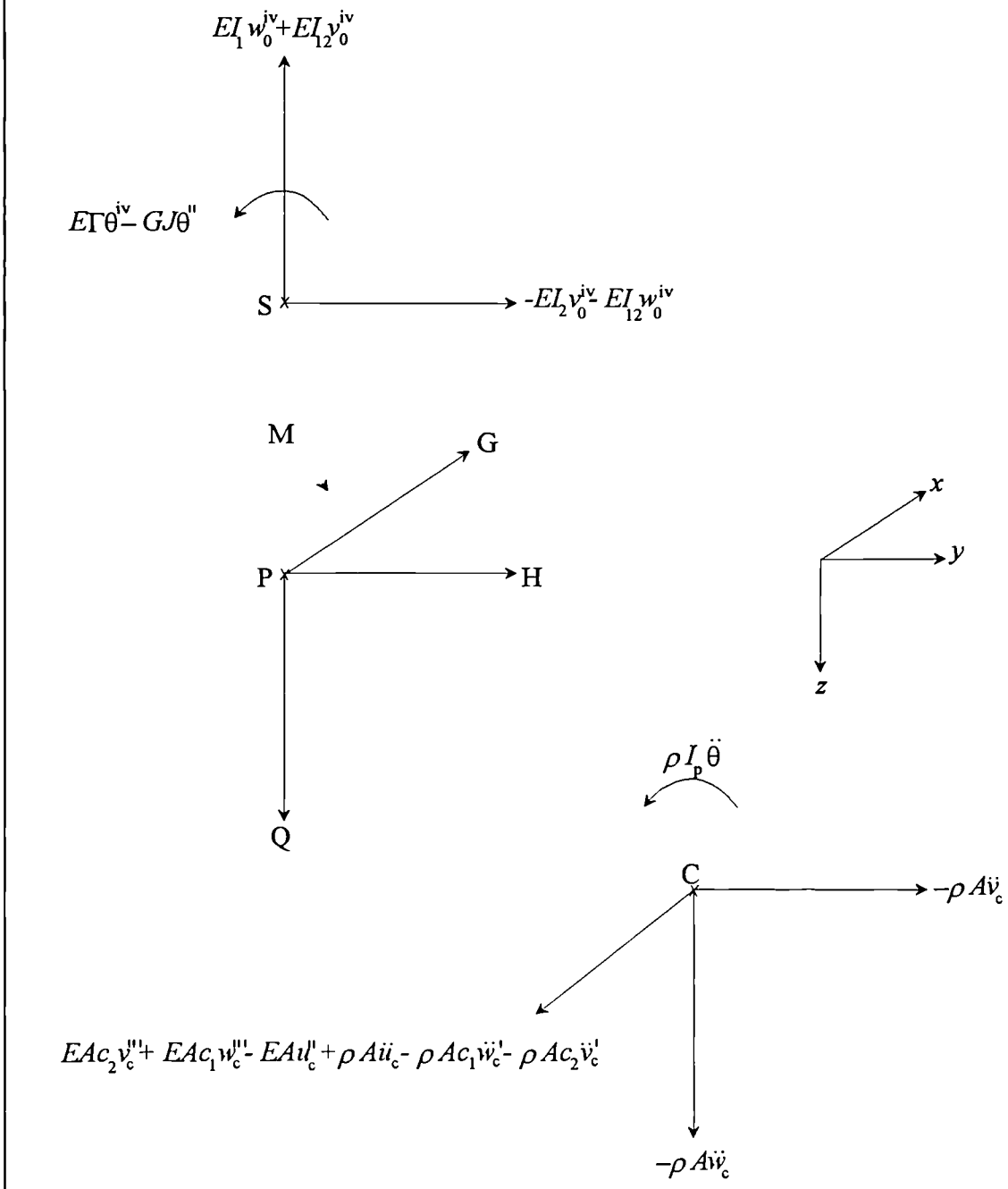

Fig. 2.4 Free body diagram of a stiffener.

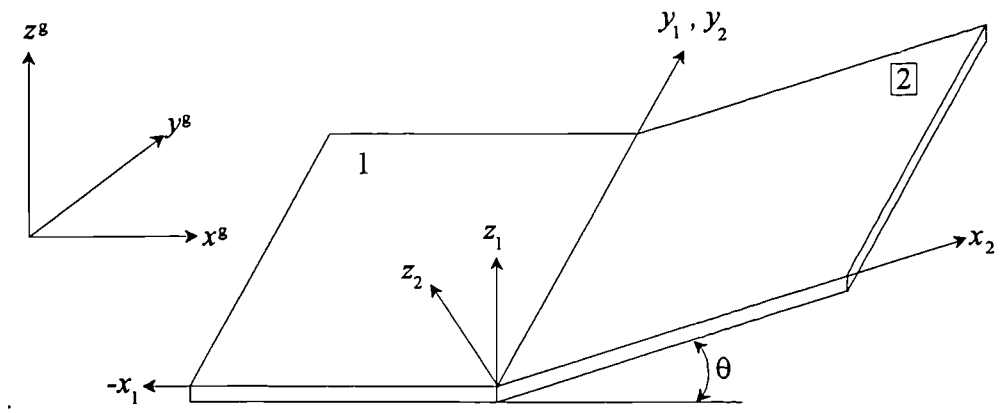

a)

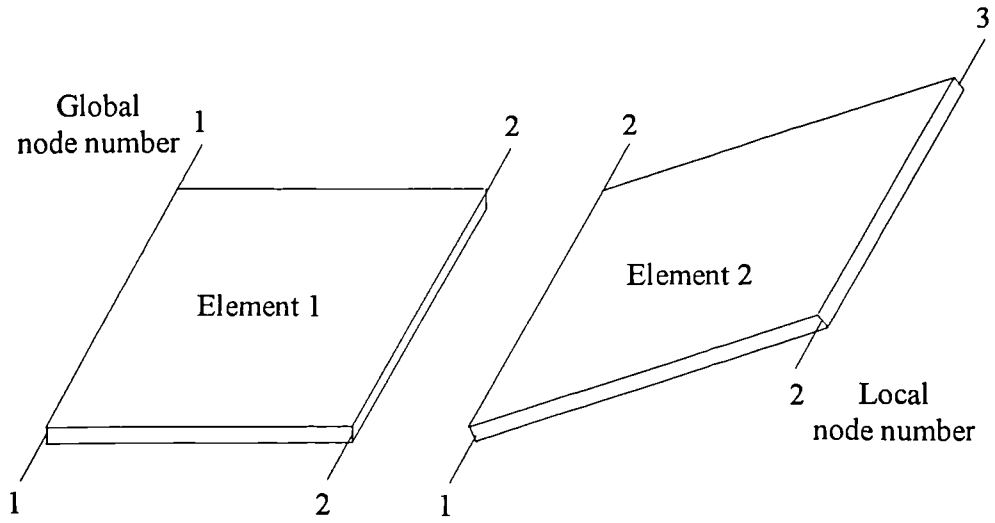

b)

Fig. 2.5
a) Local and global axes system
b) Local and global node numbers

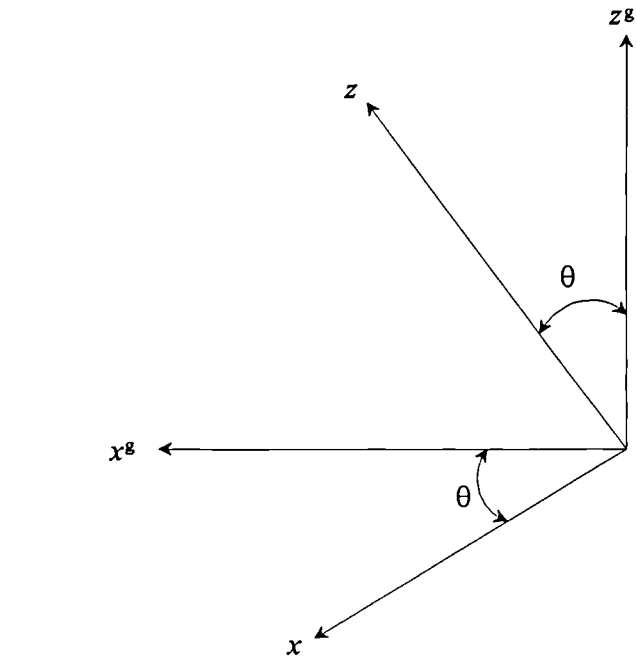

a)

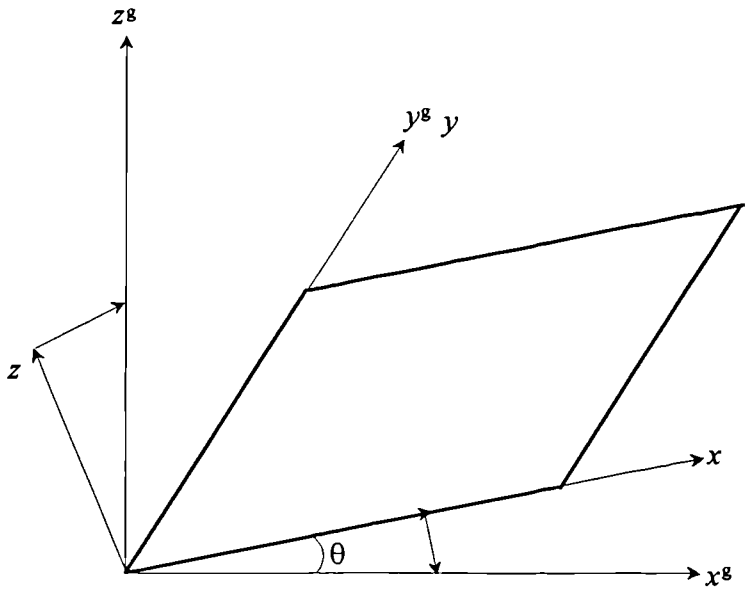

b)

Fig. 2.6

a) View of global and local axes as seen from $+y$ direction

b) Translation from local to global co-ordinates.

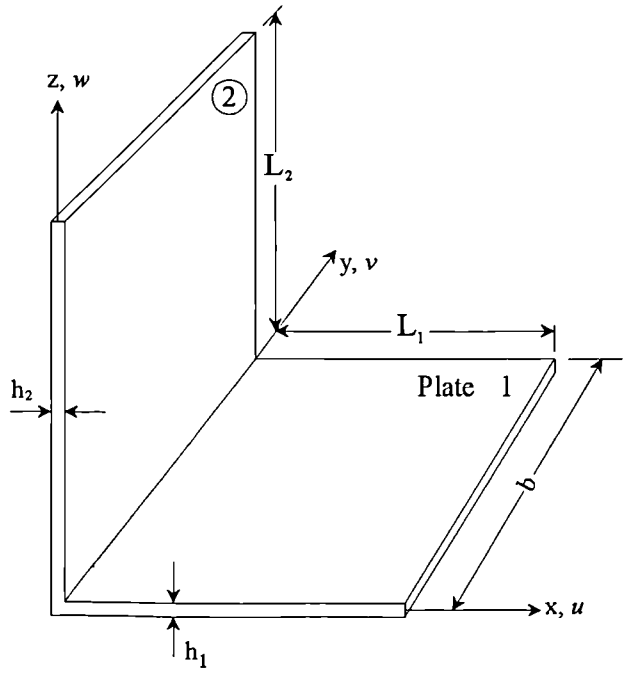

a)

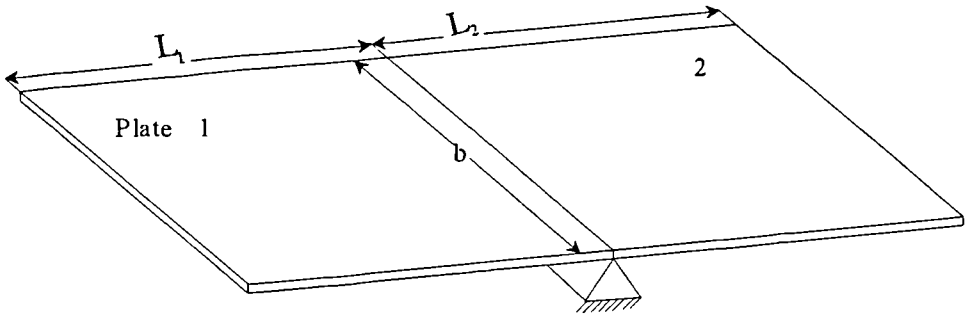

b)

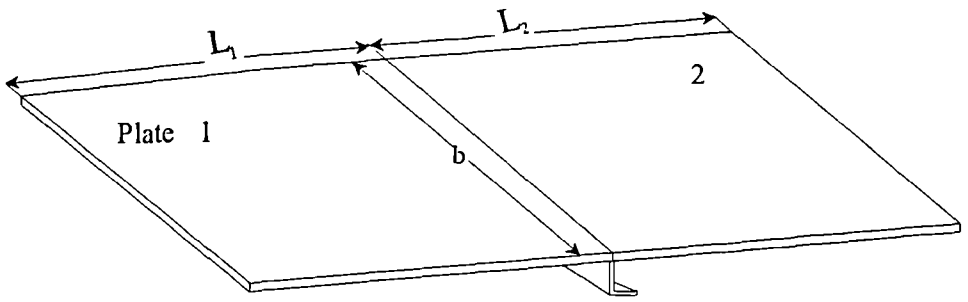

c)

Fig. 2.7 Junction Types

a) Two rectangular plates joined at right angles,
b) Two simply supported flat plates,
c) Two plates connected over a beam.

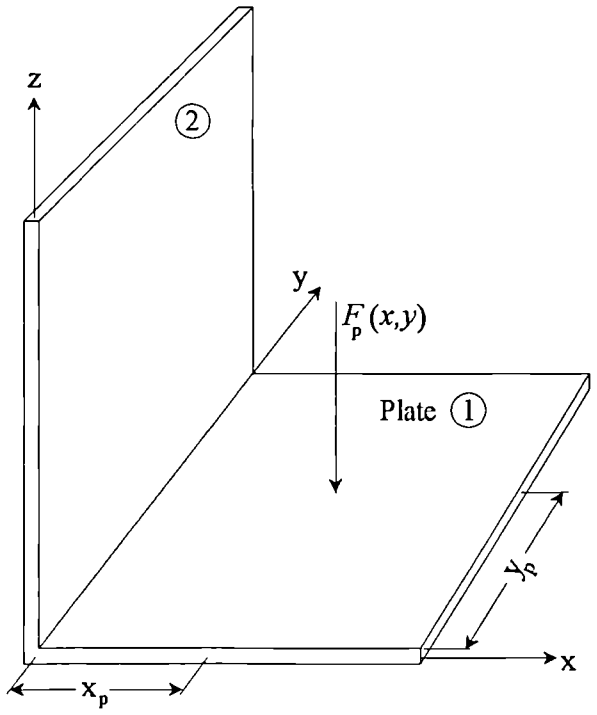

a)

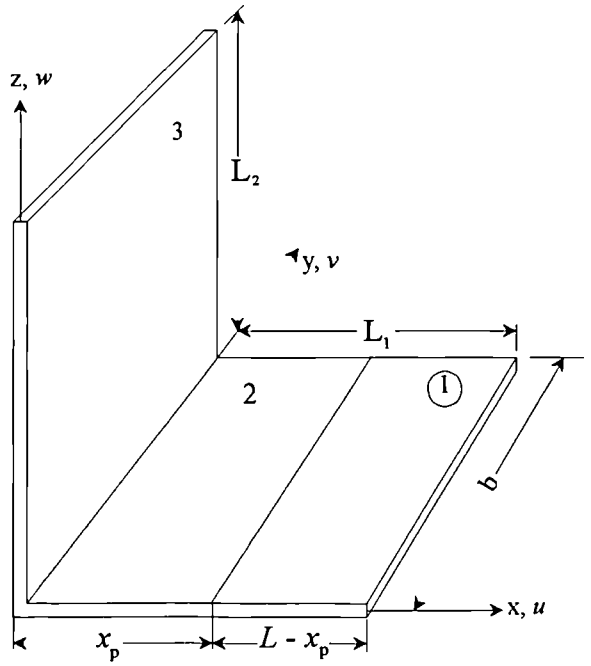

b)

Fig. 2.8 a) Concentrated force acting on the plate
b) Equivalent three plate structure.

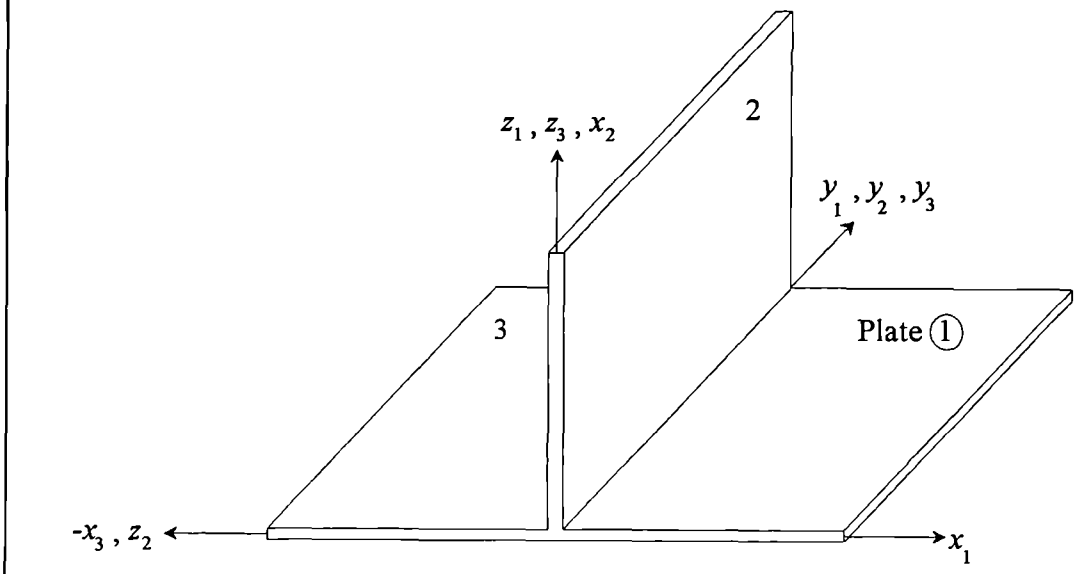

a)

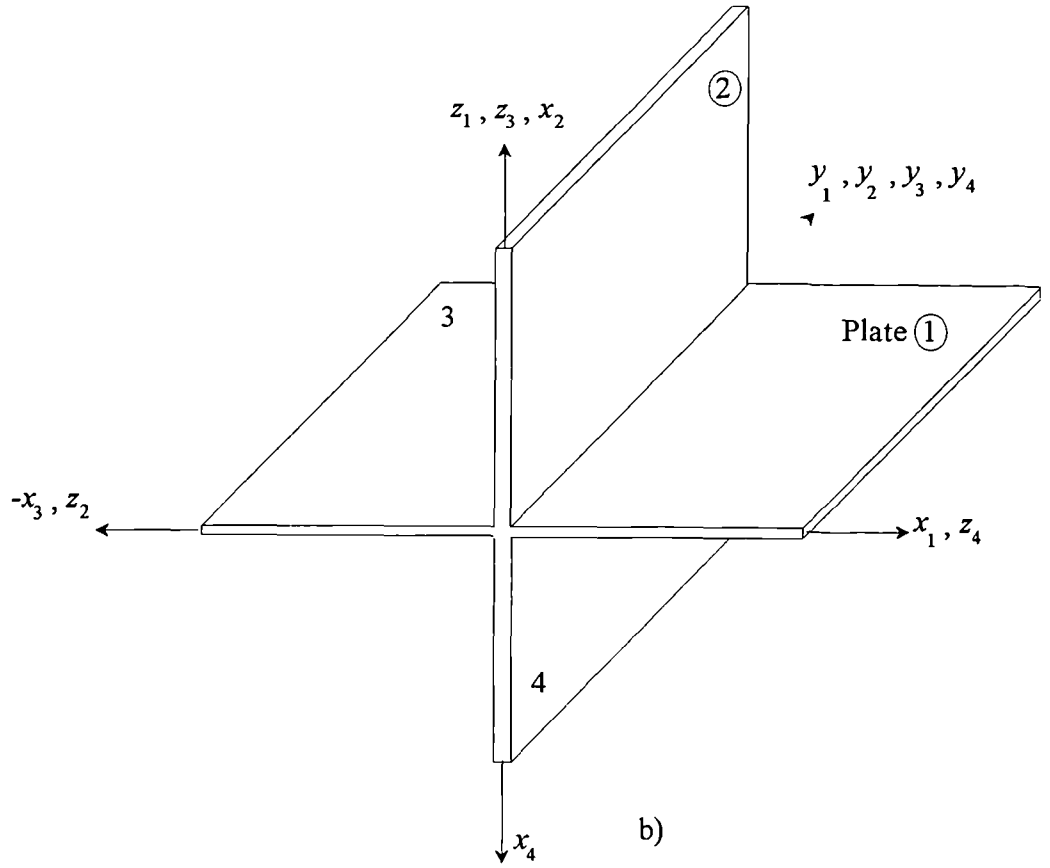

b)

Fig. 2.9 Schematic of a
a) T junction
b) Cross junction

3 STATISTICAL ENERGY ANALYSIS.

In this chapter the aim is to describe briefly, rather than to derive, the relationships on which statistical energy analysis is based; for full derivations and details the reader is referred to the books by Lyon [55] and Cremer *et al.* [28] and the articles by Fahy [56], and Hodges and Woodhouse [5]. The present summary is provided for two reasons:

1. Results obtained by using the dynamic stiffness method of chapter two will be used as a bench-mark against which SEA will be assessed for a range of plate structures.

2. Wave Intensity Analysis (WIA), which is described in chapter four, is an extended form of SEA. It was therefore felt necessary to review the basics of SEA as the fundamental groundwork for WIA.

3.1 METHOD OF APPROACH.

Statistical Energy Analysis (SEA), which is one of the most commonly used approaches in the high frequency vibration analysis of complex structures, is described by its originator [55] as follows
"***Statistical*** emphasises that the systems being studied are presumed to be drawn from statistical populations having known distributions of their dynamical parameters. ***Energy*** denotes the primary variable of interest. Other dynamical variables are found from the energy of vibration. The term ***Analysis*** is used to emphasise that SEA is an approach to problems rather than a particular technique."

The method is generally applied to situations where either an exact solution is quite cumbersome or impossible or at an early design stage where the details of the structure are not known clearly. Because of the lack of detailed knowledge of the structural properties (physical or geometric), SEA tries to describe the average dynamics of the system through the ensemble of the possible systems, having random parameters, excited over broad frequency bands.

The philosophy behind the SEA approach to the vibration analysis of a structure can be briefly outlined as follows:

(i). The analysis starts with the identification of a number of "subsystems" into which the system (structure) is divided.

(ii). The subsystems can be not only finite linear elastic structural components, but also wave types within a component, as in the case of flexural, longitudinal, and shear waves of a plate.

(iii). SEA uses vibrational energy to describe the state of a system, and thus the "unknown" in each subsystem is the energy level of that particular subsystem. Other response variables, such as displacement, stress, and acceleration may be estimated from the energy. The method assumes that the response of the system is mainly dominated by resonant modes, and thus the time averaged potential and kinetic energies are equal.

(iv). The energy dissipated by a subsystem is characterised by the dissipative loss factor (see equation 3.3), and that transferred to the connected subsystems by the coupling loss factor as described in section 3.2.1.

(v). SEA aims to derive a set of linear equations for subsystem energy levels by considering energy flow. The use of energy variables allows the use of simple power balance equations to describe the interaction between coupled subsystems.

The linear equations can be derived by "modal" or "wave" methods, which can be generally expected to lead to the same results [5], as discussed in the following sections.

3.1.1 MODAL APPROACH.

After dividing a complex system into several subsystems, each subsystem is described as a set of modes or "oscillators", and energy flow

relationships are established between the subsystems by considering modal coupling. The energy flow from one subsystem to another can be expected to be maximum when the uncoupled natural frequencies of the modes in the subsystems are near to each other.

If it is assumed that each mode in a subsystem has the same energy [56], (this assumption is known as the equipartition of modal energy hypothesis in SEA), and that the power exchange between two modes in different subsystems is proportional to their energy difference and is not affected by the presence of other modes, then the energy flow between two subsystems may be found by adding the power between all modes. This type of analysis is actually an extension of the analysis of two coupled simple oscillators in which energy flow is modelled akin to that of heat flow between coupled conductors [5]. Thus, the study of two coupled oscillators may be considered as the fundamental element in the modal approach of SEA equations [23].

The main advantage of the modal approach is that in principle it enables one to formulate systems possessing any kind of arbitrary complexity and dimensionality [57].

3.1.2 WAVE APPROACH.

This approach is based on the consideration of two continuous subsystems, rather than the two coupled oscillators of modal analysis [55,58].

In this approach the power exchange is considered to be due to the transmission of waves incident upon a subsystem boundary. The energy flow between the subsystems is modelled by a wave transmission process which uses the transmission coefficients to calculate the coupling loss factors, as described in section 3.3.

Central to this procedure is the assumption that the wave field is "*diffuse*", which means that the wave intensity per unit angle of incidence is constant for all incidence angles [49]. This is the analogy of the "equipartition" assumption of the modal approach.

3.2 FUNDAMENTAL SEA EQUATIONS.

The statistical energy analysis of a system starts with writing the power balance equation of any arbitrary subsystem *j*, regardless of which one of the aforementioned approaches is used. Considering some kind of external source that delivers power into subsystem *j*, this power input is either dissipated in the subsystem or transferred to other coupled subsystems. Conservation of energy implies that the sum of dissipated power and transferred power should be equal to the input power to the subsystem. In mathematical terms this can be expressed as

$$\Pi_j^{in} = \Pi_j^{diss} + \sum_{i \neq j}^{k} \Pi_{ji}^{coup} \tag{3.1}$$

where Π^{in} and Π^{diss} are the input and dissipated powers, and Π^{coup} is the energy flowing from subsystem *j* to all other subsystems to which subsystem *j* is coupled. The main concern of SEA is with the temporal averages of the energy flow, and hence by averaging all energy flows over time, equation (3.1) may be rewritten as

$$\left\langle \Pi_j^{in} \right\rangle = \left\langle \Pi_j^{diss} \right\rangle + \sum_{i \neq j}^{k} \left\langle \Pi_{ji}^{coup} \right\rangle \tag{3.2}$$

where the angle brackets represent time averages. The dissipated power in subsystem *j* may be written as

$$\left\langle \Pi_j^{diss} \right\rangle = \omega \eta_j \left\langle E_j \right\rangle \tag{3.3}$$

where the constant η is the average internal loss factor, and $\langle E_j \rangle$ is the temporal average of the total stored energy, which is equivalent to twice the mean kinetic energy.

Assuming that the input power in the subsystem is known or can be estimated, the unknowns in equation (3.2) are the coupling powers and the averaged response energies. SEA aims to write the average coupling power from subsystem *j* to *i* in terms of the energy variables E_j, so that

equation (3.2) becomes a set of linear equations in these variables [55]. The way of doing this constitutes the topic of the next section.

3.2.1 TWO COUPLED OSCILLATORS

Fig. 3.1.a depicts the most general system of two linearly coupled oscillators [58], in which inertia, gyrostatic, and stiffness coupling are all included. It is assumed that the coupling through the spring of modulus k_c is light and the forces $f_1(t)$ and $f_2(t)$ are weakly stationary, random processes. Fig. 3.1.b represents the equivalent SEA model of the oscillator set schematically. Using equation (3.3) and introducing a *coupling loss factor*, η_{ji}, it can be shown [55] that the power balance equation between the oscillator set may be expressed as

$$\langle \Pi_1^{in} \rangle = \eta_1 \omega \langle E_1 \rangle + \omega \eta_{12} \left(\langle E_1 \rangle - \langle E_2 \rangle \right) \tag{3.4}$$

$$\langle \Pi_2^{in} \rangle = \eta_2 \omega \langle E_2 \rangle + \omega \eta_{21} \left(\langle E_2 \rangle - \langle E_1 \rangle \right) \tag{3.5}$$

where E_1 and E_2 are the total energies of the oscillators 1 and 2 respectively, and the coupling loss factor, η_{ji}, is a parameter which relates the transmission of energy from one oscillator to the other. These results have been shown to be valid [58] for any arbitrary coupling strength, provided that the oscillator energies are suitably defined.

Equation (3.4) and (3.5) constitute the basis of the SEA approach, which states that energy flow is proportional to the difference in the modal energy levels of two coupled subsystems. This is similar to heat flow in thermodynamics, the modal energies of the subsystems being analogous to temperature [55].

3.2.2. MULTI MODAL SUBSYSTEMS.

Having obtained the two oscillator result, at the second stage SEA tries to extend these results to the case of two coupled subsystems which each contain many modes or oscillators; unfortunately the foregoing results are no longer valid for the power exchange between any two oscillators

[58]. However, it has been shown that the results hold provided that the coupling of one subsystem to all the oscillators of the second subsystem is *weak* [23] and that the external generalised forces are statistically independent [59].

If the energy produced by the excitation source in the directly excited subsystem is greater than the energy transferred to the indirectly driven subsystem, per unit time, then the subsystems are said to be "*weakly coupled*" [59], although this is not the only definition of weak coupling. A more comprehensive definition and discussion of weak coupling is given by Langley [34]. If the coupling is strong, the power flow relationships need to be modified, leading to a much more complex form than those of weak coupling relationships [31].

The requirement for statistically independent generalised forces arises from the need for the modal responses to be uncorrelated. To this end, it is normally assumed that the excitation has uniform power spectral density, and that the spatial cross correlation is zero [5]. Such an excitation is termed as "*rain-on-the roof*". This type of excitation also excites all modes equally, leading to the equipartition of modal energy in a uniform structure, as well as satisfying the modal incoherence assumption because of the orthogonality of the modes [5]. Even though most of the studies on SEA are generally concerned with rain-on-the roof type of excitation, it has been shown [33] that the usual SEA energy flow and energy expressions may be derived if the system is excited by random point loads, provided that energy flow and energy variables are averaged over the range of point load locations.

From a wave point of view, the modal incoherence assumption is analogous to requiring the system to be reverberant. This means that a wave that is incident on the boundary reflects many times before it eventually dies out after building up a reverberant field in which distribution of energy is uniform [5]. One criterion as to whether the system is reverberant is that if the reverberant stored energy is greater than the direct stored energy, the system is said to be reverberant [60]. A more direct method of measuring the reverberance is discussed in section 5.5.

If the necessary conditions are met then the power balance equations for two multi-modal subsystems are found to be [56]:

$$\left\langle \Pi_1^{in} \right\rangle = \eta_1 \omega \langle E_1 \rangle + \omega n_1 \eta_{12} \left(\frac{\langle E_1 \rangle}{n_1} - \frac{\langle E_2 \rangle}{n_2} \right) \tag{3.6}$$

$$\left\langle \Pi_2^{in} \right\rangle = \eta_2 \omega \langle E_2 \rangle + \omega n_2 \eta_{21} \left(\frac{\langle E_2 \rangle}{n_2} - \frac{\langle E_1 \rangle}{n_1} \right) \tag{3.7}$$

where n_1 and n_2 are modal densities (the average number of natural frequencies of the structure per unit of frequency in a specified excitation band [28]) of subsystem 1 and 2 respectively, and ω is the central frequency of the frequency band. This band is assumed to be wide enough to contain several resonant frequencies to get a reliable estimate of the energy levels within the subsystems. $<E_1>$ and $<E_2>$ represent the total energies of the two subsystems; equations (3.6) and (3.7) thus state that the energy flow is proportional to the difference in the average modal energy.

The choice of the frequency bandwidth plays an important role in SEA, since it is assumed that the response of each subsystem is controlled by the response of modes whose resonance frequencies lie within the particular frequency band, $\Delta\omega$, and that contribution of non-resonant modes is negligible [56]. However in some cases the contribution of non-resonant modes needs to be considered [43]. It has been shown that to represent a subsystem accurately, the width of frequency band should be enough to ensure a minimum of five to seven resonant frequencies within the frequency band [31,41], and yet the ratio of bandwidth to the centre frequency should be substantially less than unity [61], i.e. $\Delta\omega / \omega << 1$.

Finally, equations (3.6) and (3.7) may be conveniently written in matrix form

$$\begin{bmatrix} \langle \Pi_1^{in} \rangle \\ \langle \Pi_2^{in} \rangle \end{bmatrix} = \omega \begin{bmatrix} (\eta_1 + \eta_{12})n_1 & -\eta_{12}n_1 \\ -\eta_{21}n_2 & (\eta_2 + \eta_{21})n_2 \end{bmatrix} \begin{bmatrix} \langle E_1 \rangle / n_1 \\ \langle E_2 \rangle / n_2 \end{bmatrix} \tag{3.8}$$

The coupling loss factors corresponding to the power flow in each direction are related by the reciprocity principle, which may be stated as [32]

$$n_1\eta_{12} = n_2\eta_{21} \tag{3.9}$$

Thus the square matrix which appears in equation (3.8) is symmetric.

Expression (3.8) relates to only two multi modal subsystems, although it can be easily extended for many multi-modal subsystems. For such a system the power flow expressions can be written in matrix form as

$$\langle \overline{\Pi}^{in} \rangle = \mathbf{A} \langle \overline{\mathbf{E}} \rangle \tag{3.10}$$

where $\langle \overline{E}_j \rangle = \langle E_j \rangle / n_j$ and the entries of matrix A may be expressed as

$$A_{ji} = -\omega\eta_{ji}n_j, \qquad A_{jj} = \omega\left(\eta_j + \sum_{i \neq j}^{k} \eta_{ji}\right)n_j, \qquad j \neq i \tag{3.11),(3.12}$$

where k is the total number of subsystems.

3.3 SEA PARAMETERS RELATED TO PLATES.

In the foregoing section a parameter uniquely associated with SEA known as the coupling loss factor was defined. For plate substructures this parameter may be expressed as [28]

$$\eta_{ji} = \frac{c_g L}{\pi\omega A_j} < \tau_{ji} > \tag{3.13}$$

where c_g is the group velocity of the incident wave, L is the junction length, A_j is the area of the source plate, and $< \tau_{ji} >$ is the diffuse wave field transmission coefficient.

The angular dependent transmission coefficient $\tau(\theta)$ can be derived from a wave analysis of corresponding semi-infinite plates [56]. It is defined as the ratio of the transmitted wave intensity to the incident wave intensity for any of the wave types generated in the source or receiver plate [49]. If this transmission coefficient is known, by assuming that the waves are incident to the junction with equal probability from all the angles between $-\pi/2$ and $\pi/2$ then by integrating $\tau(\theta)$ multiplied by an appropriate weighting factor, over all angles of incidence in the range $-\pi/2$ to $\pi/2$, the diffuse wave field transmission coefficient may be obtained: that is to say;

$$< \tau_{ji} >= \frac{1}{2} \int_{\pi 2}^{\pi/2} \tau(\theta) \cos\theta \, \mathrm{d}\theta \tag{3.14}$$

In the present work the wave transmission coefficients have been found by using the analysis of reference [29].

The modal density, n_j, which appears in equation (3.11), may be found by considering the natural frequencies which lie within the quarter circle of the modal lattice (see Fig. 3.2) that corresponds to a simply supported rectangular plate of dimensions L_1 and L_2 [28]. As can be seen from Fig. 3.2, k_c may be written as

$$k_c^2 = \left(\frac{m_1 \pi}{L_1} \right)^2 + \left(\frac{m_2 \pi}{L_2} \right)^2 \tag{3.15}$$

As the portion of area that corresponds to each mode of the plate is $\left(\pi^2/L_1 L_2\right)$, the number of modes below the wave number k_c=k becomes

$$N(k) = \frac{\pi k^2}{4} \frac{L_1 L_2}{\pi^2} \tag{3.16}$$

Then the modal density as a function of wave number may be expressed as

$$n_j(k) = \frac{\mathrm{d}N(k)}{\mathrm{d}k} = \frac{kL_1L_2}{2\pi} \tag{3.17}$$

The modal density as a function of frequency may be written as

$$n_j(\omega) = \frac{kL_1L_2}{2\pi}\frac{\mathrm{d}k}{\mathrm{d}\omega} \tag{3.18}$$

Equation (3.18) can be recast into the form

$$n_j(\omega) = \frac{L_1L_2\omega}{2\pi c_j c_{gj}} \tag{3.19}$$

where c_j and c_{gj} are phase velocity and group velocity of the wave respectively and related to wave number k and frequency ω in the form

$$c_j = \frac{\omega}{k_j} \qquad \text{and} \qquad c_{gj} = \frac{\mathrm{d}\omega}{\mathrm{d}k_j} \tag{3.20}$$

The modal density of bending waves can be shown to be [28]:

$$n_{\mathrm{B}} = \left(\frac{12\rho(1-\nu^2)}{E}\right)^{1/2}\frac{A}{2h} \tag{3.21}$$

where ρ is the density of the plate, E is modulus of elasticity, ν is the Poisson ratio and A and h represent area and thickness respectively. The longitudinal, n_{L}, and shear, n_{S}, modal densities can be similarly expressed in the forms

$$n_{\mathrm{L}} - \frac{\rho(1-\nu^2)A}{E}f, \text{ and} \qquad n_{\mathrm{S}} = \frac{2\rho(1+\nu)A}{E}f \tag{3.22),(3.23}$$

where f is the frequency in Hertz. It should be noted that the units of modal densities in equations (3.21)–(3.23) are modes/Hz.

Finally, for most of the theoretical analysis it is common practice to take the loss factor, η_j, between 0.01 and 0.02 [28].

The foregoing analysis is applied to a range of plate structures in chapter 5.

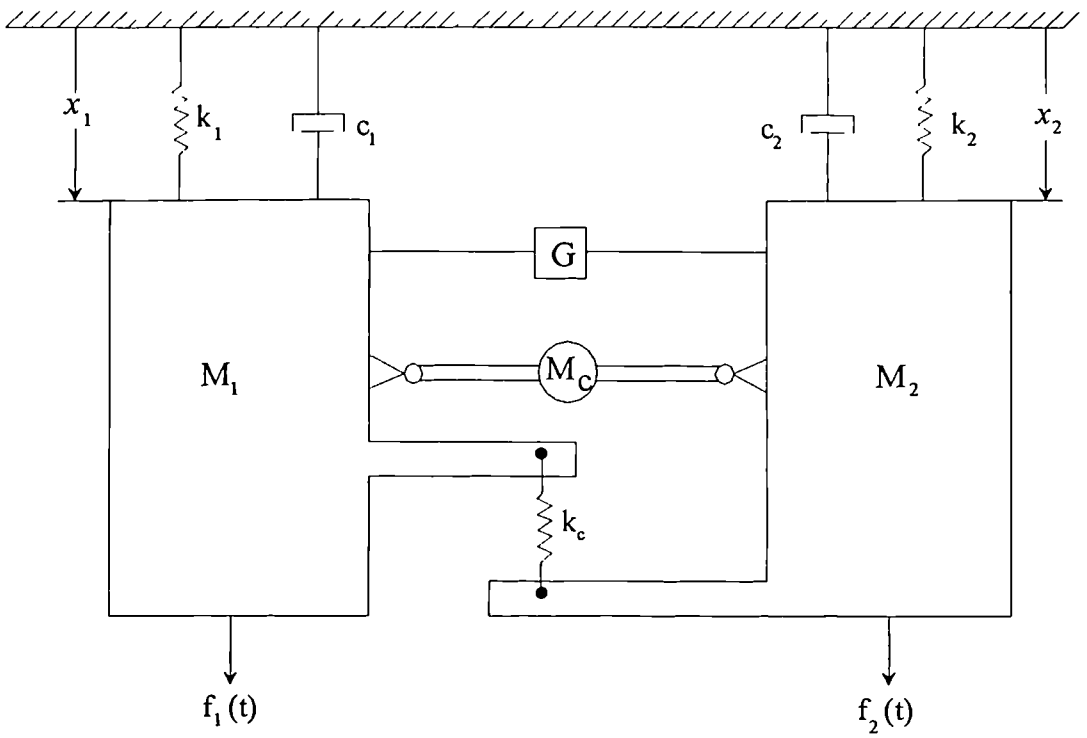

Fig. 3.1.a Schematic of two coupled oscillators

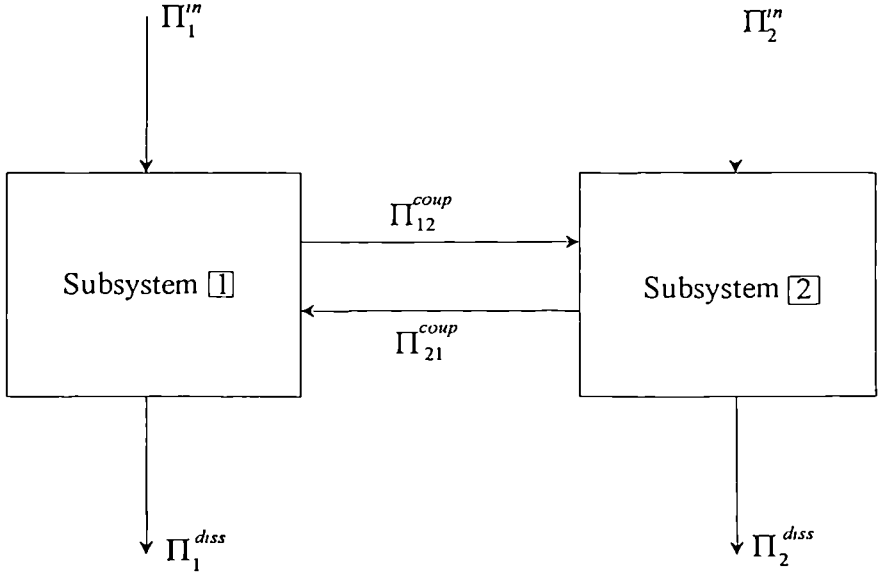

Fig. 3.1.b SEA model of two oscillators

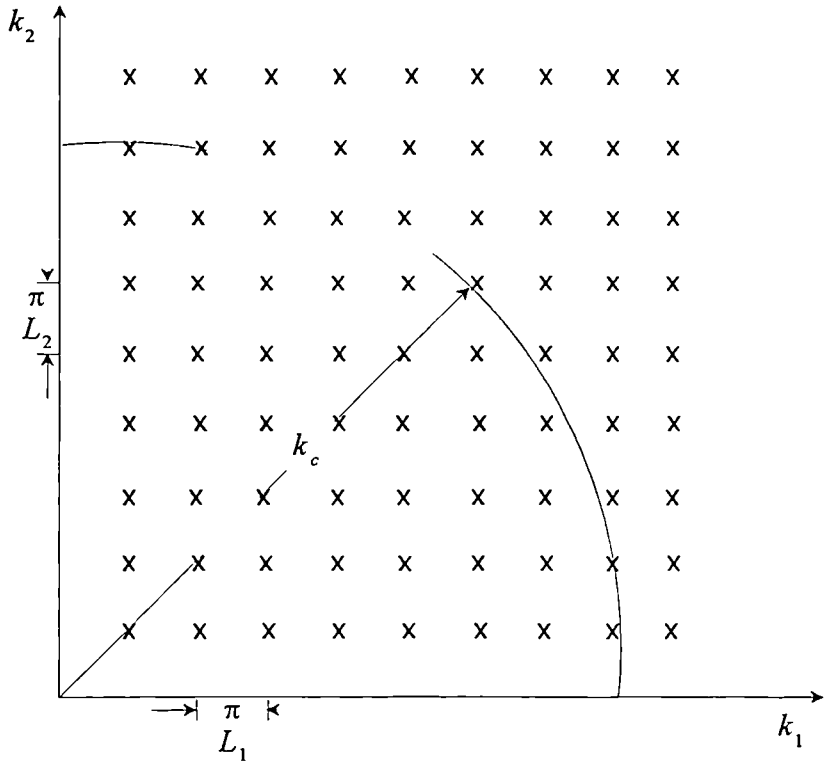

Fig. 3.2 Modal Lattice for a Rectangular Plate

4. WAVE INTENSITY ANALYSIS.

4.1 SYSTEM MODELLING FOR WIA.

As mentioned in section 1.3.2 WIA is an extended form of SEA. Therefore the method follows almost the same procedure as SEA with regard to system modelling. In this respect, the initial step in the application of WIA to any system is the determination of subsystems.

In SEA the subsystems, as explained in section 3.1, can be not only the structural components, but also different wave types in a component. Unless each structural component bears just one wave type, subsystem *j* will not refer to wave type *j* in component *j*. Therefore to avoid confusion between the structural components and the various wave types, here only the different wave types in a component will be referred to as subsystems, in which case a structure composed of two plates will support six subsystems. The first three subsystems will belong to the first component, and the latter three to the second component, corresponding to out-of-plane bending, in-plane longitudinal and in-plane shear wave types.

The main difference between the SEA and WIA system descriptions is in the construction and size of the energy coefficient matrix, which occurs in the linear equations for the subsystem energy levels. In SEA, according to the diffuse wave field assumption, the energy is taken to be constant per unit incidence angle, whereas in WIA the angular dependence of the wave energy in each subsystem is represented in terms of shape functions the number of which vary depending on the accuracy required. A particular Fourier component of the subsystem energy will be referred to here as a "subset" to avoid confusion with the term subsystem.

In WIA the unknowns are taken to be the subsets for each wave subsystem. Considering the plate example described above: if the directional dependence of each wave type is represented by, say, two shape functions, then in the system there are; 2 components, 6 subsystems and a

total of 12 subsets. Thus the size of the WIA energy matrix for this particular case is 12x12, whereas the SEA matrix is 6x6.

In general, considering all three wave types that a plate may carry, if there are Y components in a structure and the same number of shape functions, Z, for each wave type, then the dimension of energy matrix would be, $(3YZ)$x$(3YZ)$. However, it should be noted that each subsystem may not necessarily be expanded by the same number of shape functions.

The system modelling technique of WIA will be explained in some detail in section 4.3 by an illustrative example. In the following section the energy flow equations, which are necessary to derive a set of linear equations, will be obtained for a particular wave type.

4.2 ENERGY FLOW EQUATIONS.

If it is assumed that the wave field is not diffuse, but rather the intensity is dependent on the wave incidence angle, θ, then equation (3.1) which expresses the conservation of energy principle in a subsystem will take a slightly different form. This new form of the energy flow equilibrium expression for heading θ of subsystem j may be written as

$$\Pi_j^{in}(\theta,\omega) = \Pi_j^{diss}(\theta,\omega) + \Pi_j^{cout}(\theta,\omega) - \Pi_j^{cin}(\theta,\omega) \tag{4.1}$$

where Π_j^{in} represents the power input to wave heading θ of wave type j via the external forcing (this can be estimated by assuming that the plate is infinite in which case it takes a form independent of heading angle for an isotropic plate), Π_j^{cin} is the power input due to coupling with other wave types at the plate boundaries, Π_j^{cout} is the output energy flow from subsystem j to other wave types at the boundary, and Π_j^{diss} represents the power dissipated, which can be expressed as [28]

$$\Pi_j^{diss}(\theta,\omega) = \omega\eta_j E_j(\theta,\omega) = \omega\eta_j A_j e_j(\theta,\omega) \tag{4.2}$$

Here η_j is the loss factor, E_j represents the mean stored total energy, A_j is the area of substructure to which subsystem j belongs, and $e_j(\theta,\omega)$ is the energy density of wave type j at a specific frequency ω, propagating in the direction of incidence angle θ. The intensity, or energy flow vector, related to this wave may be expressed as

$$\mathbf{I}_j(\theta,\omega) = e_j(\theta,\omega)c_{gj}(\theta,\omega)\mathbf{r}(\theta) \tag{4.3}$$

where $\mathbf{r}$ is a unit vector in the θ direction, and c_{gj} is the group velocity of wave type j, as defined in section 3.3

Then the power output at a plate boundary may be expressed in terms of intensity in the form [63]

$$\Pi_j^{cout}(\theta,\omega) = L\mathbf{I}_j(\theta,\omega).\mathbf{s} \tag{4.4}$$

where L is the length of the boundary and $\mathbf{s}$ is the outward pointing unit normal. Substituting $\mathbf{I}_j$ from equation (4.3) equation (4.4) may be written in the form

$$\Pi_j^{cout}(\theta,\omega) = Le_j(\theta,\omega)c_{gj}(\theta,\omega)\mathbf{r}(\theta).\mathbf{s} \tag{4.5.a}$$

or

$$\Pi_j^{cout}(\theta,\omega) = Le_j(\theta,\omega)c_{gj}(\theta,\omega)\cos\alpha \tag{4.5.b}$$

where α is the angle between unit vectors $\mathbf{r}$ and $\mathbf{s}$ as illustrated in Fig. 4.1, and may be termed as the total incidence angle. Power output takes place when the scalar product in equation (4.5.a) is positive, or rather $\cos\alpha$ of equation (4.5.b) is non-negative. As can be seen in Fig. 4.1, α may be written in terms of the wave heading angle, θ, and the orientation of the boundary, ψ, in the form

$$\alpha = \theta + \frac{\pi}{2} - \psi \tag{4.6}$$

The output boundary can be any of the four boundaries of the plate depending entirely on the wave heading angle θ (see the discussion at the end of this section). To obtain the total power output from wave type j, a summation over all output boundaries needs to be introduced into equation (4.5), which expresses the power output at a single boundary. Hence the total output power takes the form

$$\Pi_j^{cout}(\theta,\omega) = e_j(\theta,\omega)c_{gj}(\theta,\omega)\sum_p L_p \cos\left(\theta+\frac{\pi}{2}-\psi_p\right) \tag{4.7}$$

The modal density which is given by equation (3.19), in the present notation may be written in the form

$$n_j = \frac{\omega A_j}{2\pi c_j c_{gj}} \tag{4.8}$$

Making use of the definition of modal density equation (4.7) may be rewritten as

$$\Pi_j^{cout}(\theta,\omega) = \left(\frac{\omega}{2\pi c_j}\right)\left[\frac{E_j(\theta,\omega)}{n_j}\right]\sum_p L_p \cos\left(\theta+\frac{\pi}{2}-\psi_p\right) \tag{4.9}$$

Finally, the expression for the energy flow transmitted to heading θ of subsystem j needs to be derived. Assuming this power is provided by heading ϕ of subsystem m then an appropriate form of input power is

$$\Pi_j^{in}(\theta,\omega)\,\mathrm{d}\theta = \mathbf{I}_m(\phi,\omega).\mathrm{s}L\,\tau_{mj}(\phi,\mathrm{s})\,\mathrm{d}\phi \tag{4.10}$$

where τ_{mj} is the transmission coefficient from wave type m to j for the boundary, and $\mathrm{d}\theta$ and $\mathrm{d}\phi$ are direction bands.

It should be noted that if a wave encounters a boundary or line support, it will be partially or wholly reflected as well as transmitted depending on the incidence angle. Thus there is a possibility of subsystem j inputting power to itself in which case subsystems m and j are identical and

the energy transmission coefficient is replaced by a reflection coefficient.

Using equation (4.3), equation (4.10) may be rearranged in the form

$$\Pi_j^{cin}(\theta,\omega)\,\mathrm{d}\,\theta = e_m(\phi,\omega)c_{gm}(\phi,\omega)\cos\left(\phi+\frac{\pi}{2}-\psi\right)L\tau_{mj}(\phi+\frac{\pi}{2}-\psi)\,\mathrm{d}\,\phi \quad (4.11)$$

The incidence angles θ and ϕ may be related by using Snell's Law which enables ϕ to be written as a single valued function of θ, and $\mathrm{d}\,\phi$ to be determined in terms of $\mathrm{d}\,\theta$. For incidence angles θ and ϕ the statement of Snell's Law may be made with reference to Fig. 4.2 in which tangential trace wavelengths (the component of wave lengths in y direction) should be equal to each other [28], thus

$$\frac{\sin(\phi+\pi/2-\psi)}{c_m} = \frac{\sin(\theta+\pi\,2-\psi)}{c_j} \quad (4.12)$$

Using equation (4.12), $\mathrm{d}\,\theta$ and $\mathrm{d}\,\phi$ may be eliminated from equation (4.11) giving rise to

$$\Pi_j^{cin}(\theta,\omega) = \left(\frac{\omega}{2\pi c_j}\right)\left[\frac{E_m(\theta,\omega)}{n_m}\right]L\cos\left(\theta+\frac{\pi}{2}-\psi\right)\tau_{mj}\left(\phi+\frac{\pi}{2}-\psi\right) \quad (4.13)$$

As in the case of power output, this expression gives the power input by subsystem m at a single boundary, the total power transferred into the wave type j may be acquired by summing over not only all input boundaries, but also wave types. The latter summation is due to the contribution of wave types that can make an input to the wave type j, thus total power input may be written as

$$\Pi_j^{cin}(\theta,\omega) = \left(\frac{\omega}{2\pi c_j}\right)\sum_q\sum_m\left[\frac{E_m(\phi_{qm},\omega)}{n_m}\right]L_q\cos\left(\theta+\frac{\pi}{2}-\psi_q\right)\tau_{mj}^q\left(\phi_{qm}+\frac{\pi}{2}-\psi_q\right)$$

(4.14)

where the indices q and m represent all the input boundaries and wave types respectively.

At this stage directional dependence of each wave type may be introduced in terms of a set of shape functions into the energy terms, $E_j(\theta,\omega)$ and $E_m(\phi,\omega)$ of previous power flow expressions, leading to

$$E_j(\theta,\omega)=\sum_a E_{ja}(\omega)N_a^j(\theta) \tag{4.15}$$

$$E_m(\phi,\omega)=\sum_c E_{mc}(\omega)N_c^m(\phi) \tag{4.16}$$

Equations (4.15) and (4.16) may represent a Fourier series expansion of wave energy. Then they will take the form

$$E_j(\theta,\omega)=E_{j0}1/2\pi+E_{j1}\cos(\theta)+E_{j2}\cos(2\theta)+\cdots+E_{ja}\cos(a\theta) \tag{4.17}$$

where a represents the number of shape functions in the series, and E_{j0}, E_{j1}, ... are the subsets of the subsystem j. A similar expression may be written for wave type m by substituting j for m.

So far all the unknowns of the general power expression (4.1) have been identified. After application of the following three procedures, a power balance expression, which involves not only wave type j, but also the other wave types via the power input terms, may be obtained. These steps are:-

(i). Substitute equations (4.2), (4.7) and (4.13) together with equations (4.15) and (4.16) into the general power expression (4.1).

(ii). Multiply by shape function $N_d^j(\theta)$ where d=0,1,2,3,...

(iii). Integrate over the range of incidence angle θ.

Then the form of power balance expression of subsystem j becomes

$$\int_0^{2\pi} \Pi_J^{in}(\theta,\omega) N_d^J(\theta)\,\mathrm{d}\theta = \omega\eta_J \sum_a E_{Ja}(\omega) \int_0^{2\pi} N_a^J(\theta) N_d^J(\theta)\,\mathrm{d}\theta$$

$$+\left(\frac{\omega}{2\pi c_J}\right)\sum_a\left(\frac{E_{Ja}}{n_J}\right)\sum_p L_p \int_{\beta_p} N_a^J(\theta) N_d^J(\theta)\cos\left(\theta+\frac{\pi}{2}-\psi_p\right)\mathrm{d}\theta$$

$$-\left(\frac{\omega}{2\pi c_J}\right)\sum_q\sum_m\sum_c\left(\frac{E_{mc}}{n_m}\right)L_q \int_{\beta_q} N_c^m(\phi_{cm}) N_d^J(\theta)\cos\left(\theta+\frac{\pi}{2}-\psi_q\right)\tau_{mJ}^q\left(\phi_{qm}+\frac{\pi}{2}-\psi_q\right)\mathrm{d}\theta$$

(4.18)

where β_p and β_q respectively are the range of wave heading angles for which the boundary under consideration is output and input boundary.

The input and output boundaries are determined by the incidence angle of the wave and an edge of the plate is identified as an output boundary when the scalar product of equation (4.5.a) is positive. As the wave heading angle changes, so the input and output boundaries of the plate change as well and an edge which is an input boundary for a specific heading angle may become output boundary for a different incidence angle. The range of incidence angles for which an edge of the plate is an output boundary is depicted in Fig. 4.3, and overall input and output boundaries for the whole range of incidence angles are tabulated in Table 4.1.

Table 4.1

Input and output boundaries for the whole range of incidence angles

Range of θ	*Output Boundary*	*Input Boundary*
$0<\theta<\pi/2$	1,2	3,4
$\pi/2<\theta<\pi$	2,3	4,1
$\pi<\theta<3\pi/2$	3,4	1,2
$3\pi/2<\theta<2\pi$	4,1	2,3

Repeating these three steps for each wave type in the system, a set of linear equations may be obtained. These linear equations may be expressed in matrix form as

$$\Pi = \mathbf{Q}\overline{\mathbf{E}} \tag{4.19}$$

where the vector $\overline{\mathbf{E}}$ contains the coefficients E_{jd}/n_j in which index j spans over the wave types in the structure (j=1,2,...) index d represents the shape functions (d=0,1,2,...), the elements of matrix $\mathbf{Q}$ and input vector Π may be expressed as

$$Q_{jd,mc} = \delta_{jm}\left\{\omega\eta_j n_j \int_0^{2\pi} N_d^j(\theta)N_c^j(\theta)\,\mathrm{d}\,\theta\right.$$

$$\left.+\left(\frac{\omega}{2\pi c_j}\right)\sum_p L_p \int_{\beta_p} N_d^j(\theta)N_c^j(\theta)\cos(\theta+\frac{\pi}{2}-\psi_p)\,\mathrm{d}\,\theta\right\}$$

$$-\left(\frac{\omega}{2\pi c_j}\right)\sum_q L_q \int_{\beta_q} N_d^j(\theta)N_c^m(\phi_{qm})\cos\left(\theta+\frac{\pi}{2}-\psi_q\right)\tau_{mj}^a\left(\phi_{qm}+\frac{\pi}{2}-\psi_q\right)\mathrm{d}\,\theta \tag{4.20}$$

$$\Pi_{jd} = \int_0^{2\pi} \Pi_j^m(\theta,\omega)N_d^j(\theta)\,\mathrm{d}\,\theta \tag{4.21}$$

4.3 AN EXAMPLE APPLICATION: L-SHAPED PLATES.

In this section the intent is to illustrate the way of constructing the energy flow equilibrium equations of the previous section by applying the method to the simplest case of two plates connected at a right angle. As depicted in Fig. 4.4 a wave impinging on the junction with an incidence angle θ is partly transmitted to the other plate and partly reflected back to the same plate losing all of the power it carries either to a reflected wave or to a transmitted wave.

Attaching a unique identification number (i.e. 1,2,3 for bending, longitudinal and shear waves of first plate respectively and 4,5,6 for the waves in the second plate) to each wave type, one would end up having six subsystems (j=6) for the two coupled plates. Assuming, for the sake of simplicity, that the Fourier series expansion of each subsystem has been truncated after the third term in the series, then there exist a total of 18 subsets in the system. The three shape functions would take the form

$$N_0^j = \frac{1}{2\pi}, \qquad N_1^j = \cos\theta, \quad \text{and} \quad N_2^j = \cos 2\theta \tag{4.22}$$

A schematic energy flow diagram for this case is shown in Fig. 4.5. The figure shows each subsystem coupled to every other subsystem and the energy of each subsystem consists of directional dependent components. Even though external power may be injected into any wave type that may be considered to be appropriate, the majority of energy transmission analyses of this type generally consider the external power input to be via the flexural modes of the first plate and the response of all the other subsystems is investigated [62]. Thus the constant term of Fourier representation of flexural wave energy in plate 1 is attributed to an external input power.

The calculation of the transmission and reflection coefficients for each wave heading angle at a junction is central to this approach, as equation (4.10) expresses the power transfer between wave types in terms of the energy transmission coefficients. In the present work the wave transmis-

sion coefficients have been found by using the analysis of reference [29].

Although at a junction (the boundary where two or more plates meet) there may be transmission and reflection to flexural, longitudinal, and shear wave types of the two components (see Fig. 4.5) regardless of the type of incident wave, at a free edge (the boundary of a plate which is not connected to other plates) there will be only reflection and transmission between waves of the same component, and the nature of the reflection and transmission is determined by the type of the impinging wave. If it is a bending wave, then it will be completely reflected back and there will be no transmission to in-plane waves. Such an edge may be termed as a purely reflecting boundary for flexural waves. However, if the wave is either of longitudinal or shear type, it may be reflected and transmitted to the other in-plane wave, but *not* to a flexural wave as illustrated in Fig. 4.6. The figure shows the transmission coefficients from subsystem j to other subsystems as a function of incident angle at boundary 1. At all other boundaries there is no transmission from flexural to other subsystems, but a pure reflection from bending to bending, and reflection and transmission between in-plane subsystems.

The effect of pure reflection should be embodied into the assumed angular distribution of wave energy of the flexural subsystems. This can be achieved by ensuring that incident wave energy is equal to the reflected wave energy, that is

$$E_j(2\psi-\theta,\omega)=E_j(\theta,\omega) \tag{4.23}$$

where $2\psi-\theta$ is the heading angle of the reflected wave. The above equality may be satisfied by ensuring that the requirement is fulfilled by each shape function.

As mentioned before, the dimension of the matrix $\mathbf{Q}$ entirely depends on the number of subsystems in the model and shape functions which are used in the Fourier series expansion of the wave energy; for the present example considering the six subsystems and three shape functions for

each subsystem, the dimension of matrix **Q** will be 18x18. Several representative elements of matrix **Q** are given below

A diagonal element, $Q_{12,12}$, (the energy coefficient for the subset 2 of the subsystem 1) will take the form

$$Q_{12,12} = \underbrace{\omega\eta_1 \int_0^{2\pi} N_2^1 N_2^1 \, \mathrm{d}\theta}_{A} + \underbrace{\left(\frac{\omega}{2\pi c_1}\right)\sum_p L_p \int_{\beta_p} N_2^1 N_2^1 \cos(\theta + \frac{\pi}{2} - \psi_p)\,\mathrm{d}\theta}_{B}$$

$$\underbrace{-\left(\frac{\omega}{2\pi c_1}\right)\sum_q L_q \int_{\beta_q} N_2^1 N_2^1 \cos(\theta + \frac{\pi}{2} - \psi_q)\, \tau_{11}^q(\phi_{q1} + \frac{\pi}{2} - \psi_q)\,\mathrm{d}\theta}_{C} \qquad (4.24)$$

Substituting the shape functions from expression (4.22) the terms labelled as *A*, *B* and *C* may be written as

$$A = \omega\eta_1 \int_0^{2\pi} \cos^2\theta \,\mathrm{d}\theta \qquad (4.25)$$

As can be seen from Fig. 4.5 the orientation angle, ψ, of boundaries 1,2,3, and 4 are, respectively

$$\psi_1 = \frac{\pi}{2}, \qquad \psi_2 = \pi, \qquad \psi_3 = \frac{3\pi}{2}, \qquad \psi_4 = 2\pi \qquad (4.26)$$

Substituting those values into expression (4.24), using appropriate angular range of output boundaries from Table 4.1, term *B* may then be rewritten as

$$B = \left(\frac{\omega}{2\pi c_1}\right)\left\{ L_1 \int_{\pi 2}^{\pi 2} \cos^2\theta \cos\theta \,\mathrm{d}\theta + L_2 \int_0^{\pi} \cos^2\theta \cos(\theta - \frac{\pi}{2})\,\mathrm{d}\theta \right.$$

$$+L_3\int_{\pi/2}^{3\pi/2}\cos^2\theta\cos(\theta-\pi)\,\mathrm{d}\,\theta+L_4\int_{\pi}^{2\pi}\cos^2\theta\cos(\theta-\frac{3\pi}{2})\,\mathrm{d}\,\theta\Big\} \qquad (4.27)$$

Assuming that the transmission coefficient for each wave heading angle is already known, term C, which is the expression for input wave energy, would take the form

$$-\left(\frac{\omega}{2\pi c_1}\right)\Big\{L_1\int_{\pi 2}^{3\pi 2}\cos^2\theta\cos\theta\,\tau_{11}^{1}(\phi_{11})\,\mathrm{d}\,\theta+L_2\int_{\pi}^{2\pi}\cos^2\theta\cos(\theta-\frac{\pi}{2})\,\mathrm{d}\,\theta$$

$$+L_3\int_{3\pi 2}^{5\pi 2}\cos^2\theta\cos(\theta-\pi)\,\mathrm{d}\,\theta+L_4\int_{0}^{\pi}\cos^2\cos(\theta-\frac{3\pi}{2})\,\mathrm{d}\,\theta\Big\} \qquad (4.28)$$

As another example, the coupling entry, $Q_{13,52}$, (coupling energy coefficient between subset 3 of subsystem 1 and subset 2 of subsystem 5) may be expressed as

$$Q_{13,52}=-\left(\frac{\omega}{2\pi c_1}\right)\sum_q L_q\int_{\beta_q}N_2^5N_3^1\cos(\theta+\frac{\pi}{2}-\psi_q)\,\tau_{51}^{q}(\phi_{q5}+\frac{\pi}{2}-\psi_q)\,\mathrm{d}\,\theta \qquad (4.29)$$

By inserting the shape functions and integration range for the boundaries the above expression may be recast into the form

$$Q_{13,52}=-\left(\frac{\omega}{2\pi c_1}\right)\Big\{L_1\int_{\pi 2}^{3\pi 2}\cos\theta\cos 2\theta\cos\theta\,\tau_{51}(\phi_{15})\,\mathrm{d}\,\theta\Big\} \qquad (4.30)$$

It is emphasised that ϕ is written in terms of θ by using Snell's Law (see equation (4.12)) before carrying out the integration.

In a similar fashion all elements of matrix **Q** may be constructed. By using the standard matrix inversion techniques expression (4.19) may be solved to yield subset energies. Considering that there are three subsets,

in this example, for each subsystem, the sum of these three subsets gives the energy of the subsystem to which they belong.

4.4 THE DIFFUSE WAVE FIELD VERSION OF WIA.

If it is assumed that the wave field is diffuse, it will be no longer necessary to consider the angular dependence of wave energy, as the energy per unit angle of incidence will be constant. In this case equation (4.15), which expresses directional dependence of each wave type would take the form

$$E_j(\theta,\omega)=\frac{E_j(\omega)}{2\pi} \tag{4.31}$$

If this result is substituted into equations (4.19)–(4.21) a diffuse wave field version of the power balance equations may obtained. For the generalised input power, which is given by the left side of equation (4.19), to correspond to the actual input power, it will be appropriate to multiply both sides of equation (4.19) by 2π. Then a typical coupling element in matrix **Q** may be written as

$$Q_{j1,m1}=-\left(\frac{\omega}{2\pi c_j}\right)\sum_p L_p\frac{1}{2\pi}\int_{\beta_p}\cos(\theta+\frac{\pi}{2}-\psi_p)\tau^p_{mj}(\phi_{pm}+\frac{\pi}{2}-\psi_p)\,\mathrm{d}\theta \tag{4.32}$$

The reciprocity principle implies that

$$\tau^p_{mj}(\phi_{pm}+\frac{\pi}{2}-\psi_p)=\tau^p_{jm}(\theta+\frac{\pi}{2}-\psi_p) \tag{4.33}$$

Then the expression (4.32) may be rewritten as

$$Q_{j1,m1}=-\omega n_j\sum_p \eta^p_{jm} \qquad \eta^p_{jm}=\frac{L_p c_{gj}<\tau^p_{jm}>}{\pi\omega A_j} \tag{4.34),(4.35}$$

where $<\tau^p_{jm}>$ is the diffuse wave field transmission coefficient as given by equation (3.14). In the present notation this takes the form

$$< \tau_{jm}^{p} >= \frac{1}{2}\int_{\beta_p} \cos(\theta+\frac{\pi}{2}-\psi_p)\,\tau_{jm}^{p}(\theta+\frac{\pi}{2}-\psi_p)\,\mathrm{d}\,\theta \tag{4.36}$$

In the same way, a diagonal entry of matrix **Q** may be written as

$$Q_{j1,j1} = \omega\eta_j n_j + \left(\frac{\omega}{2\pi c_j}\right)\sum_q L_q \frac{1}{2\pi}\int_{\beta_q} \cos(\theta+\frac{\pi}{2}-\psi_q)\,\mathrm{d}\,\theta$$

$$-\left(\frac{\omega}{2\pi c_j}\right)\sum_p L_p \frac{1}{2\pi}\int_{\beta_p} \cos(\theta+\frac{\pi}{2}-\psi_p)\,\tau_{jj}^{p}(\theta+\frac{\pi}{2}-\psi_p)\,\mathrm{d}\,\theta \tag{4.37}$$

In this case the indices p and q span over the boundaries of the plate that carries wave type j. If the subsystem j is a flexural wave, at a free boundary the transmission, rather reflection coefficient from subsystem j to j is unity, then the last two terms of equation (4.37) cancel. If there is another plate connected to a particular boundary of the plate, τ_{jj}^{p} is the internal reflection coefficient. Assuming that the coupling at the boundary is non-dissipative, it can be expressed as

$$\tau_{jj}^{p}(\theta+\frac{\pi}{2}-\psi_p) = 1-\sum_{m\neq j}\tau_{jm}^{p}(\theta+\frac{\pi}{2}-\psi_p) \tag{4.38}$$

Then equation (4.37) may be rewritten as

$$Q_{j1,j1} = \omega\eta_j n_j + \omega n_j \sum_p \sum_{m\neq j} \eta_{jm}^{p} \tag{4.39}$$

As can be seen equations (4.19), (4.34), and (4.39) are exactly the same as the SEA expressions as given by equations (3.10), (3.11) and (3.12) respectively. This shows that the diffuse wave field version of WIA is the same as SEA; therefore WIA can be considered as an extended form of SEA.

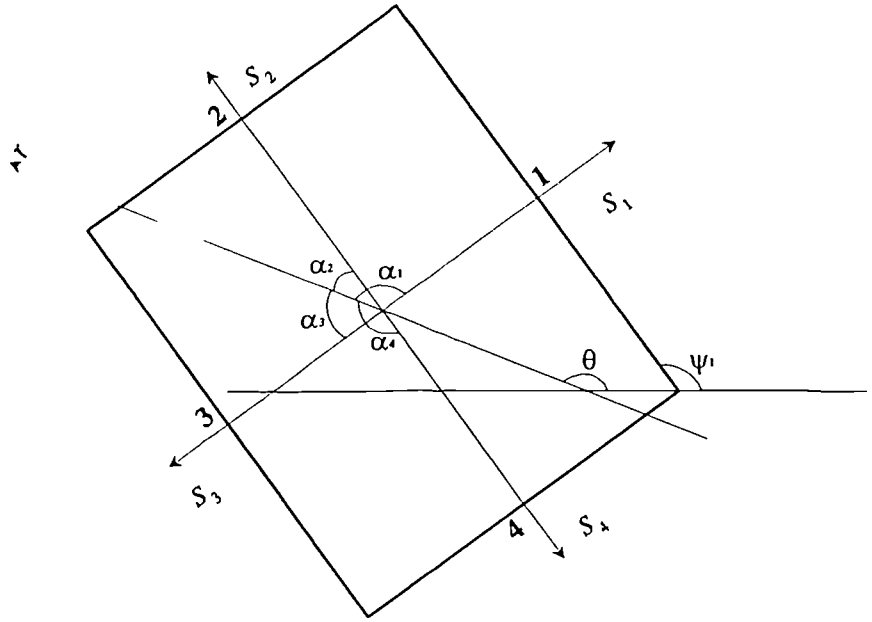

Fig. 4.1 Wave incidence at a boundary with arbitrary orientation.

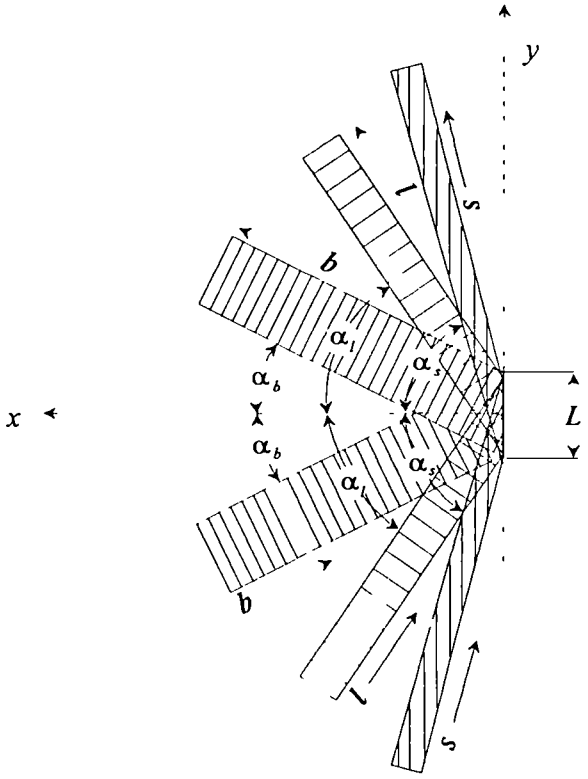

Fig. 4.2 Reflection of all three wave types at a junction.

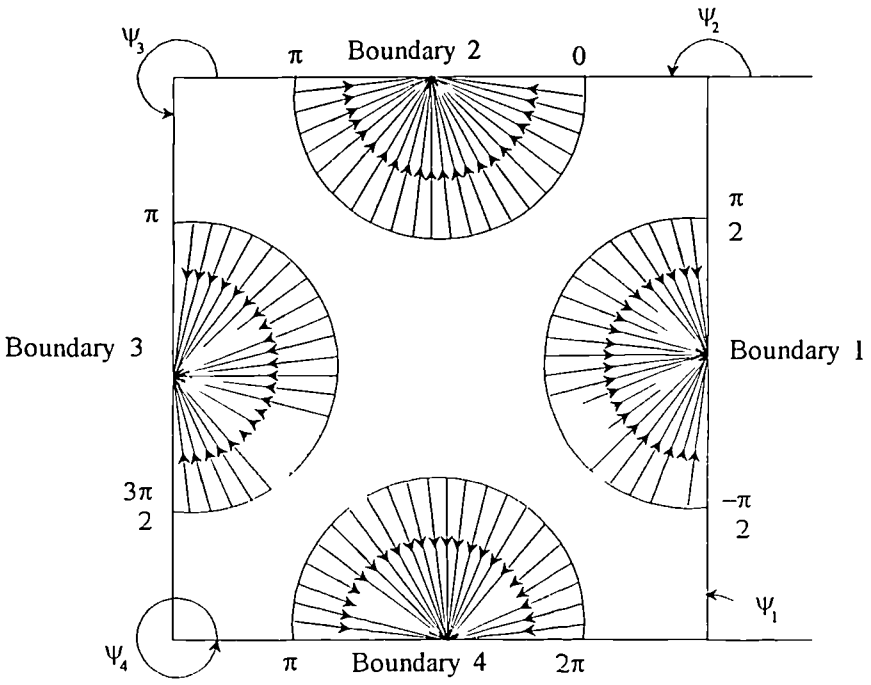

Fig. 4.3 Angular range of output boundaries with respect to incidence angles.

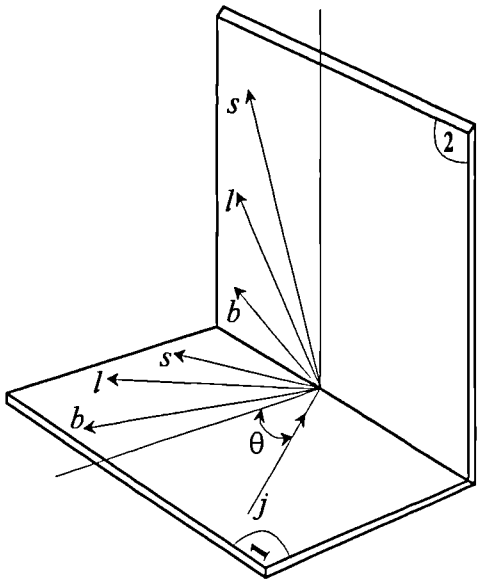

Fig. 4.4 Wave transmission through the junction between two plates.
θ : Angle of incidence of j 'th type wave.

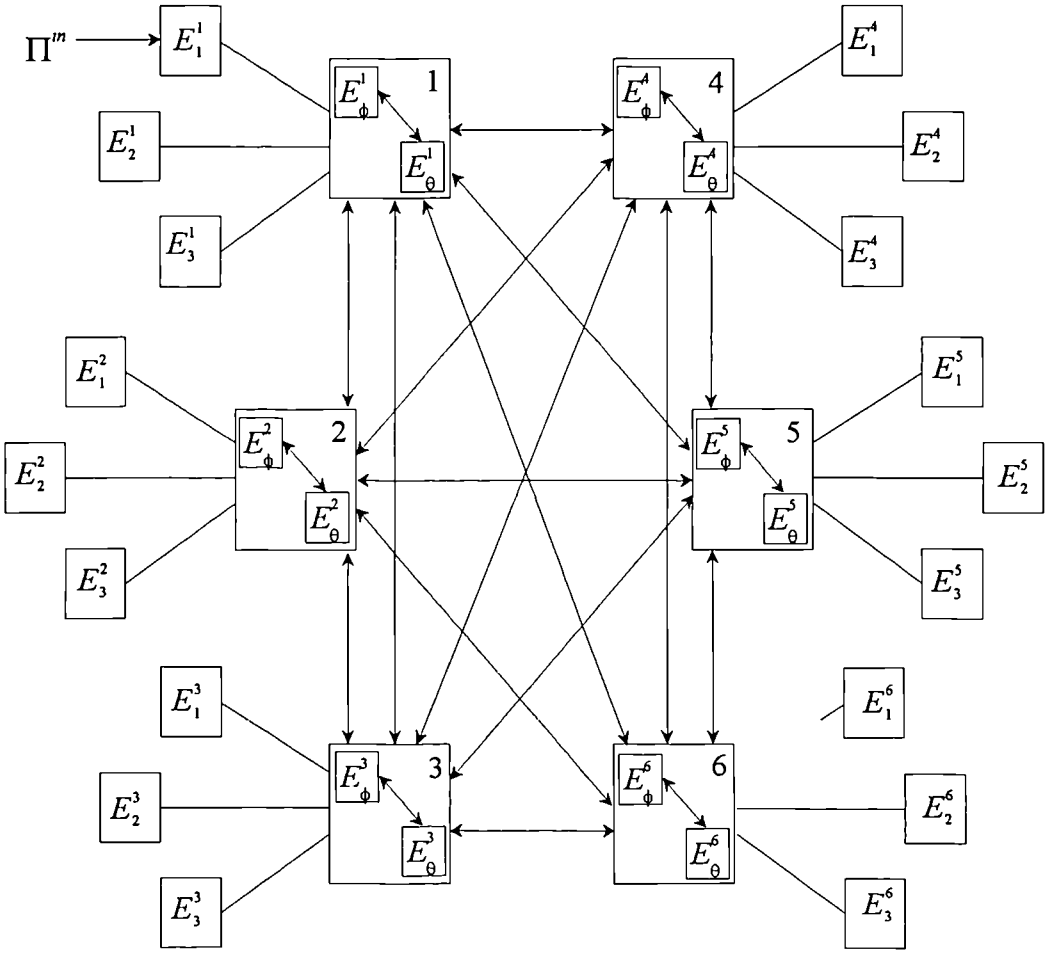

Fig. 4.5 Energy flow diagram for the two plate model.

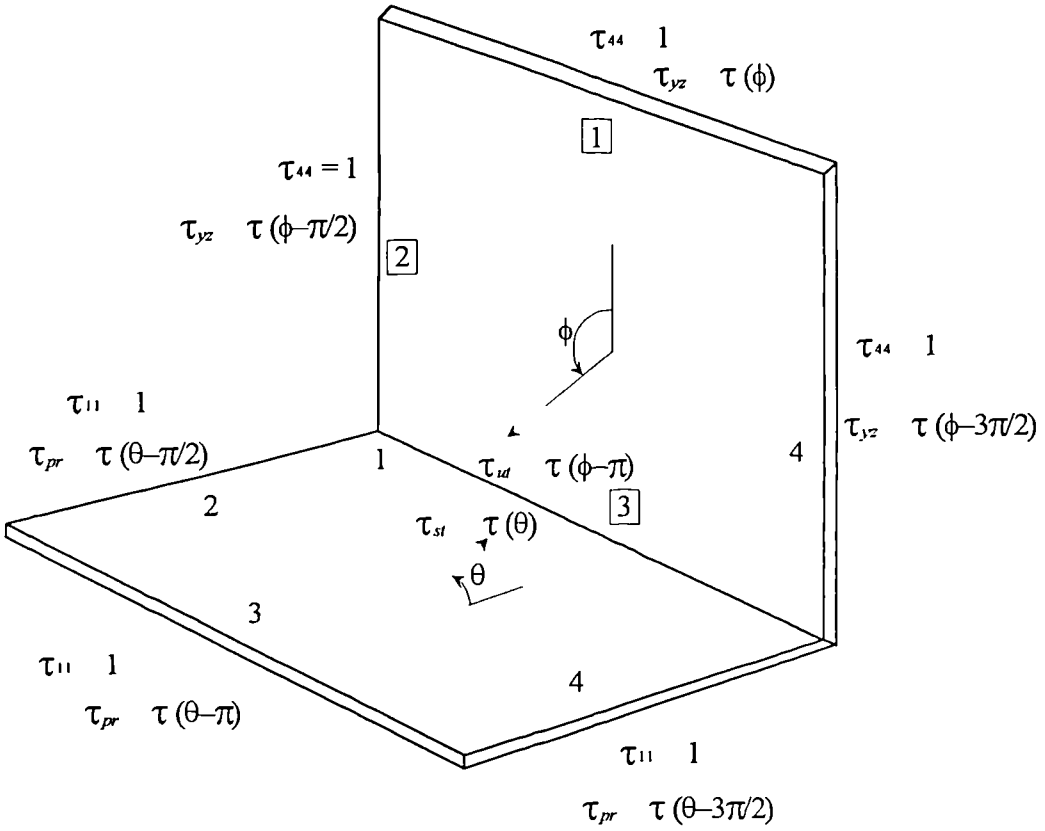

s =1,2, or 3 p–r =2, or 3

u 4,5, or 6 y–z =5, or 6

t 1,2,3,4,5, or 6

Fig. 4.6 Schematic represenation of the transmission coefficients at boundaries of the two plate model.

5 RESULTS AND COMPARISONS.

5.1 PRELIMINARIES.

It was stated in chapter 2 that the formulation (equations 2.12, 2.35, 2.36, 2.61, 2.98) of the dynamic stiffness method relates to a prescribed value of the Fourier term number, n. Therefore the set of equations has to be solved for as many "n" values as needed for the series to converge. However only a finite number of modes contribute significantly to the energy flow at any particular frequency: the series may be truncated by considering the well known formula for the natural frequencies of a simply supported plate of length L and width b:-

$$\omega_{mn} = \sqrt{\frac{D}{\rho h}}\left[\left(\frac{m\pi}{L}\right)^2 + \left(\frac{n\pi}{b}\right)^2\right] \tag{5.1}$$

The maximum number of Fourier terms, n_{max}, that contribute to the overall response of the structure in a particular frequency band may be found from this formula by taking m=0; thus n=$n_{max.}$ becomes

$$n_{max} = \frac{b}{\pi}\omega_{max}^{1/2}\left(\frac{\rho h_{max}}{D}\right)^{1/4}$$

where ω_{max} is the maximum frequency of the band, and h_{max} is the maximum plate thickness in the structure. Then the total energy of a plate may be obtained by adding the energies due to each n between 1 to n_{max}. Although there are infinite number of modes contributing to the overall response of a plate, clearly the loop can not be extended to the infinity, hence the truncation procedure is dictated by the physics. Although n_{max} limit the frequency summation to those modes whose natural frequencies lie in the band or below it, and does not consider the modes whose natural frequencies are above the band, these modes are known to be non-resonant modes and neglecting their contribution does not greatly alter the results.

As mentioned in section 4.4 the use of a single component in the Fourier series expansion of the wave energy reduces the WIA method to conventional SEA, in which case the results of WIA become exactly the same as those of SEA. However, so as to provide an unbiased set of results from an independent source, the SEA results which will be presented in this chapter were acquired by running the SEA program of McWilliam [64]. In order to implement the dynamic stiffness method and WIA, two separate FORTRAN-77 programs were developed. Brief descriptions of these programs may be found in Appendix A.

The plate structures that are analysed in this section can be divided into four broad groups. These are:

(i). Plate assemblies that consist of several plates either connected in a row over a simple support or joined rigidly at a right angle. (See, for example, Fig. 5.1).

(ii). A closed section formed by four plates as depicted in Fig. 5.53.

(iii). Complex-junction plate structures, i.e. structures which have a junction that contains more than two plates as illustrated in Fig. 5.62

(iv). Symmetrically or asymmetrically stiffened plate rows (see Figs. 5.72 and 5.83).

The plates of group **(i)**, **(ii)**, and **(iii)** were considered to be made of steel and those of group **(iv)** made of aluminium with the material properties given in Table 5.1.

Table 5.1

The material properties of the plates considered.

Material	Mod. of Elas. E (N/m^2)	Density ρ (kg/m^3)	Poisson Rat. ν	Loss Factor η
Steel	$2\text{x}10^{11}$	7800	0.3	0.01
Aluminium	$7.3\text{x}10^{10}$	2800	0.33	0.01

In the dynamic stiffness method it is assumed that the external disturbance is due to a point force acting perpendicular to the plate surface (the locations of the point forces with which the exact results of the next section are obtained are given in section 5.3.1); in WIA and SEA this is equivalent to injecting power into the flexural modes of the plate. In all of the cases considered the external input is via the first plate (the reasoning behind this approach was explained in section 4.3) and the energy level of the other plates in the structure with respect to the excited plate is expressed in terms of dB (decibels) i.e. $10\text{Log}_{10}(E_p/E_1)$, where the suffix "p" refers to a particular plate in the system.

In what follows the specifications of the plates within the four aforementioned groups of structures are given, and the results of all three methods are presented without elaborating on any specific point, as a detailed analysis of the results will be performed in later sections.

Almost all of the graphs referred to in the following sections relate to logarithmic flexural mean energy ratios in sixteen one-third octave frequency bands ranging between 600 Hz to 20 kHz as tabulated in Table 5.2.

Table 5.2

One-third octave central frequencies and bandwidths.

Band	Central Freq (Hz)	Min. Freq. (Hz)	Max. Freq. (Hz)	Band Width (Hz)
1	630.0	561.3	701.1	145.8
2	793.8	707.1	890.9	183.8
3	1000.6	890.9	1122.5	231.6
4	1260.0	1122.5	1414.3	291.8
5	1587.5	1414.3	1781.9	367.6
6	2000.1	1781.9	2245.0	463.1
7	2520.0	2245.0	2828.6	583.6
8	3175.0	2828.6	3563.8	735.2
9	4000.3	3563.8	4490.1	926.3
10	5040.0	4490.1	5657.2	1167.1
11	6350.0	5657.2	7127.6	1470.4
12	8000.5	7127.6	8980.3	1852.7
13	10080.0	8980.3	11314.4	2332.1
14	12700.0	11314.4	14255.2	2940.8
15	16001.0	14255.2	17960.5	3705.3
16	20160.0	17960.5	22628.8	4668.3

5.2 PRESENTATION OF RESULTS.

5.2.1 PLATE ASSEMBLIES.

Plate assemblies which consist of 3, 4, 8, and 15 plates were considered in this group, and for each of them there are bending and in-plane models. The bending model is basically a row of plates in which only out-of-plane motion occurs; in the in-plane model the plates are connected at a right angle; therefore due allowance needs to be made for the in-plane longitudinal and shear modes (or waves) during energy transmission calculations.

Three Plate Assembly.

The bending and in-plane models of the three plate assembly are shown in Figs. 5.1.a and b respectively. The dimensions of the structure and the bending, n_B, longitudinal, n_L, and shear, n_S, modal densities, which were calculated using the equations 3.21 to 3.23, are given in Tables 5.3-5.5 for three different cases. The main difference between these three cases is the thicknesses of the plates in the structure. In case 1 all the plates have the same thickness, in case 2 there is a gradual reduction in the thickness moving from plate 1 to 3, and in case 3 the thickness first decreases from plate 1 to 2 then increases from plate 2 to 3. Additionally, the plates of case 3 are larger in comparison to the other two cases.

As can be seen in Figs. 5.2 and 5.3 which relate to case 1, there are two separate graphs for each plate under consideration. Figs. 5.2.a and 5.2.b present respectively the results of the bending and in-plane models for plate 2 across the range of frequencies. In these figures the term "exact" refers to the predictions of the dynamic stiffness method, while the term "full" shows the results of in -plane model in which the contribution of the in-plane modes in the energy transmission has been fully taken into account.

Similar energy distribution curves are presented for cases 2 and 3 in Figs. 5.4 to 5.7.

Table 5.3

Dimensions and modal densities of the three plate assembly

Case 1

Plate	h (mm)	L (m)	$n_B x10^2$	$n_L x10^8/f$	$n_S x10^8/f$
1	4	0.90	6.24	2.71	7.75
2	4	0.80	5.54	2.41	6.89
3	4	0.65	4.50	1.96	5.60

Table 5.4

Dimensions and modal densities of the three plate assembly

Case 2

Plate	h (mm)	L (m)	$n_B x10^2$	$n_L x10^8/f$	$n_S x10^8/f$
1	10	0.90	2.49	2.71	7.75
2	7.4	0.80	2.99	2.41	6.89
3	4.8	0.65	3.75	1.96	5.60

Table 5.5

Dimensions and modal densities of the three plate assembly

Case 3

Plate	h (mm)	L (m)	$n_B x10^2$	$n_L x10^8/f$	$n_S x10^8/f$
1	9.5	0.90	2.62	2.71	7.76
2	3.2	1.30	11.3	3.92	11.2
3	5.5	1.10	5.54	3.32	9.48

In all cases width of the plates: b=0.85 m

Four Plate Assembly.

Three different four plate assemblies have been studied which are quite similar to the foregoing three plate assemblies. The dimensions and modal densities of these cases are tabulated in Tables 5.6-5.8.

The plate energy ratios for case 1 are plotted in Figs. 5.8-5.10, and Figs. 5.11-5.16 present these ratios for cases 2 and 3.

Table 5.6

Dimensions and modal densities of the four plate assembly

Case 1

Plate	h (mm)	L (m)	$n_B x10^2$	$n_L x10^8/f$	$n_S x10^8/f$
1	4	0.90	6.24	2.71	7.76
2	4	1.37	9.49	4.13	11.8
3	4	1.45	10.1	4.37	12.4
4	4	1.10	7.62	3.32	9.48

Table 5.7

Dimensions and modal densities of the four plate assembly

Case 2

Plate	h (mm)	L (m)	$n_B x10^2$	$n_L x10^8/f$	$n_S x10^8/f$
1	10	0.90	2.49	2.71	7.76
2	7.4	1.37	5.13	4.13	11.8
3	4.8	1.45	8.37	4.37	12.4
4	2.2	1.10	13.8	3.32	9.48

Table 5.8

Dimensions and modal densities of the four plate assembly

Case 3

Plate	h (mm)	L (m)	$n_B x10^2$	$n_L x10^8/f$	$n_S x10^8/f$
1	10	0.90	2.49	2.71	7.76
2	6.5	1.37	5.84	4.13	11.8
3	8.4	1.45	4.78	4.37	12.4
4	3.6	1.10	8.47	3.32	9.48

In all cases width of the plates: b 0.85 m

Eight Plate Assembly.

The bending and in-plane models of the eight plate assembly is depicted in Fig. 5.17. The structures are obtained by adding four more plates to

case 2 of the four plate assembly. The specifications of the last four plates are listed in Table 5.9.

The graphs which show 1/3rd octave frequency bands energy distribution in sixteen frequency bands for plates 2 to 8 may be found in Figs. 5.18-5.24.

Table 5.9

Dimensions and modal densities of the eight plate assembly

Plate	h (mm)	L (m)	$n_B x10^2$	$n_L x10^8/f$	$n_S x10^8/f$
5	4.5	0.70	4.31	2.11	6.03
6	6.3	1.10	4.84	3.32	9.48
7	5.5	0.90	4.54	2.72	7.76
8	3.0	0.55	5.08	1.66	4.74

Width of the plates: b–0.85 m

Fifteen Plate Assembly.

Two cases are considered for the fifteen plate assembly. Case 1 is formed by attaching seven more plates to the eight plate assembly; the details of these plates are shown in Table 5.10. Although in practice it is unlikely for the plates of different thickness couple together in a structure, here the plate thicknesses are varied to encourage bending to in-plane conversion or vice versa. Whereas case 2 corresponds to a practical structure: all fifteen plates have the same thickness h=5 mm, length L 0.9 m, and width b=1.1 m.

Figs. 5.25-5.38 show the energy levels across the range of plates for case 1, while the results for case 2 are shown in Figs. 5.39-5.52.

Table 5.10

Dimensions and modal densities of the fifteen plate assembly

Case 1

Plate	h (mm)	L (m)	$n_B x10^2$	$n_L x10^8/f$	$n_S x10^8/f$
9	4.4	0.75	4.72	2.26	6.46
10	5.6	1.10	5.45	3.32	9.48
11	6.0	0.70	3.23	2.11	6.03
12	4.0	0.65	4.51	1.96	5.60
13	3.5	0.95	7.53	2.87	8.19
14	5.2	0.78	4.16	2.35	6.72
15	6.5	1.15	4.91	3.47	9.91

5.2.2 CLOSED SECTIONS.

The closed section structure is illustrated in Fig. 5.53, and two distinct cases are considered. For case 2 the various parameters are listed in Table 5.11, while for case 1 the plates have the same length as in case 2, but the thickness of all the plates is 10 mm.

Table 5.11

Dimensions and modal densities of the four plate box assembly

Case 2

Plate	h (mm)	L (m)	$n_B x10^2$	$n_L x10^8/f$	$n_S x10^8/f$
1	10	0.90	2.49	2.71	7.76
2	7.4	1.37	5.13	4.13	11.8
3	4.8	0.90	5.20	2.71	7.76
4	2.2	1.37	1.73	4.13	11.8

Width of the plates: b=0.85 m

It should be noted that the bending models of the previous structures were obtained essentially by flattening the in-plane model. However this approach cannot be used in the case of the box structure; here the bending results which are shown in Figs. 5.54-5.59 are yielded by restraining

the in-plane degrees of freedom of the structure in the exact method, and by using the flexural energy transmission coefficients in SEA and WIA.

5.2.3 COMPLEX-JUNCTION PLATE ASSEMBLIES.

In all of the previous structures there are only two plates at a junction. Two more complex geometries are shown in Figs. 5.61 and 5.62. Table 5.12 shows the dimensions of the plates for case 2 (Fig. 5.62), and case 1 (Fig. 5.61) is constructed by using only the first four plates of case 2.

The plate energy ratios for these cases are presented in Figs. 5.63-5.71.

Table 5.12

Dimensions and modal densities of the complex-junction plate model

Case 2

Plate	h (mm)	L (m)	$n_B x10^2$	$n_L x10^8/f$	$n_S x10^8/f$
1	9.0	0.9	2.77	2.71	7.76
2	6.0	0.7	3.24	2.11	6.03
3	5.0	0.5	2.77	1.51	4.31
4	3.0	0.4	3.69	1.21	3.45
5	2.0	0.55	7.63	1.66	4.74
6	4.5	0.4	2.47	1.21	3.45
7	1.5	0.8	14.8	2.41	6.90

Width of the plates: b 0.85 m

5.2.4 STIFFENED PLATES.

Figure 5.72 illustrates a symmetrically stiffened row of six plates. Two cases are considered: the dimensions and modal densities of the plates for case 1 are given in Table 5.13. In case 2 every plate has the dimensions of plate 1 of case 1. In both cases the stringers are taken to have thickness t=3 mm and height H=20 mm.

Table 5.13

Dimensions and modal densities of six plates with stringers

Case 1

Plate	h (mm)	L (m)	$n_B x10^2$	$n_L x10^8/f$	$n_S x10^8/f$
1	2	0.30	2.40	0.51	1.53
2	2	0.26	2.08	0.44	1.32
3	2	0.33	2.64	0.56	1.68
4	2	0.28	2.24	0.47	1.42
5	2	0.24	1.92	0.41	1.22
6	2	0.36	2.88	0.62	1.83

Width of the plates: b–0.5 m

The plate energy ratios are shown in Figs. 5.73-5.82. Since the stringers are symmetric there is no in-plane motion, and therefore these cases are analogous to the bending model of the previous cases.

An asymmetrically stiffened panel has also been considered (see Fig. 5.83). This is identical to the previous panel apart from the attachment configuration of the stringers. Again, two cases were considered, and the results are shown in Figs. 5.84-5.93.

5.3 FACTORS INFLUENCING THE EXACT RESULTS.

5.3.1 EFFECT OF POINT LOAD LOCATIONS.

As pointed out in section 2.6.1, the dynamic stiffness method calculates the energy transmission by exciting the structure by point loads, whereas in SEA it is often assumed that the excitation is of "rain-on-the roof" type. It is shown [33] that a response similar to that arising from rain-on-the roof excitation may be achieved if the plate is excited by several point loads and the resulting response is averaged over the point load locations. This procedure has been implemented to yield the "exact" energy ratios which are presented in the previous section. The sensitivity

of the response, especially when the in plane motion is present, to the selection of the point load locations requires further investigation.

To this end two sets of force positions have been chosen, as shown in Fig. 5.94. The figure shows the plan view of a typical excited plate and the accompanying table gives the co-ordinates of the force positions for force sets 1 and 2. Each set consists of nine excitation points which are randomly distributed over the plate. Although there is no general criterion for the selection of the force positions, the dynamic stiffness program encounters numerical problems in the calculation of the stiffness matrix if the excitation point is too close to the edge of the plate. This happens because of the scaling procedure which was performed in section 2.2.1 while trying to avoid numerical overflow at the higher frequencies in the exponential terms of the dynamic stiffness matrix, they became too small when the point force is near to the edge of the plate. Since an averaging over the point load locations is performed, provided that the force which quite near to the edge of the plate does not yield very different response the average response of the plate would not be greatly affected. However this shortcoming does not restrict the comparison between the results of the dynamic stiffness method and SEA or WIA, as the latter two method do not favour large deviations from the mean response level. Besides, it has been suggested [41] that in this type of analysis, exciting the plate too near to the junction should be avoided as this would lead to biased results due to the existence of nearfield waves near the junction.

Figs. 5.95-5.97 show the relative ranges (the difference between the energy ratios of sets 1 and 2 for a particular plate after averaging over possible load locations) for the bending and in-plane models of case 2 of the four plate assembly. Generally as the frequency increases the difference between the two sets decreases. This trend is clear for both bending and in-plane energy transmission and it can be concluded that the results are relatively insensitive to the choice of the averaging points.

The scatter over the nine excitation points of set 1 is examined in Figs. 5.98-5.100. The figures show the dB range (the difference between maximum and minimum energy levels for the individual point forces at a

particular one-third octave frequency band) for the same four plate assembly. Although the dependency of the response to the individual point load locations decreases with increasing frequency, and the bending curve becomes relatively smooth after 5 kHz, there is still a 2 dB difference at 10 kHz. When the in-plane modes are included the system is more sensitive to the force position. This is most marked in plate 4, where the range is as high as 5 dB at 8 kHz when the actual ratio is -17 dB. The Fig. 5.100.a shows the full energy ratio of the last plate for the same case due to each of the nine driving point: as can be observed while the force locations 5 and 7 respectively yield the maximum and minimum energies at 600 Hz, thus result in 12 dB scatter; 5 dB scatter which occurs around 8 kHz is caused by the driving points 6 and 9.

5.3.2 EFFECT OF BOUNDARY CONDITIONS.

The boundary conditions imposed in the dynamic stiffness method are that the two longitudinal edges of each plate are taken to be simply-supported so that an exact solution to the governing equations may be derived. Having this limitation does not prevent a direct comparison between the exact results and the SEA or WIA approach, since the latter two analyses assume that the energy transmission is "independent" of the boundary conditions. With regard to transverse edges, all of the exact results (other than those of the box section) which are presented in section 5.2 have been obtained by clamping the extreme transverse edges.

The validity of the SEA assumption concerning the boundary conditions may be checked with the exact method by changing the boundary conditions at the extreme transverse edges of the plate assembly from clamped to simply supported. It has been shown previously [50] that if the above procedure is implemented then the bending energy is redistributed over the entire frequency range, although the effect diminishes as the frequency increases. However the detailed effect of changing from clamped to simple support boundary condition has not been considered in the presence of in-plane motion, and needs to be investigated.

For this purpose the clamped left-hand transverse edge of the four plate assembly has been changed to a simple support: the results are plotted in

Figs. 5.101-5.103. It is observed that at low frequencies the energy in the last plate decreases while it increases in the second plate. On the other hand at sufficiently high frequencies the simple-support and clamped curves converge to the same value. This phenomenon is thought to be a direct consequence of phase effects, which are not considered in SEA.

From a wave point of view, the effect of the boundary conditions is to change the phase of the various wave components. Considering a wave impinging on a boundary, the amplitude of the reflected wave would be equal in magnitude to that of the incident wave regardless of the type of support. However the phase of the returning wave, relative to that of the original incident wave, will depend on the boundary condition. Phase effects are more marked at low frequencies, as shown in Figs. 5.101-5.103. The reason for this is that at the higher frequencies the phase effects tend to fluctuate rapidly with frequency, and they thus tend to average out over a frequency band.

The consequences of changing the right-hand boundary condition from clamped to simply-supported have also been investigated. The results are not reported here, since for the present plate assembly no significant effect has been observed.

5.4 FACTORS INFLUENCING THE WIA RESULTS.

5.4.1 EFFECT OF THE NUMBER OF SHAPE FUNCTIONS FOR PLATE ASSEMBLIES.

Equation (4.15) expresses the dirccttional dependency of the wave energy in terms of a set of shape functions corresponding to a finite Fourier series. In the selection of the Fourier components of equation (4.17) care must be exercised since, equation (4.23) imposes constraints due to the presence of purely reflecting boundaries for bending waves.

For the plate assemblies which are considered in this study, there are at least two purely reflecting boundaries: two longitudinal edges of any

plate in the assembly, in which case the Fourier terms may take the form: $\cos d\theta$, where d–0,1,2,3,.... In addition, in the first and last plate of all the assemblies considered, save the box section, there is a transverse purely reflecting boundary. For these plates due to the constraint of equation (4.23), the shape functions of the bending waves should take the form: $\cos d\theta$ with d=0,2,4,.... However for in-plane waves there are no purely reflecting boundaries (see section 4.3); therefore in the extreme components the same type of shape functions as in intermediate plates may be used for these two wave types.

Convergence checks on various plate assemblies were performed and case 2 of the four plate assembly is reported in detail here. Initially three and five Fourier terms are used in the extreme and intermediate plates respectively, and the resulting wave energy distribution with respect to incidence angle is plotted for each plate in Figs. 5.104 to 5.107. In these figures an angle of zero radian represents a wave normally incident on the junction. The centre frequency of the one-third octave excitation band is taken as 20 kHz. The results correspond to the in-plane model of the four plate assembly.

As can be seen in these figures there is some negative energy for certain incident angles in plate 2, and the amount increases moving away from the excited plate. For physical reasons the presence of negative energy is not permissible, and the result arises from the truncation of the Fourier series after just a few terms. To investigate this effect the number of Fourier terms in the outer plates was increased to five and in the middle plates to nine. Fig. 5.105 indicates that the negative energy is almost halved in plate 2, and has virtually disappeared in plate 3, (Fig. 5.106) although it still appears in plate 4. Finally the number of Fourier components was raised to fifteen in plates 2 and 3, and eight in plates 1 and 4. In this case no negative energy occurred in any of the plates as may be seen from the curve which corresponds to 15 terms in Figs. 5.105 and 5.106, and 8 terms in Fig. 5.107.

In order to investigate the effect of the number of shape functions on the energy level of the various plates in the structure, for each set of Fourier

terms the wave energies were obtained by integrating $E_j(\theta,\omega)$ over the heading θ, as indicated by equation (4.18).

In the WIA program the integration is carried out numerically by using the "trapezoidal" rule. To increase the accuracy of integration as the number of Fourier terms is raised, the number of increments within the angular range of integration has been increased by a suitable amount: in the three cases considered there were respectively 50, 80, and 120 increments.

For each one-third octave frequency band considered, the mean quantities are obtained by averaging over the range of the band, starting with the band minimum frequency which is at 17960.5 Hz and ending with the band maximum frequency at 22628.8 Hz for band 16 (Table 5.2). It was found that the method is not sensitive to the number of increments taken between the minimum and maximum frequency of the band; in fact, two increments were found to be sufficient.

The plate energy ratios obtained by using an increasing number of Fourier terms are given in Table 5.14.

Table 5.14

Energy ratios (dB) *for case 2 of four plate assembly.*
Third-octave band results with centre frequency 20 kHz

Terms	E_2/E_1	E_3/E_1	E_4/E_1
3, 5	-11.35	-15.37	-21.52
5, 9	-11.40	-15.25	-21.72
8, 15	-11.46	-15.36	-21.77

Although the detailed angular energy distribution (and the phenomenon of negative energy) is affected by the number of Fourier terms, it is clear that converged estimates of the total energy are obtained with relatively few terms.

The reason for this effect is that the energy curves oscillate below and above the zero line when there are few Fourier terms, but on balance the positive and negative portions cancel as can be observed most clearly in Fig. 5.107. On the other hand if there are many components, the oscillations do not take place, and the curve just follows the zero line for certain ranges of incidence angles. Therefore in each case almost the same total level of energy is predicted.

5.4.2 EFFECT OF THE NUMBER OF SHAPE FUNCTIONS FOR STIFFENED PLATES.

In the convergence checks for the stiffened plates, it was found that the use of a small number of Fourier terms can lead to not only negative energy at certain incident angles, but also poor total response predictions.

The results of calculations performed by using five and three Fourier components in the middle and outer plates respectively are shown in Fig. 5.77. It is seen that although the WIA results for the symmetrically stiffened plates are quite close to the exact results up to 12 kHz, at this frequency the WIA curve (as well as the exact curve) makes a dip but does not recover afterwards. At 20 kHz the difference between the exact and WIA results is as high as 7 dB in the last plate. To eliminate the negative energy from the system, and to improve the response predictions, the number of Fourier terms was raised gradually. Good agreement with the exact results was obtained for 20 and 41 Fourier terms in the extreme and intermediate plates respectively. In this case the discrepancy for the final plate at the highest frequency reduced to 0.63 dB, and the negative energies disappeared entirely, as may be noted from the Figs. 5.108-5.113.

An explanation of the observed trend can be made by considering the wave transmission coefficients which are shown in Fig. 5.114. The figure shows the bending wave transmission coefficient between two stiffened plates at two discrete frequencies, and also the transmission coefficient between plates 1 and 2 in the case 2 four plate model. In the latter case the plates are coupled across a simple support.

The transmission coefficients of the simply supported junction are independent of frequency and vary smoothly with wave heading angle. However the transmission coefficients of the stiffened plate junction are dependent on both the incidence angle and the frequency of excitation. The coefficient of the stiffened junction has very narrow peaks at 20 kHz, but at 1 kHz the variation of the transmission coefficient with the incidence angle is relatively smooth. Thus the study of transmission coefficient leads to the following conclusions:

(i). In simply-supported plates five Fourier components are enough for convergence, as the transmission coefficients vary smoothly with the incidence angle.

(ii). In stiffened plates five Fourier terms are still sufficient up to moderate frequencies because of the reason given in **(i)**, and as evidenced by the two WIA curves following virtually the same path up to 12 kHz in Fig. 5.77.

(iii). At higher frequencies the transmission coefficients are characterised by very narrow peaks with small angular range, and thus many Fourier terms are needed to yield the desired accuracy for stiffened plates.

5.5 TYPICAL RESULTS AT LOW FREQUENCIES.

Before proceeding to fully analyse the results produced by the approximate methods, it is worth studying the behaviour of SEA at low frequencies to highlight the various possible reasons which are considered to lead to "wrong" answers in the SEA model.

To this end an additional set of results was obtained within the frequency range of 25 Hz to 280 Hz for case 2 of the four plate assembly. One-third octave band mean energy ratios and discrete frequency energy ratios are plotted in Figs. 5.115-5.117.

An examination of the one-third octave band mean response graphs for plates 2 and 3 reveals that SEA and WIA almost give the average of the exact predictions. However, if desired, these average values may be corrected to yield the maximum response if they are multiplied by $\coth(0.5\pi M)$ (M: modal overlap factor) [65], since an engineer is much more concerned with the peak response.

Although this correction may in principle be applied to the one-third octave band energy ratios, the peaks and troughs of the exact curve are relatively washed out because of the averaging process. Thus the procedure is illustrated here for the discrete frequency energy ratios of the four plate model. As may be seen in Fig. 5.115.b the corrected SEA curve goes through the peaks which are exhibited by the exact method.

As stated in section 1.3.1 and chapter 2, the requirements which are put forward for successful application of SEA are:-

(i). The components should be weakly coupled.

(ii). The modal overlap factor must be greater than unity.

(iii). The frequency band should be wide enough to contain at least five to seven modes.

(iv). Each component of the structure should be reverberant.

An observation that can be made from Fig. 5.115.a is that the SEA mean energy ratio of the plate 2 is almost zero across the frequency range. This implies that the energy in plate 2 is as large as the energy in the driven plate, meaning that plates are "strongly" coupled. Therefore the present system does not satisfy the weak coupling requirement.

The modal overlap factors each plate are also tabulated in Figs. 5.115.a to 5.117.a, as can be seen they increase with frequency. For example for the one-third octave band with centre frequency 280 Hz, the modal overlap factors of the individual components are between 0.07-0.38. As these values are substantially less than unity, it has been shown [40] that

in such a case the coupling loss factors which are obtained by a wave transmission analysis are far greater than the actual values. Although in plate 4 (Fig. 5.117.a) the SEA curve is above the exact curve, the predictions of SEA in the plates 2 and 3 are fair representation of the average response. Therefore, the results of the present case do not fully support the conclusion of reference [40] where the case studied was two coupled beams.

For the same centre frequency the number of modes which are excited in the plates varies between 1.61-8.83. It should be noted that although the product of the modal density and the bandwidth usually yields a non-integer value, in order to perform a modal summation the number of modes is rounded to the nearest integer value.

Although the number of modes in the final plate is around eight at the highest frequency, it is less than five at low frequencies. Also, for the entire frequency range there are just a few modes in the other plates, and therefore the system does not satisfy condition **(iii)** completely.

Finally, the structure may be checked for reverberance by using the following formula [28] which is a measure of the decay in a wave each time it reflects from the boundaries. Therefore a value which is closer to unity implies that a wave is reflected many times before it is absorbed: thus resulting in a reverberant wave field.

$$r = \exp(-0.5\omega\eta x/c_g)\begin{cases} r \approx 0.98 & \text{reverberant,} \\ r \ll 0.98 & \text{non-reverberant} \end{cases} \qquad (5.2)$$

where x is the length of the plate, and c_g and η represent the group velocity and loss factor respectively. For the present model the values of r at 280 Hz are between 0.94-0.98 which implies that the system is highly reverberant.

Although in this section it has been seen that the SEA results are an average of the exact response, particularly in plates 2 and 3, and knowledge of the maximum response may be obtained by introducing a correction factor, the present system is strongly coupled, has low modal over-

lap factor and the average number of modes excited is less than five across the one-third octave frequency bands. In what follows the situations where the four conditions of SEA are duly satisfied will be investigated in relation to the results of section 5.2.

5.6 COMPARISON OF RESULTS: BENDING ONLY.

As pointed out earlier there are two distinct graphs for each component of the structures presented in section 5.2; one for the bending model in which only flexural motion exists, and one for the in-plane model of the same structure. Here, the discussions will concern only the bending energy transmission, and the contribution of the in-plane motion will be treated separately in section 5.7.

5.6.1 PLATE ASSEMBLIES.

The simplest structure that is considered in this study is the one that consists of three plates. An examination of the three plate assembly results reveals that although SEA initially overestimates the energy level of plate 2, the agreement between SEA and the exact predictions is quite good at high frequencies: in case 1 SEA starts off high and as the frequency increases the two curves converge to the same value (Fig. 5.2.a); in case 2 the discrepancy seems to be larger at low frequencies, but it never exceeds 3 dB after 5 kHz; in case 3 the exact curve is smoother since the modal density is higher in comparison to other the two cases, and thus the agreement is extremely good. The difference is around 1.5 dB and 0.01 dB at 500 Hz and 20 kHz, respectively.

In the second plate for case 1, WIA yields a good average of the exact response up to 5 kHz, although from this frequency onwards it starts to underpredict the mean response. In case 2 there is some overprediction of the response, but not as high as in SEA. In case 3 the WIA and exact results start off almost from the same point, and the exact curve oscillates around the WIA curve up to 6 kHz. Beyond this point the WIA results diverge slightly from the exact results and the difference reaches around 0.5 dB at the highest one-third octave band.

For plate 3, as may be observed from Fig. 5.3.a, SEA first overestimates the response and then as the frequency increases it starts to underestimate the response. This effect is better seen in plate 3 of case 3 (Fig. 5.7.a).

For all the cases WIA yields a much improved estimate of the energy in plate 3, when compared to SEA. For example in case 1 starting from mid-range frequencies up to the highest frequency the discrepancy never exceeds 0.5 dB. Even though in case 2 the exact results are erratic, WIA predicts the energy levels reasonably well. In case 3 the WIA predictions are still quite good, while the underprediction of SEA reaches as much as 3 dB.

The main difference between the three plate assemblies is the thicknesses of the plates. The results show the influence of this factor on the energy transmission: there is a greater energy flow between plates of similar thickness. This tendency is predicted by all three methods.

In the four plate assemblies the plates are relatively larger than in the three plate models, and thus the exact curve is fairly smooth even at low frequencies. In the second and third plates SEA and WIA exhibit similar behaviour as in the three plate models: in the second plate SEA overpredicts the mean response at all frequencies, and while WIA is quite close to the exact curve at low frequencies, it slightly underpredicts at high frequencies.

The reason behind this phenomenon can be better understood if Fig. 5.118 is examined. The figure shows the wave energy distribution in the excited plate, as predicted by SEA and WIA for case 2 of the four plate model. Since it is assumed in SEA that the wave field is diffuse, the wave energy distribution predicted by this method is constant for all wave heading angles; this assumption is not made in WIA, and the distribution depends on the incidence angle. As can be seen in the figure, at normal incidence where the majority of the transmission takes place, the amount of wave energy travelling towards the neighbouring plate is 30% less in WIA than in SEA: as the SEA and WIA curves are scaled by dividing the maximum energy in the plate a direct comparison between

them can be made. This phenomenon leads to an overprediction in SEA and underprediction in WIA in the second plate. Fig. 5.119, which shows the WIA wave energy distribution in plates 2, 3, and 4, suggests that the wave field is not diffuse in these components.

In the eight plate assembly, which is an extended form of case 2 of the four plate assembly, the same characteristics demonstrated by the previous models also occur for the first three indirectly driven plates, as may be seen in Figs. 5.18.a to 5.20.a. From plate 5 onwards the error in the SEA prediction increases with frequency, reaching 18 dB in plate 8 at 20 kHz. However, WIA is still close to the exact results in the final plate, the disagreement at 20 kHz being 2.7 dB (Fig. 5.24.a).

In case 1 of the fifteen plate assembly, which is an extended form of the eight plate assembly, the situation is similar. SEA diverges from the exact results not only as the frequency increases, but also as the plates become remote from the driven plate. Although WIA starts to underpredict from plate 6 onwards, the discrepancy is weakly dependent on the frequency and remoteness of the plate.

To highlight the severity of the SEA underprediction, the energy discrepancies for the last eight plates are tabulated in Table 5.15, for the one-third octave band with centre frequency 20 kHz.

Table 5.15

The discrepancy (dB) *between results of the exact and the approximate methods for case 1 of the 15 plate assembly; centre frequency:* 20 kHz

	dB range			dB range	
Plate	SEA	WIA	Plate	SEA	WIA
8	26.12	5.93	12	43.71	8.62
9	30.07	5.46	13	46.08	7.21
10	37.19	8.60	14	51.31	7.73
11	41.18	8.82	15	54.43	6.77

The dimensions of the previous models all have been relatively random. To investigate the effect of structural regularity, a further fifteen plate structure has been considered (case 2) in which each plate is identical. The results appear similar to those of case 1 as shown in Figs. 5.39 to 5.52: in the remote plates SEA severely underestimates the response. However, in this case it seems that the energy transmission is predicted incorrectly by the approximate methods: this may be due to periodicity of the structure which is not modelled neither by the traditional SEA nor the WIA. However the work of Keane and Price [66] addresses this issue in SEA: by introducing non-uniform frequency statistics, SEA can be used in the dynamic analysis of periodic structures.

It is known [28] that periodic structures exhibit alternate "pass bands" and "stop bands": if the frequency of a wave impinging on the junction lies in a pass band, then the wave will travel unattenuated from one component to another, and there occurs only a phase change between consecutive plates. However, if the frequency of a wave is within the range of the stop band, then there will be greatly reduced transmission to the connecting plate, but the wave will either grow or decay at the boundaries. To give an indication of the pass bandwidth consider the case where $n=11$. Were the plates connected through simple supports then each pass bands would have a lower bounding frequency which corresponds to the natural frequency of a single panel with simply supported transverse edges, and an upper bounding frequency which corresponds to the natural frequency for clamped edges. Considering for example the 10 kHz one-third octave band, the pass band corresponding to 23 half wave lengths along the panel has a lower bounding frequency of 9 kHz and an upper bounding frequency of 9.2 kHz. The next pass band begins at 9.7 kHz which indicates a pass bandwidth of 200 Hz and a stop bandwidth of 500 Hz. Obviously the detailed structure of the pass and stop bands for stiffener connections is complex but these figures give some indication of the pass and the stop bandwidths.

Thus far the best agreement between the SEA and exact results has been achieved in case 3 of the three plate assembly, particularly in the second plate. The worst agreement has arisen in the final plate of fifteen plate

model. These two cases may be further studied in relation to the four conditions of section 5.5, which are usually postulated for the successful application of SEA.

Referring to these two plates as the "best" and "worst" cases; in each of them, in all the models considered here, the weak coupling requirement is satisfied as proven by the low values of the energy ratios. Although there is no clear quantification of coupling strength in the literature, here a drop of 6 dB in the energy ratios (factor of 4) is considered to satisfy weak coupling requirement. The values of the other parameters: the modal overlap factor, M, the number of modes excited, N, and the reverberation parameter, *r*, are given for the best and worst case in Table 5.16 at the highest centre frequency.

Table 5.16

The modal overlap factor, number of modes excited, and reverberation factor for the best and worst models with centre frequency 20 kHz.

Case	M	N	*r*
Best	22.6	527	0.60
Worst	9.82	229	0.73

Although M and N for the best case are quite high, these values for the worst case are clearly well above the required limit, and both of the plates may be considered to be reverberant. Hence both the "best" and "worst" cases satisfy the aforementioned requirements. However the performance of SEA for the fifteen plate structure is extremely poor, while the WIA results are relatively accurate. The main reason for the poor performance of SEA can be put down to the diffuse wave field assumption, which is relaxed in the WIA approach.

It has already been shown [50] that the diffuse wave field assumption leads to an overestimate in the component which is next to the excited plate and an underestimate elsewhere. The present results confirm these findings: since the transmission coefficients are dependent on the wave

incidence angle, the wave energy becomes more and more "filtered" as it passes down the structure. Those waves which have a high transmission coefficient dominate the wave field, and the resulting energy flow is much greater than that predicted by SEA.

An additional four plate model in which the wave field is expected to be reasonably diffuse has also been studied. The structure, which has the same thicknesses as in case 2 of the box assembly, is depicted in Fig. 5.120. The dimensions and boundary orientation angles are randomly selected so that a wave will not come to the same point after travelling through other boundaries, which should result in a much more diffuse wave field.

Unfortunately, this structure can not be analysed by the exact method, and therefore only the predictions of WIA and SEA are presented in Figs. 5.121 to 5.123. In this figures "WIA, rectangular" refers to the results of an equivalent structure in which the plates are rectangular, but have the same area as in the irregular model.

The general impression from these figures is that the irregular geometry does make the wave field more diffuse, leading to closer agreement between SEA and WIA, particularly for plate 2. This example suggests that WIA can deal with the irregular geometry, although the lack of a validating exact analysis is unfortunate.

5.6.2 CLOSED SECTIONS.

Case 1 of the four plate closed section assembly is basically a symmetric structure in which each plate has the same thickness . The energy levels in plates 2 and 4 are therefore identical, as can be seen in Figs. 5.54 and 5.56. In plate 3 both SEA and WIA underestimate the exact results.

Much better predictions are yielded by the approximate methods for case 2 of the box assembly, which is formed by closing case 2 of the four plate row. It can be noted from Fig. 5.57.a that the response of the second plate is almost the same as for the open model, but the energy ratio of fourth plate is increased by about 5 dB. This is expected since

the final component is directly connected to the driven plate. In this component the discrepancy of SEA has been reduced to 0.05 dB which compares with the error of 4 dB in the open plate row. The improved SEA prediction is due to the fact that in a closed structure the wave field tends to become more diffuse.

5.6.3 COMPLEX-JUNCTION PLATE ASSEMBLIES.

The results for the complex-junction plate assemblies do not differ greatly from the previous cases. The effect of the number of junctions on the performance of SEA can be clearly observed in the results of the seven plate model, Figs. 5.66.a to 5.71.a.

For example, on the seventh plate of the complex-junction model the discrepancy at 20 kHz is about 4 dB, whereas on the equivalent plate of the eight plate model it is 16 dB, although the properties of the plates in both structure are more or less the same. The explanation of this phenomenon rests on the number of junctions that a wave energy travels through: in the present model a bending wave emanating from the excited plate encounters only three junctions before it reaches the seventh plate, but in the eight plate model there are twice as many junctions between the excited and penultimate plate.

5.6.4 STIFFENED PLATES.

As the main concern of this section is with bending only energy transmission, attention here is focused on the symmetrically stiffened plate rows.

As can be seen in Fig. 5.73, in plate 2 the SEA prediction lies well above the exact curve, and the overestimation is the highest of all the cases that have been discussed so far. However, WIA is fairly close to the exact results and the slight underestimation which were observed for the second plates of the other assemblies at the higher frequencies does not take place here.

In previous models, plate 3 was the component in which SEA began to underestimate at mid-range frequencies, but in this case such behaviour is not exhibited; rather it has been shifted to plate 4. A possible reason for this effect is that a significant amount of energy is transmitted to the second plate, and the energy flowing from plate 2 to plate 3 is higher than in the previous cases.

Throughout the structure at about 12 kHz, there is a dip in the curves predicted by all three methods, this being more marked towards the last plate. Up to this frequency the energy level gradually decreases, and then it starts to increase. Although the WIA results closely follow the trend of the exact results, the SEA curve does not rise after the dip, causing a very high discrepancy at 20 kHz. Fig. 5.77 shows that the underprediction at this frequency is around 16.5 dB. As explained in section 5.4.2, WIA behaves in a similar way to SEA, if an insufficient number of shape functions are used.

Figs. 5.124 to 5.129 compare the energy distributions as predicted by WIA and the exact method for case 1 of the symmetrically stiffened plates at 20 kHz. As can be more clearly observed from Figs. 5.128 and 5.129 WIA determines the angles of maximum energy transmission very accurately. The figures are constructed by relating the incidence angles of WIA to number of half wave lengths the in exact method: considering a bending wave incident at an angle θ (when θ is zero the wave is normally incident), the component of bending wave number along the junction may be written as

$$k = k_B \sin\theta$$

where k_B is the bending wave number, given by

$$k_{\mathrm{B}} = \left(\frac{\omega^2 \rho 12(1-\nu^2)}{Eh^2} \right)^{1/4} \tag{5.3}$$

Then the half-wavelength of the bending waves may take the form

$$\frac{1}{2}\lambda = \frac{\pi}{k_B \sin\theta} \tag{5.4}$$

For a junction with length b, the half-wavelength may be related to the number of half wave lengths, as

$$\frac{1}{2}\lambda = \frac{b}{n} \tag{5.5}$$

The energy values due to each n may be readily obtained in the exact method, and therefore, if desired, they may be converted to the angular energy distribution by relating n to $\sin\theta$, using the equations (5.4) and (5.5)

$$\sin\theta = \frac{n\pi}{bk_B} \tag{5.6}$$

Equation (5.6) was used for plotting the exact energy distribution curves in Figs. 5.124 to 5.129.

Case 2 for the stiffened panel corresponds to a periodic version of case 1. There is not much change in the general trend of the curves; there is about a 2 dB increase in amount of the energy transferred throughout the structure.

5.6.5 SUMMARY OF MAIN FINDINGS FOR BENDING ONLY CASES.

SEA and WIA exhibit the following trends for the structures that have been examined thus far:

(i). In the immediate vicinity of the excited plate, SEA always overestimates the mean response, while WIA is quite close to the exact results up to the mid-range frequencies, beyond which it slightly underpredicts the mean energy.

(ii). In the third plate of each structure, other than the closed and stiffened models, SEA initially overestimates the response, and then as the frequency increases it starts to underestimate. The predictions of WIA are rather accurate in this component, and regardless of the number of plates in the structure WIA usually follows the trend of the exact results. However in the periodic structures, for example case 2 of the fifteen plate assembly, WIA may yield quite poor predictions.

(iii). In structures which have many components that are connected in a row, the response is always underpredicted by SEA from the fourth plate onwards. The discrepancy is maximum at the highest one-third octave frequency in the furthest plate.

(iv). Since the wave field tends to become diffuse in box structures, the energy values predicted by SEA are fairly accurate.

(v). In complex-junction structures the predictions of SEA are more accurate than for flat plate assemblies with the same number of plates, since the extreme panels are separated by fewer junctions.

(vi). In the second plate of the symmetrically stiffened plate assembly, SEA is initially several decibels above the exact curve, meaning that the predicted energy flow is much greater than in the other models. This prevents the underprediction which usually occurs in the third plate. In later components however, the discrepancy is high, and SEA can not model the system accurately. Provided that enough Fourier components are used, WIA is capable of representing the true physical model with great accuracy. It can even determine the regions of maximum energy transmission as illustrated in Figs. 5.124-5.129.

(vii). Fulfilment of weak coupling, high modal overlap, many excited modes, and high reverberance does not guarantee the successful application of SEA.

5.7 THE EFFECT OF IN-PLANE VIBRATIONS.

5.7.1 GENERAL EFFECTS.

While the previous sections were concerned with pure bending energy transmission, in this section an assessment of effect of in-plane motion will be made. It should be emphasised that the energy ratios which are referred to as "full" in the graphs of section 5.2 are *not* the ratio of the total (sum of bending, longitudinal, and shear) energy of a particular plate in the system to the total energy of the excited plate; they are bending energy ratios for which the effects of in-plane motion have been fully accounted.

An obvious difference between the pure bending and the full graphs is that there is a reduction to a certain extent in the energy level of the plate which is next to the driven plate. This phenomenon may be observed in almost all of the cases considered in this study. A physical explanation of the observed trend is as follows: in the pure bending calculations it is assumed that a bending wave impinging on the junction is either partly reflected or transmitted to another bending wave in the neighbouring plate. On the other hand, if due allowance is made for the presence of in-plane waves, then some of the incident flexural wave energy will be converted into in-plane waves in the second plate. Therefore the amount of transmitted bending wave energy decreases in comparison to the pure bending case.

Having observed that there is a definite reduction in the bending energy level of the plate which is next to the excited one, the following question arises: "What are the factors that foster bending to in-plane conversion?" For instance, although the areas of the plates in cases 1 and 2 of the three plate assembly are the same, the difference in the predictions of the exact method between bending and full is 1.6 dB and 3.5 dB for case 1 and 2 respectively.

This can be explained by considering the bending and in-plane shear wavelengths: if the ratio of the shear to the bending wavelength (λ_S λ_B)

is much greater than unity, then clearly there will be very little in-plane motion generated. Snell's Law (see equation (4.12)) implies that for propagation of a wave from one component into another one, the tangential trace wavelengths of the two waves in these components have to be equal. Therefore there will be no bending to shear wave conversion at the junction if

$$\sin\theta > \frac{k_S}{k_B}.$$

The bending waves arriving at angles of incidence that satisfy the above inequality thus are totally reflected, and the angle θ is known as [28] the "critical angle" beyond which no transmission occurs. Obviously, as the ratio k_S/k_B decreases, the range of incidence angles at which there may be bending to in-plane transmission decreases as well.

Therefore the condition for significant in-plane conversion becomes

$$\frac{k_S}{k_B} \geq 1. \tag{5.7}$$

Using the definition of bending wavenumber from equation (5.3), and shear wavenumber from the following expression

$$k_S = \left(\frac{2\rho\omega^2(1+\nu)}{Eh}\right)^{1/2},$$

neglecting the contributions of $[12(1-\nu^2)]^{1/4}$ and $[2(1+\nu)]^{1/2}$, and assuming that the mass densities of the two plates are almost the same, then equation (5.7) may be rewritten as

$$\frac{k_S}{k_B} \approx \omega^{1/2}\left(\frac{\rho}{E}\right)^{1/4}\left(\frac{h_1}{h_2}\right)^{1/2} \geq 1.$$

Here h_1 and h_2 are respectively the thicknesses of the plates on which the bending wave emanates and the in-plane waves are generated. The

in-plane longitudinal wave is encompassed by this equation, since the longitudinal wave number k_L is less than k_S.

The above result shows that bending to in-plane conversion is directly proportional to the square root of the frequency of excitation and the ratio h_1/h_2. This explains why the in-plane effect is greater in case 2: in case 1 all the plates have the same thickness and there is little in-plane transmission, while in case 2 there is a reduction in the plate thickness, leading to the generation of in-plane waves.

An examination of the transmission coefficients shown in Fig. 5.130, confirms that the degree of conversion of bending waves in the source plate to in-plane waves in the adjoining component is strongly dependent on the thickness ratio of these plates. Fig. 5.130.a shows the in-plane shear wave transmission coefficient from plate 1 to 2 at a corner junction with respect to incident angle when a bending wave is incident to the junction. To show the degree of transformation vividly, the coefficients are presented for three different h_1/h_2 ratios at a constant frequency, and Fig. 5.130.b presents transmission coefficients for longitudinal waves under similar conditions. The bending wave energy transmission coefficient is not independent of frequency when the in-plane waves are taken into account.

5.7.2. PLATE ASSEMBLIES.

Referring to Figs. 5.2.b to 5.7.b, it can be seen that in the second component of the three plate models SEA captures the behaviour of the exact curve: with increasing frequency there is a decrease in the energy flow from the excited plate. However it still exhibits the same tendency as in the pure bending case, overestimating across the frequency range, although the amount of overestimation has been reduced fractionally. The underestimation which is observed at high frequencies in the WIA predictions has also been reduced. This is particularly evident in plate 2 of case 2 where there is about 1.2 dB difference between the exact results and WIA for the pure bending case, while in the full case this reduces to 0.07 dB.

In the third plate of the first two cases of the three plate model the exact results for the full model again show a lower energy level than for the bending only model. This is more marked in case 2 than in case 1, due to the further reduction in the plate thickness from plate 2 to 3. On the other hand, in case 3 of the same model the full energy ratio of the last plate is higher than for pure bending. This is due to the conversion of plate 2 in-plane waves into bending waves in the thicker plate 3. These trends are closely followed by the approximate methods.

In the plates two and three of the four plate models, all three methods exhibit a behaviour similar to that of three plate assemblies, depending on whether thickness increases or decreases down the structure.

However in the fourth plate, for all three cases the full analysis leads to an increase in the response regardless of the thickness of the plate. As an example in case 2, the increase in the results of the exact, SEA, and WIA at 20 kHz are 2.27, 3.94, and 1.93 dB respectively.

A further comparison between the exact and the WIA results can be made from Figs. 5.131-5.134 which show the energy distribution as predicted by two methods for case 2 of the four plate assembly at 20 kHz. As can be seen, WIA does not give the fine details of the peaks which occur in the exact results, but rather it yields a smooth envelope: similar curves as in the case of stiffened plates would have been obtained (Figs. 5.124-5.129) if many shape functions have been employed. The two WIA curves shown in the Figs. 5.132 and 5.133 correspond to the ranges $0<\theta<\pi/2$ and $\pi/2<\theta<\pi$, which are not distinguished by the exact method. It can be seen WIA gives a reasonable, smoothed, estimate of the energy distribution.

An examination of the energy ratios of the eight plate assembly (Figs. 5.18.b to 5.24.b) reveals that the response of the plates which are close to the source plate conform to the observations made for previous assemblies. From the fifth plate onwards, the energy predictions for the full model are always greater than for the bending only model. The agreement between the exact and the approximate methods is closer for the full model. For instance in the final plate at 20 kHz it is already

known that bending only SEA underestimates by about 18 dB; however with the inclusion of in-plane waves this discrepancy reduces to 13 dB. For the same case bending only WIA overpredicts 2.7 dB, yet in the full case this drops to 1.4 dB.

Similar observations can be made for case 1 of the fifteen plate assembly: moving away from the excited plate the energy increases; by the time wave types reached to the fifteenth component, they have travelled through fourteen junctions. On this plate even at mid range frequencies the increase in the full bending energy level, in comparison to pure bending energy results, is quite high as illustrated in Fig. 5.135. Figure shows the difference between the bending only and the full results, as given by the exact method for the last plate of the various models, as a function of the average number of in-plane modes per component. The horizontal axis in this figure is effectively a scaled form of frequency. As can be seen there are two main factors that lead to an increase in the energy transmission: the number of junctions in the system, and the number of in-plane modes excited. Even though the average number of in-plane modes in the four plate structure is almost three times that in the fifteen plate structure, the latter structure displays a much greater change in the energy transmission, due to the increased number of junctions.

If attention is focused on the remote components for case 1 of the fifteen plate model, it can be observed that both SEA and WIA exhibit similar trends to the exact results: the effect of the in-plane waves increases as the plate becomes more remote. Further the difference between the exact and the approximate methods decreases when in-plane effects are present. This is shown in Table 5.17, where the difference between the energy ratios of the exact and the approximate of the last five plates and the reduction in the discrepancies relative to pure bending case at the highest centre frequency are presented.

Table 5.17

The discrepancy (dB) *between the exact and the approximate methods after the inclusion of in-plane waves, and reduction relative to pure bending discrepancies.*

Case 1

	dB range		Reduction (dB)	
Plate	SEA	WIA	SEA	WIA
11	23.46	0.40	17.72	8.42
12	26.25	0.94	17.46	7.68
13	32.25	0.53	13.83	6.68
14	35.72	0.07	15.59	7.66
15	40.37	0.51	14.06	6.26

Although in both approximate methods the discrepancies have been reduced substantially in comparison to the pure bending case, and the two curves are shifted towards the exact results, the effect of in-plane energy transmission on SEA and WIA are not the same: the WIA results come much closer to the exact results.

An understanding of what is happening can be obtained comparing the in-plane energies which are predicted by the various methods. These results are shown in Table 5.18 for 20 kHz; the in-plane energy of a particular plate due to a particular method has been divided by the bending energy of the source plate. The differences between the exact and approximate methods are shown, so that a value which is close to zero implies good agreement with the exact method.

Table 5.18

In-plane longitudinal and shear energy ratios (dB) *of* WIA *and* SEA *to exact for the last five plate of case 1 of the fifteen plate assembly.*

	Longitudinal		Shear	
Plate	SEA	WIA	SEA	WIA
11	-34.62	-6.45	-34.15	-4.80
12	-36.19	-4.11	-36.10	-2.91
13	-39.06	-3.06	-39.50	-1.77
14	-46.86	-5.72	-46.71	-4.27
15	-46.21	-2.58	-48.15	-1.44

An important observation which can be made from the table is that as the plate becomes further from the source plate the deviation of SEA from the exact results becomes worse. The reason for this phenomenon must lie in the diffuse wave field assumption, as WIA yields much improved results. As mentioned in the previous sections, the diffuse wave field assumption overpredicts the energy flow from the source plate to the connecting plate, tends to underpredict the energy flow for subsequent junctions. A similar problem occurs in the presence of in-plane waves: it is known that the majority of conversion from bending to in-plane waves takes place when a bending wave is heading towards a junction at normal or near to normal angles. Since only a small amount of energy is incident at such angles in SEA, the bending to in-plane conversion is underestimated, and thus in later junctions the in-plane to bending conversion can not be modelled properly, thus resulting in a large deviation from the exact results.

5.7.3 CLOSED SECTIONS.

In both cases of the box structure the in-plane energy transmission reduces the bending energy in plates 2 and 4 since they are directly connected to the excited plate. As in the previous models, WIA is much more sensitive to the presence of in-plane waves, and rapidly converges towards the exact curve.

In the third plate for the symmetric assembly (case 1, Fig. 5.55) where the exact curve was much higher than WIA and SEA curves for pure bending, here there is about 2 to 3 dB reduction in the results of the exact method, and therefore the predictions of the approximate methods seem to be improved.

In the third plate of case 2, SEA has improved relative to the pure bending case: the characteristic underestimation at mid-range frequencies has disappeared. It predicts a response around 1 dB above the WIA results across the frequency range.

5.7.4 COMPLEX-JUNCTION PLATE ASSEMBLIES.

When the four plate complex-junction results which are presented in Figs. 5.63.b to 5.65.b are examined, conclusions akin to the four plate assembly of section 5.7.2 may be drawn. The only difference is: in the third plate SEA does not underestimate up to the last two one-third octave band frequencies, it then slightly underpredicts.

In the seven plate model, the contributions of in-plane vibrations are highly significant in the last two plate (Figs. 5.70.b and 5.71.b), as can also be observed from the Fig. 5.135, the difference between the pure bending and the full results as given by the exact method is as high as fifteen plate assembly in the last plate. However in the plates which are close two the excited plate, the effect of in-plane vibrations is similar to previously studied assemblies.

An explanation of the observed trend is made by Lyon [48] in the context of statistical energy analysis of ship structures. He shows that the increase in transmissibility caused by in-plane waves becomes more important as the distance from driven plate is increased in such structures. The in-plane waves act as "flanking-paths" for flexural wave energy, and generate more marked effects because of multiple junctions. As can be seen in Fig. 5.62, in-plane waves in plate 5 may be converted into bending waves in plates, thus giving a flanking path.

It is interesting to note that in-plane energy transmission increases the mean response of the final plate by almost the same amount in all methods at the highest centre frequency. That is, the differences between the pure bending results and the full results as yielded by the exact, SEA and WIA methods are respectively 17.5, 19, and 18 dB.

5.7.5 STIFFENED PLATES.

In the asymmetrically stiffened plates it is found that the energy predictions of all three methods decrease down the structure compared to case 1 of the symmetrically stiffened plate assembly. This is not thought to be due to in-plane waves but, rather the high torsional stiffness of the asymmetric stringer. In both the symmetrical and asymmetrical models the dimensions of the stringers are the same, but in the latter model the stringers are attached at the tip, and thus the torsional stiffness with respect to attachment point is large. This resists bending energy transmission from one plate to another at the junction.

If a comparison is made between the exact and approximate methods, there is no change in the typical underestimation characteristics of SEA at the higher frequencies and in remote plates. Although the accuracy of WIA is very good; as many as forty Fourier terms were required to achieve these results.

5.7.6 SUMMARY OF MAIN FINDINGS FOR IN-PLANE INCLUSIVE CASES.

From the foregoing results the following points arise regarding the effects of in-plane vibrations:

(i). In the component which is directly connected to the excited plate there is a reduction in the bending energy compared to the pure bending calculations, since some of the bending waves in the source plate are transmitted as in-plane waves in the adjoining plate.

(ii). Although in the third component of some of the models the energy ratio may increase or decrease depending on the thickness of this plate, from the fourth/fifth plate onwards the energies increase regardless of the thickness of the plates.

(iii). There are three main factors which affect the in-plane to bending wave conversion: **(a)** the number of in-plane modes excited, **(b)** the number of junctions in the structure, **(c)** the number of plates at each junction. The last two factors are particularly influential. Broadly speaking, once bending waves are converted to in-plane waves, after travelling through a couple of junctions, they dominate the energy transmission. The further a plate lies from the source plate, the greater the increase in energy arising from including in-plane vibrations.

(iv). In general both SEA and WIA follow the trends of the exact results in the presence of in-plane waves.

(v). The fact that there are more excited modes in the system when the in-plane motion is taken into consideration, means that the WIA predictions are even more accurate for this case than for the bending only case. The method improves with increasing frequency, where for example the slight underprediction which is seen in the second components disappears. Regardless of the type of the structure, the results yielded by WIA tend to be conservative.

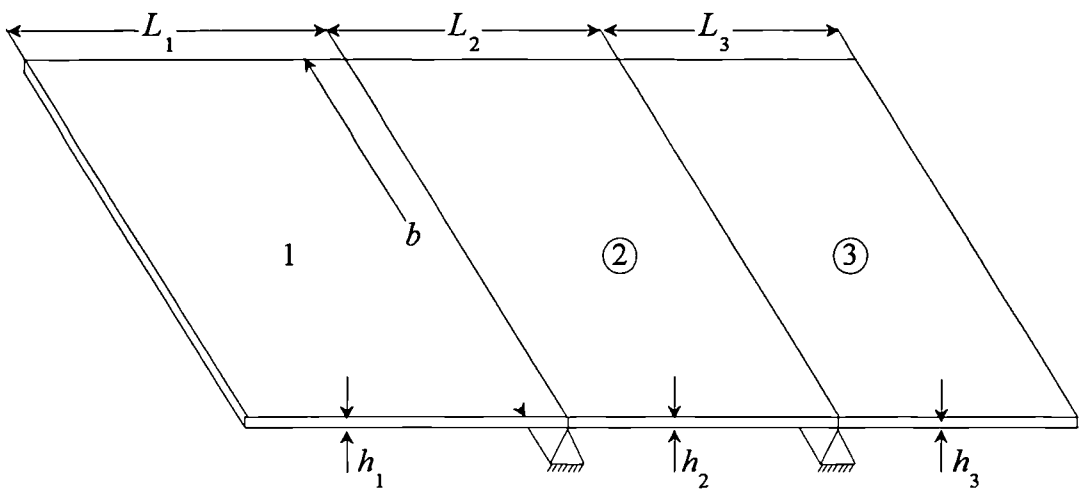

a)

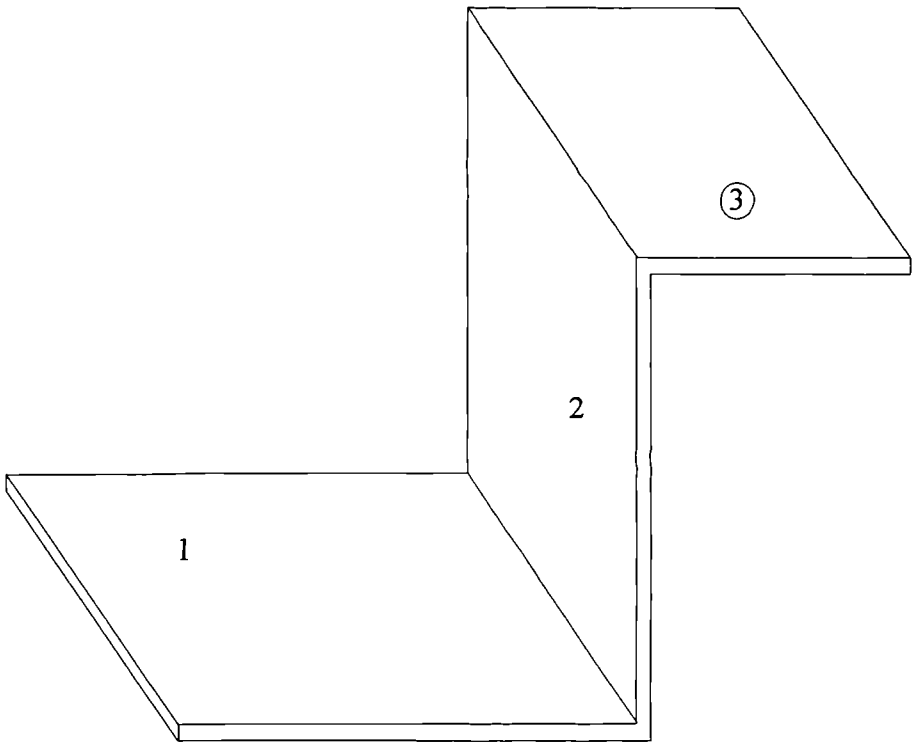

b)

Fig. 5.1 Three plate assembly
a) Bending model
b) In-plane model

Three Plate Assembly
Third Octave Band Energy Ratio
Plate 2, Case 1

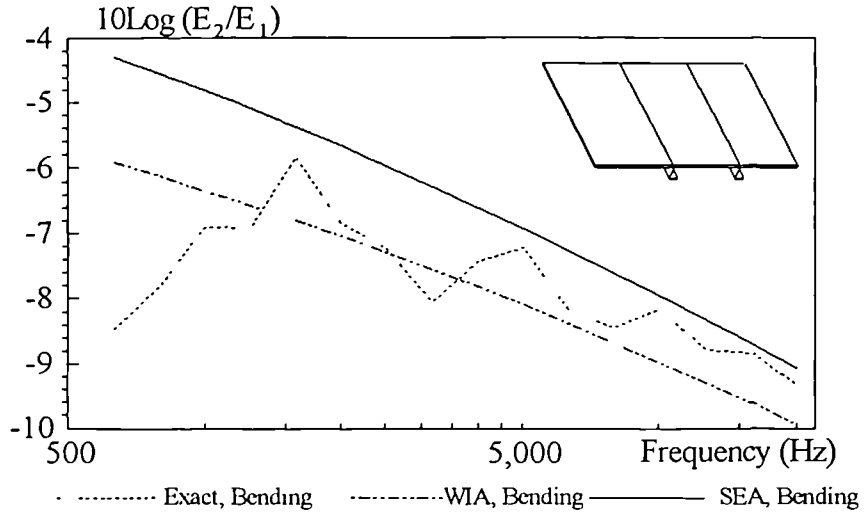

Fig. 5.2.a

Three Plate Assembly
Third Octave Band Energy Ratio
Plate 2, Case 1

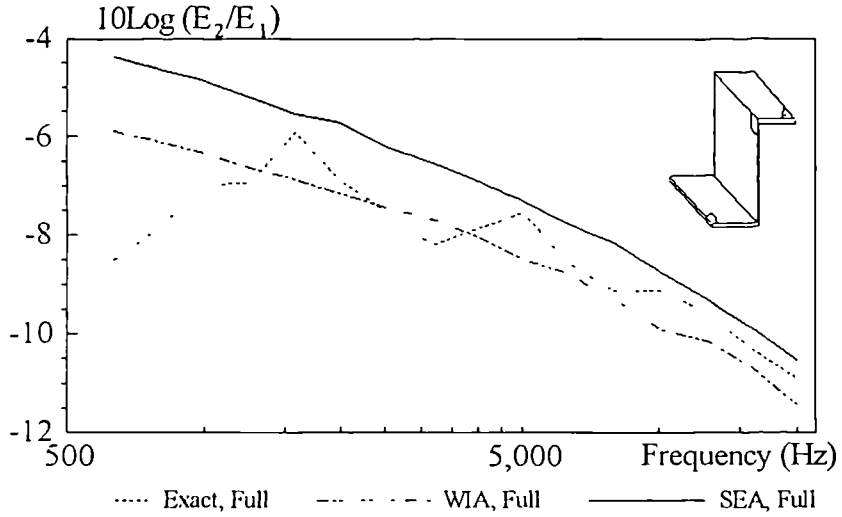

Fig. 5.2.b

Three Plate Assembly
Third Octave Band Energy Ratio
Plate 3, Case 1

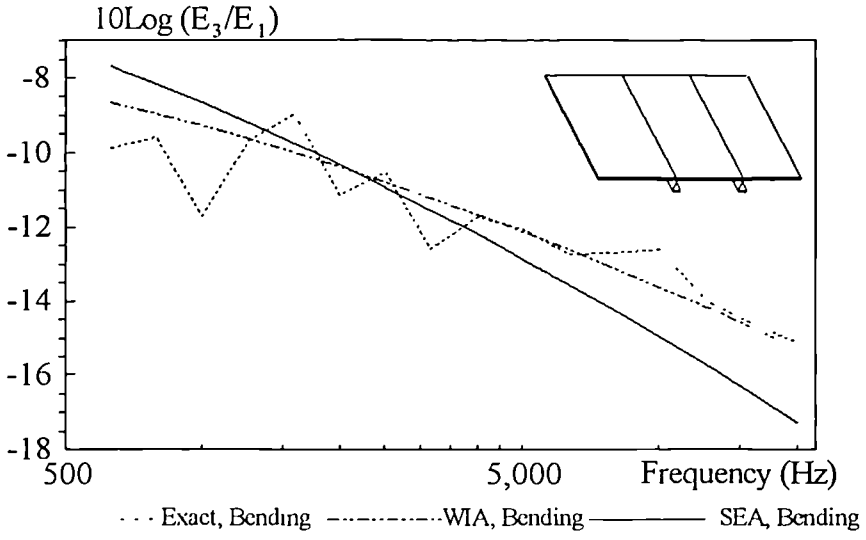

Fig. 5.3.a

Three Plate Assembly
Third Octave Band Energy Ratio
Plate 3, Case 1

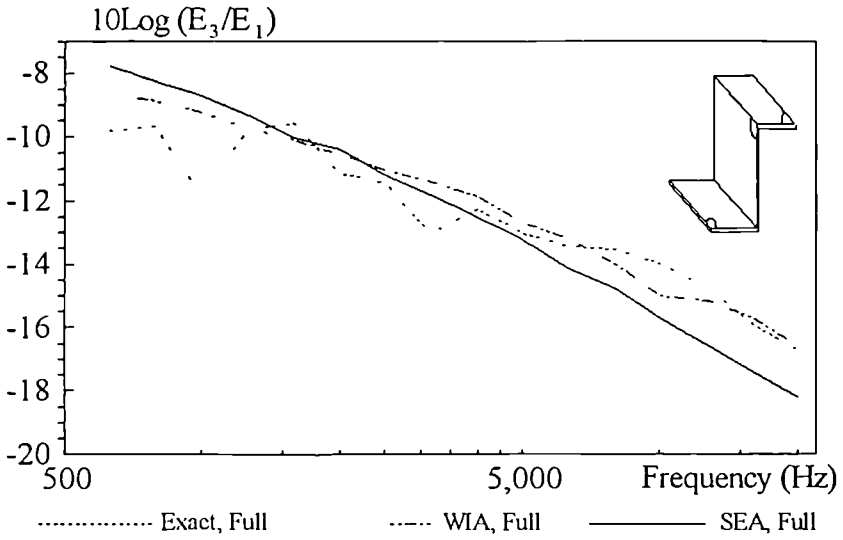

Fig. 5.3.b

Three Plate Assembly
Third Octave Band Energy Ratio
Plate 2, Case 2

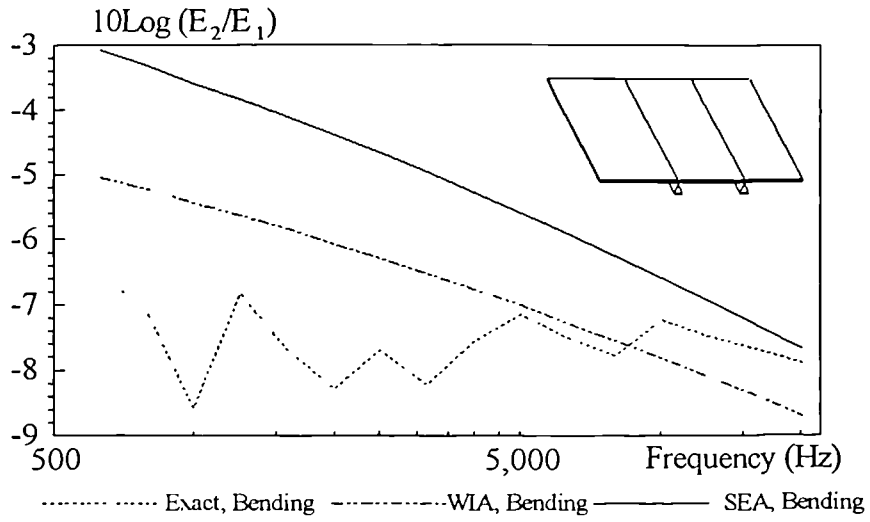

Fig. 5.4.a

Three Plate Assembly
Third Octave Band Energy Ratio
Plate 2, Case 2

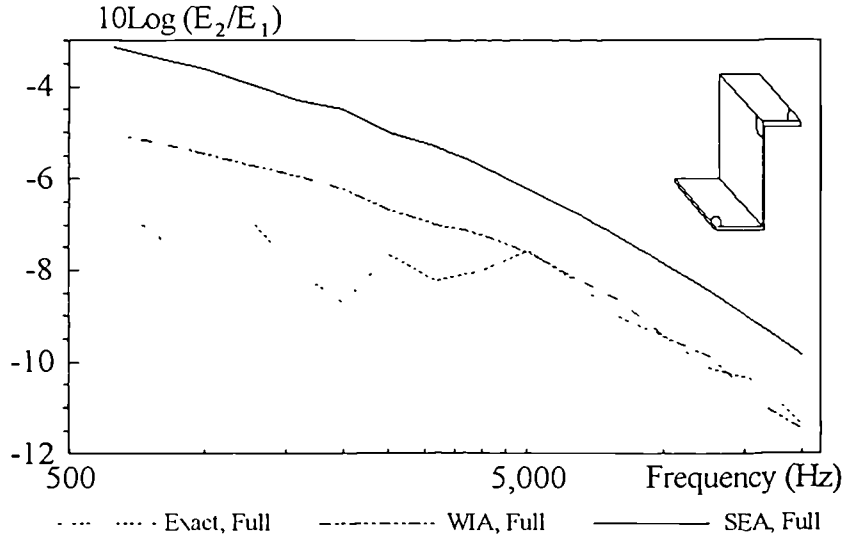

Fig. 5.4.b

Three Plate Assembly
Third Octave Band Energy Ratio
Plate 3, Case 2

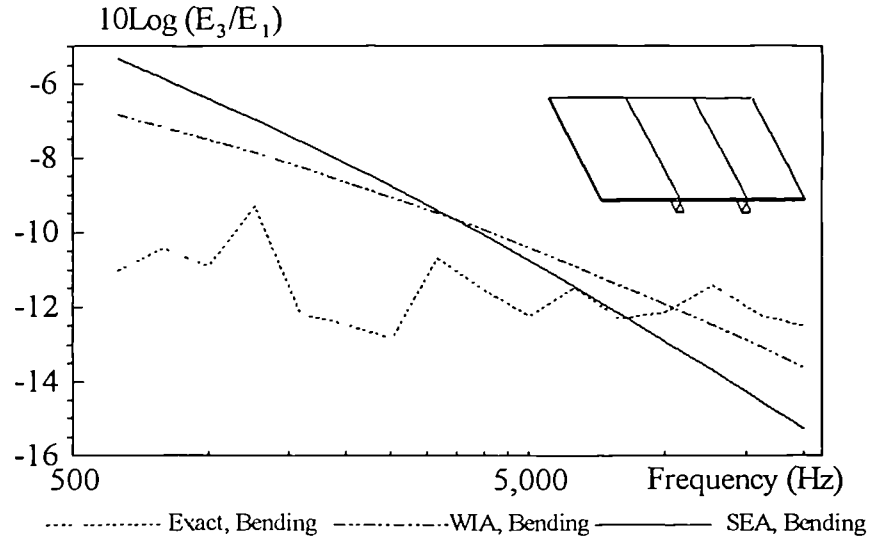

Fig. 5.5.a

Three Plate Assembly
Third Octave Band Energy Ratio
Plate 3, Case 2

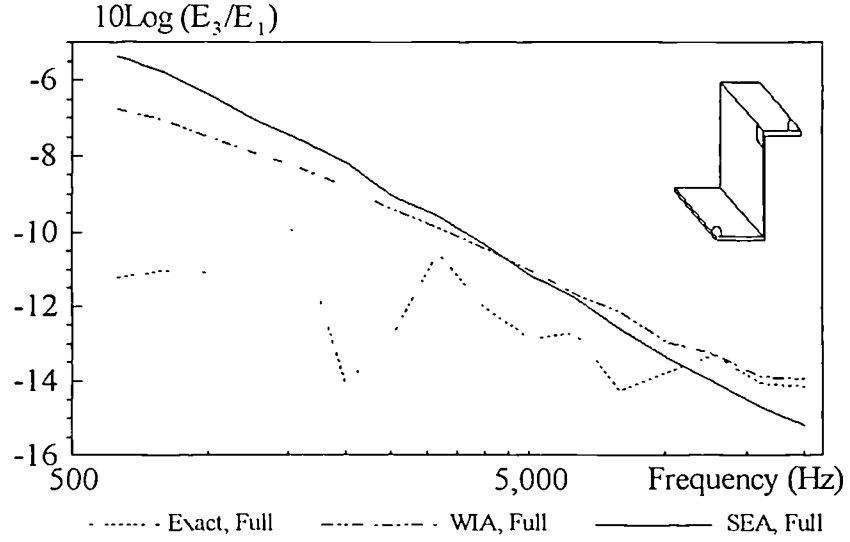

Fig. 5.5.b

Three Plate Assembly
Third Octave Band Energy Ratio
Plate 2, Case 3

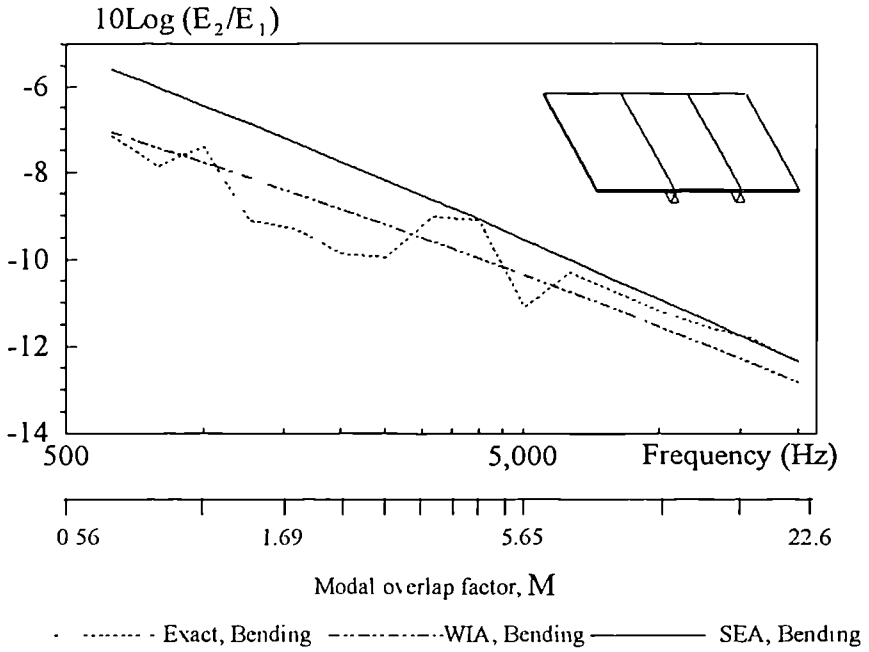

Fig. 5.6.a

Three Plate Assembly
Third Octave Band Energy Ratio
Plate 2, Case 3

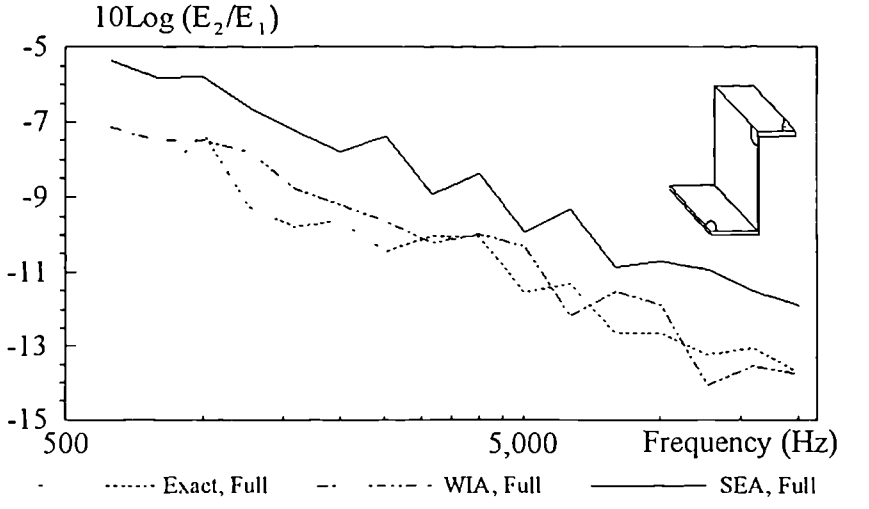

Fig 5.6.b

Three Plate Assembly
Third Octave Band Energy Ratio
Plate 3, Case 3

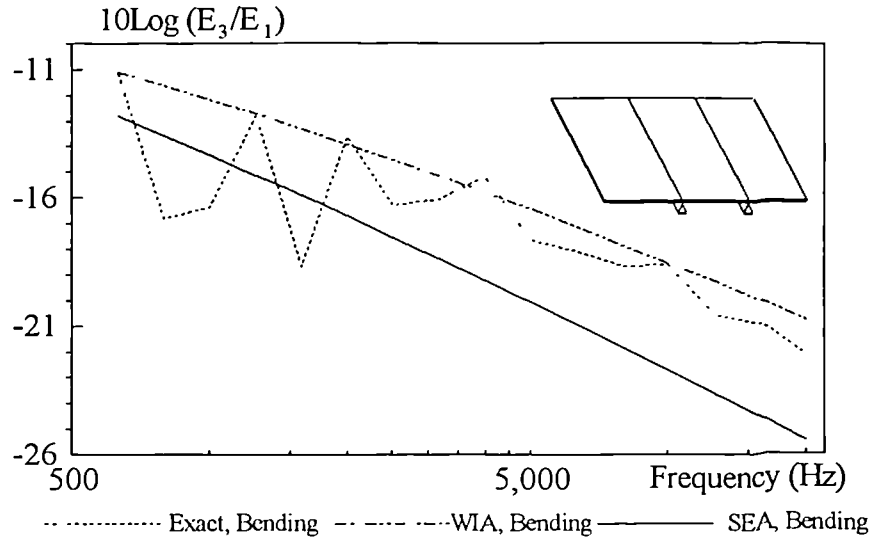

Fig. 5.7.a

Three Plate Assembly
Third Octave Band Energy Ratio
Plate 3, Case 3

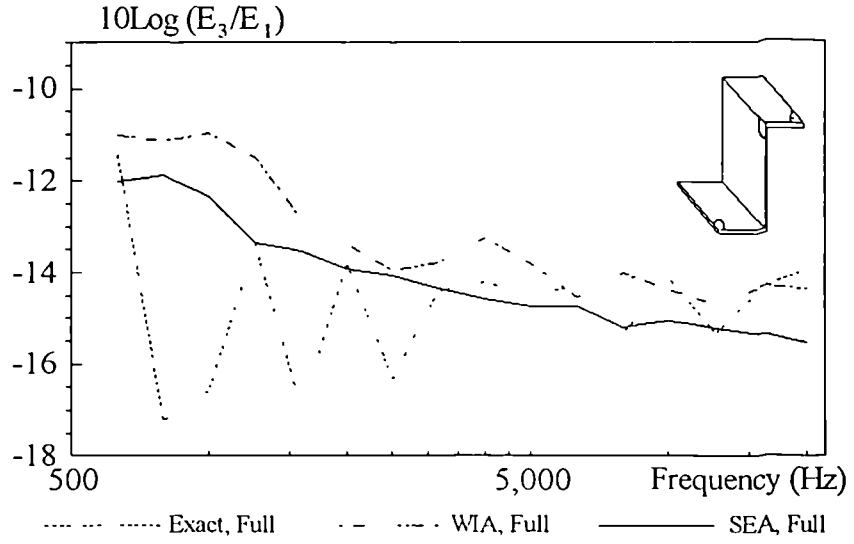

Fig. 5.7 b

Four Plate Assembly
Third Octave Band Energy Ratio
Plate 2, Case 1

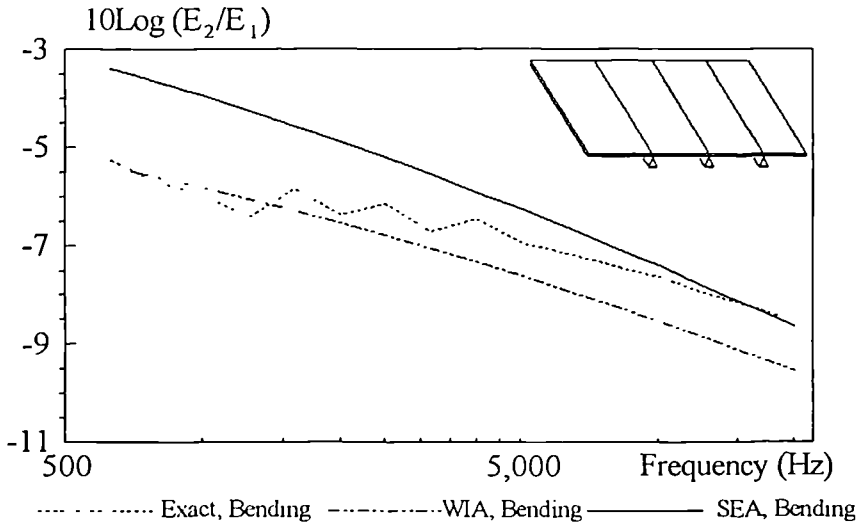

Fig. 5.8.a

Four Plate Assembly
Third Octave Band Energy Ratio
Plate 2, Case 1

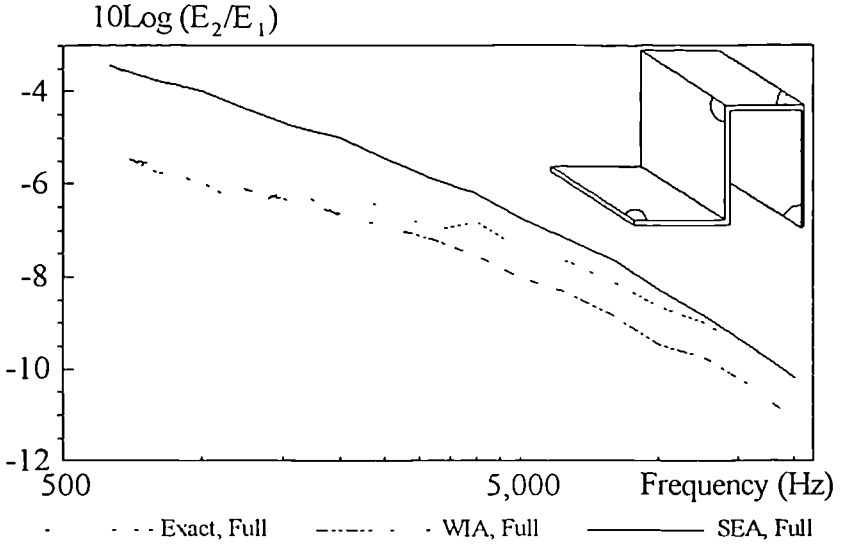

Fig 5.8.b

Four Plate Assembly
Third Octave Band Energy Ratio
Plate 3, Case 1

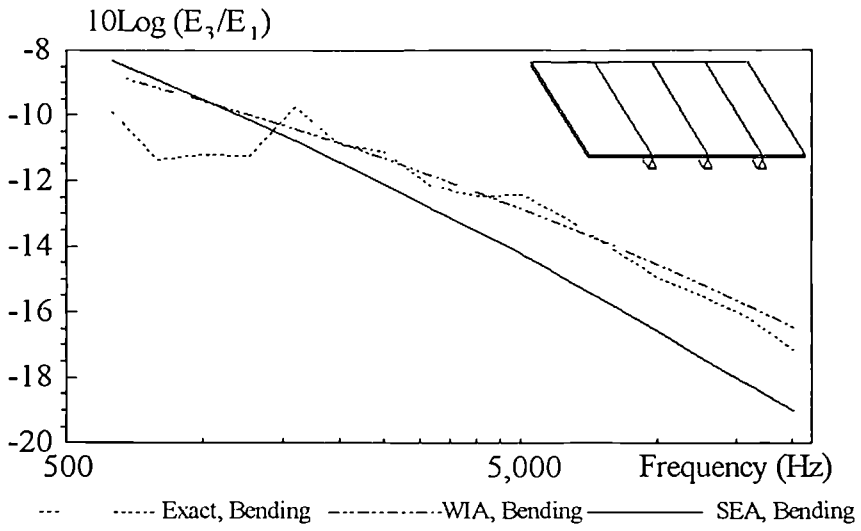

Fig. 5.9.a

Four Plate Assembly
Third Octave Band Energy Ratio
Plate 3, Case 1

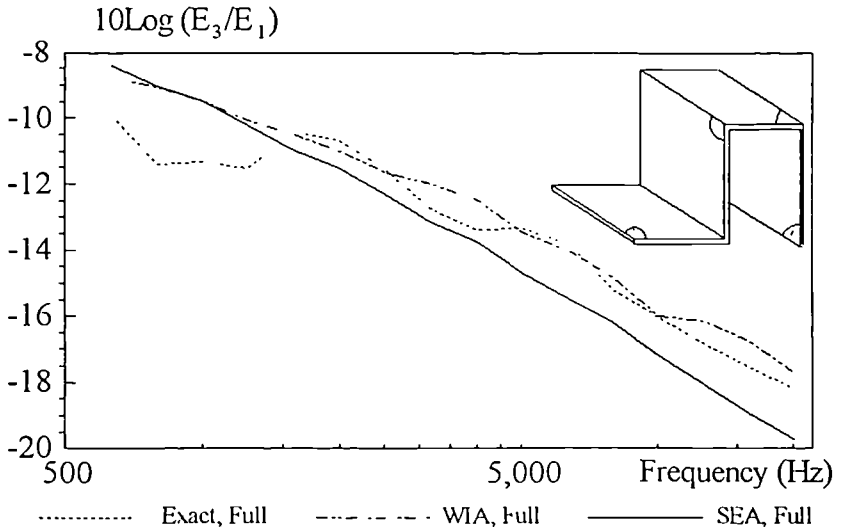

Fig. 5.9.b

Four Plate Assembly
Third Octave Band Energy Ratio
Plate 4, Case 1

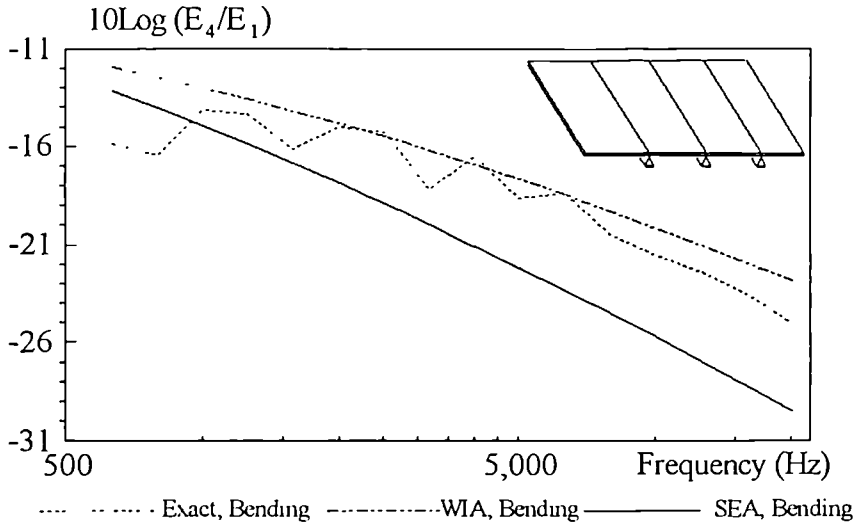

Fig. 5.10.a

Four Plate Assembly
Third Octave Band Energy Ratio
Plate 4, Case 1

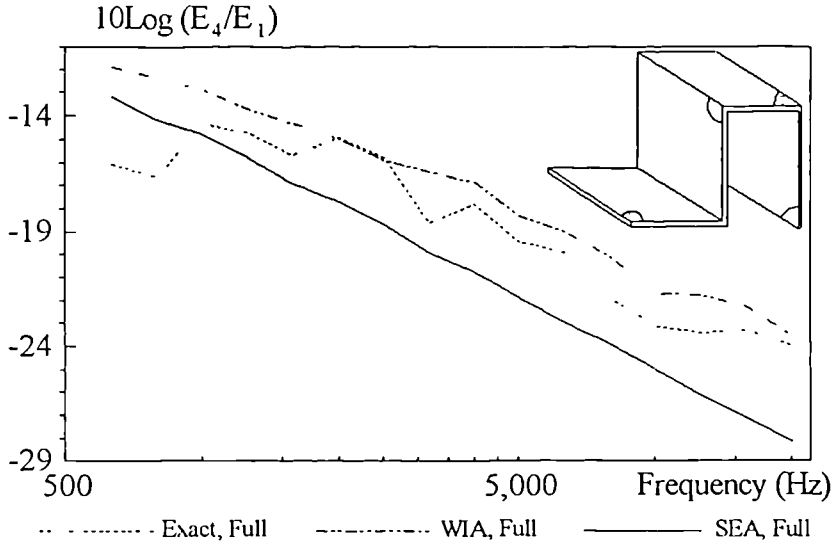

Fig. 5.10.b

Four Plate Assembly
Third Octave Band Energy Ratio
Plate 2, Case 2

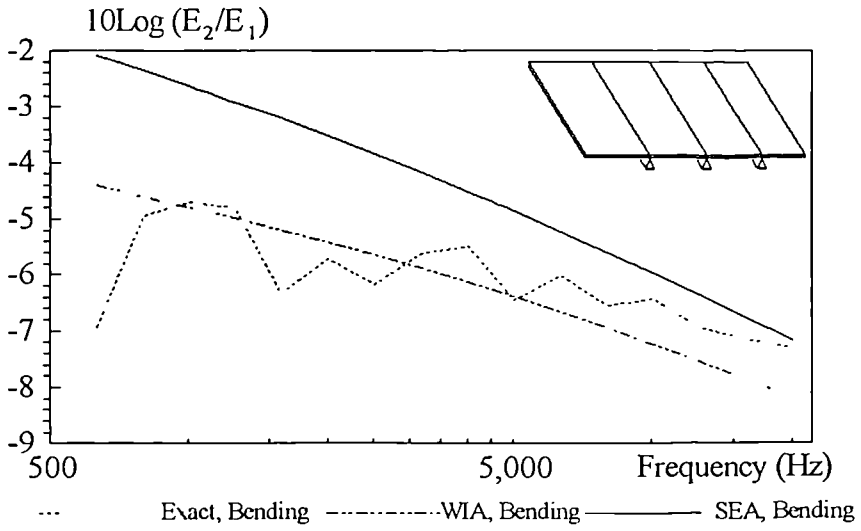

Fig. 5.11.a

Four Plate Assembly
Third Octave Band Energy Ratio
Plate 2, Case 2

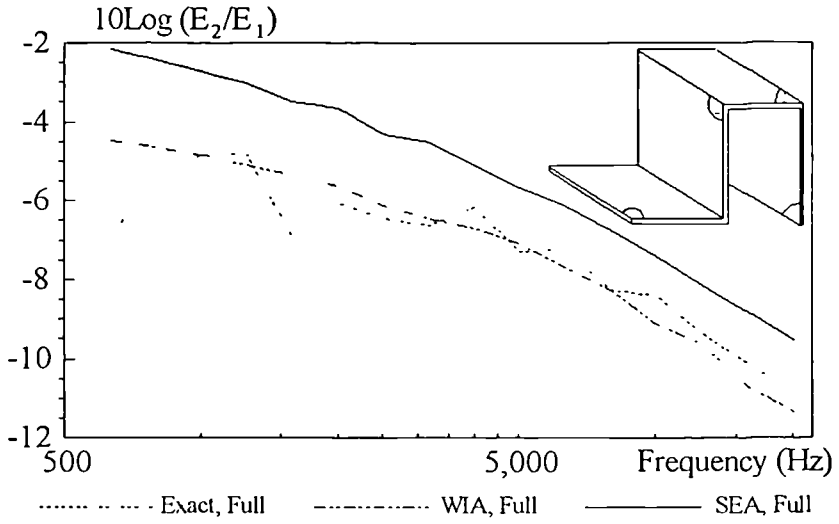

Fig. 5.11.b

Four Plate Assembly
Third Octave Band Energy Ratio
Plate 3, Case 2

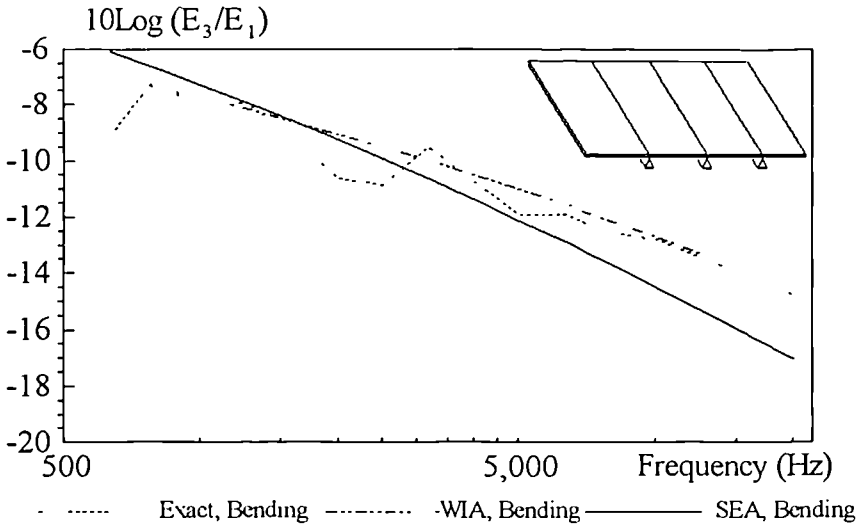

Fig. 5.12.a

Four Plate Assembly
Third Octave Band Energy Ratio
Plate 3, Case 2

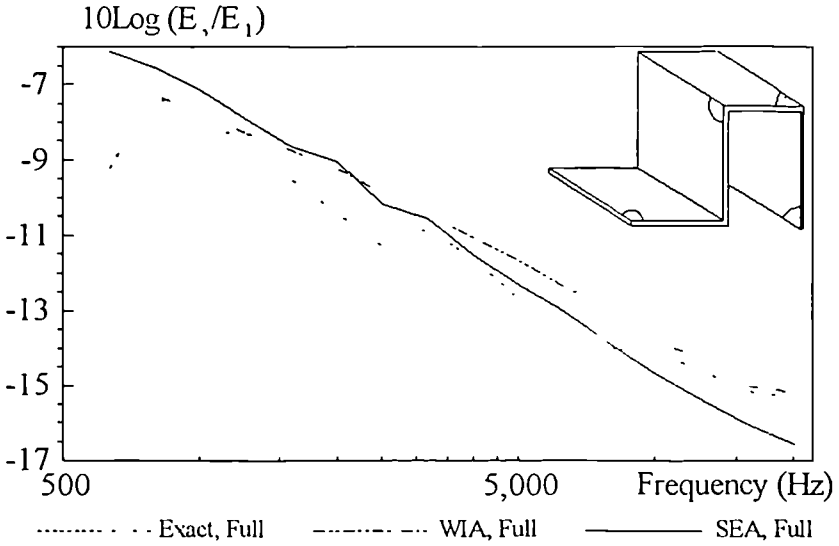

Fig. 5.12.b

Four Plate Assembly
Third Octave Band Energy Ratio
Plate 4, Case 2

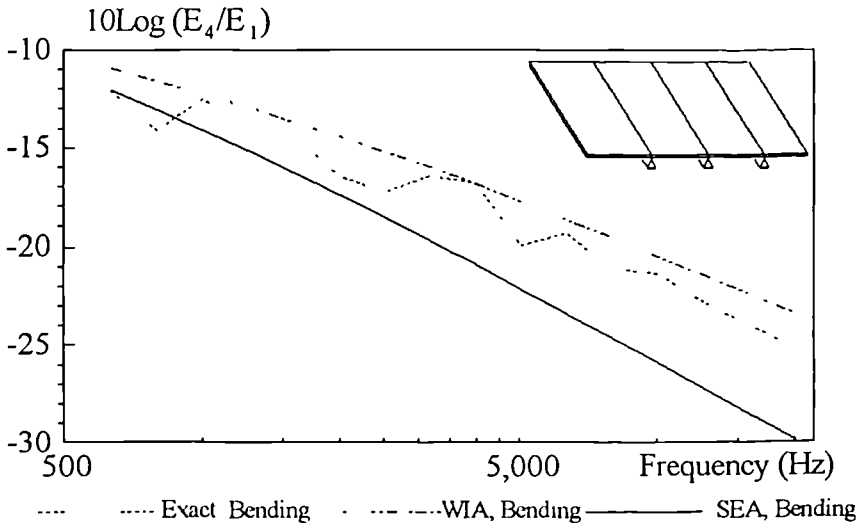

Fig. 5.13.a

Four Plate Assembly
Third Octave Band Energy Ratio
Plate 4, Case 2

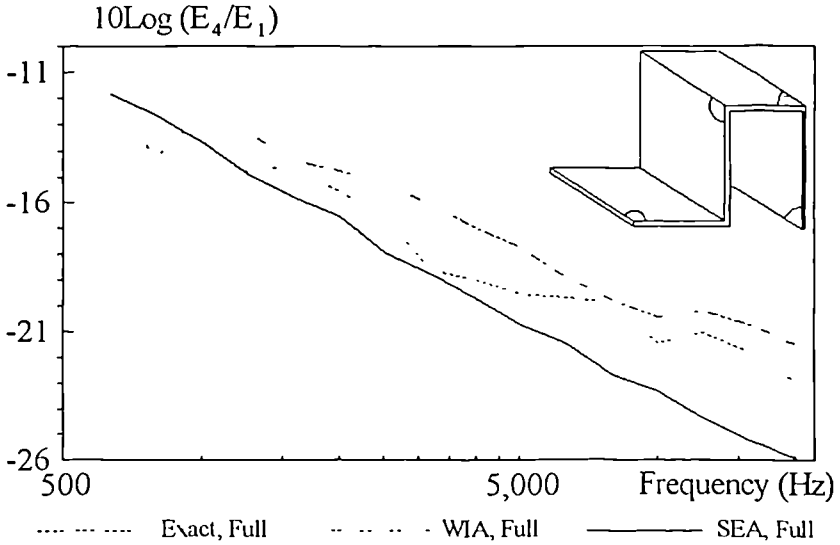

Fig. 5.13.b

Four Plate Assembly
Third Octave Band Energy Ratio
Plate 2, Case 3

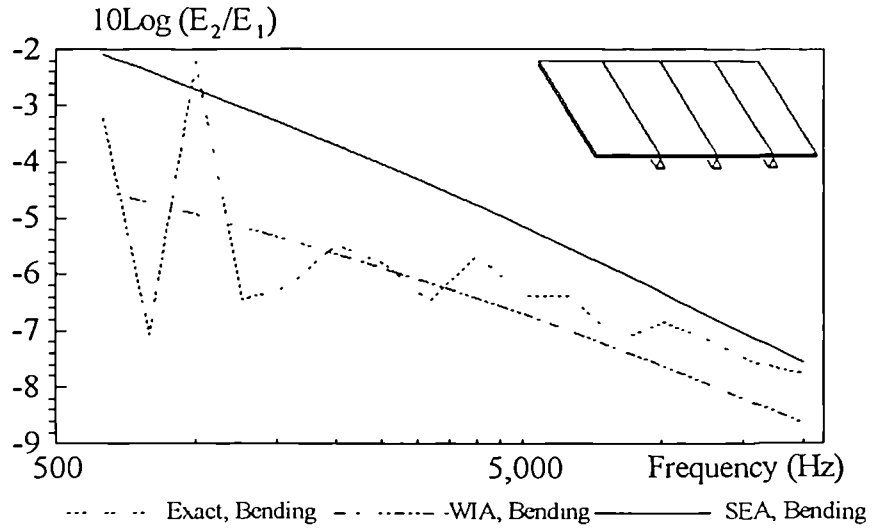

Fig. 5.14 a

Four Plate Assembly
Third Octave Band Energy Ratio
Plate 2, Case 3

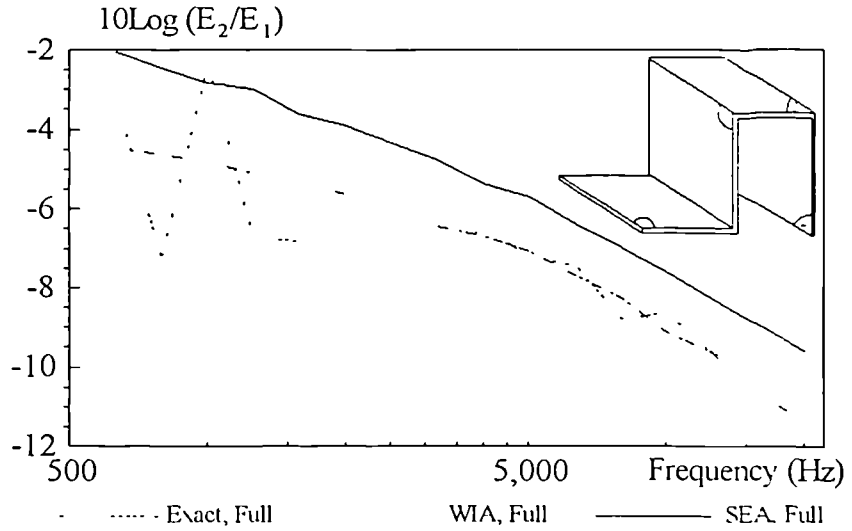

Fig 5.14.b

Four Plate Assembly
Third Octave Band Energy Ratio
Plate 3, Case 3

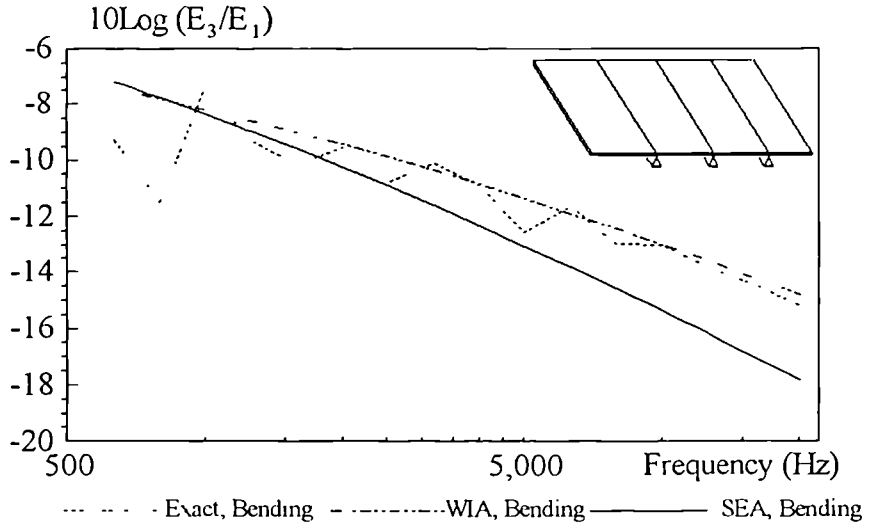

Fig. 5.15.a

Four Plate Assembly
Third Octave Band Energy Ratio
Plate 3, Case 3

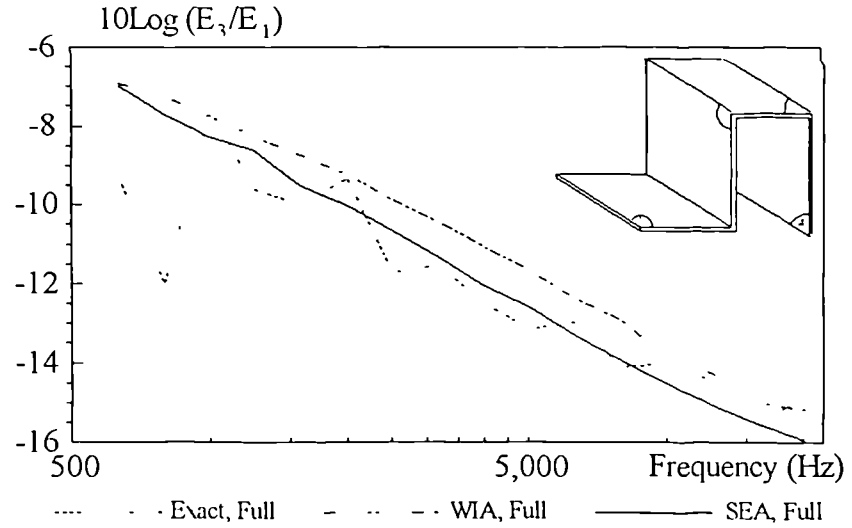

Fig. 5.15.b

Four Plate Assembly
Third Octave Band Energy Ratio
Plate 4, Case 3

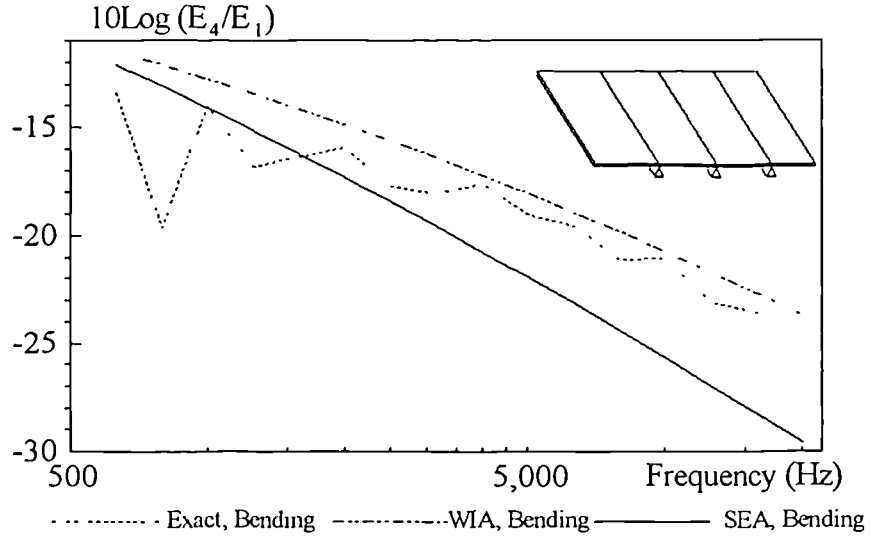

Fig. 5.16.a

Four Plate Assembly
Third Octave Band Energy Ratio
Plate 4, Case 3

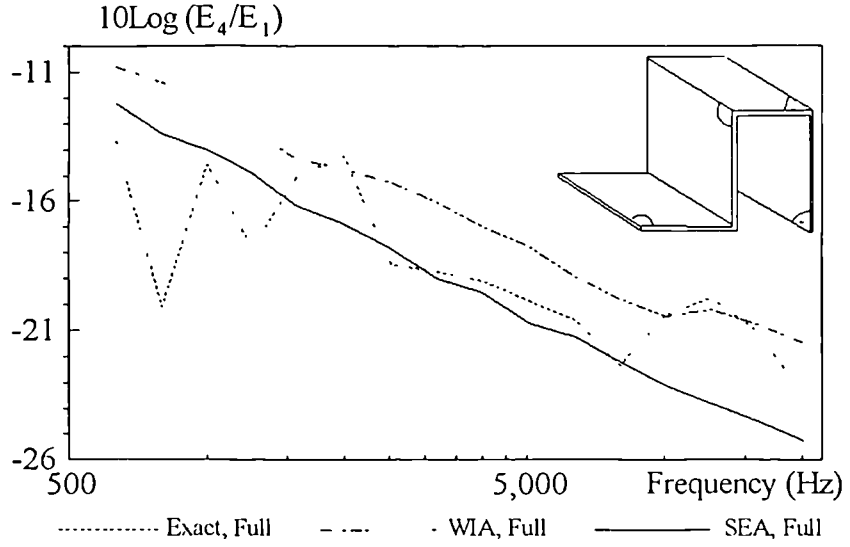

Fig. 5.16.b

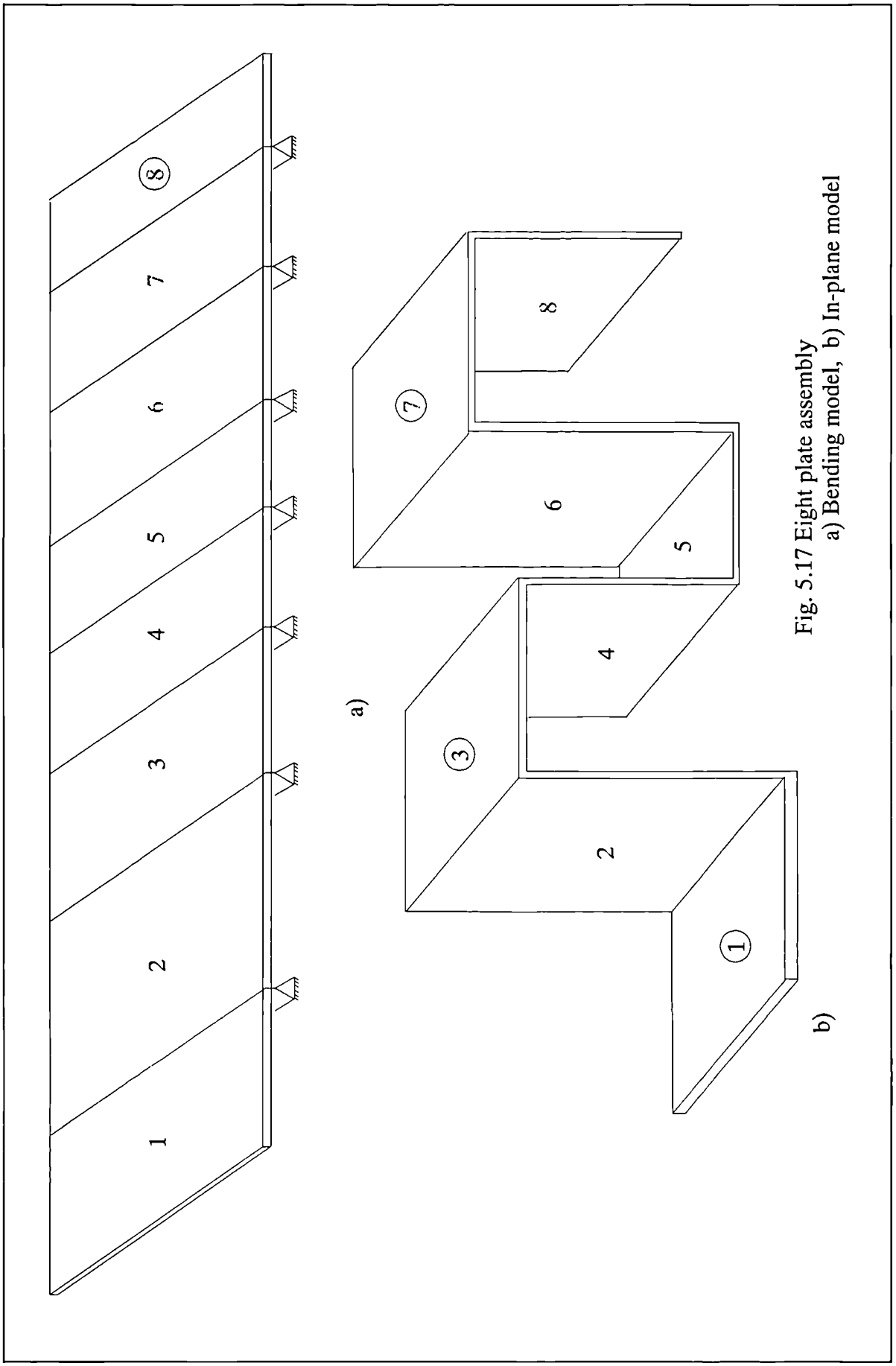

Fig. 5.17 Eight plate assembly
a) Bending model, b) In-plane model

Eight Plate Assembly
Third Octave Band Energy Ratio
Plate 2

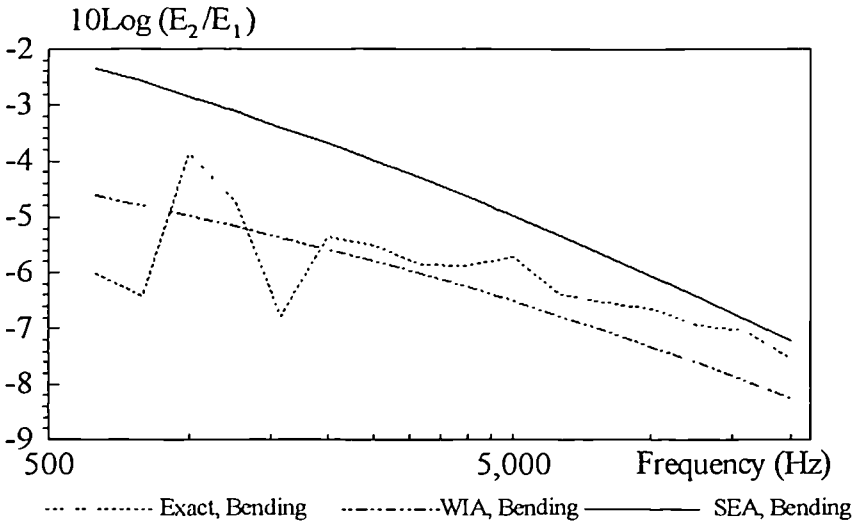

Fig. 5.18.a

Eight Plate Assembly
Third Octave Band Energy Ratio
Plate 2

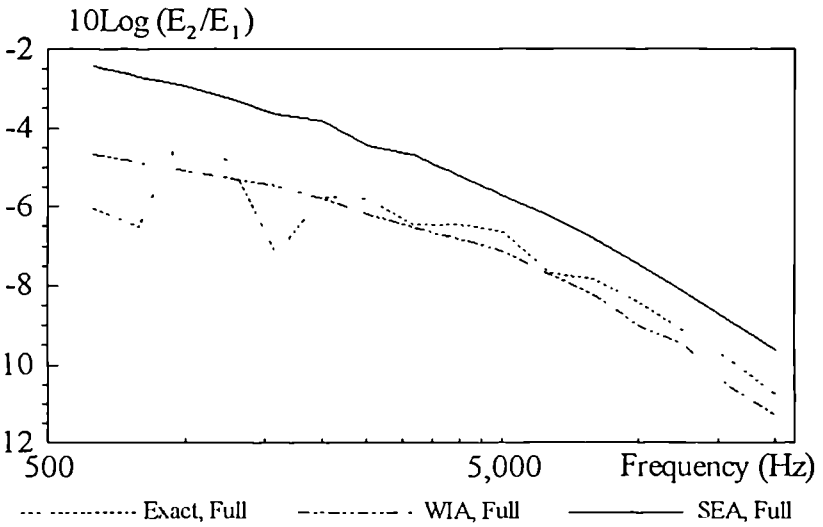

Fig. 5.18.b

Eight Plate Assembly
Third Octave Band Energy Ratio
Plate 3

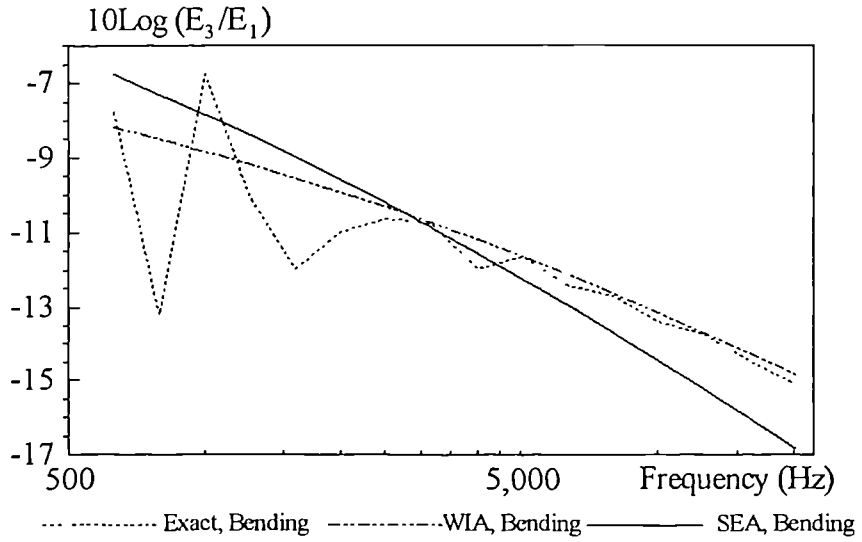

Fig. 5.19.a

Eight Plate Assembly
Third Octave Band Energy Ratio
Plate 3

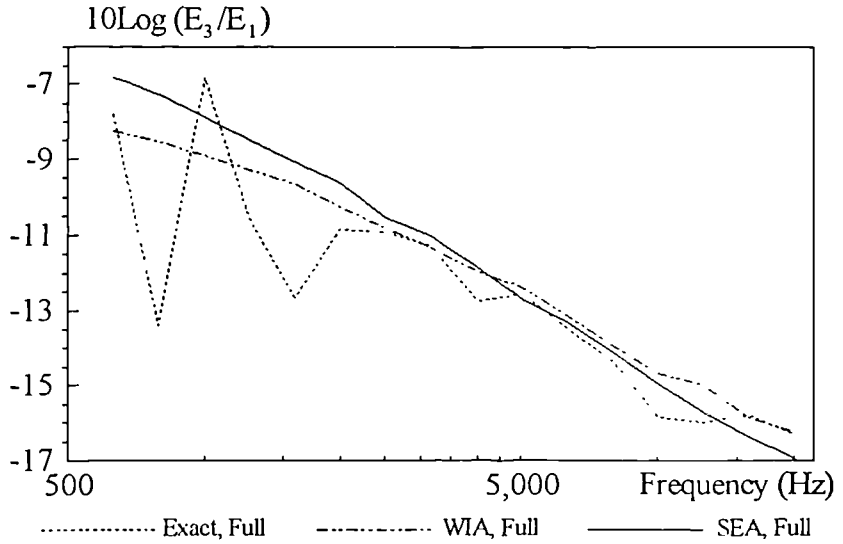

Fig. 5.19.b

Eight Plate Assembly
Third Octave Band Energy Ratio
Plate 4

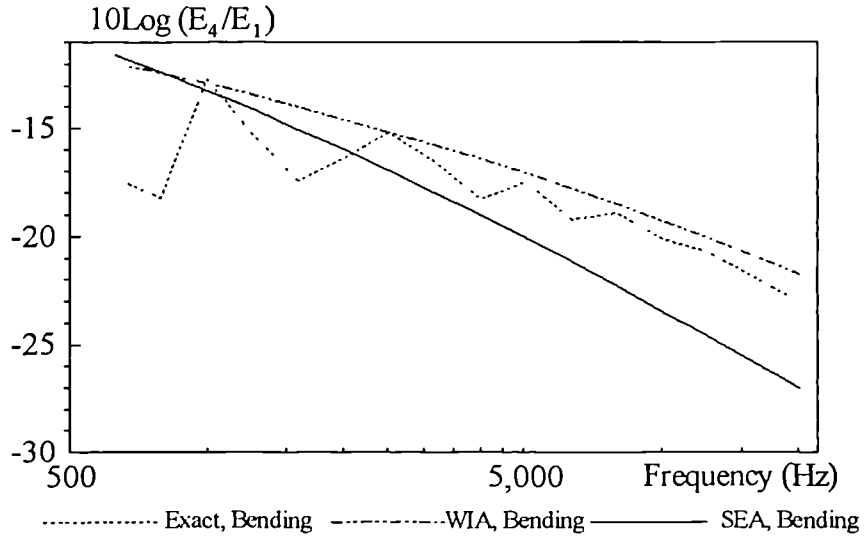

Fig. 5.20.a

Eight Plate Assembly
Third Octave Band Energy Ratio
Plate 4

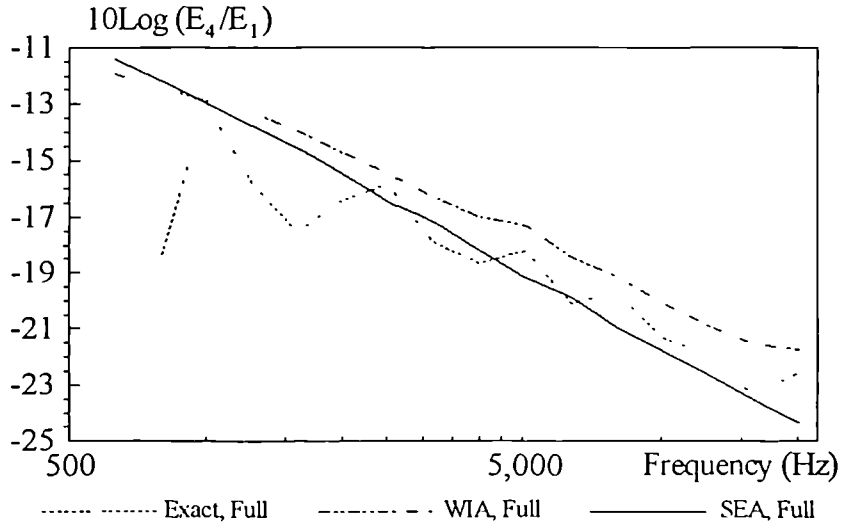

Fig. 5.20.b

Eight Plate Assembly
Third Octave Band Energy Ratio
Plate 5

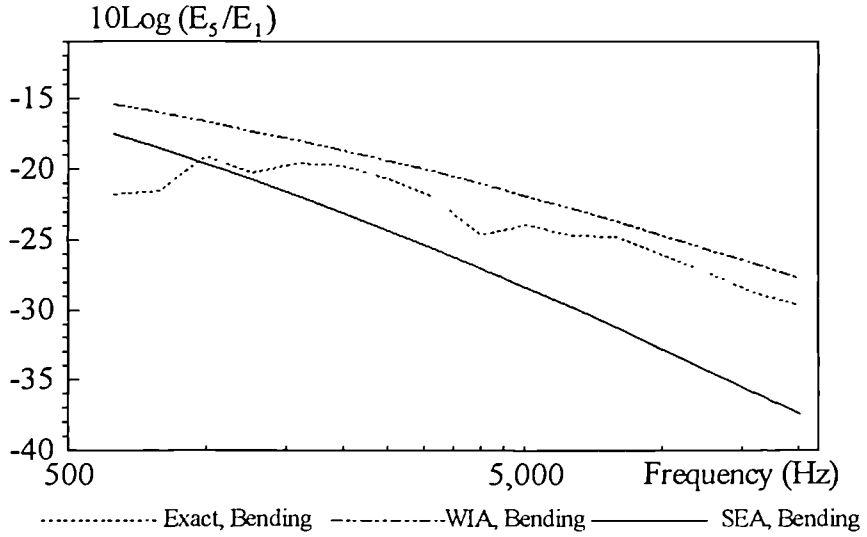

Fig. 5.21.a

Eight Plate Assembly
Third Octave Band Energy Ratio
Plate 5

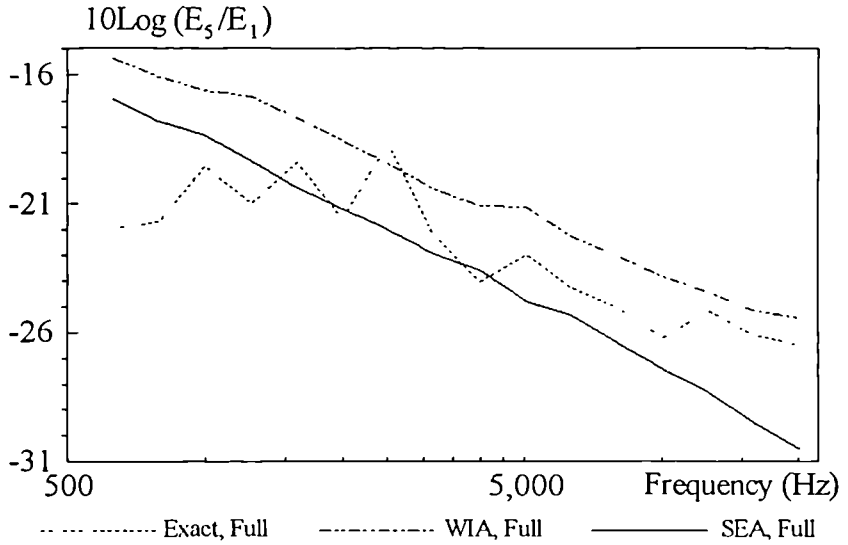

Fig. 5.21.b

Eight Plate Assembly
Third Octave Band Energy Ratio
Plate 6

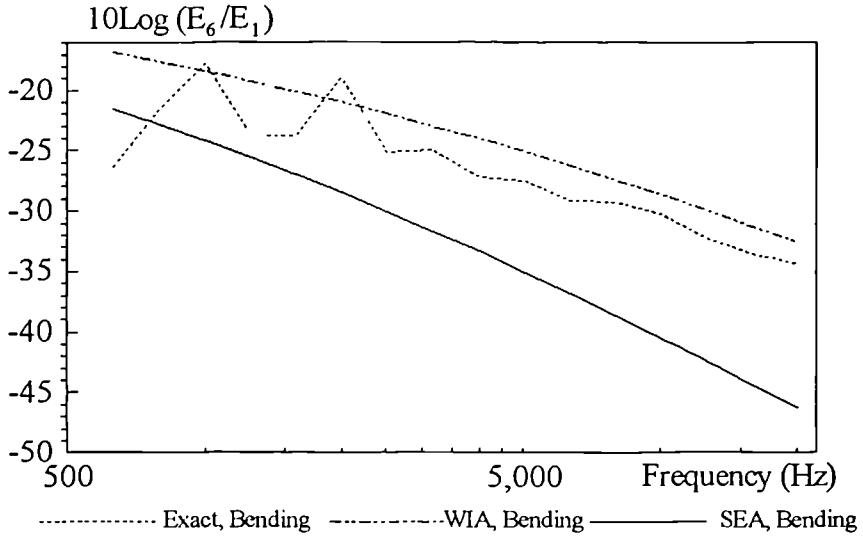

Fig. 5.22.a

Eight Plate Assembly
Third Octave Band Energy Ratio
Plate 6

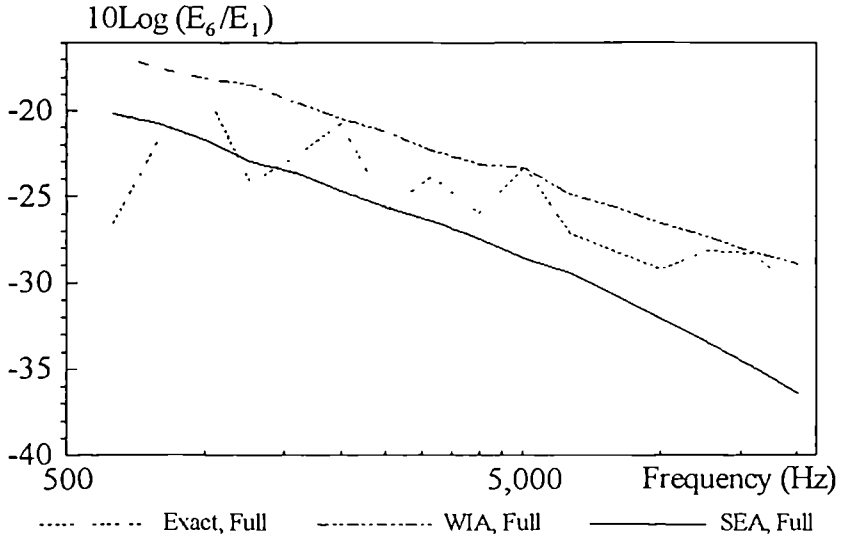

Fig. 5.22.b

Eight Plate Assembly
Third Octave Band Energy Ratio
Plate 7

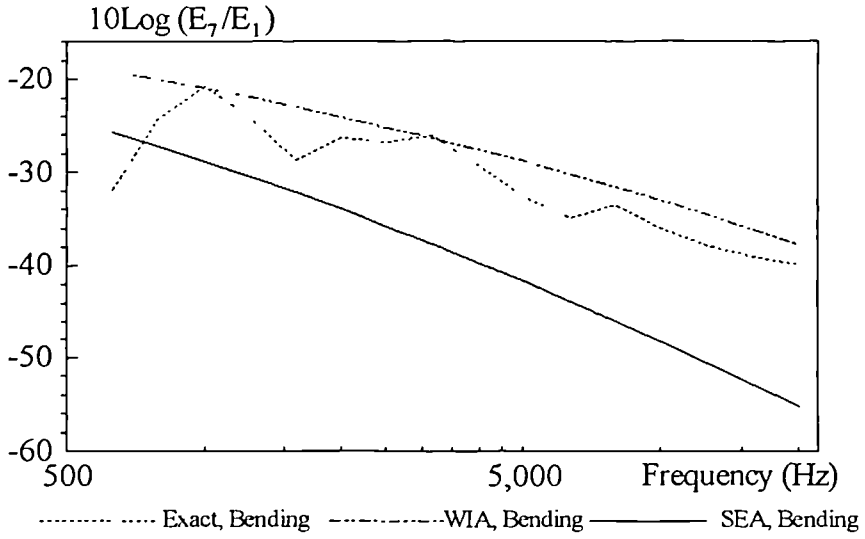

Fig. 5.23.a

Eight Plate Assembly
Third Octave Band Energy Ratio
Plate 7

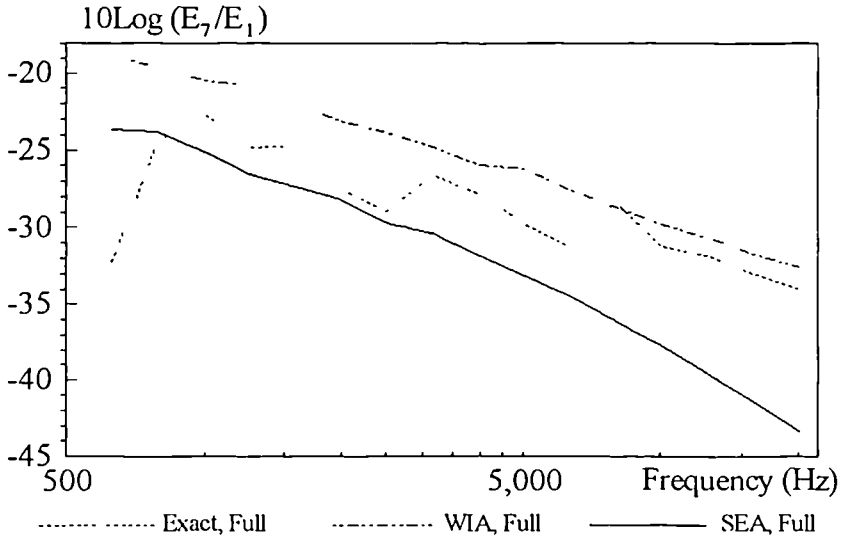

Fig. 5.23.b

Eight Plate Assembly
Third Octave Band Energy Ratio
Plate 8

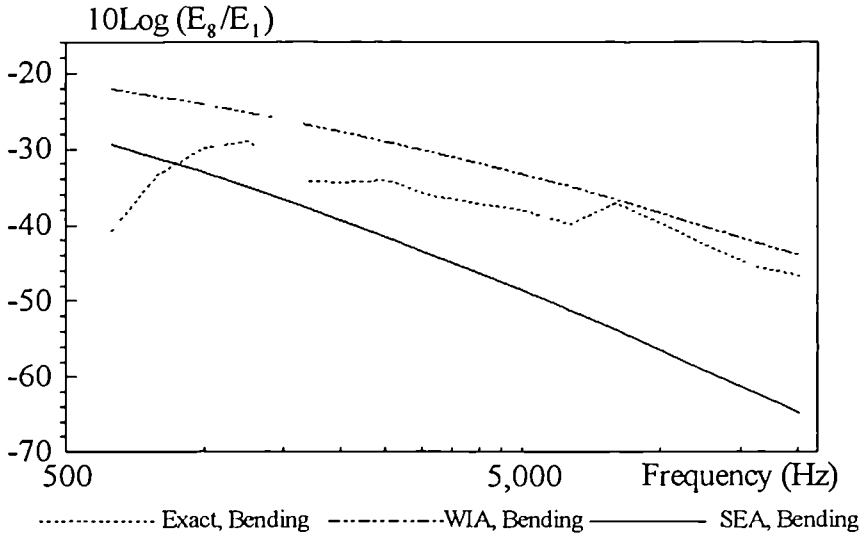

Fig. 5.24.a

Eight Plate Assembly
Third Octave Band Energy Ratio
Plate 8

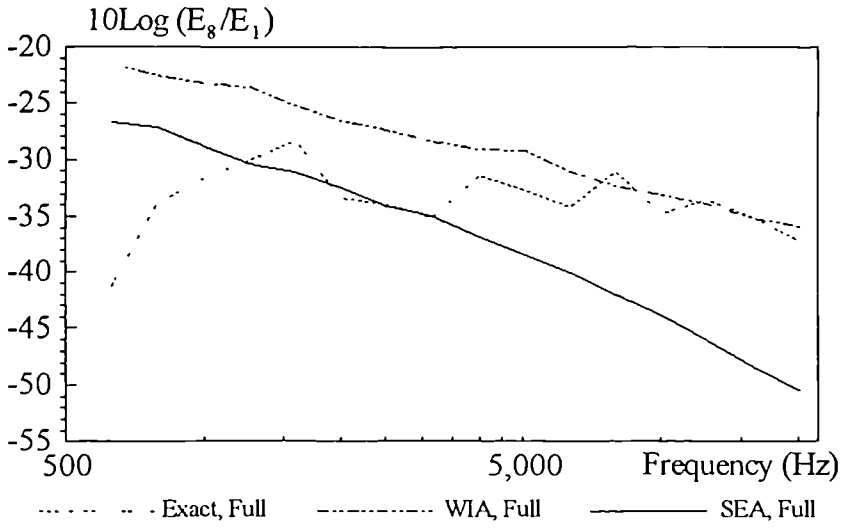

Fig. 5.24.b

Fifteen Plate Assembly
Third Octave Band Energy Ratio
Plate 2, Case 1

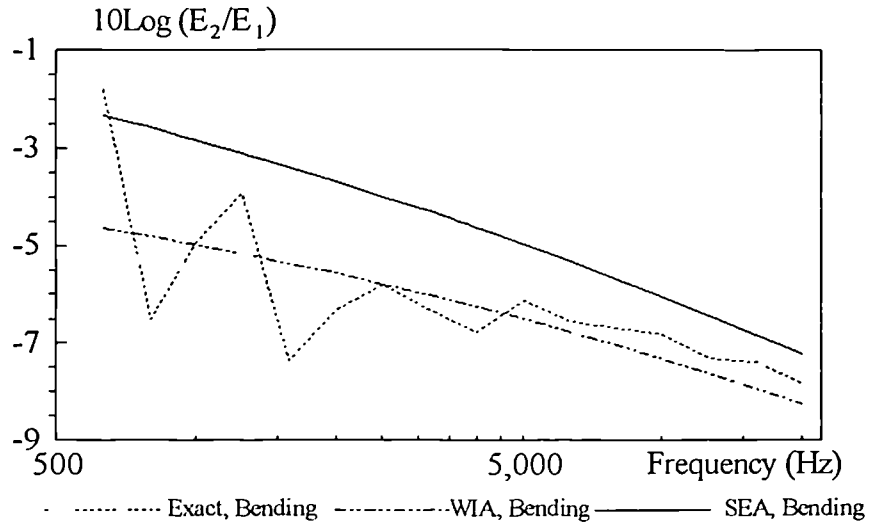

Fig. 5.25.a

Fifteen Plate Assembly
Third Octave Band Energy Ratio
Plate 2, Case 1

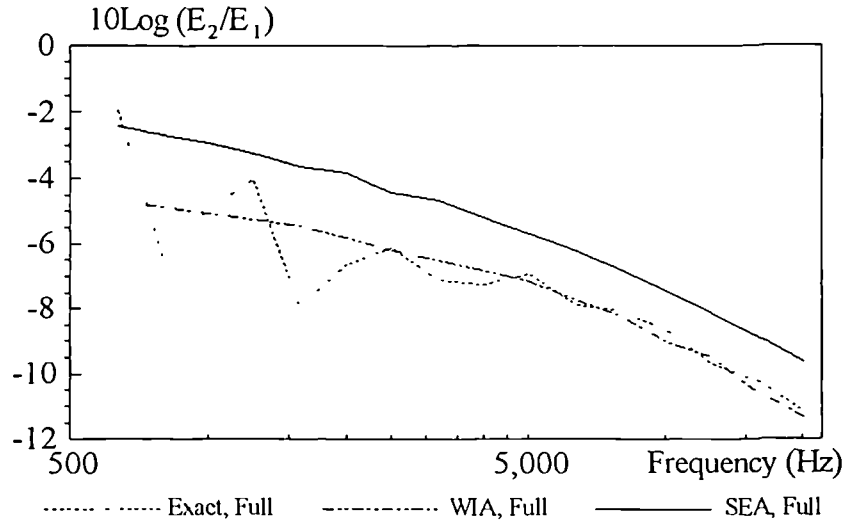

Fig. 5.25.b

Fifteen Plate Assembly
Third Octave Band Energy Ratio
Plate 3, Case 1

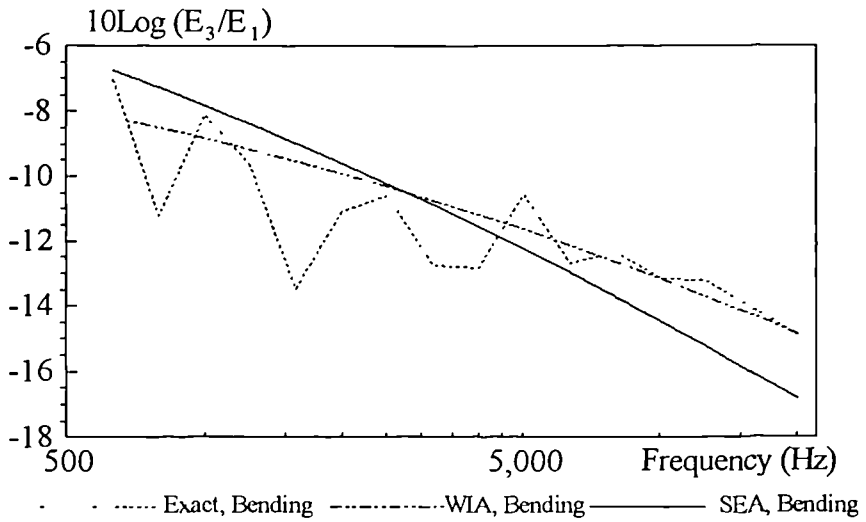

Fig. 5.26.a

Fifteen Plate Assembly
Third Octave Band Energy Ratio
Plate 3, Case 1

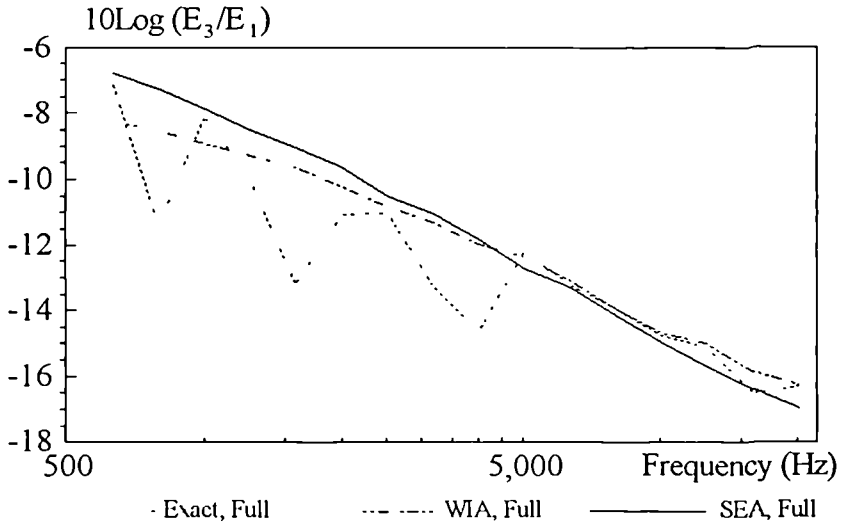

Fig. 5.26.b

Fifteen Plate Assembly
Third Octave Band Energy Ratio
Plate 4, Case 1

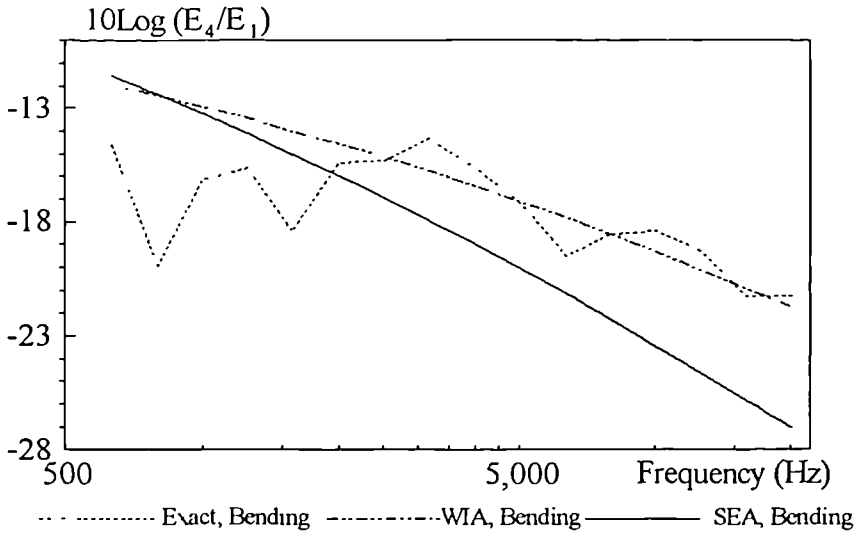

Fig. 5.27.a

Fifteen Plate Assembly
Third Octave Band Energy Ratio
Plate 4, Case 1

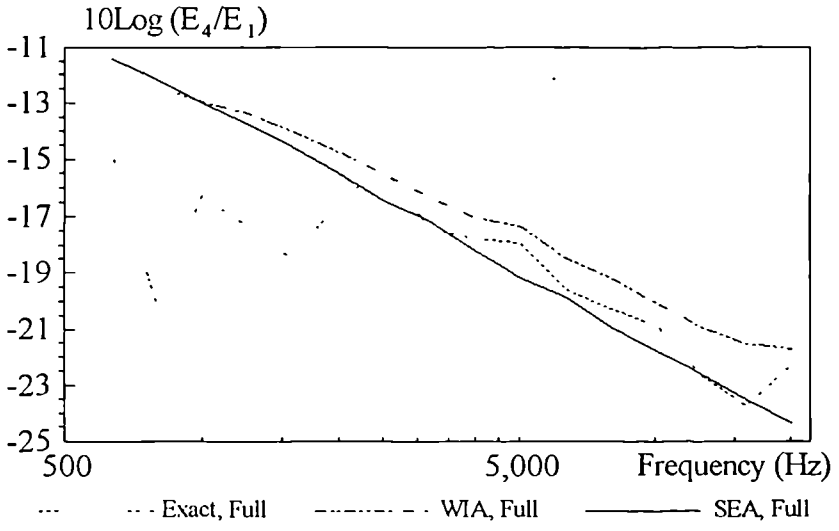

Fig. 5.27.b

Fifteen Plate Assembly
Third Octave Band Energy Ratio
Plate 5, Case 1

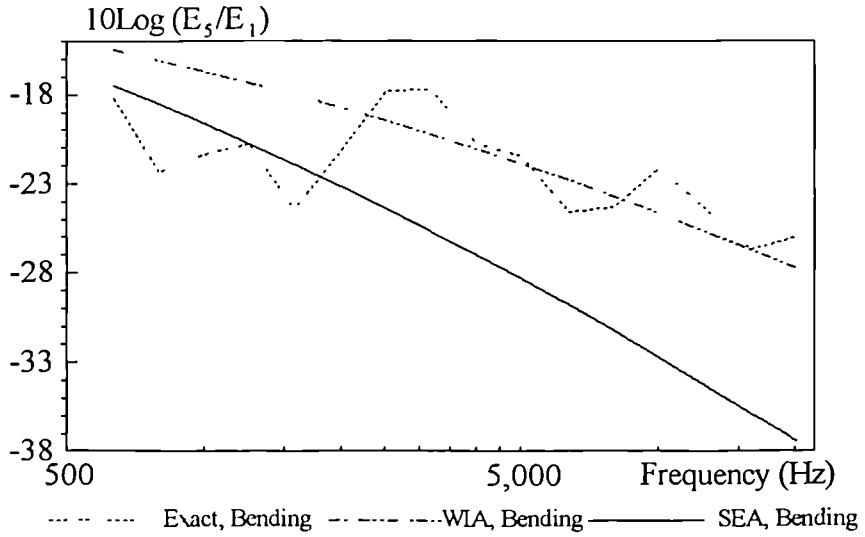

Fig. 5.28.a

Fifteen Plate Assembly
Third Octave Band Energy Ratio
Plate 5, Case 1

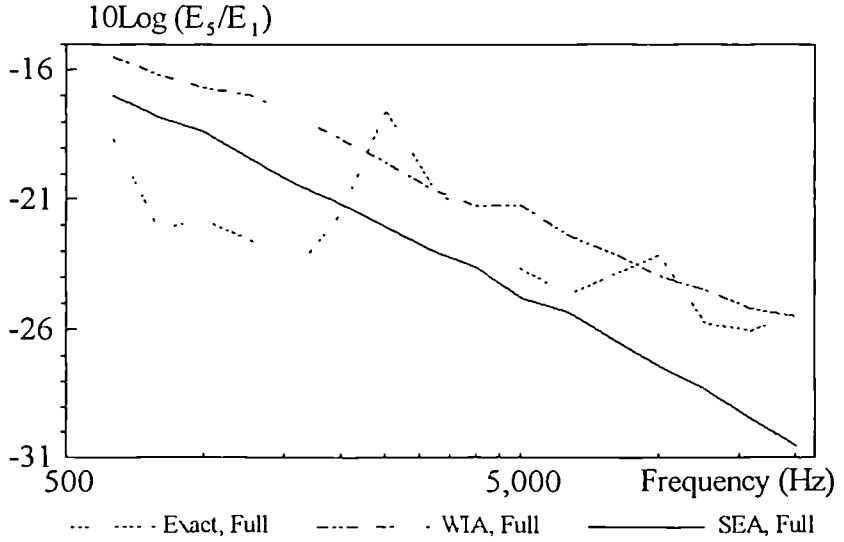

Fig. 5 28 b

Fifteen Plate Assembly
Third Octave Band Energy Ratio
Plate 6, Case 1

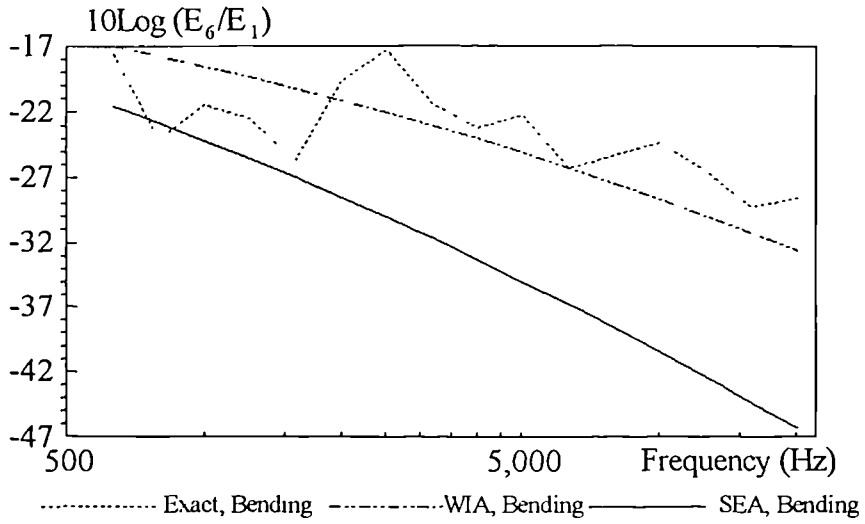

Fig. 5.29.a

Fifteen Plate Assembly
Third Octave Band Energy Ratio
Plate 6, Case 1

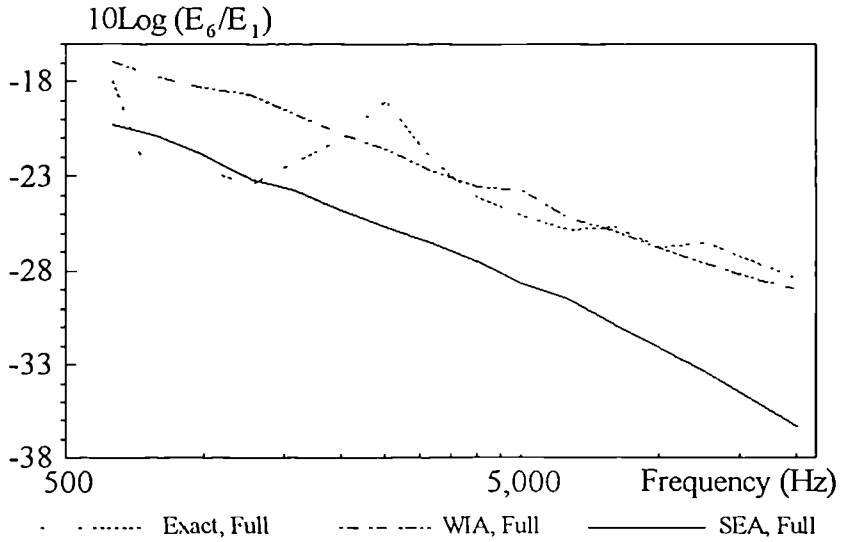

Fig. 5.29.b

Fifteen Plate Assembly
Third Octave Band Energy Ratio
Plate 7, Case 1

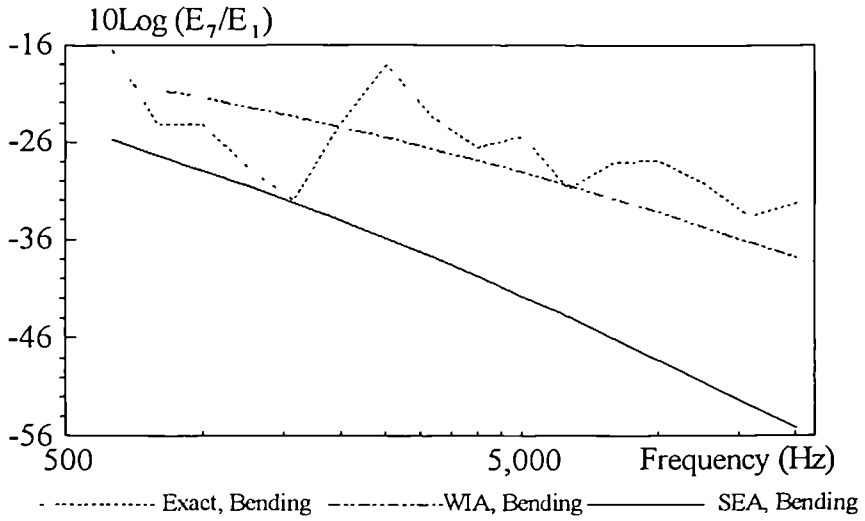

Fig. 5.30.a

Fifteen Plate Assembly
Third Octave Band Energy Ratio
Plate 7, Case 1

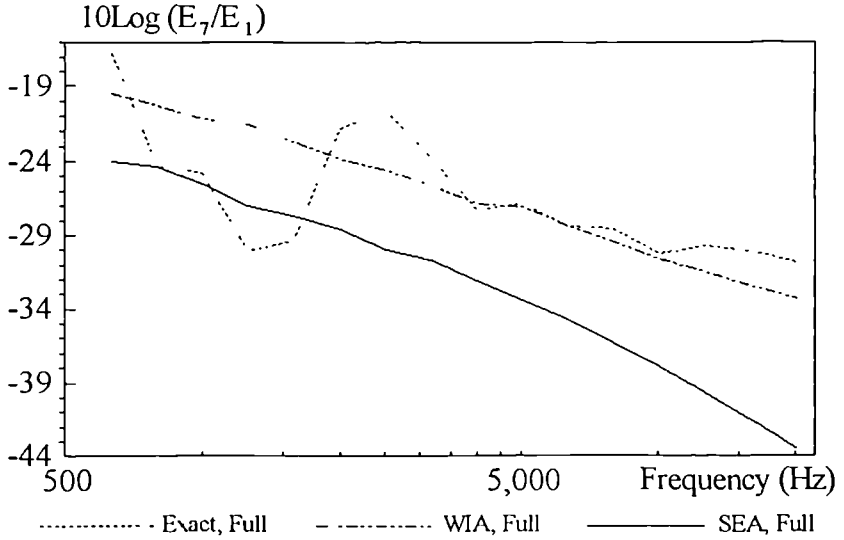

Fig. 5.30.b

Fifteen Plate Assembly
Third Octave Band Energy Ratio
Plate 8, Case 1

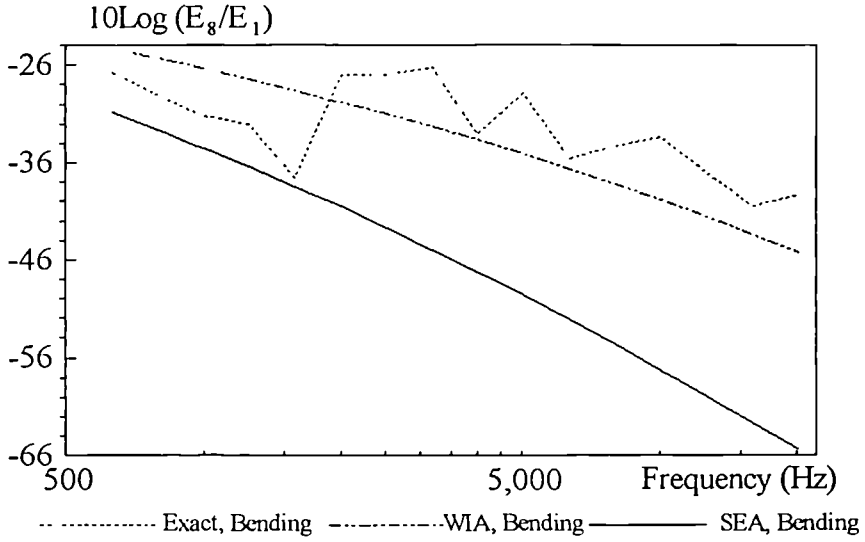

Fig. 5.31.a

Fifteen Plate Assembly
Third Octave Band Energy Ratio
Plate 8, Case 1

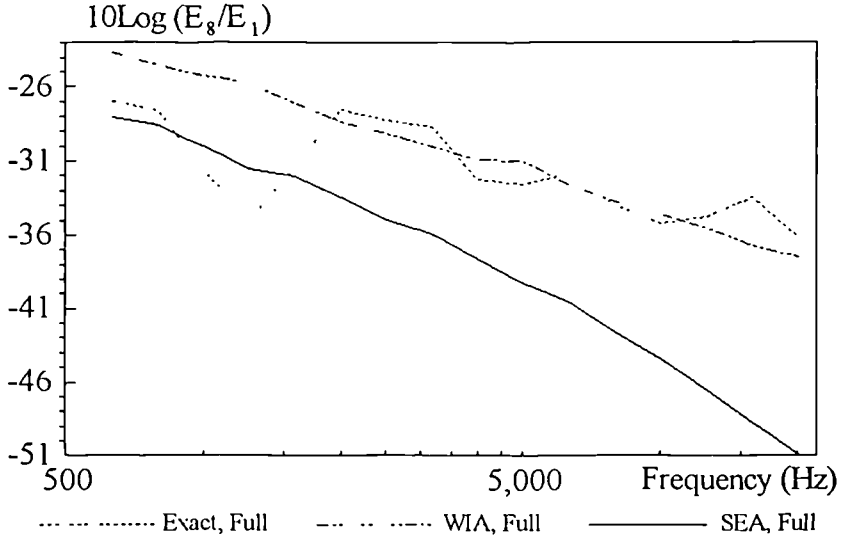

Fig. 5.31.b

Fifteen Plate Assembly
Third Octave Band Energy Ratio
Plate 9, Case 1

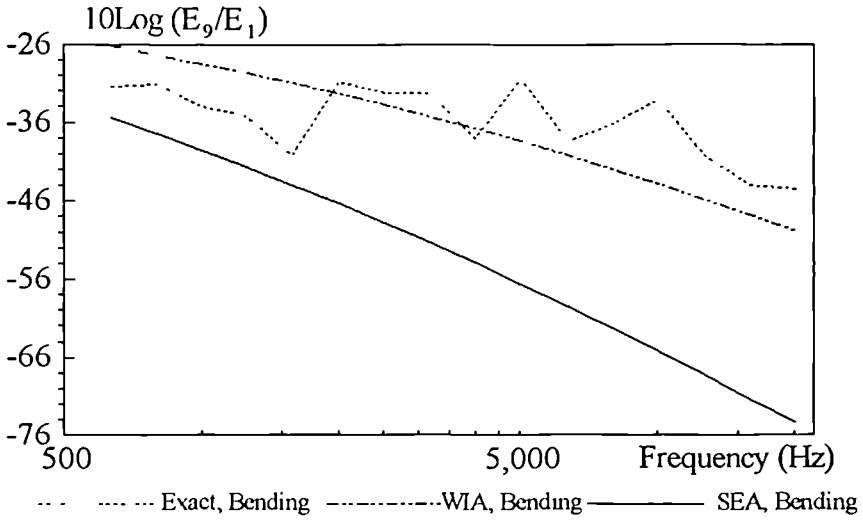

Fig. 5.32.a

Fifteen Plate Assembly
Third Octave Band Energy Ratio
Plate 9, Case 1

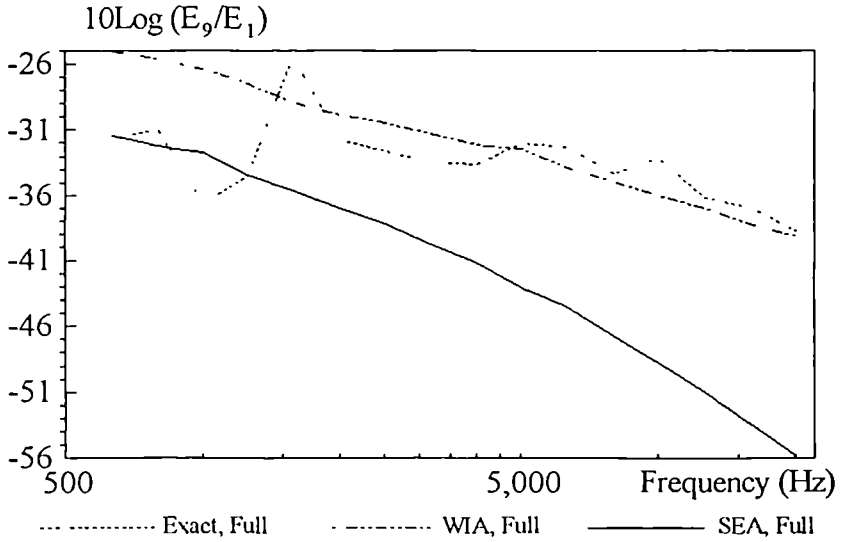

Fig. 5.32.b

Fifteen Plate Assembly
Third Octave Band Energy Ratio
Plate 10, Case 1

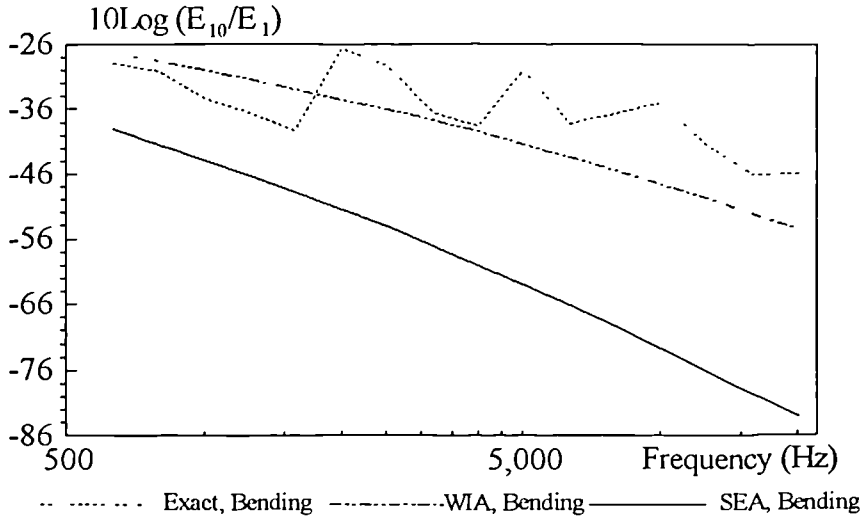

Fig. 5.33.a

Fifteen Plate Assembly
Third Octave Band Energy Ratio
Plate 10, Case 1

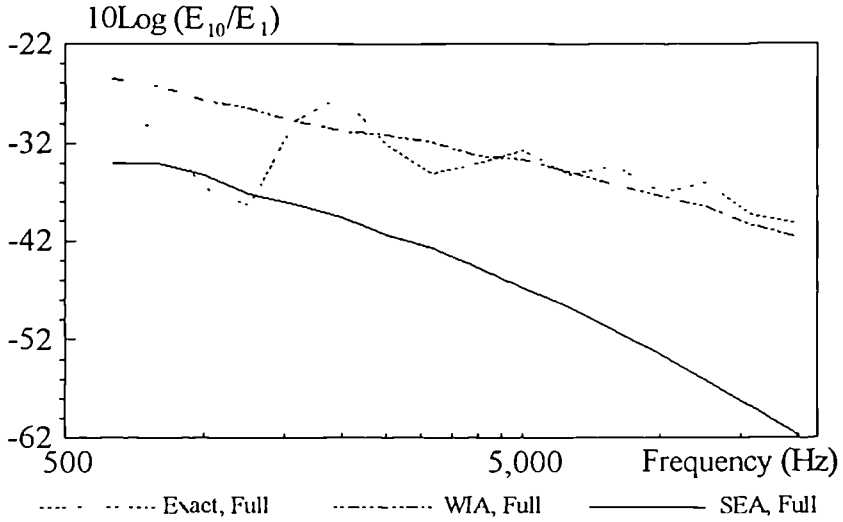

Fig. 5.33.b

Fifteen Plate Assembly
Third Octave Band Energy Ratio
Plate 11, Case 1

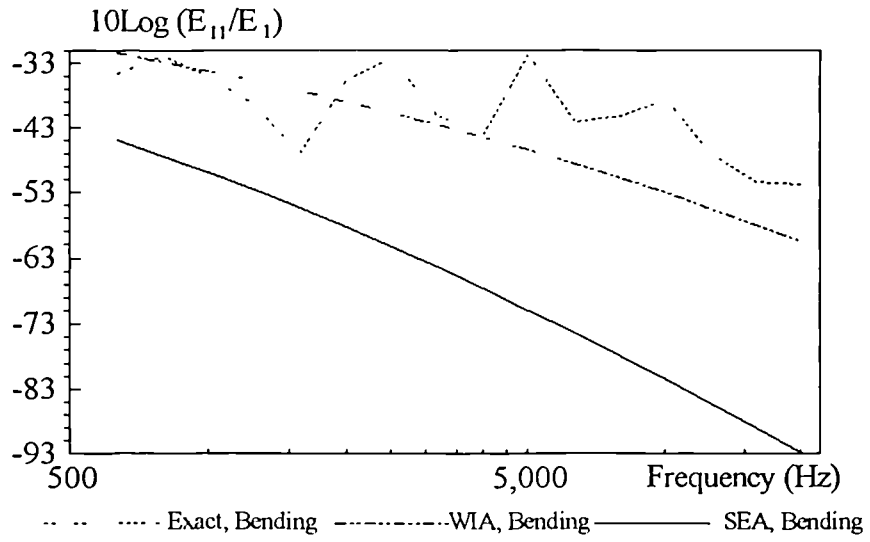

Fig. 5.34.a

Fifteen Plate Assembly
Third Octave Band Energy Ratio
Plate 11, Case 1

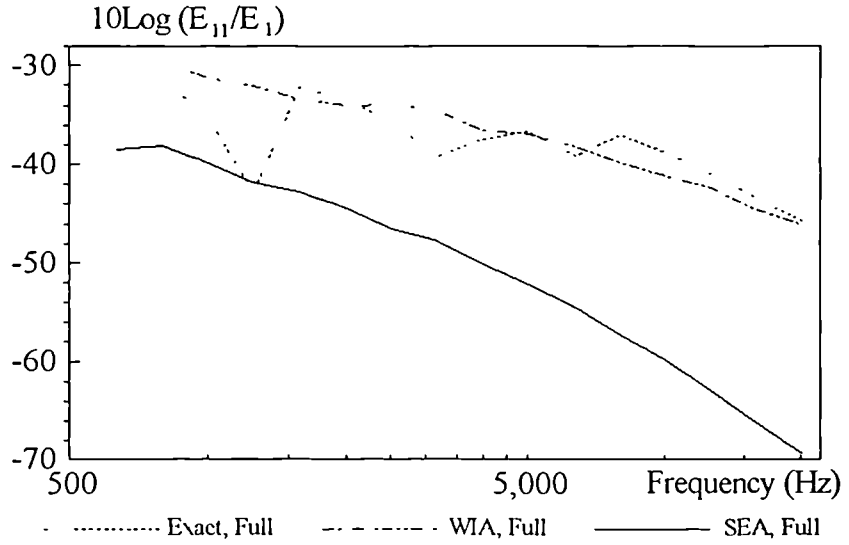

Fig. 5.34.b

Fifteen Plate Assembly
Third Octave Band Energy Ratio
Plate 12, Case 1

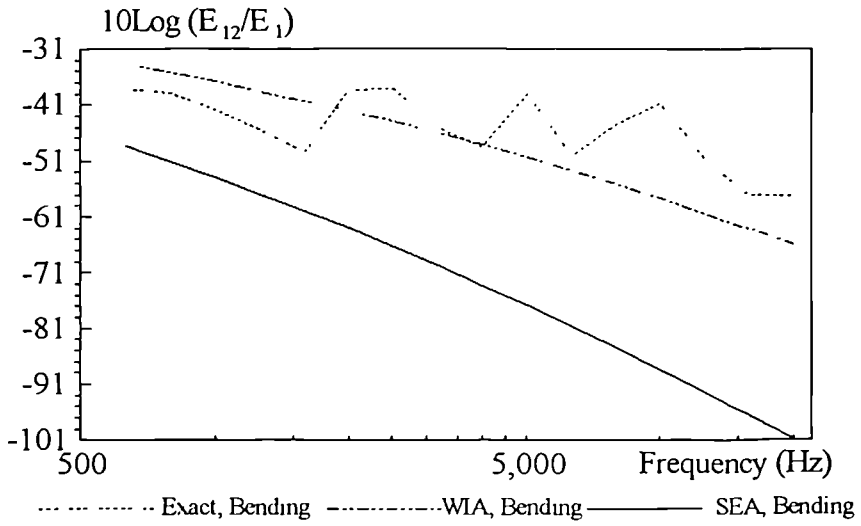

Fig. 5.35.a

Fifteen Plate Assembly
Third Octave Band Energy Ratio
Plate 12, Case 1

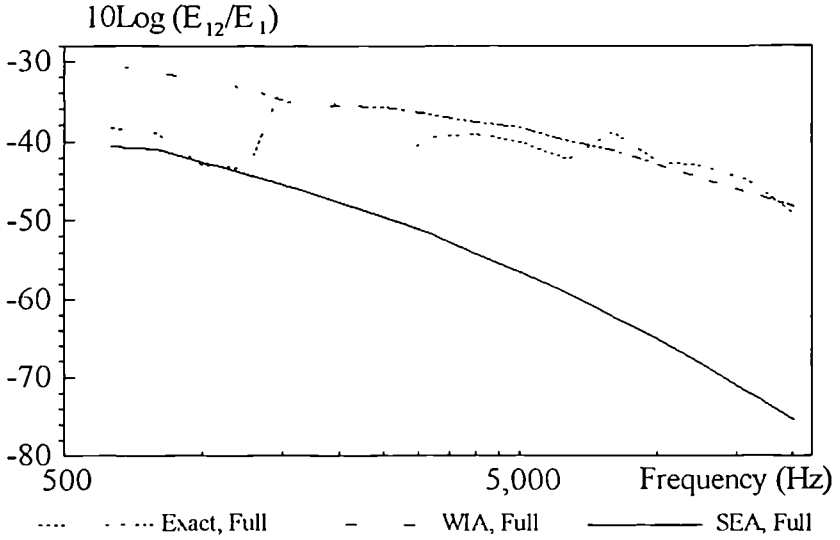

Fig. 5.35.b

Fifteen Plate Assembly
Third Octave Band Energy Ratio
Plate 13, Case 1

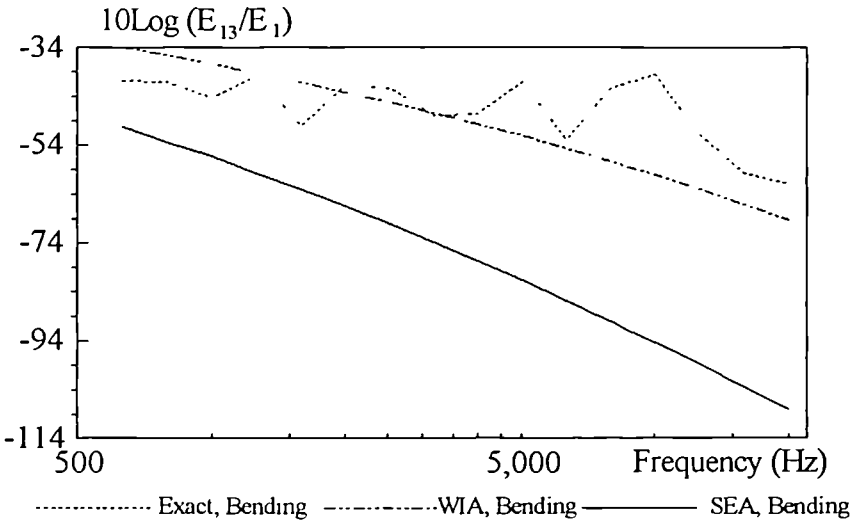

Fig 5.36.a

Fifteen Plate Assembly
Third Octave Band Energy Ratio
Plate 13, Case 1

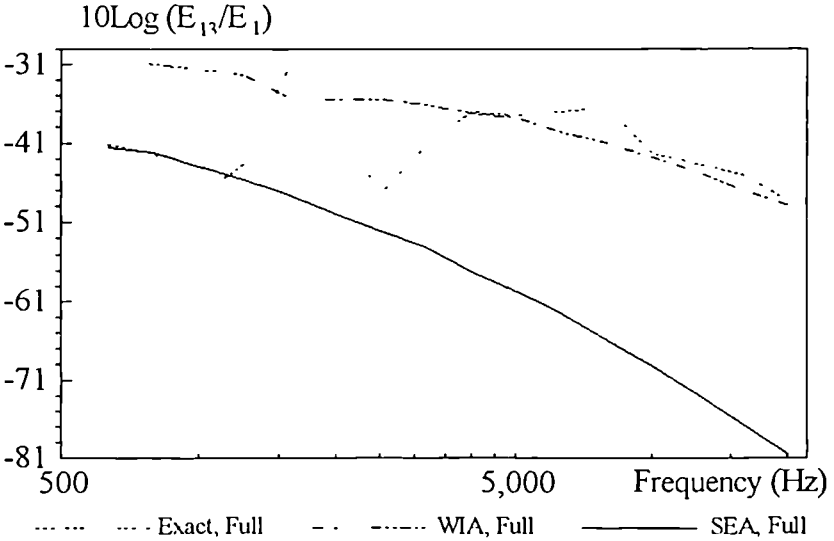

Fig. 5.36.b

Fifteen Plate Assembly
Third Octave Band Energy Ratio
Plate 14, Case 1

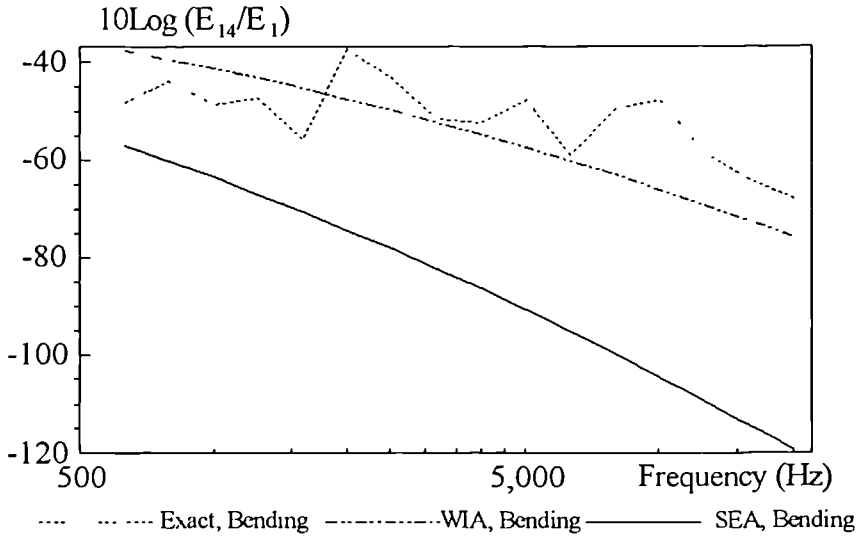

Fig. 5.37.a

Fifteen Plate Assembly
Third Octave Band Energy Ratio
Plate 14, Case 1

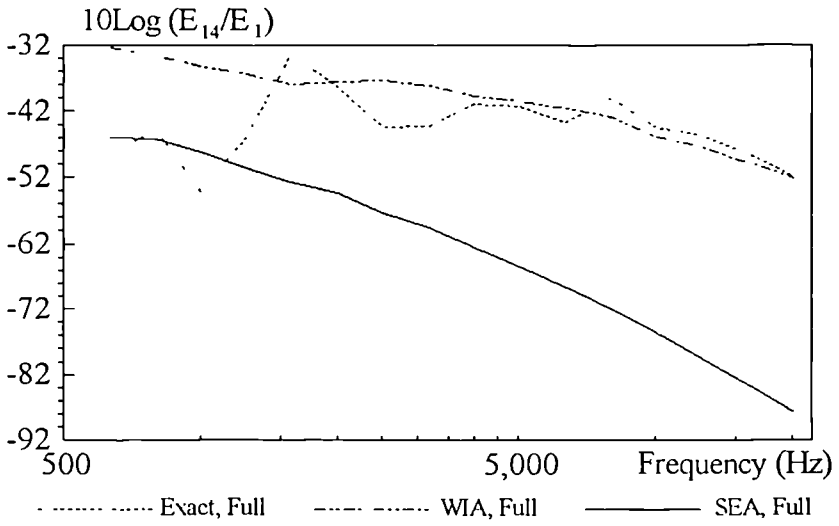

Fig. 5.37.b

Fifteen Plate Assembly
Third Octave Band Energy Ratio
Plate 15, Case 1

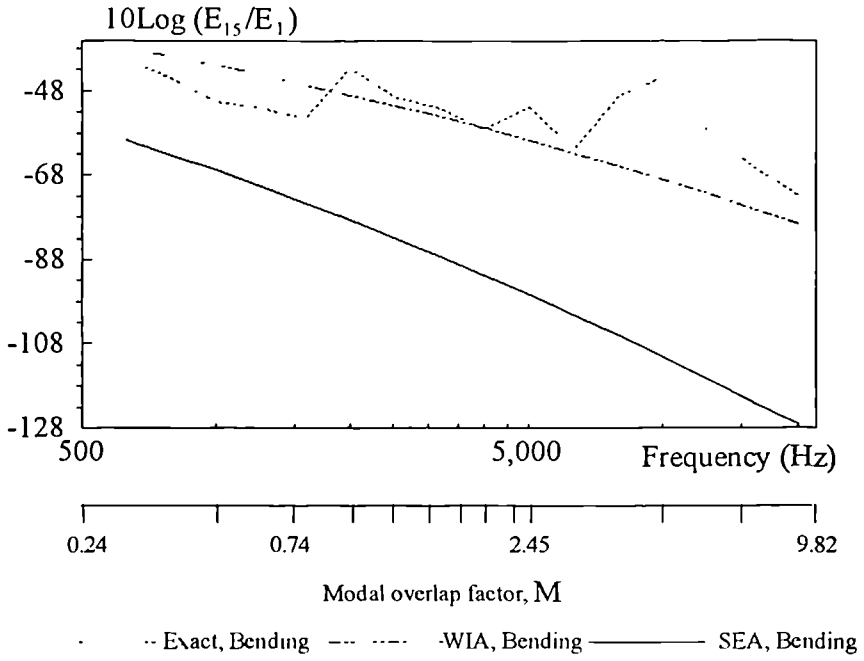

Fig. 5.38.a

Fifteen Plate Assembly
Third Octave Band Energy Ratio
Plate 15, Case 1

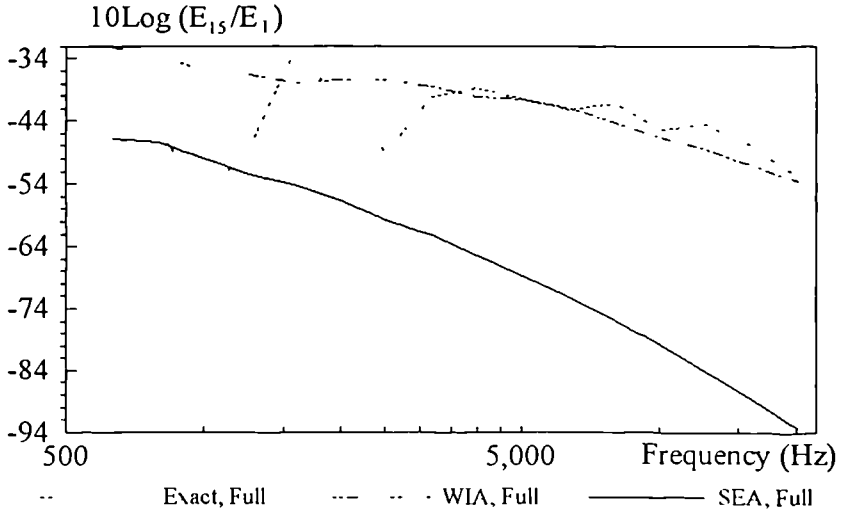

Fig. 5.38.b

Fifteen Plate Assembly
Third Octave Band Energy Ratio
Plate 2, Case 2

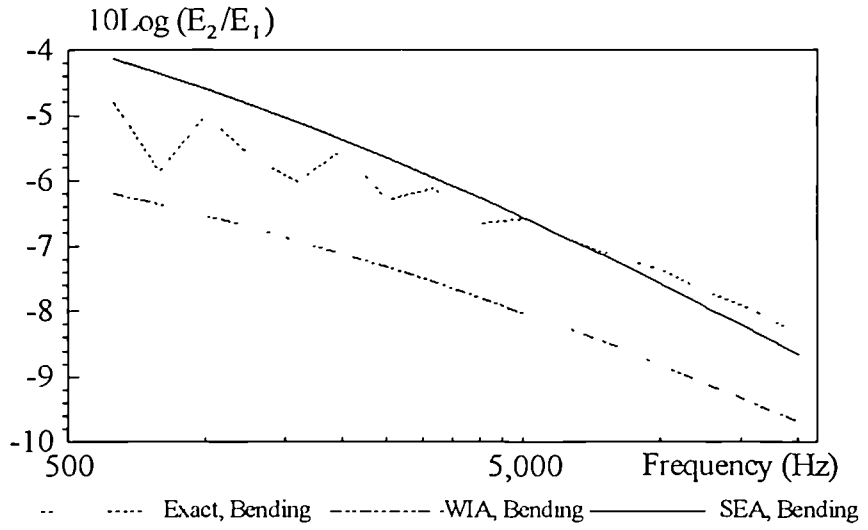

Fig. 5.39.a

Fifteen Plate Assembly
Third Octave Band Energy Ratio
Plate 2, Case 2

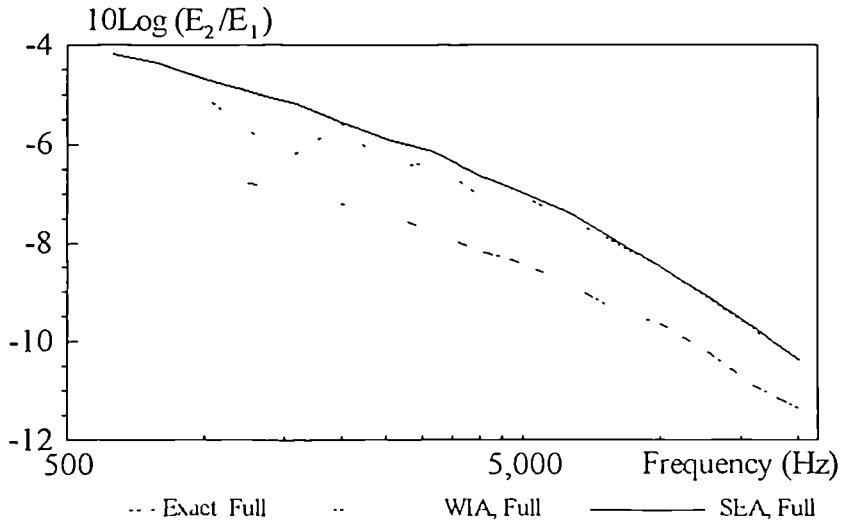

Fig. 5.39.b

Fifteen Plate Assembly
Third Octave Band Energy Ratio
Plate 3, Case 2

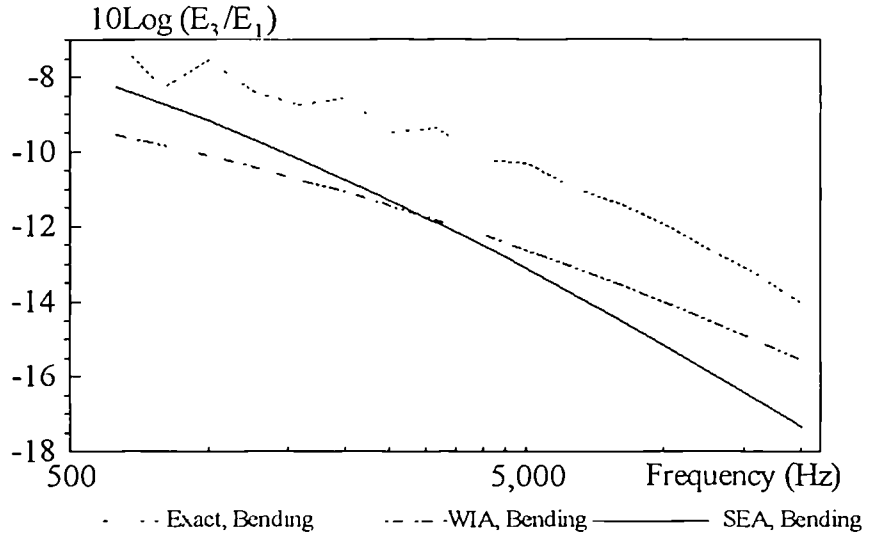

Fig 5.40.a

Fifteen Plate Assembly
Third Octave Band Energy Ratio
Plate 3, Case 2

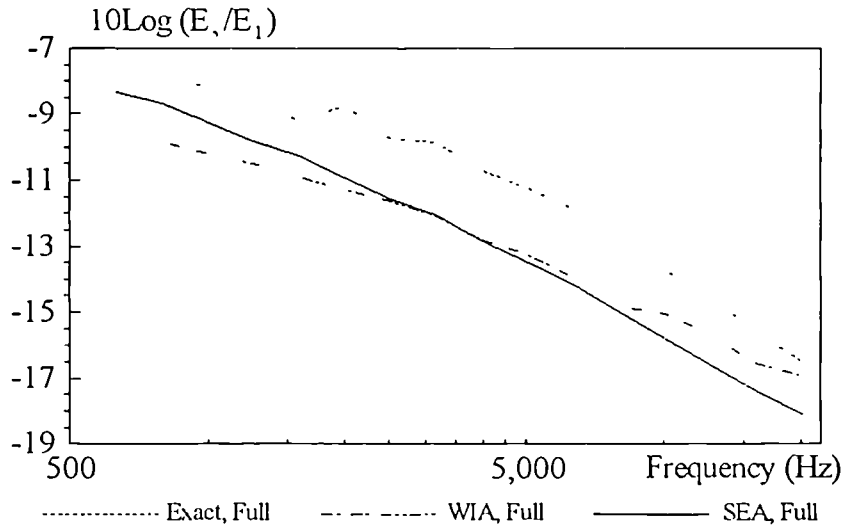

Fig. 5.40.b

Fifteen Plate Assembly
Third Octave Band Energy Ratio
Plate 4, Case 2

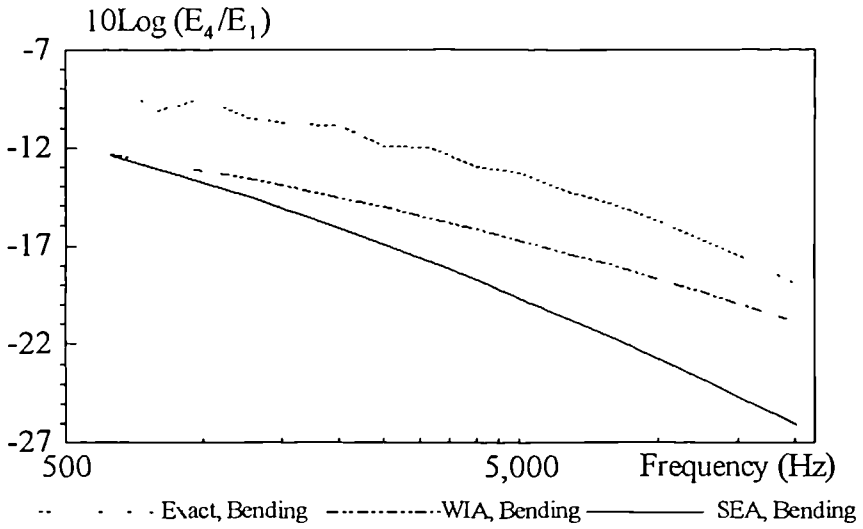

Fig. 5.41.a

Fifteen Plate Assembly
Third Octave Band Energy Ratio
Plate 4, Case 2

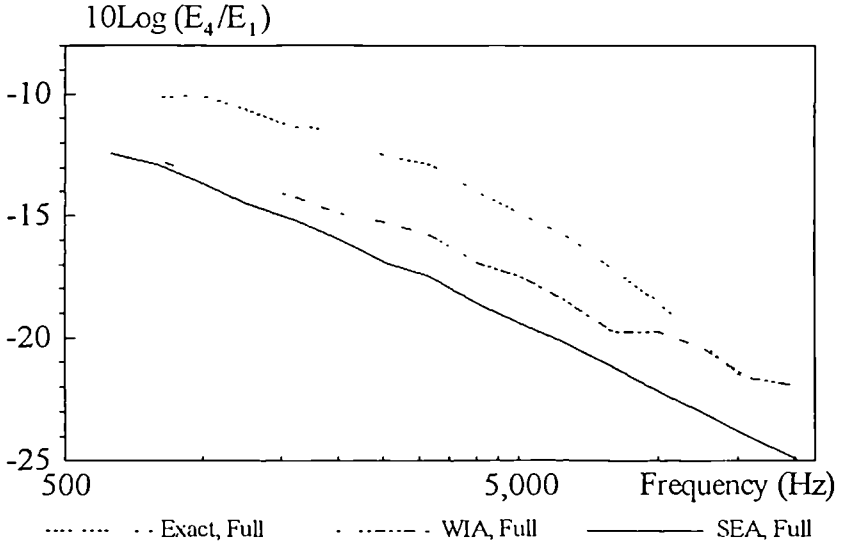

Fig. 5.41.b

Fifteen Plate Assembly
Third Octave Band Energy Ratio
Plate 5, Case 2

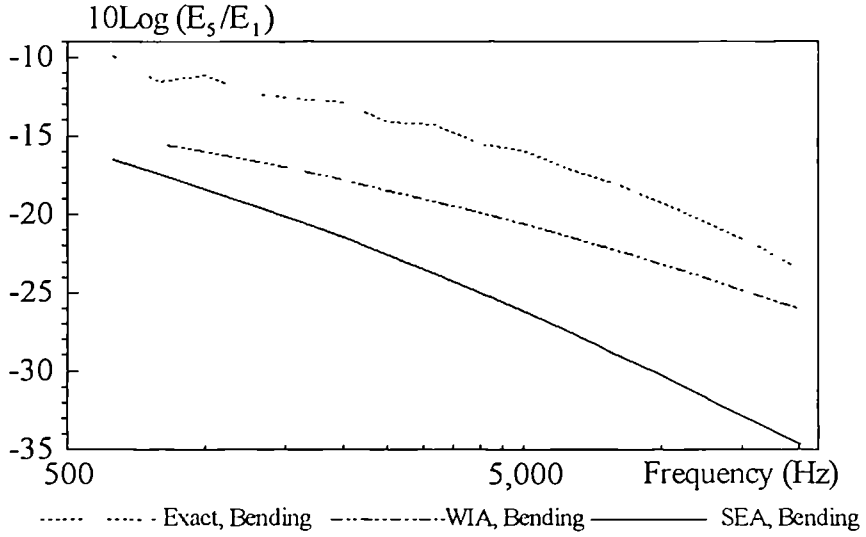

Fig. 5.42.a

Fifteen Plate Assembly
Third Octave Band Energy Ratio
Plate 5, Case 2

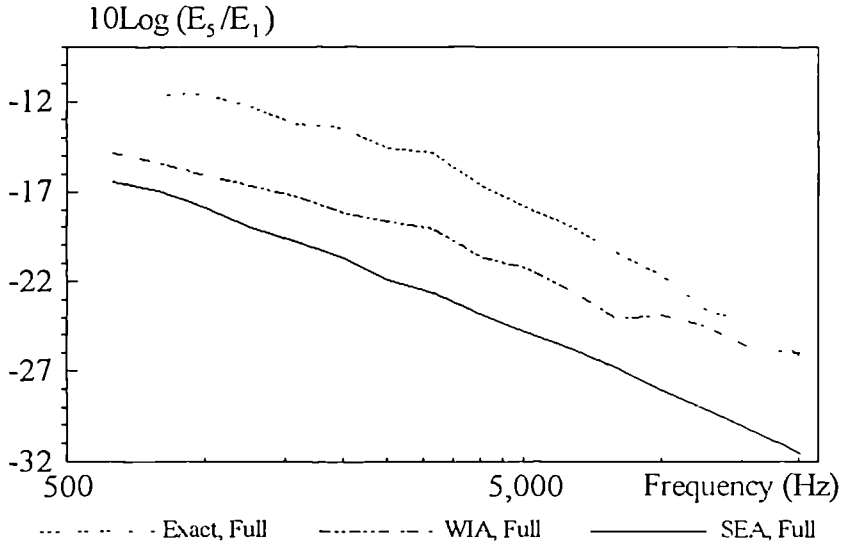

Fig. 5.42.b

Fifteen Plate Assembly
Third Octave Band Energy Ratio
Plate 6, Case 2

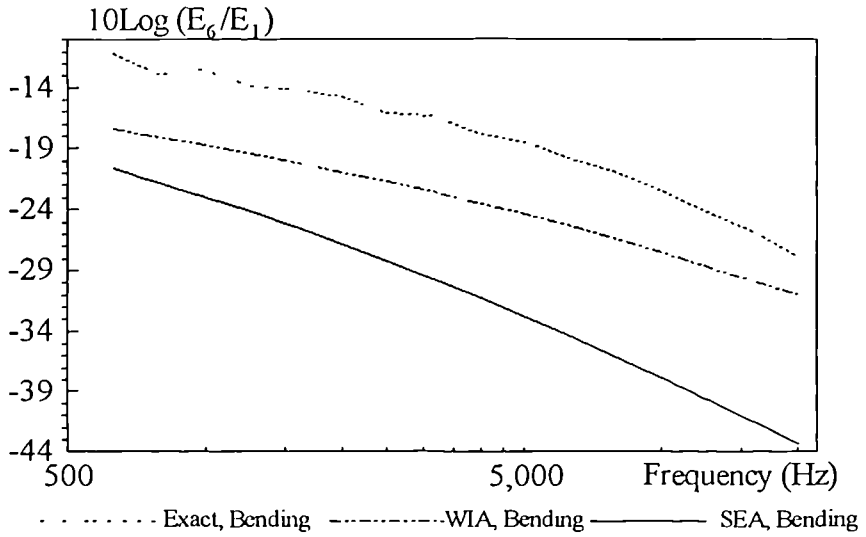

Fig. 5.43.a

Fifteen Plate Assembly
Third Octave Band Energy Ratio
Plate 6, Case 2

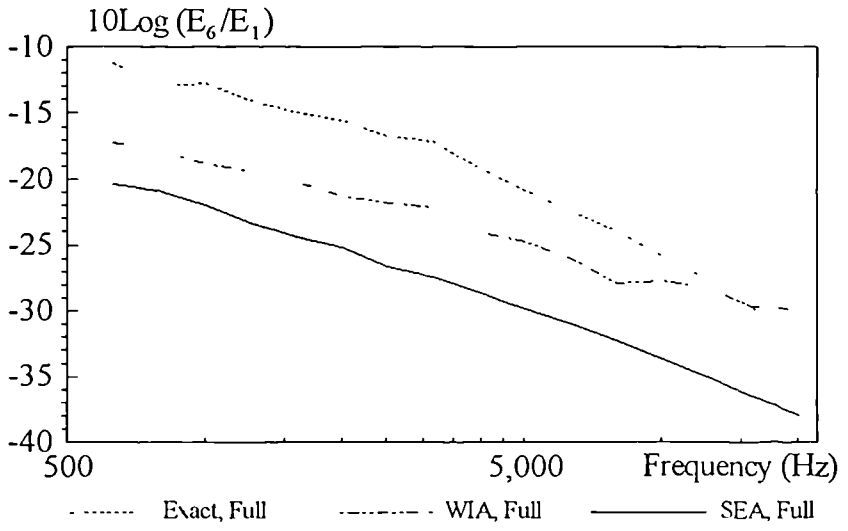

Fig. 5.43.b

Fifteen Plate Assembly
Third Octave Band Energy Ratio
Plate 7, Case 2

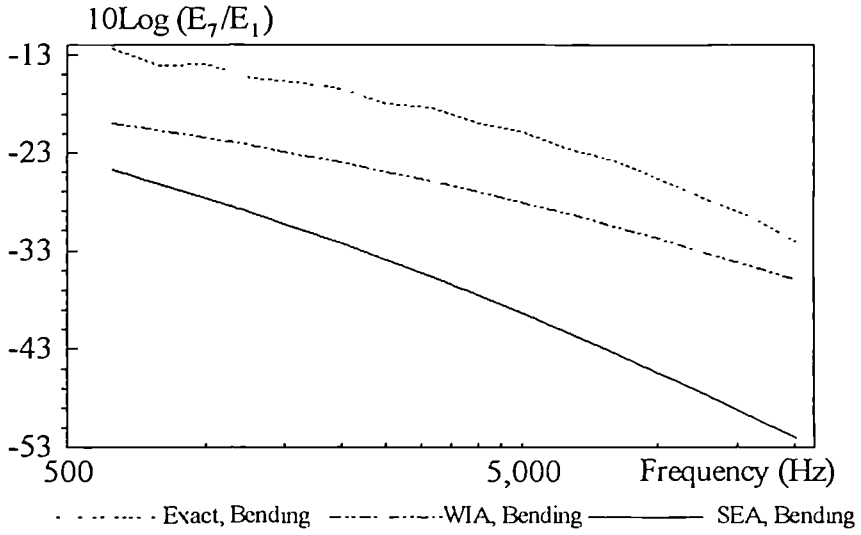

Fig. 5.44.a

Fifteen Plate Assembly
Third Octave Band Energy Ratio
Plate 7, Case 2

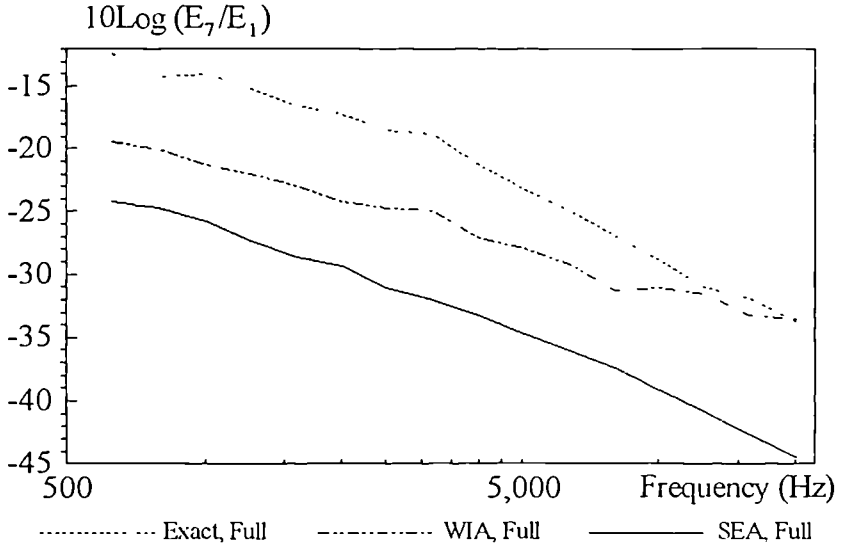

Fig. 5.44.b

Fifteen Plate Assembly
Third Octave Band Energy Ratio
Plate 8, Case 2

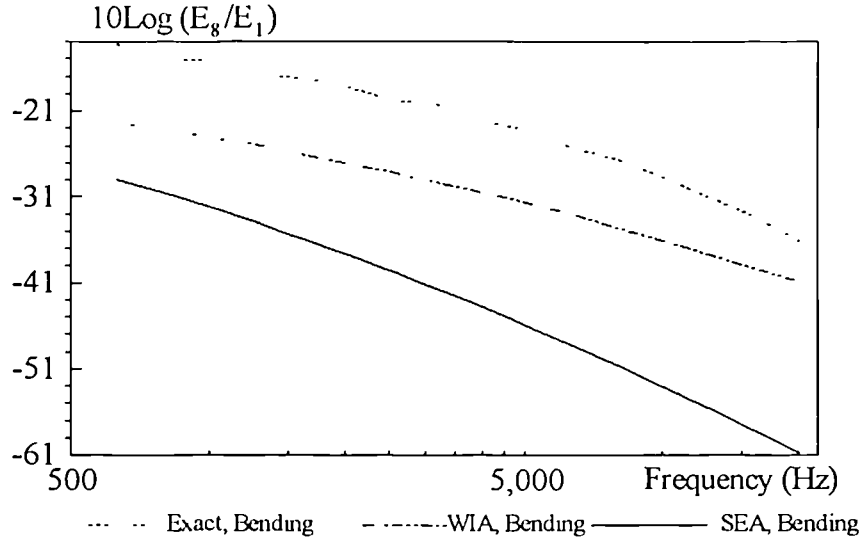

Fig 5.45 a

Fifteen Plate Assembly
Third Octave Band Energy Ratio
Plate 8, Case 2

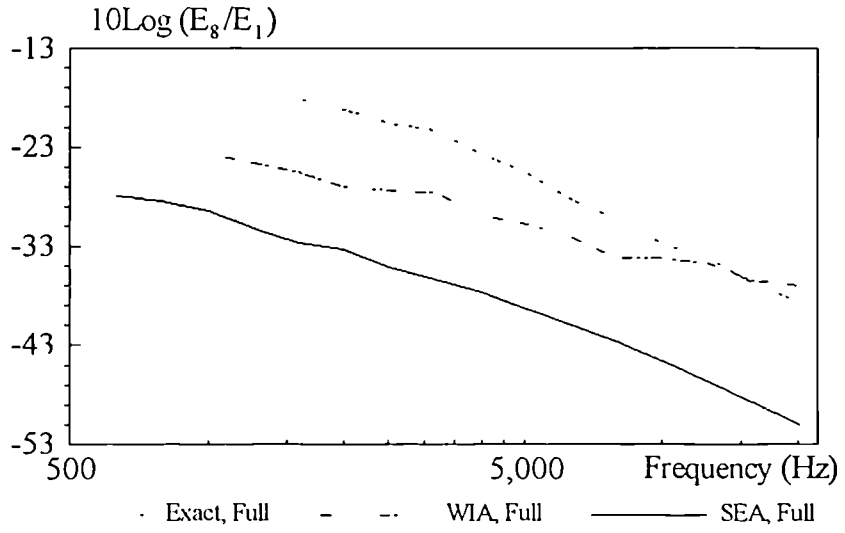

Fig. 5.45.b

Fifteen Plate Assembly
Third Octave Band Energy Ratio
Plate 9, Case 2

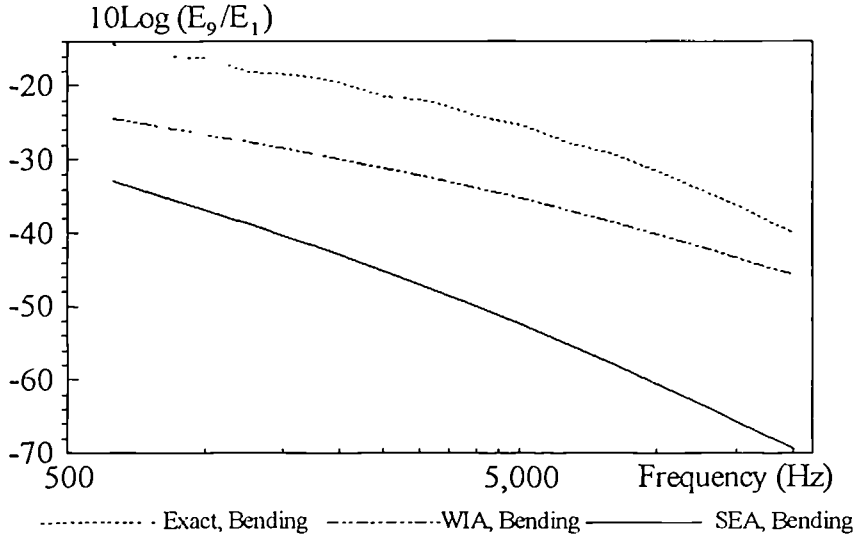

Fig. 5.46.a

Fifteen Plate Assembly
Third Octave Band Energy Ratio
Plate 9, Case 2

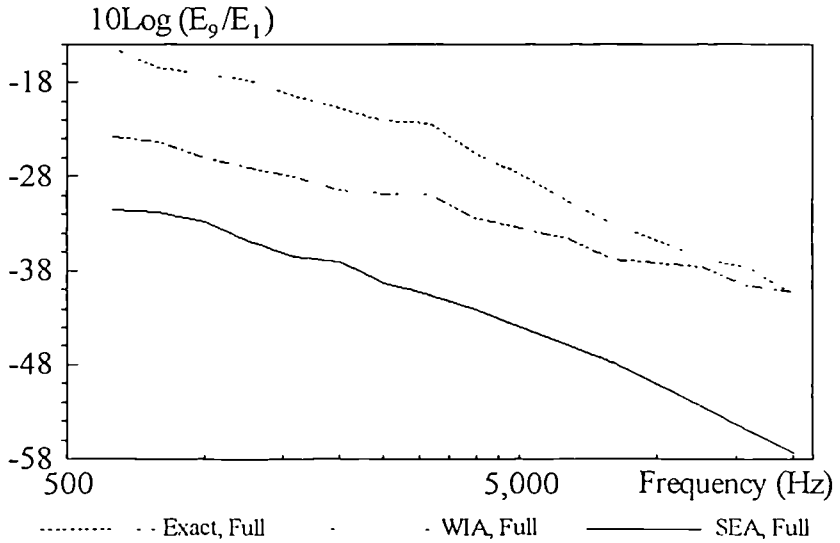

Fig. 5.46.b

Fifteen Plate Assembly
Third Octave Band Energy Ratio
Plate 10, Case 2

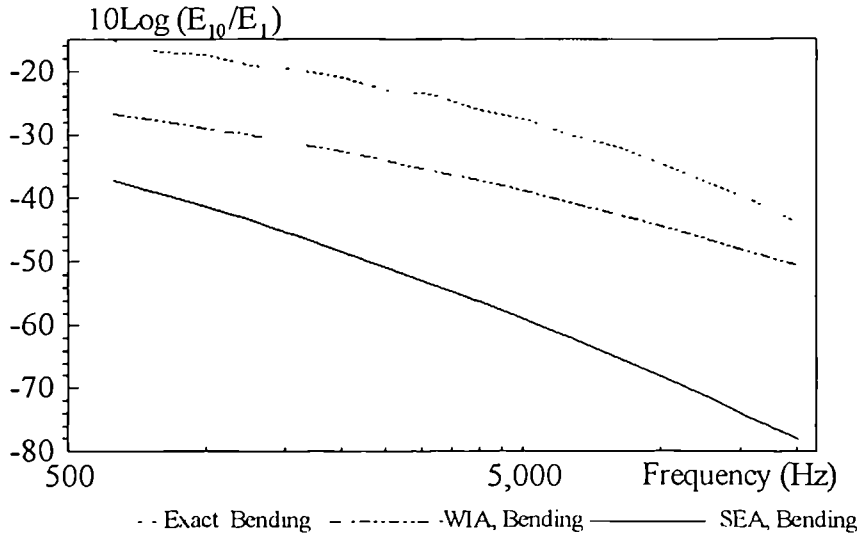

Fig. 5.47.a

Fifteen Plate Assembly
Third Octave Band Energy Ratio
Plate 10, Case 2

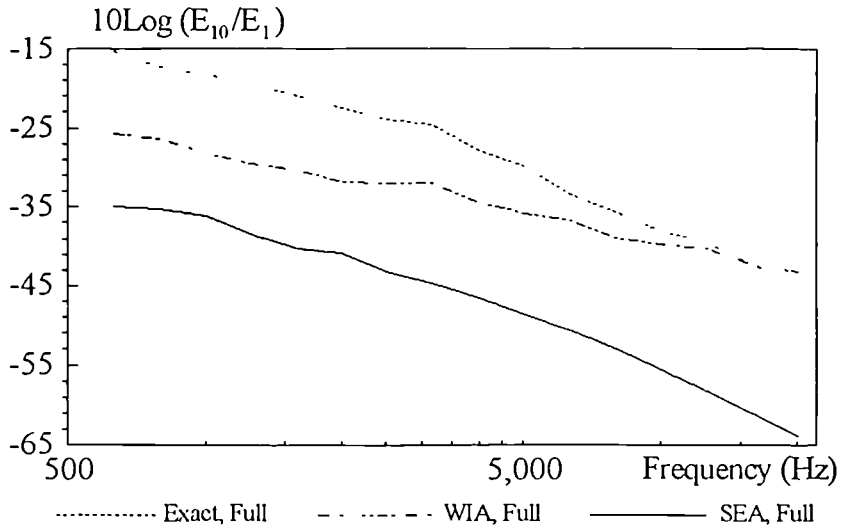

Fig. 5.47.b

Fifteen Plate Assembly
Third Octave Band Energy Ratio
Plate 11, Case 2

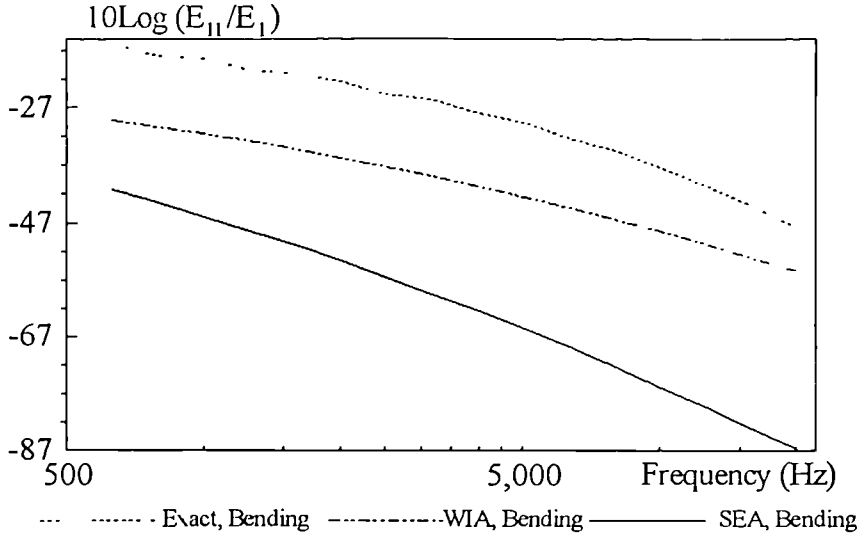

Fig. 5.48.a

Fifteen Plate Assembly
Third Octave Band Energy Ratio
Plate 11, Case 2

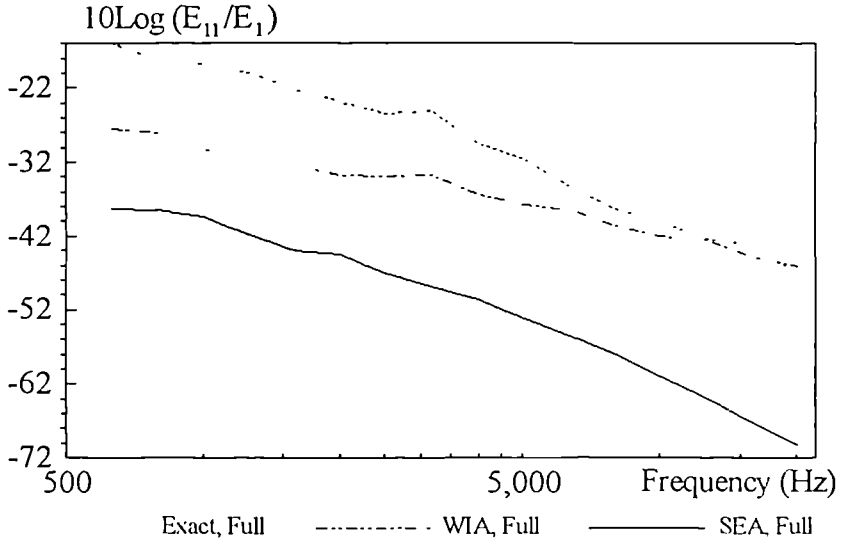

Fig. 5.48.b

Fifteen Plate Assembly
Third Octave Band Energy Ratio
Plate 12, Case 2

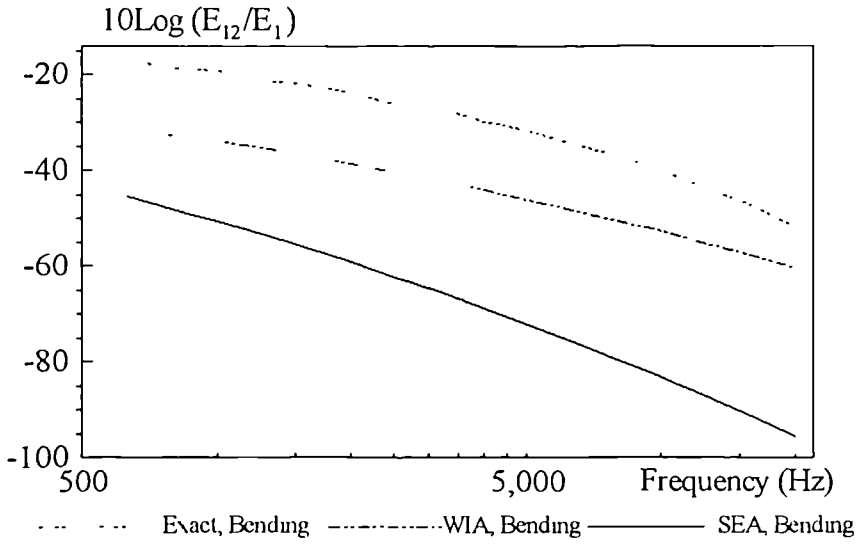

Fig. 5.49.a

Fifteen Plate Assembly
Third Octave Band Energy Ratio
Plate 12, Case 2

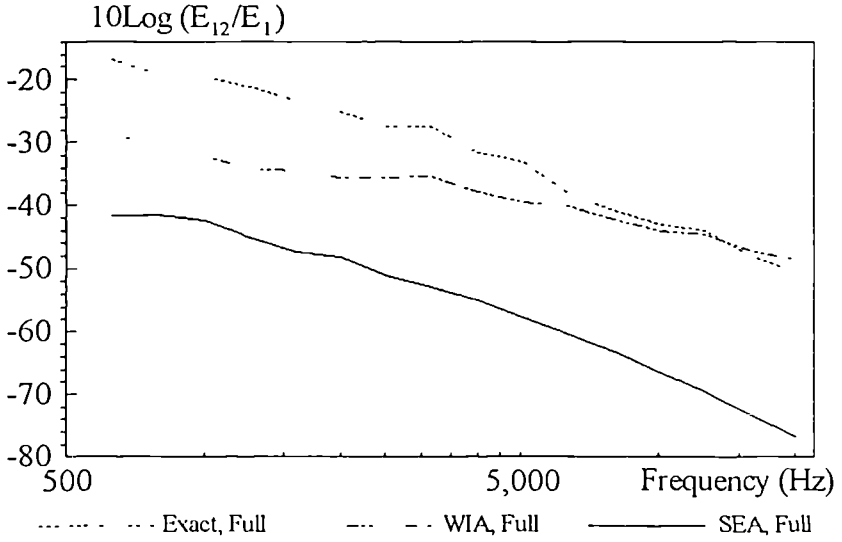

Fig. 5.49.b

Fifteen Plate Assembly
Third Octave Band Energy Ratio
Plate 13, Case 2

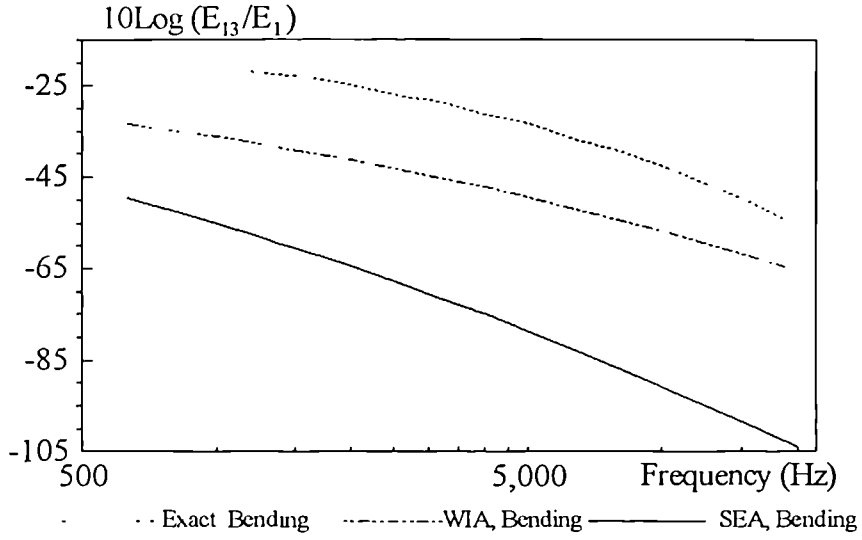

Fig. 5.50.a

Fifteen Plate Assembly
Third Octave Band Energy Ratio
Plate 13, Case 2

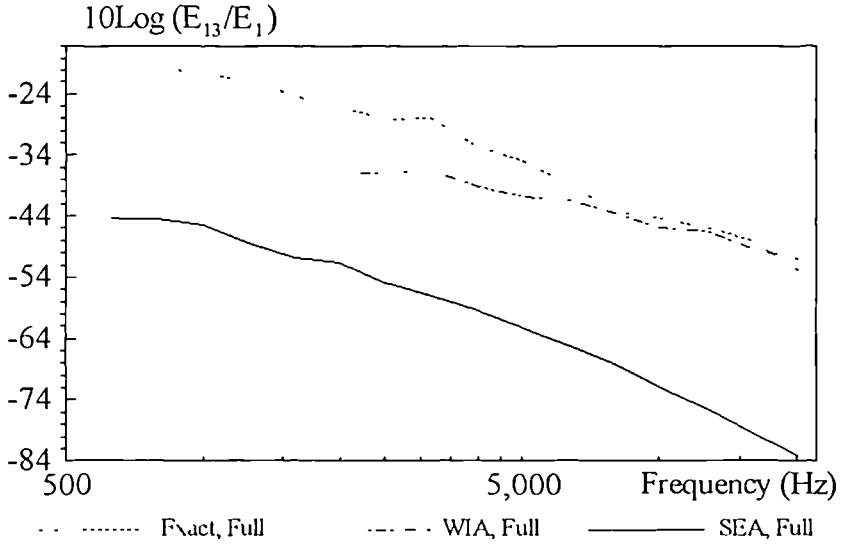

Fig. 5.50.b

Fifteen Plate Assembly
Third Octave Band Energy Ratio
Plate 14, Case 2

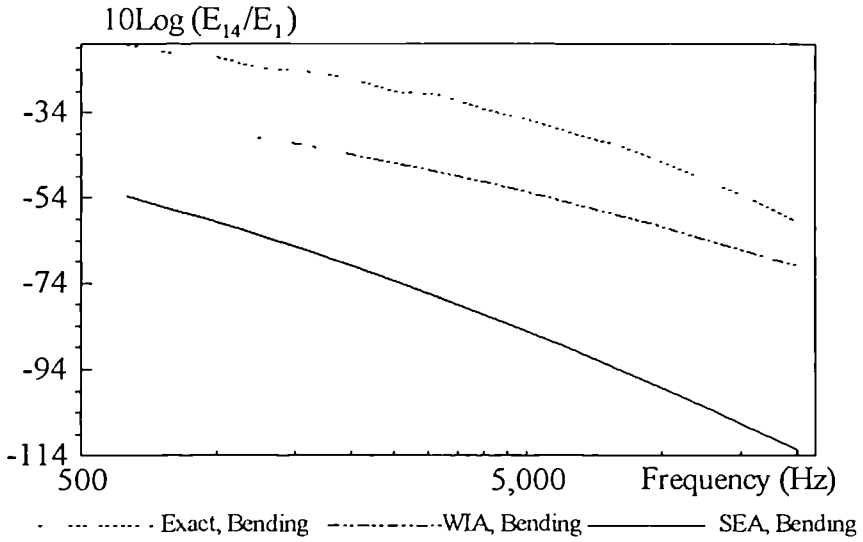

Fig. 5.51.a

Fifteen Plate Assembly
Third Octave Band Energy Ratio
Plate 14, Case 2

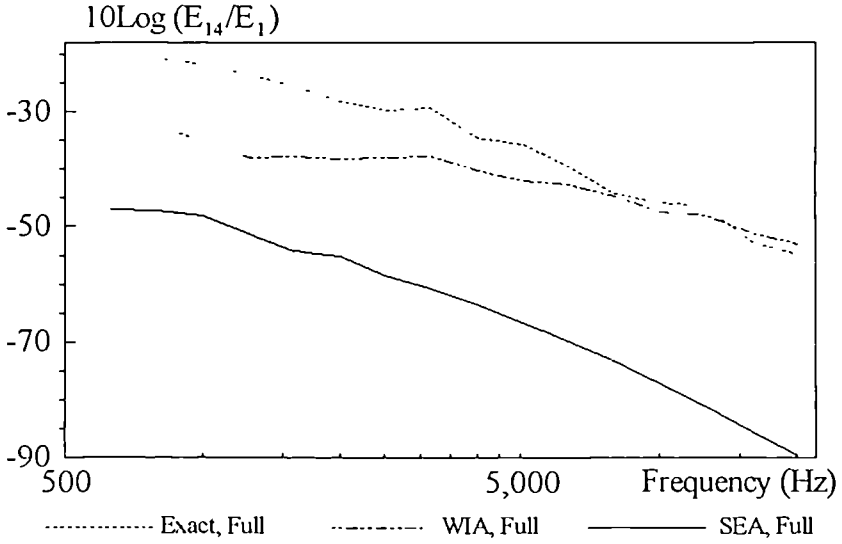

Fig. 5.51.b

Fifteen Plate Assembly
Third Octave Band Energy Ratio
Plate 15, Case 2

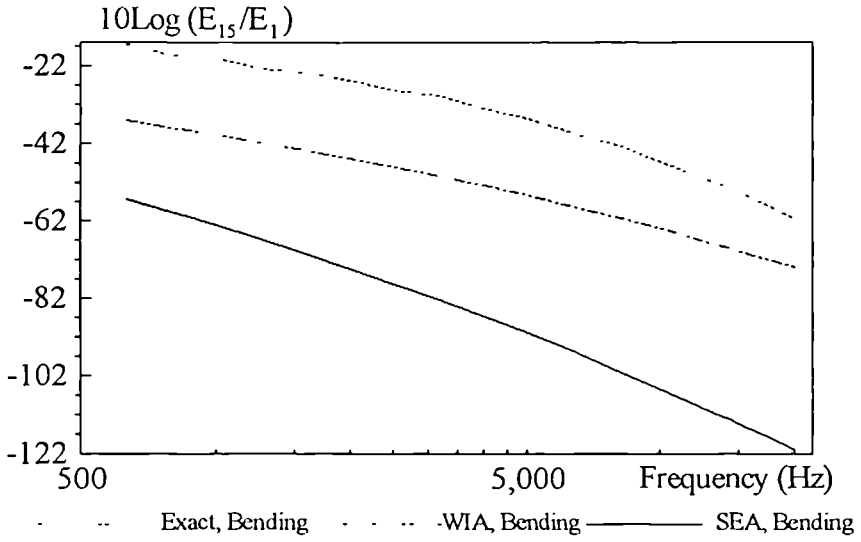

Fig 5.52.a

Fifteen Plate Assembly
Third Octave Band Energy Ratio
Plate 15, Case 2

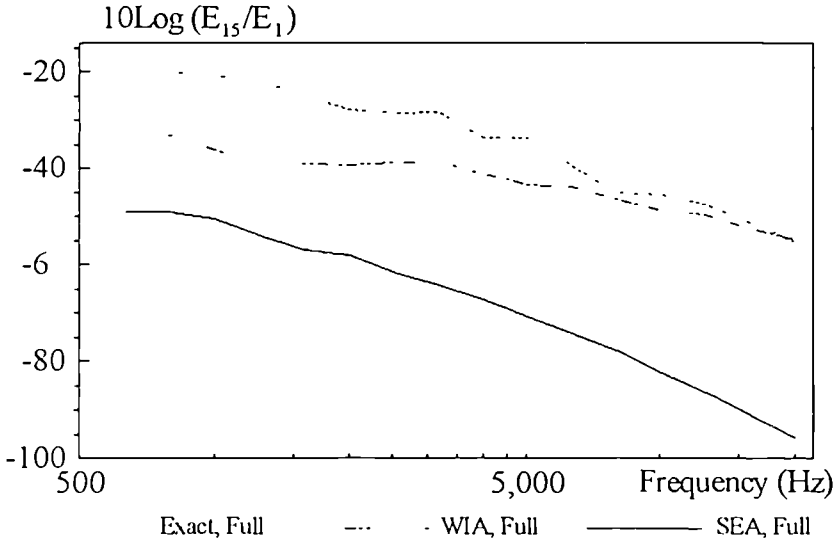

Fig. 5.52.b

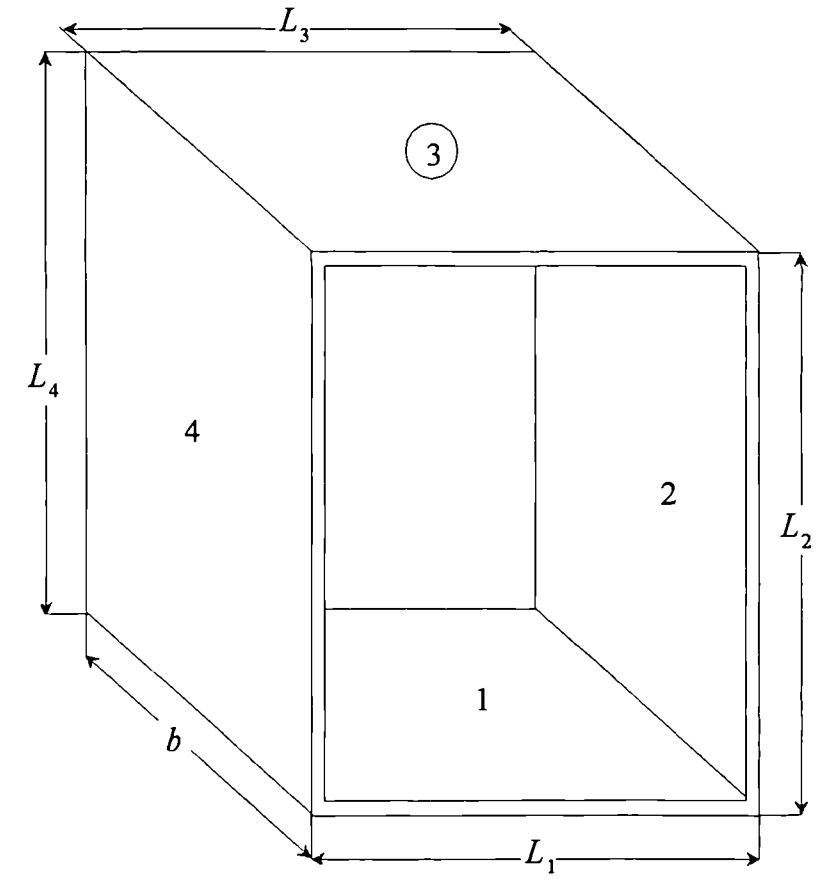

Fig. 5.53 Four plate box structure model

Four Plate Box Assembly
Third Octave Band Energy Ratio
Plate 2, Case 1

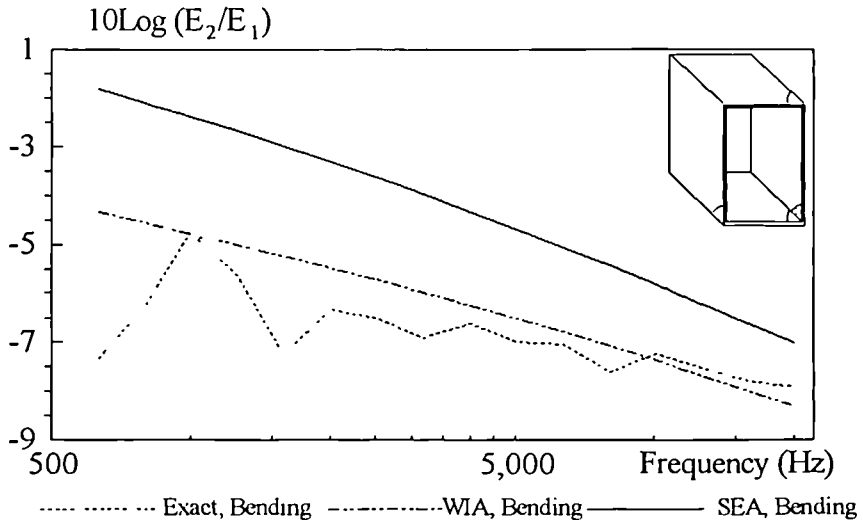

Fig. 5.54.a

Four Plate Box Assembly
Third Octave Band Energy Ratio
Plate 2, Case 1

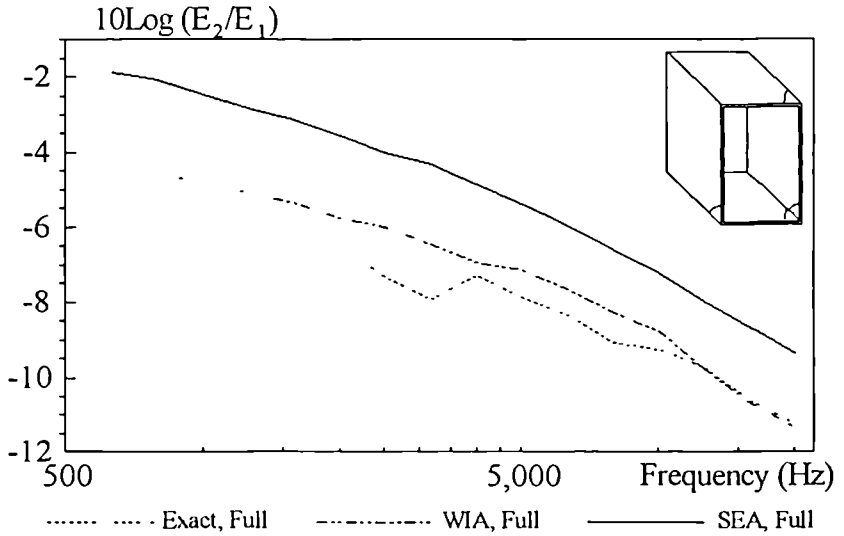

Fig. 5.54.b

Four Plate Box Assembly
Third Octave Band Energy Ratio
Plate 3, Case 1

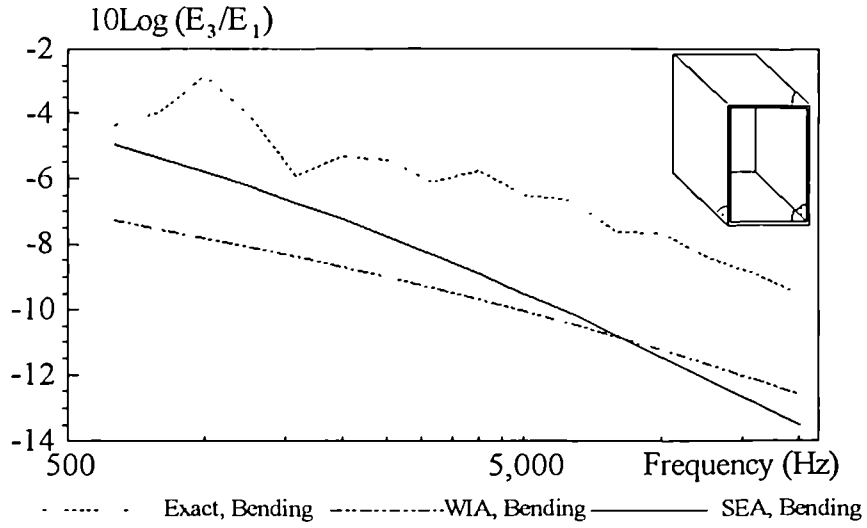

Fig. 5.55.a

Four Plate Box Assembly
Third Octave Band Energy Ratio
Plate 3, Case 1

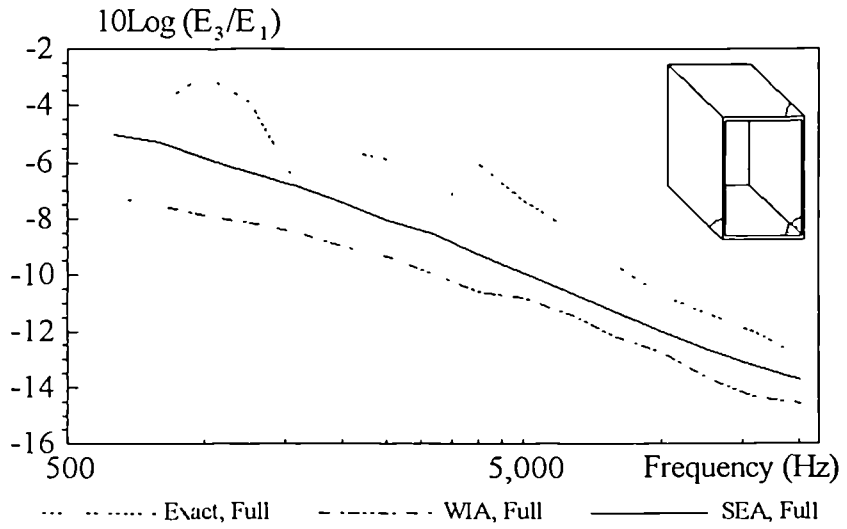

Fig 5 55.b

Four Plate Box Assembly
Third Octave Band Energy Ratio
Plate 4, Case 1

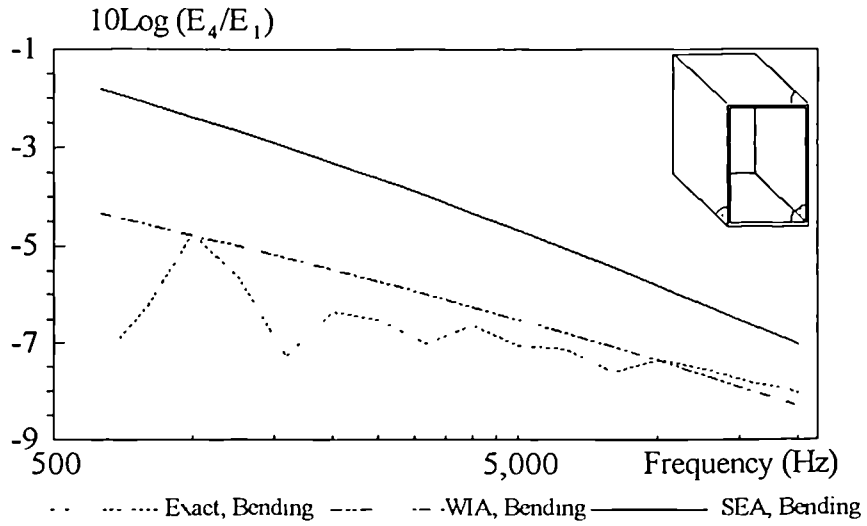

Fig. 5.56.a

Four Plate Box Assembly
Third Octave Band Energy Ratio
Plate 4, Case 1

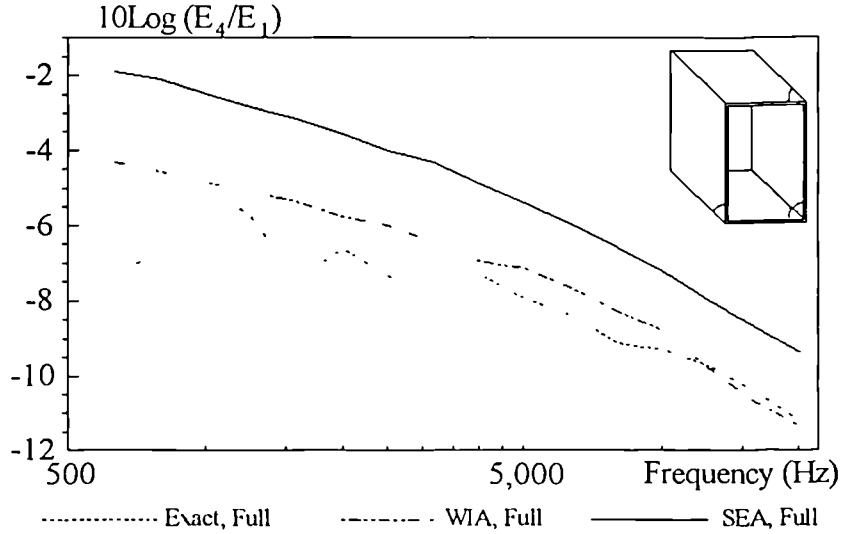

Fig. 5.56 b

Four Plate Box Assembly
Third Octave Band Energy Ratio
Plate 2, Case 2

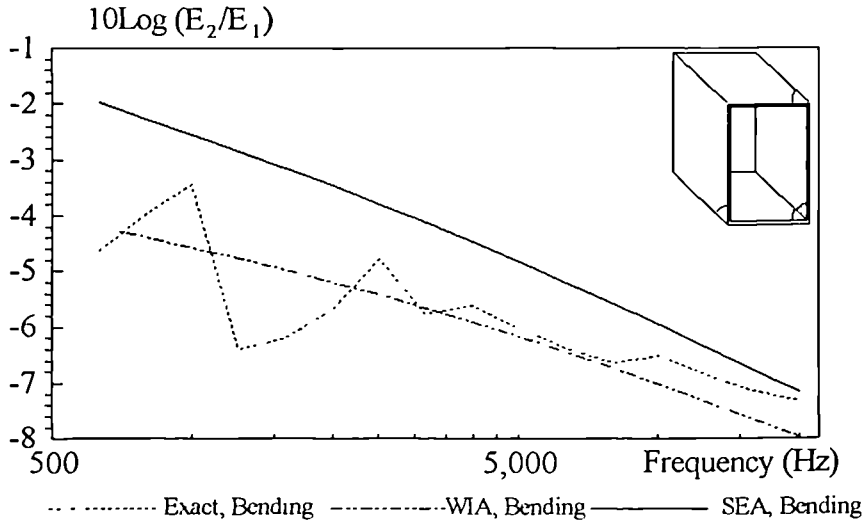

Fig. 5.57.a

Four Plate Box Assembly
Third Octave Band Energy Ratio
Plate 2, Case 2

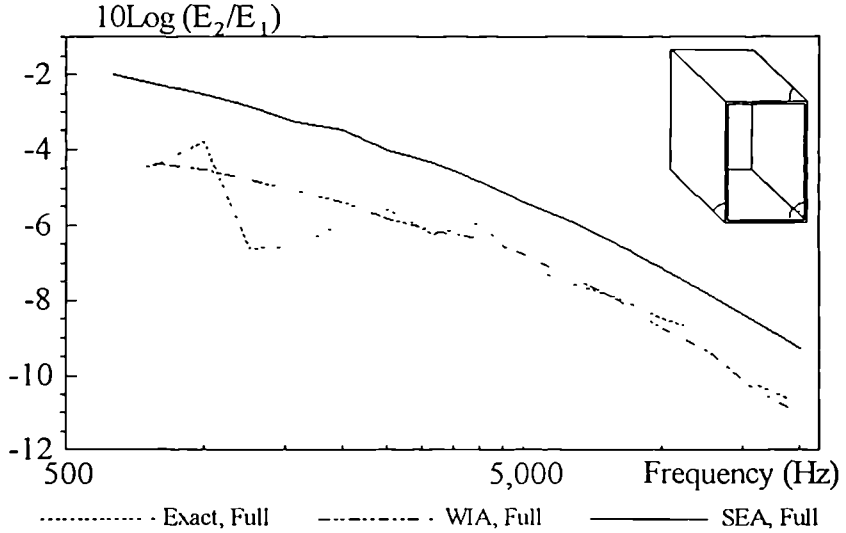

Fig. 5.57.b

Four Plate Box Assembly
Third Octave Band Energy Ratio
Plate 3, Case 2

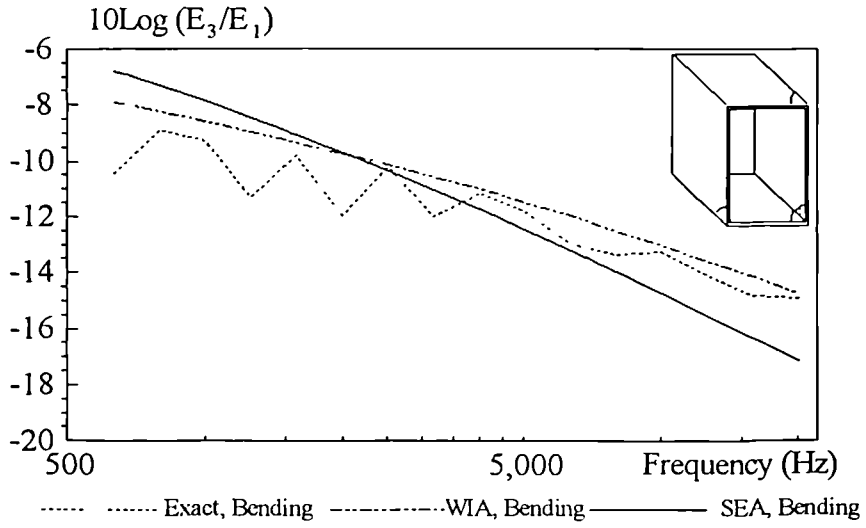

Fig. 5.58.a

Four Plate Box Assembly
Third Octave Band Energy Ratio
Plate 3, Case 2

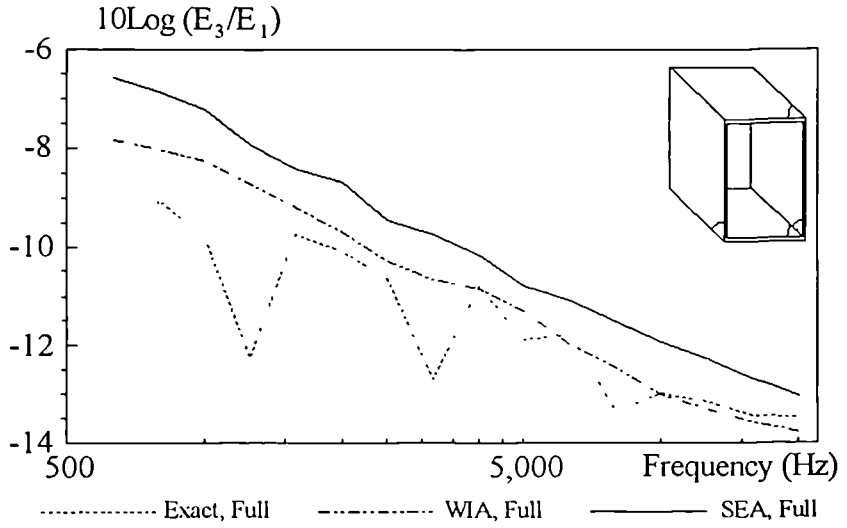

Fig. 5.58.b

Four Plate Box Assembly
Third Octave Band Energy Ratio
Plate 4, Case 2

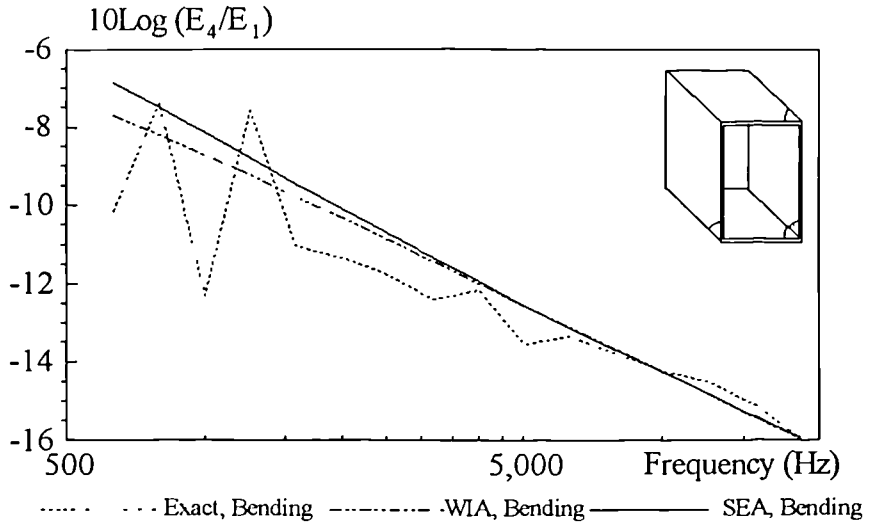

Fig. 5.59.a

Four Plate Box Assembly
Third Octave Band Energy Ratio
Plate 4, Case 2

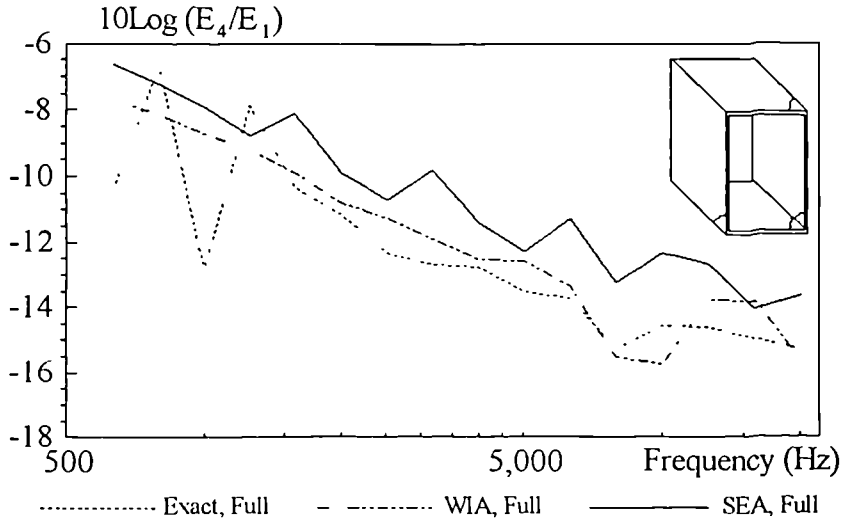

Fig. 5.59.b

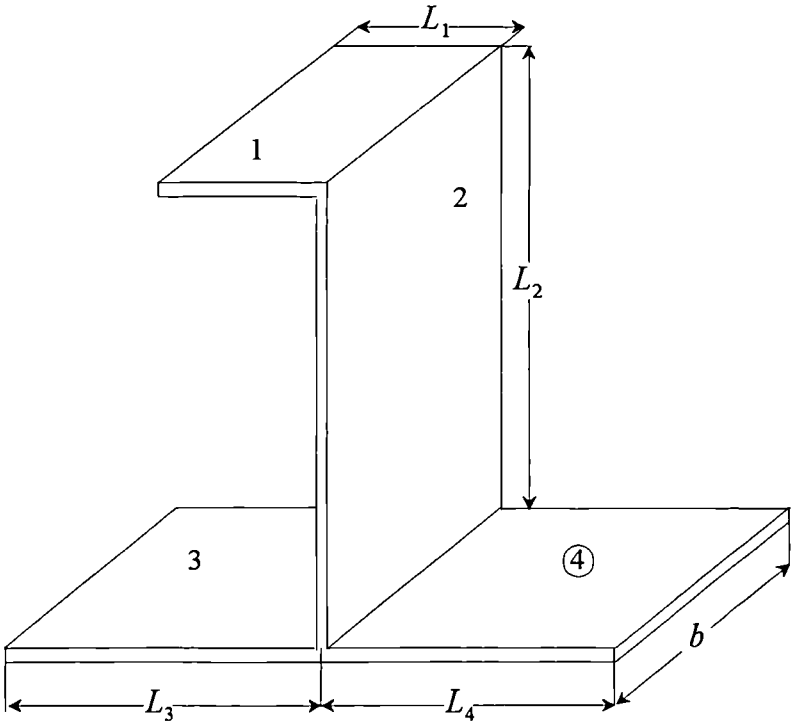

Fig. 5.61 Four plate complex-junction assembly.

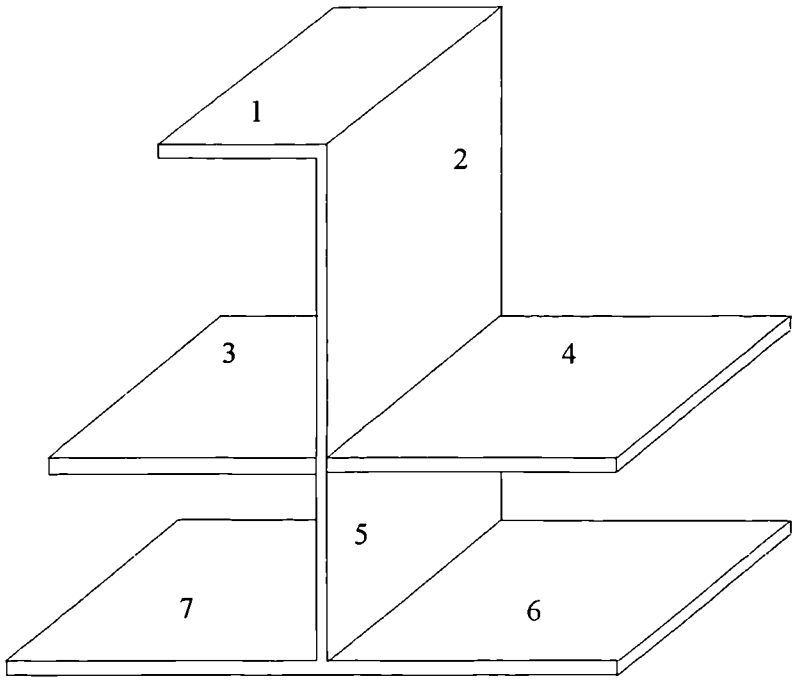

Fig. 5.62 Seven plate complex-junction assembly.

Complex-Junction Plate Assembly
Third Octave Band Energy Ratio
Plate 2, Case 1

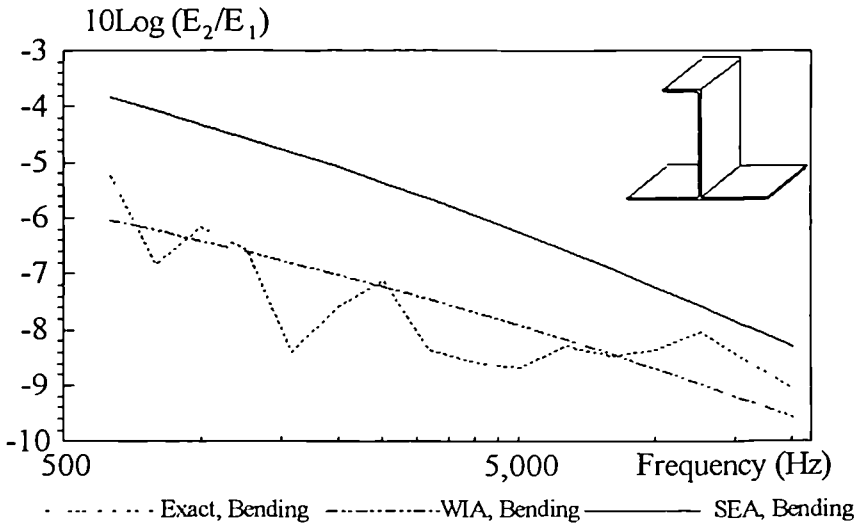

Fig. 5.63.a

Complex-Junction Plate Assembly
Third Octave Band Energy Ratio
Plate 2, Case 1

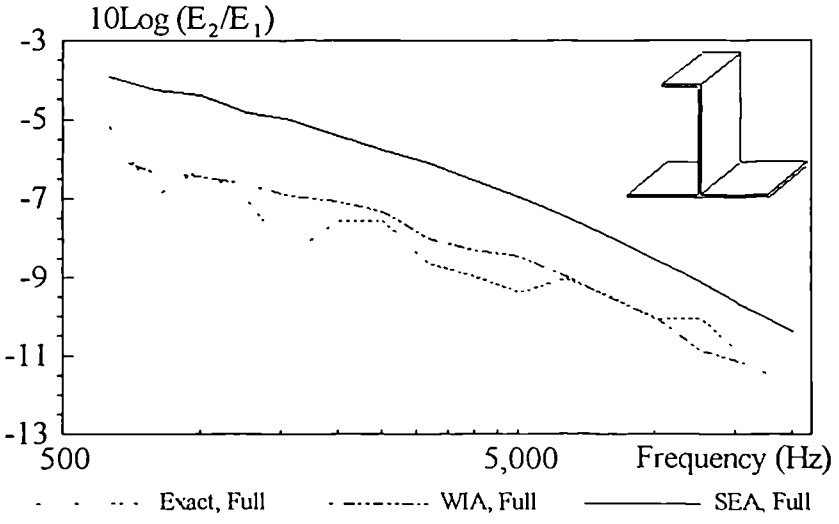

Fig. 5.63.b

Complex-Junction Plate Assembly
Third Octave Band Energy Ratio
Plate 3, Case 1

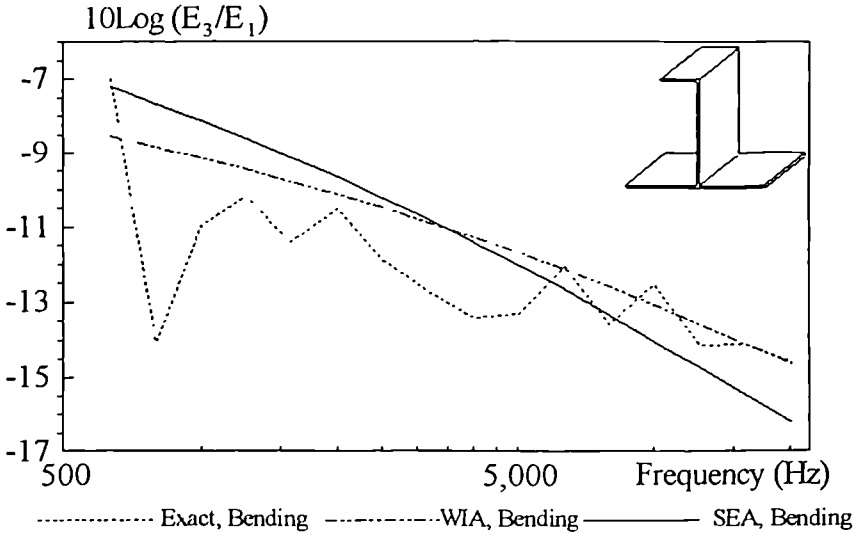

Fig. 5.64.a

Complex-Junction Plate Assembly
Third Octave Band Energy Ratio
Plate 3, Case 1

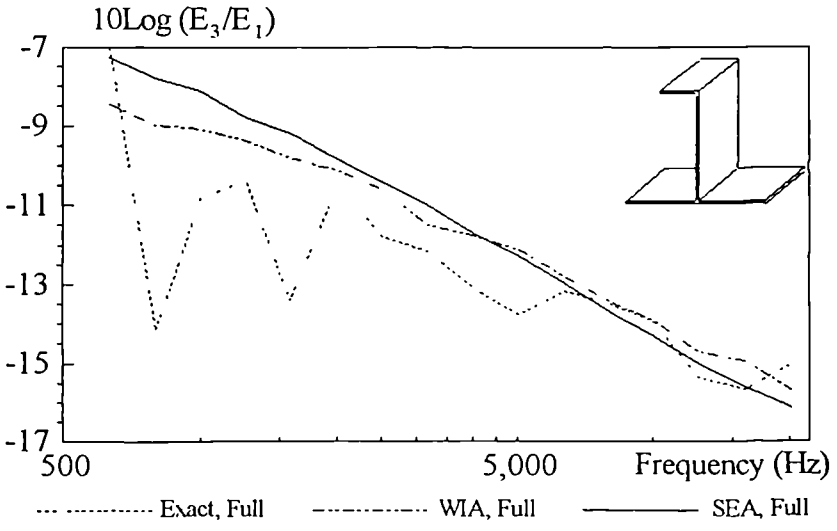

Fig. 5.64.b

Complex-Junction Plate Assembly
Third Octave Band Energy Ratio
Plate 4, Case 1

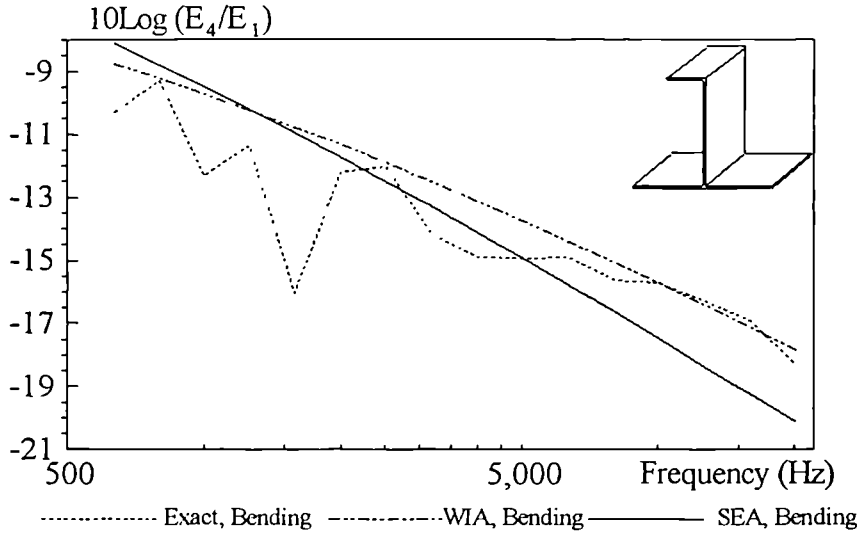

Fig. 5.65.a

Complex-Junction Plate Assembly
Third Octave Band Energy Ratio
Plate 4, Case 1

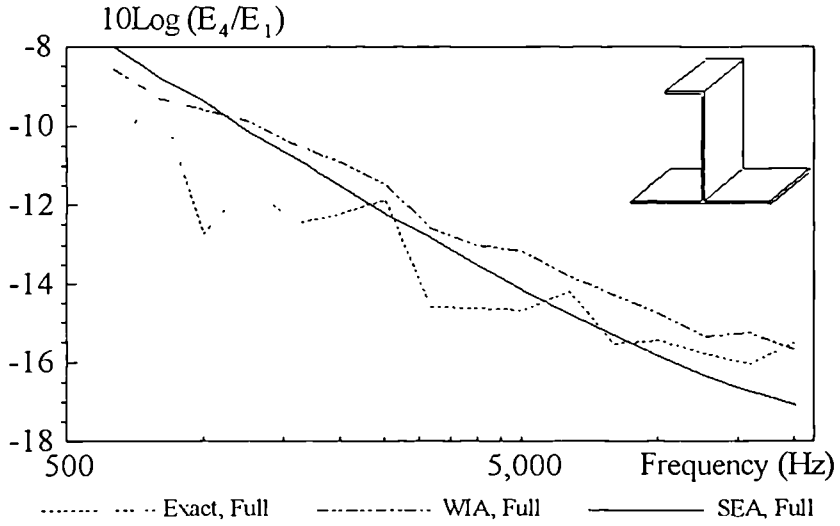

Fig. 5.65.b

Complex-Junction Plate Assembly
Third Octave Band Energy Ratio
Plate 2, Case 2

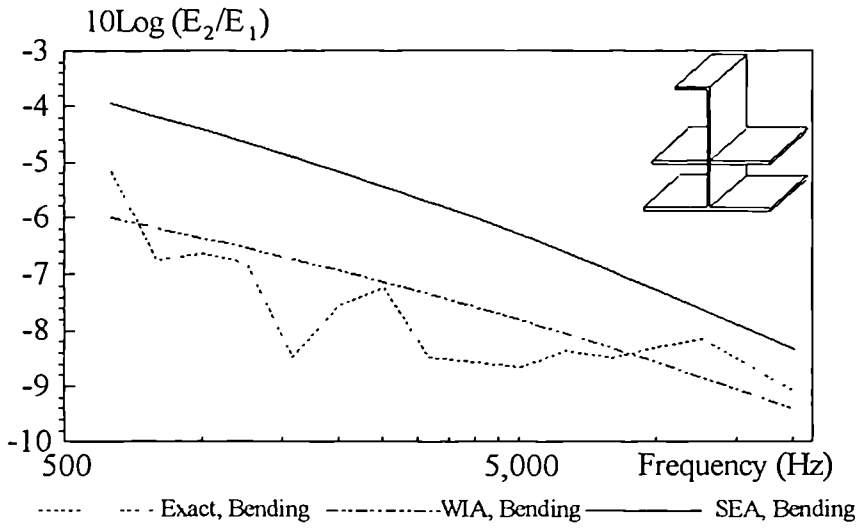

Fig. 5.66.a

Complex-Junction Plate Assembly
Third Octave Band Energy Ratio
Plate 2, Case 2

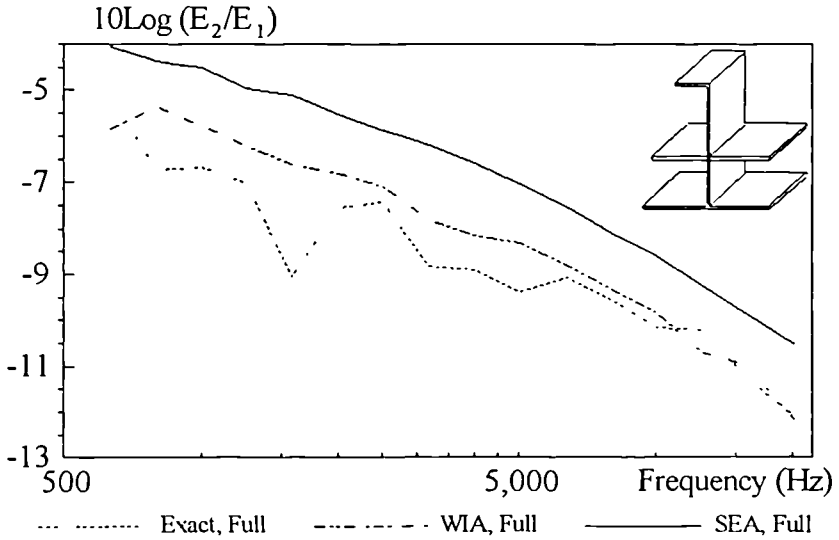

Fig. 5.66.b

Complex-Junction Plate Assembly
Third OctaveBand Energy Ratio
Plate 3, Case 2

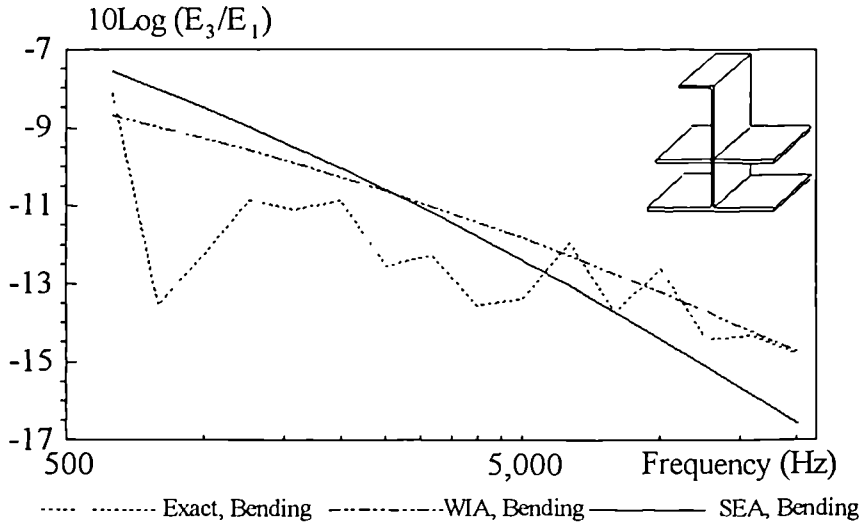

Fig. 5.67.a

Complex-Junction Plate Assembly
Third Octave Band Energy Ratio
Plate 3, Case 2

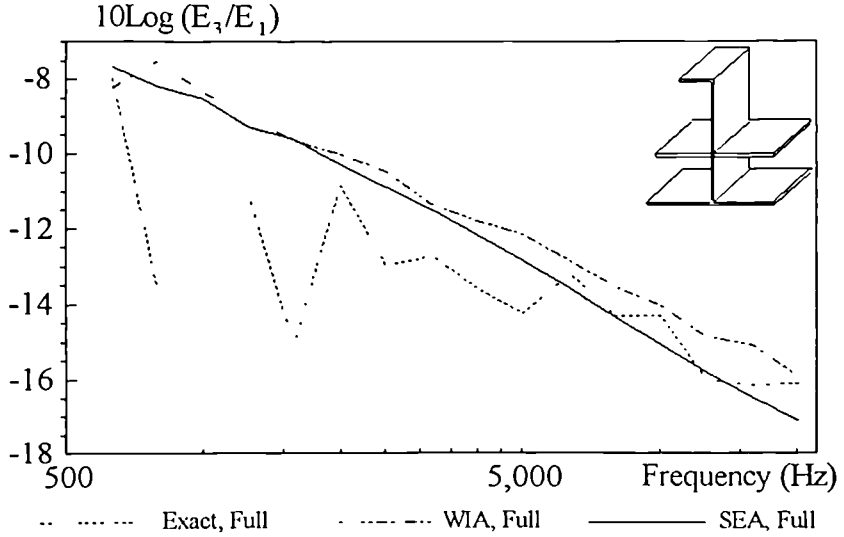

Fig. 5.67.b

Complex-Junction Plate Assembly
Third Octave Band Energy Ratio
Plate 4, Case 2

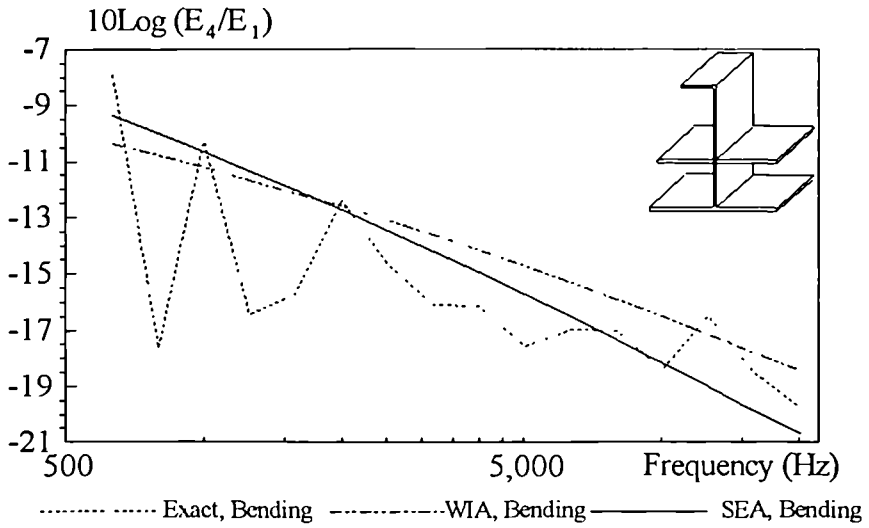

Fig. 5.68.a

Complex-Junction Plate Assembly
Third Octave Band Energy Ratio
Plate 4, Case 2

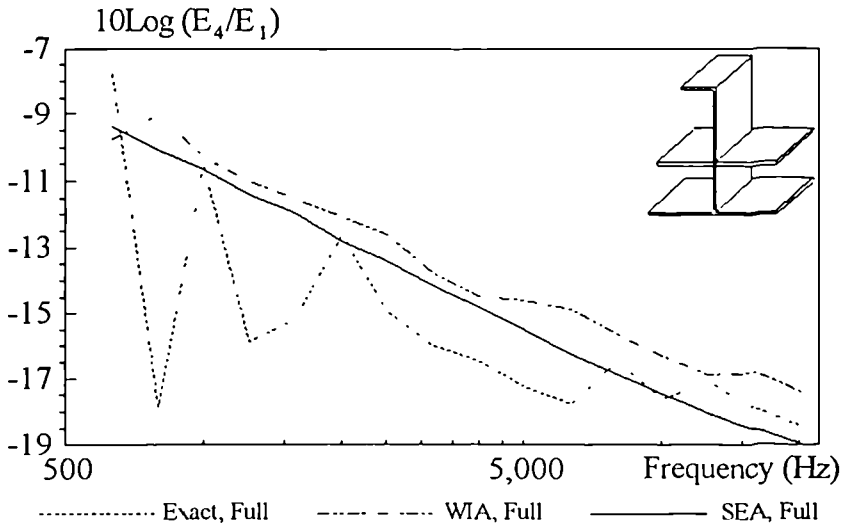

Fig. 5.68.b

Complex-Junction Plate Assembly
Third Octave Band Energy Ratio
Plate 5, Case 2

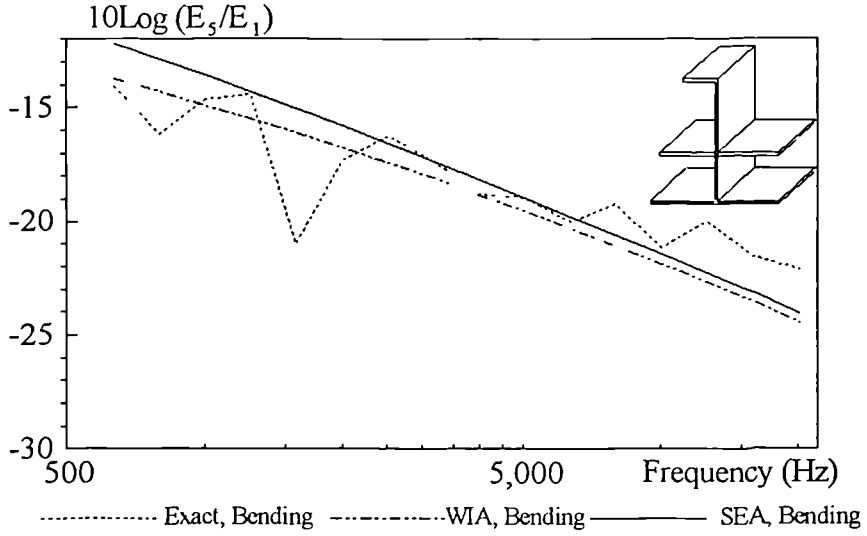

Fig. 5.69.a

Complex-Junction Plate Assembly
Third Octave Band Energy Ratio
Plate 5, Case 2

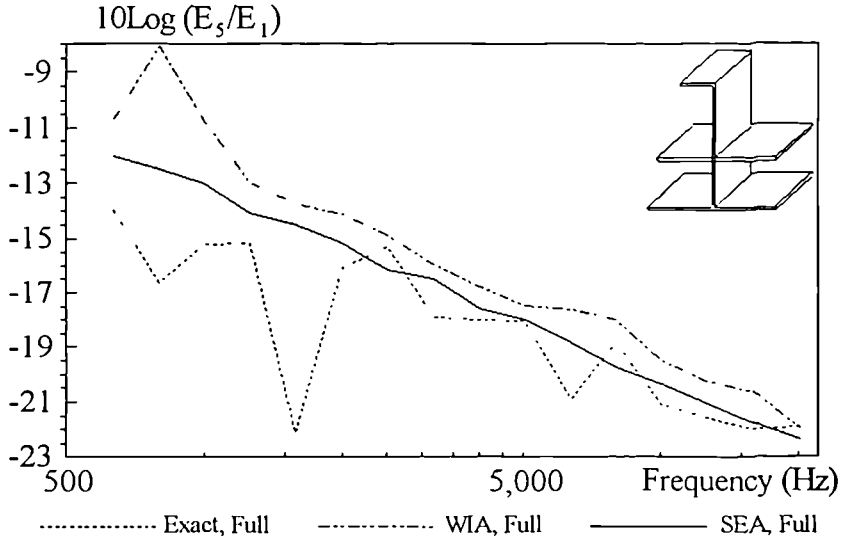

Fig. 5.69.b

Complex-Junction Plate Assembly
Third Octave Band Energy Ratio
Plate 6, Case 2

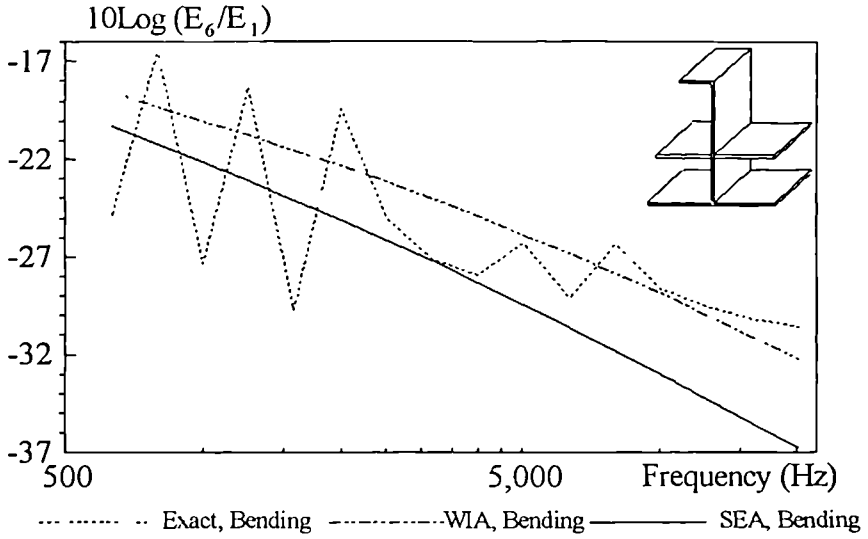

Fig. 5.70.a

Complex-Junction Plate Assembly
Third Octave Band Energy Ratio
Plate 6, Case 2

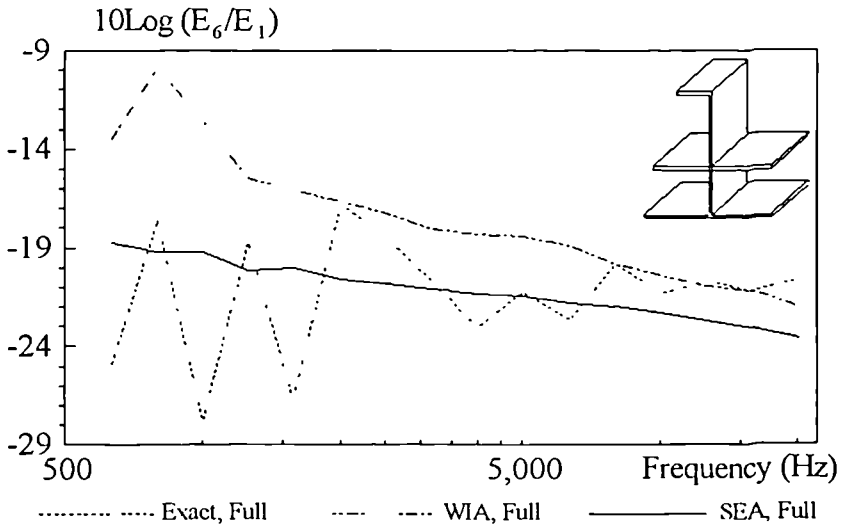

Fig. 5.70.b

Complex-Junction Plate Assembly
Third Octave Band Energy Ratio
Plate 7, Case 2

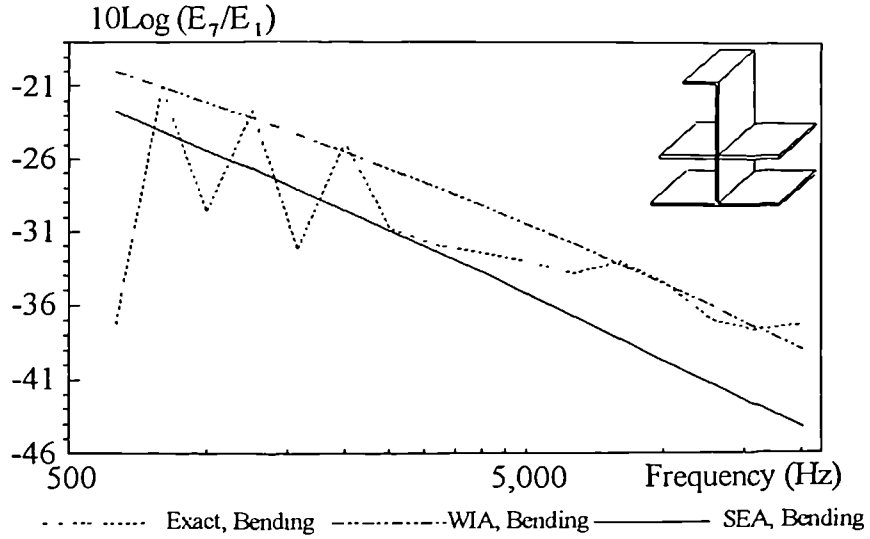

Fig. 5.71.a

Complex-Junction Plate Assembly
Third Octave Band Energy Ratio
Plate 7, Case 2

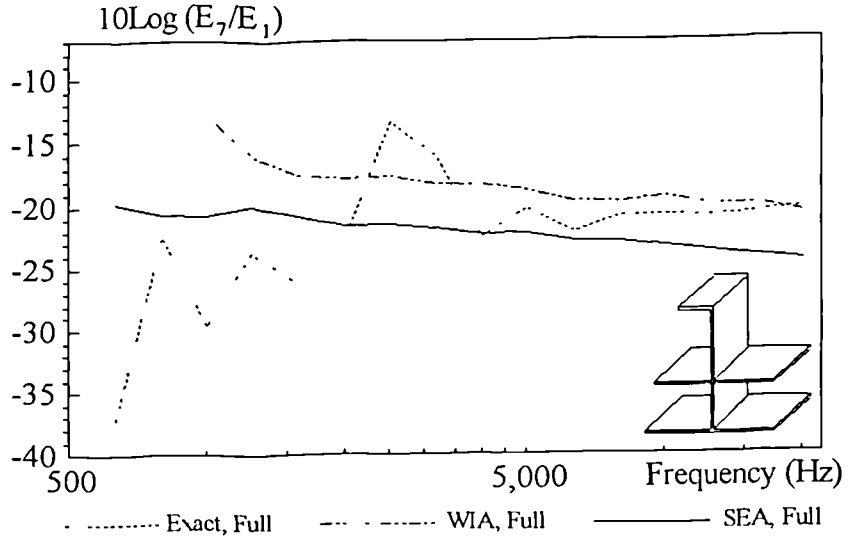

Fig. 5.71.b

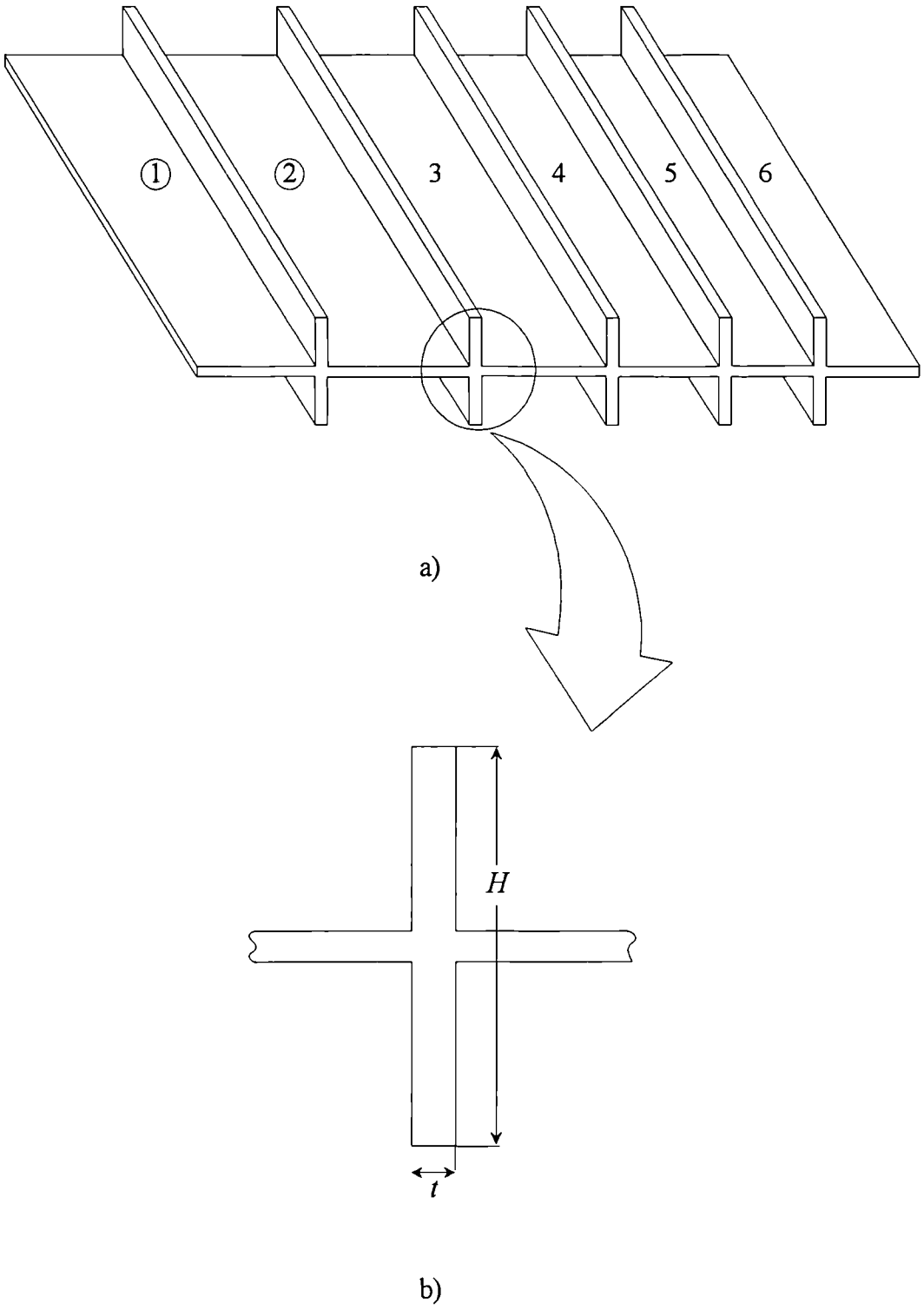

Fig. 5.72
a) Six plate assembly with five symmetric stringers
b) Stringer cross section and dimensions

Symmetrically Stiffened Plate Assembly
Third Octave Band Energy Ratio
Plate 2, Case 1

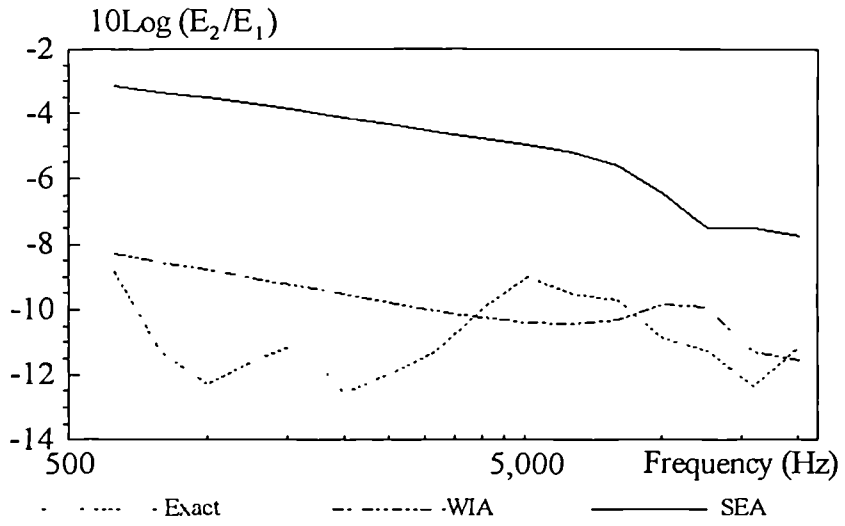

Fig. 5.73

Symmetrically Stiffened Plate Assembly
Third Octave Band Energy Ratio
Plate 3, Case 1

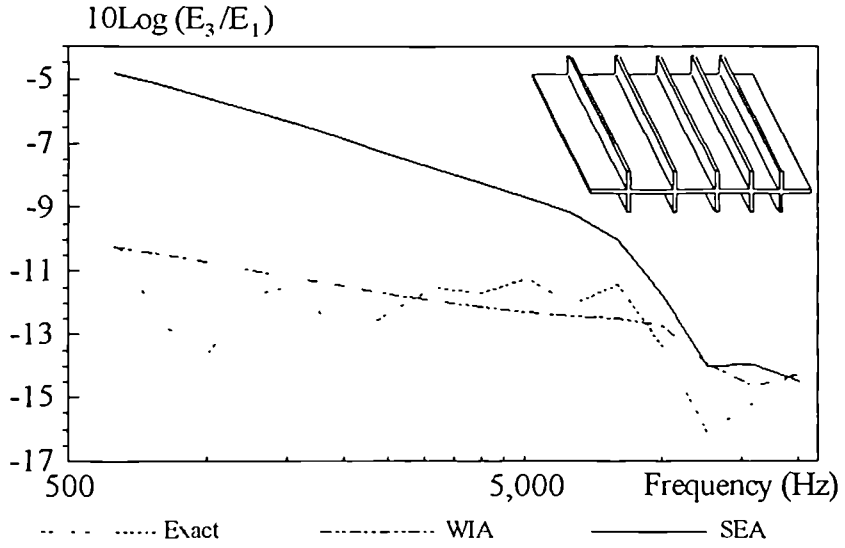

Fig 5.74

Symmetrically Stiffened Plate Assembly
Third Octave Band Energy Ratio
Plate 4, Case 1

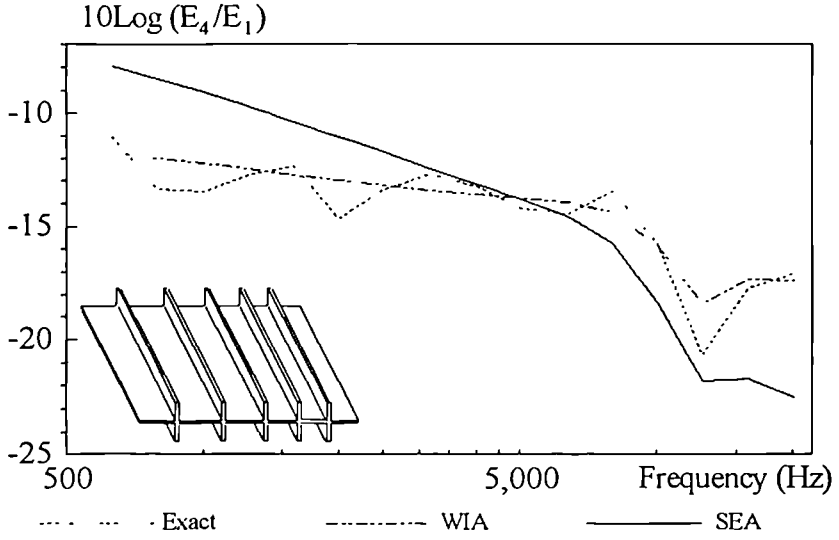

Fig. 5.75

Symmetrically Stiffened Plate Assembly
Third Octave Band Energy Ratio
Plate 5, Case 1

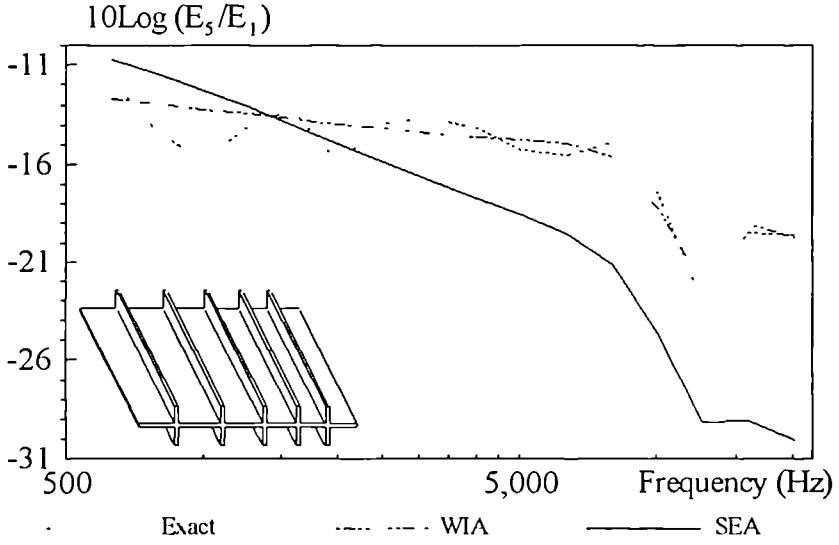

Fig. 5.76

Symmetrically Stiffened Plate Assembly
Third Octave Band Energy Ratio
Plate 6, Case 1

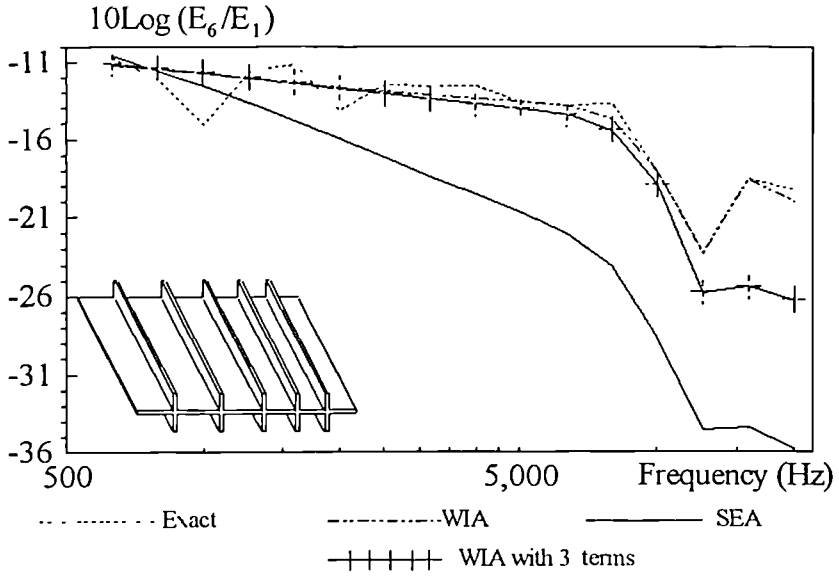

Fig. 5.77

Symmetrically Stiffened Plate Assembly
Third Octave Band Energy Ratio
Plate 2, Case 2

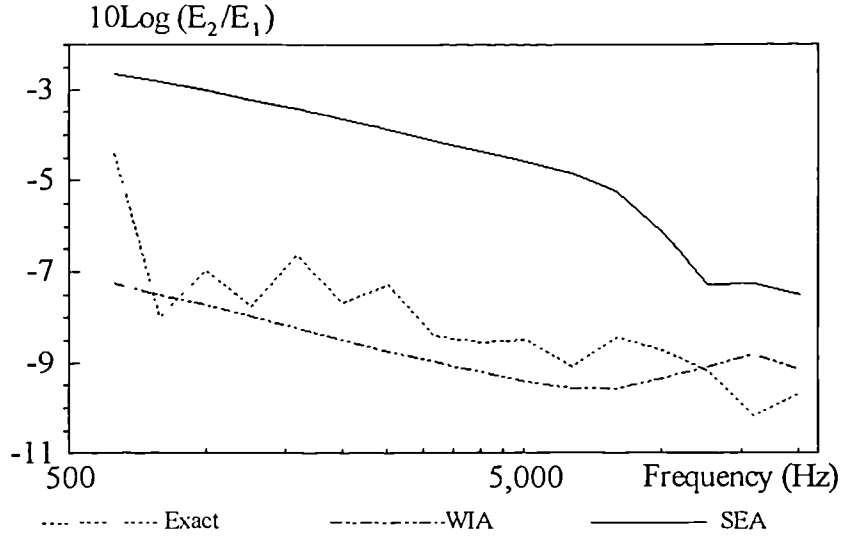

Fig. 5.78

Symmetrically Stiffened Plate Assembly
Third Octave Band Energy Ratio
Plate 3, Case 2

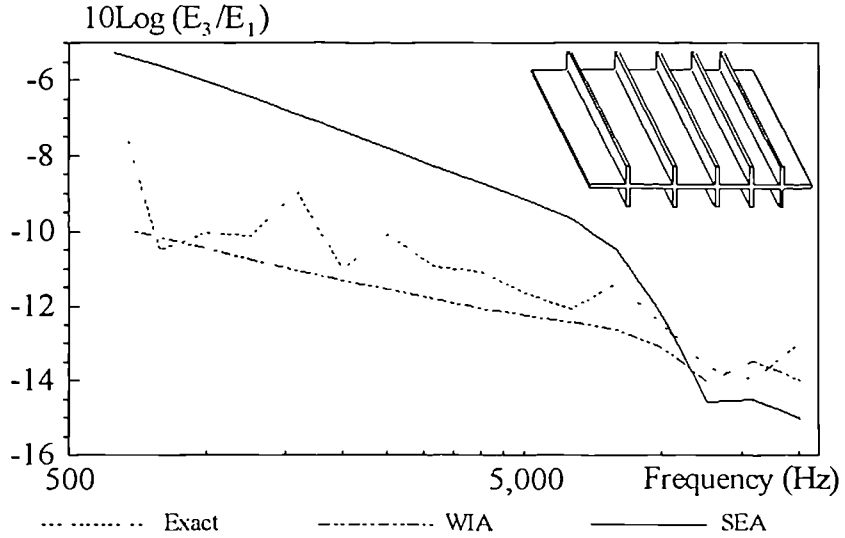

Fig. 5.79

Symmetrically Stiffened Plate Assembly
Third Octave Band Energy Ratio
Plate 4, Case 2

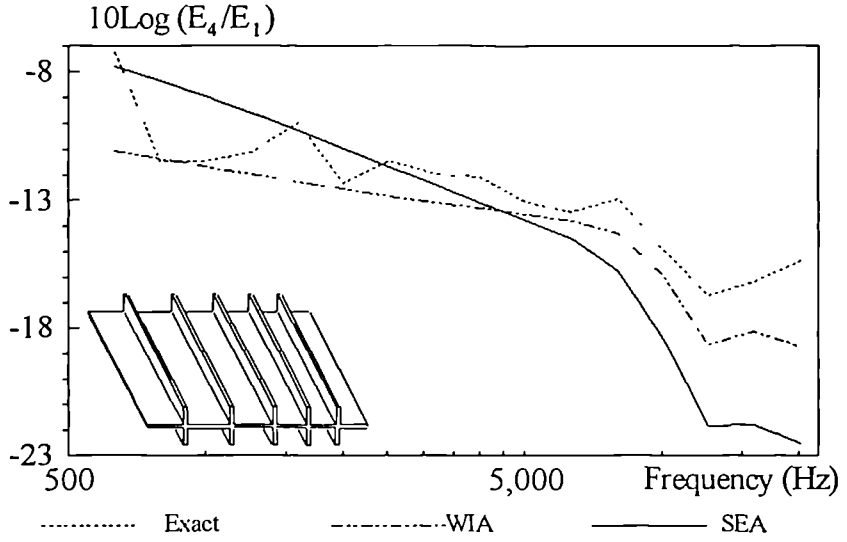

Fig. 5.80

Symmetrically Stiffened Plate Assembly
Third Octave Band Energy Ratio
Plate 5, Case 2

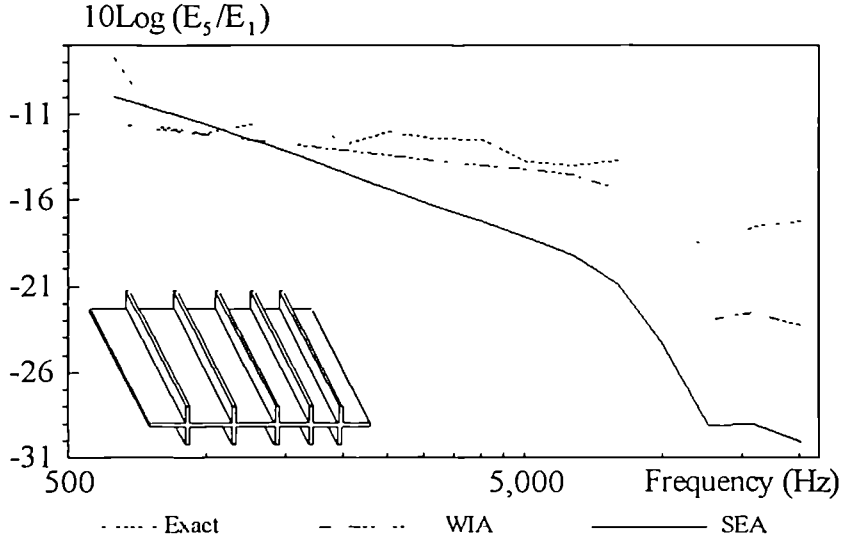

Fig. 5.81

Symmetrically Stiffened Plate Assembly
Third Octave Energy Ratio
Plate 6, Case 2

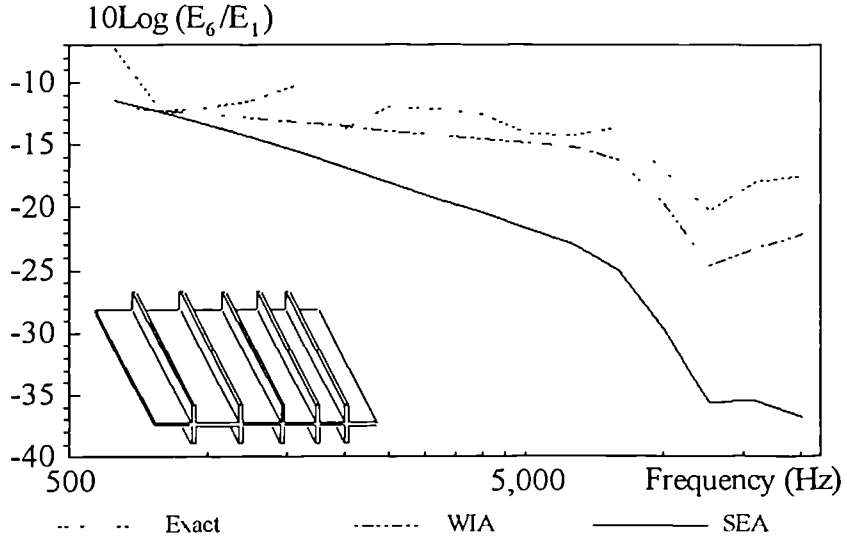

Fig. 5.82

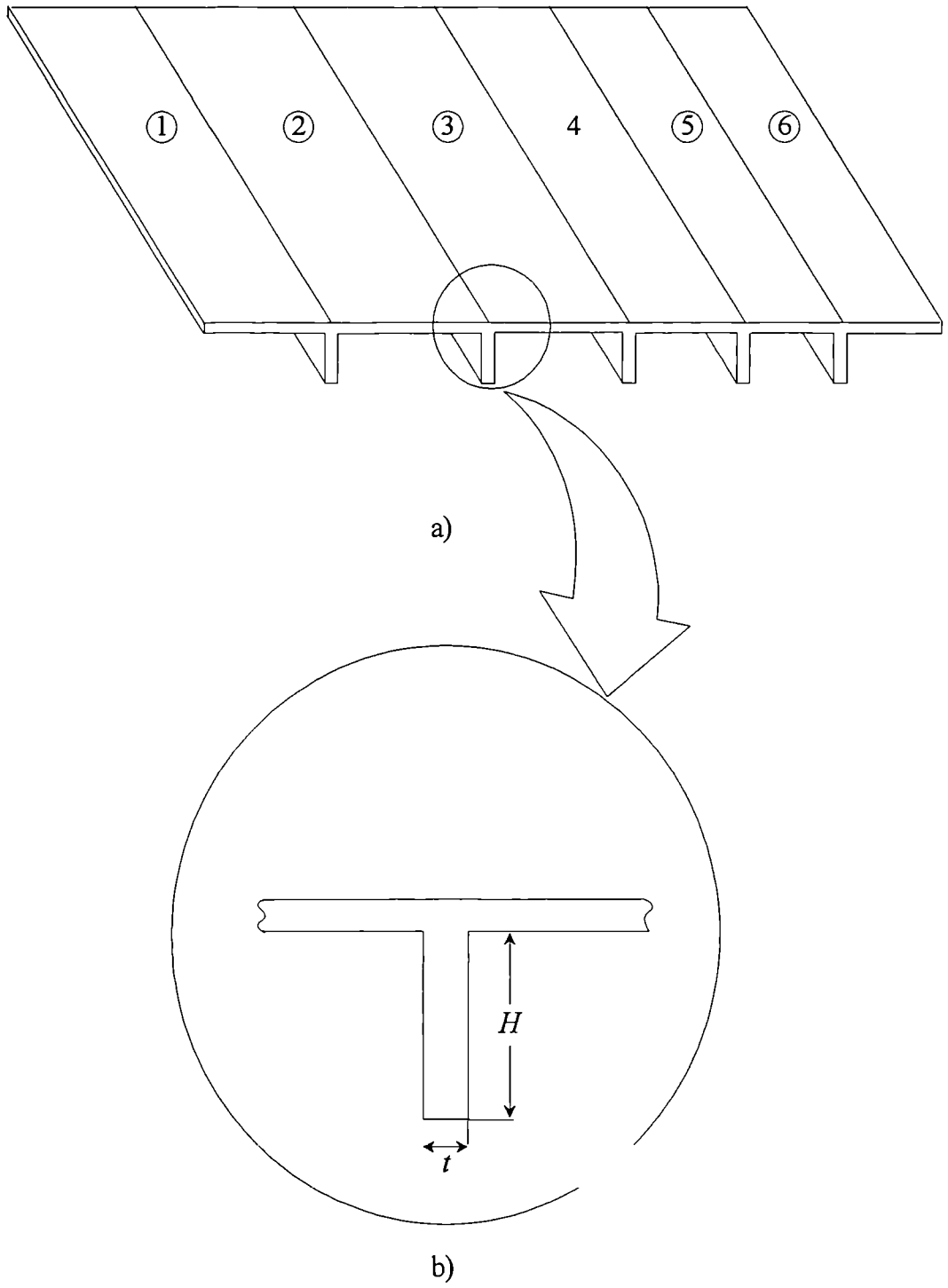

Fig. 5.83
a) Six plate assembly with five asymmetric stringers
b) Stringer cross section and dimensions

Asymmetrically Stiffened Plate Assembly
Third Octave Band Energy Ratio
Plate 2, Case 1

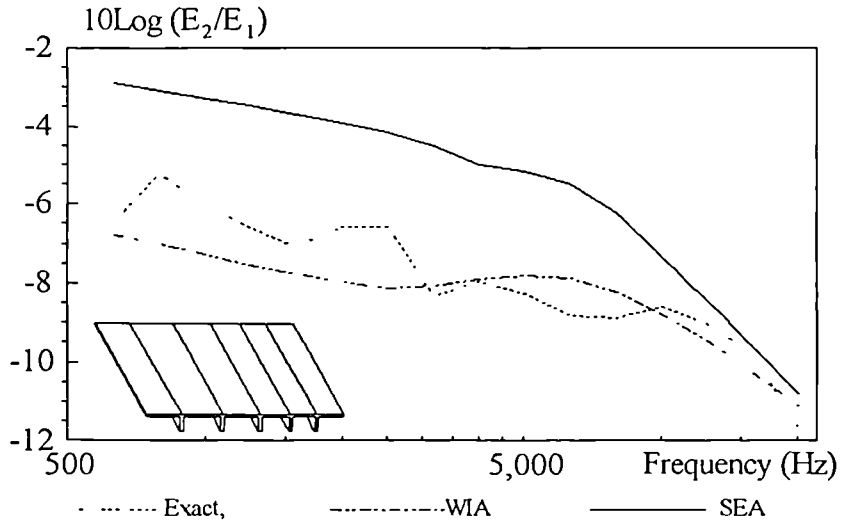

Fig. 5.84

Asymmetrically Stiffened Plate Assembly
Third Octave Band Energy Ratio
Plate 3, Case 1

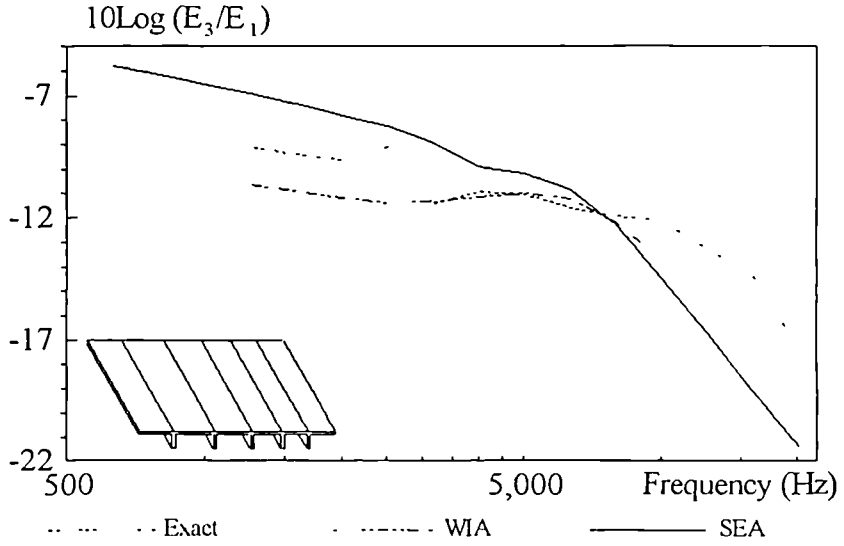

Fig. 5.85

Asymmetrically Stiffened Plate Assembly
Third Octave Band Energy Ratio
Plate 4, Case 1

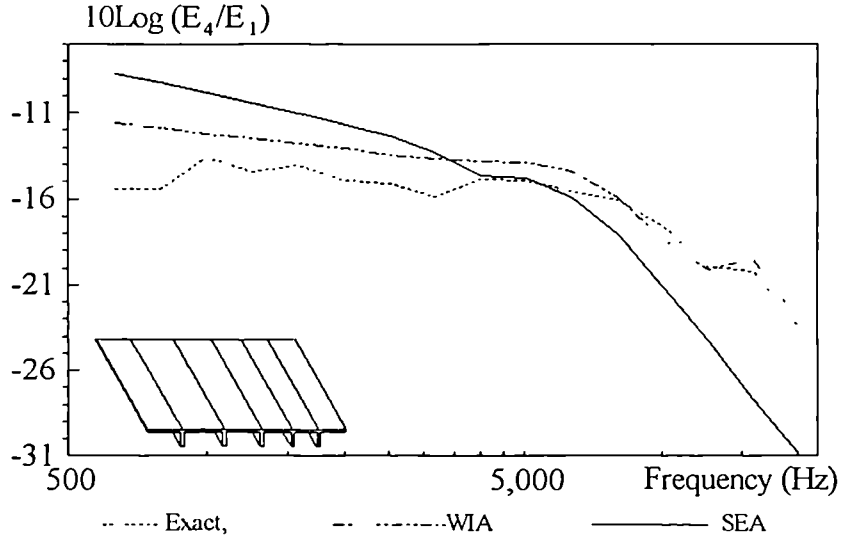

Fig. 5.86

Asymmetrically Stiffened Plate Assembly
Third Octave Band Energy Ratio
Plate 5, Case 1

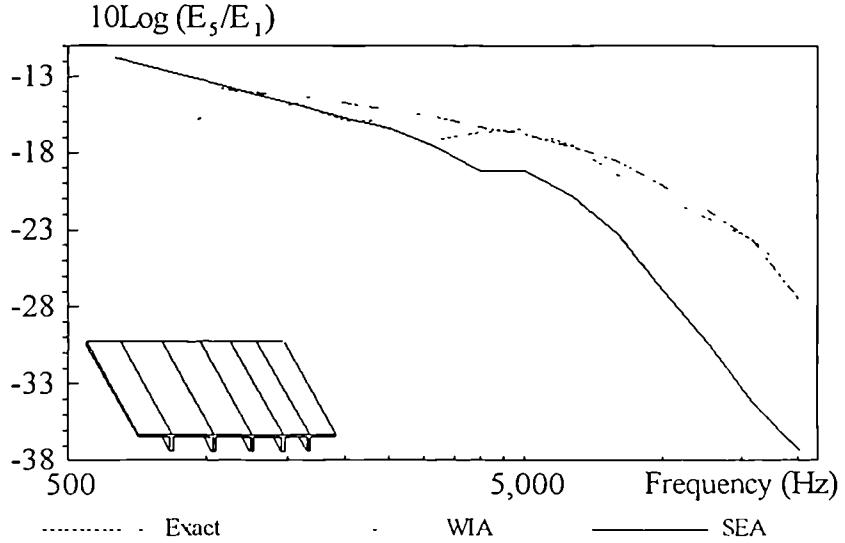

Fig. 5.87

Asymmetrically Stiffened Plate Assembly
Third Octave Band Energy Ratio
Plate 6, Case 1

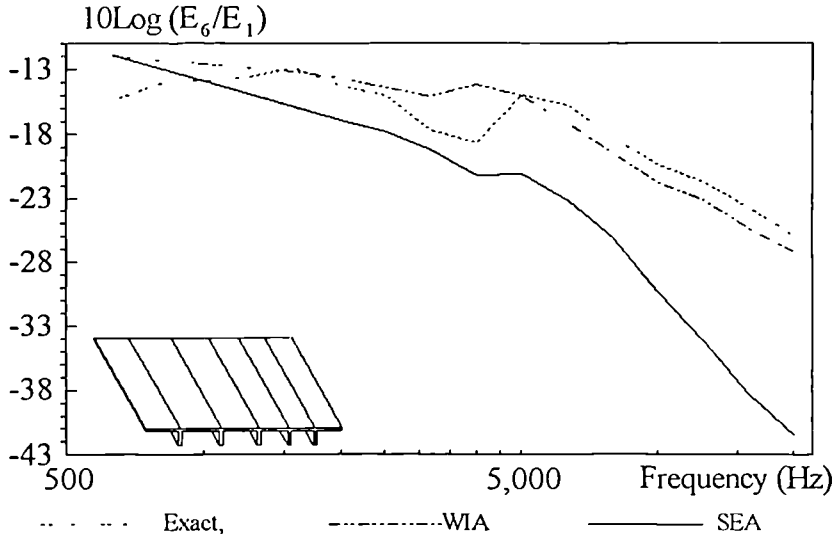

Fig. 5.88

Asymmetrically Stiffened Plate Assembly
Third Octave Band Energy Ratio
Plate 2, Case 2

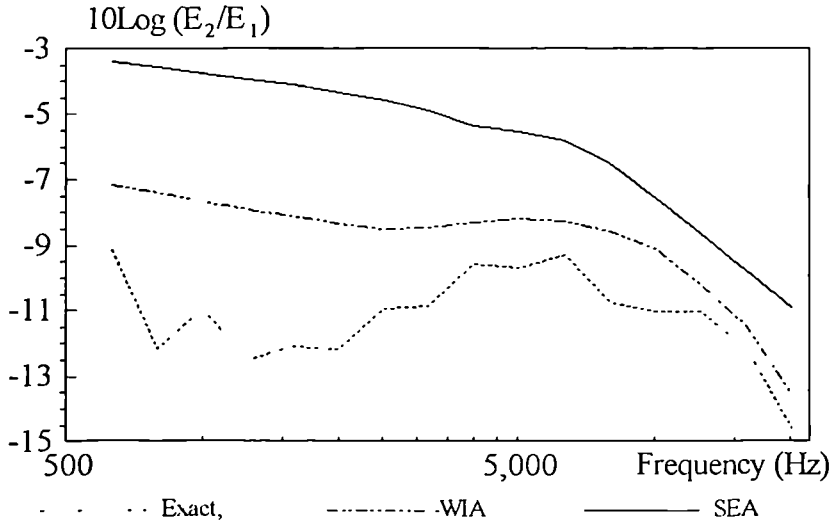

Fig. 5.89

Asymmetrically Stiffened Plate Assembly
Third Octave Band Energy Ratio
Plate 3, Case 2

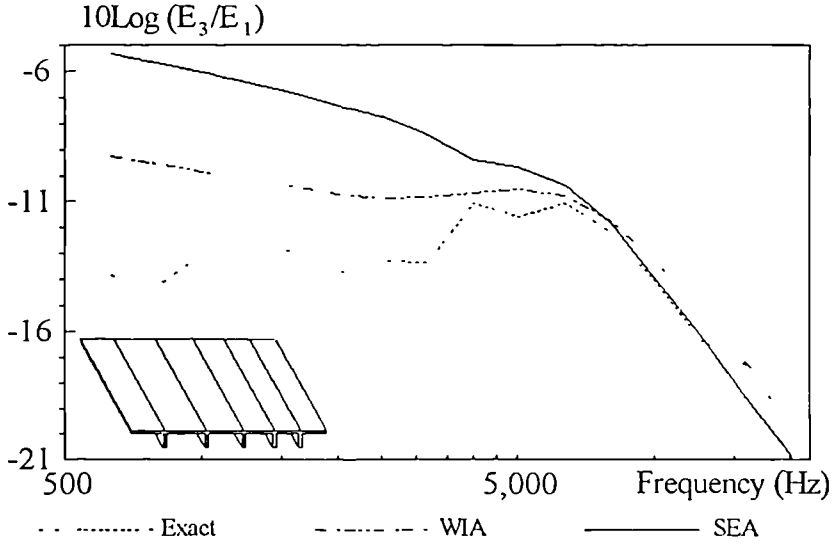

Fig. 5.90

Asymmetrically Stiffened Plate Assembly
Third Octave Band Energy Ratio
Plate 4, Case 2

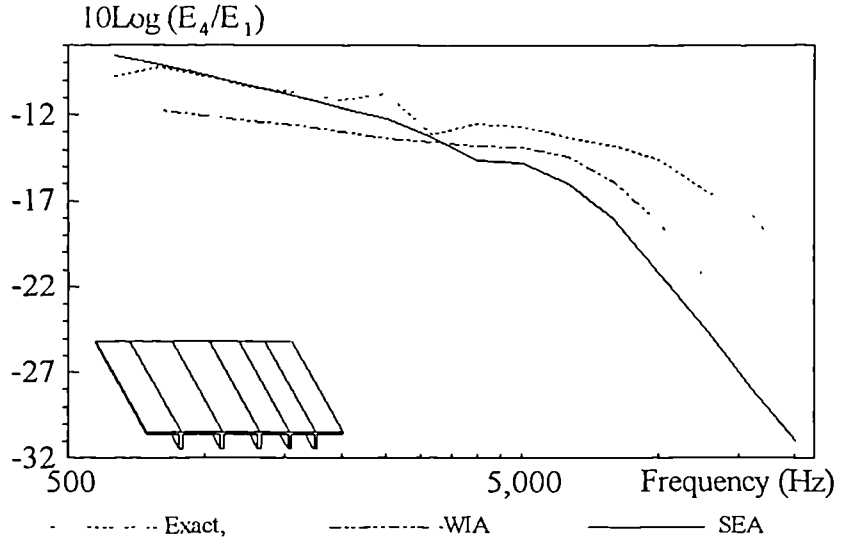

Fig. 5.91

Asymmetrically Stiffened Plate Assembly
Third Octave Band Energy Ratio
Plate 5, Case 2

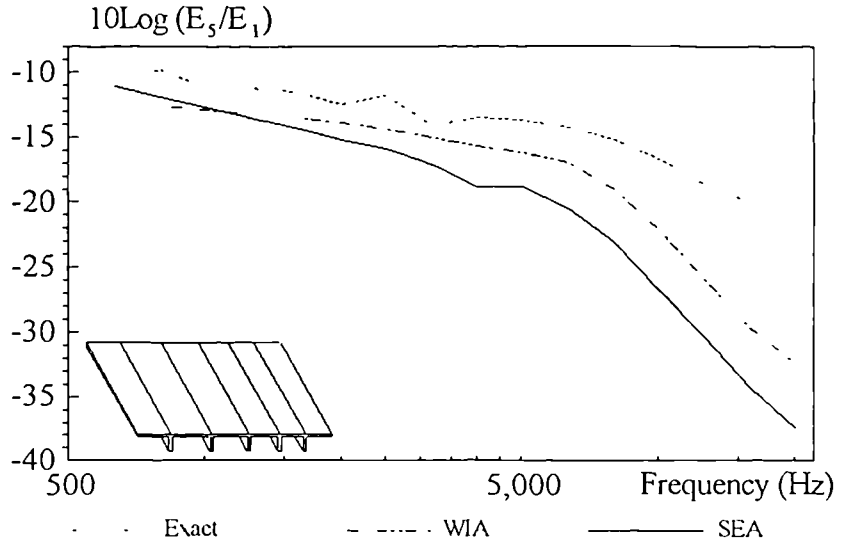

Fig. 5.92

Asymmetrically Stiffened Plate Assembly
Third Octave Band Energy Ratio
Plate 6, Case 2

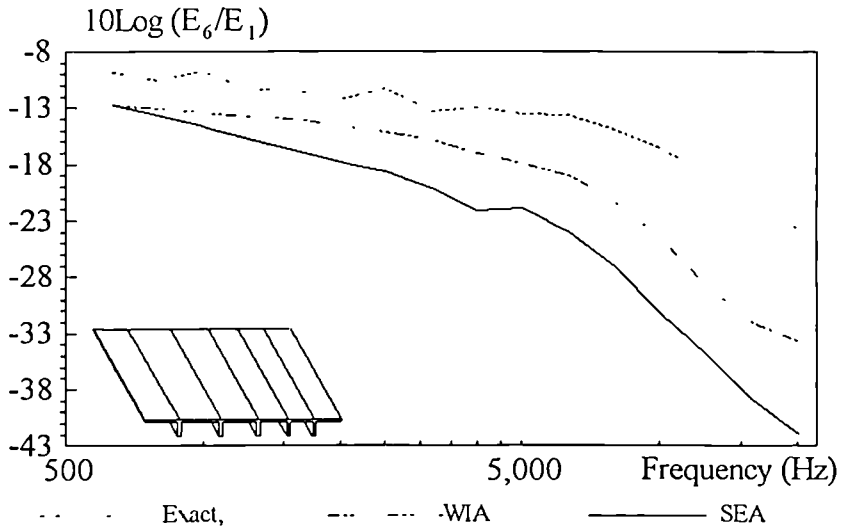

Fig. 5.93

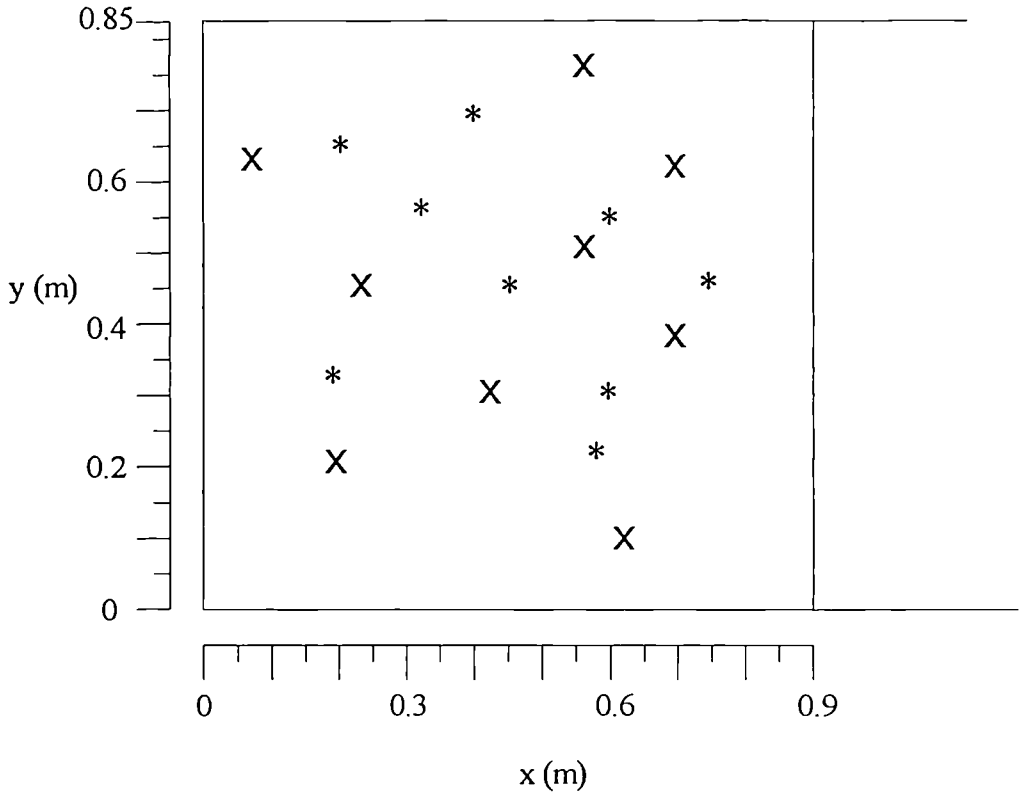

Location	Set 1 *		Set 2 X	
	x (m)	y (m)	x (m)	y (m)
1	0.595	0.540	0.110	0.605
2	0.595	0.300	0.253	0.456
3	0.415	0.700	0.552	0.701
4	0.630	0.270	0.630	0.115
5	0.752	0.450	0.702	0.615
6	0.233	0.660	0.445	0.308
7	0.242	0.312	0.242	0.212
8	0.450	0.470	0.752	0.417
9	0.318	0.550	0.502	0.525

Fig. 5.94 The selected locations of excitation points.

Four Plate Assembly (Case 2)
Relative range in the E_2/E_1 predictions of excitation set 1&2
Average range: Bending=0.27, Full=0.27

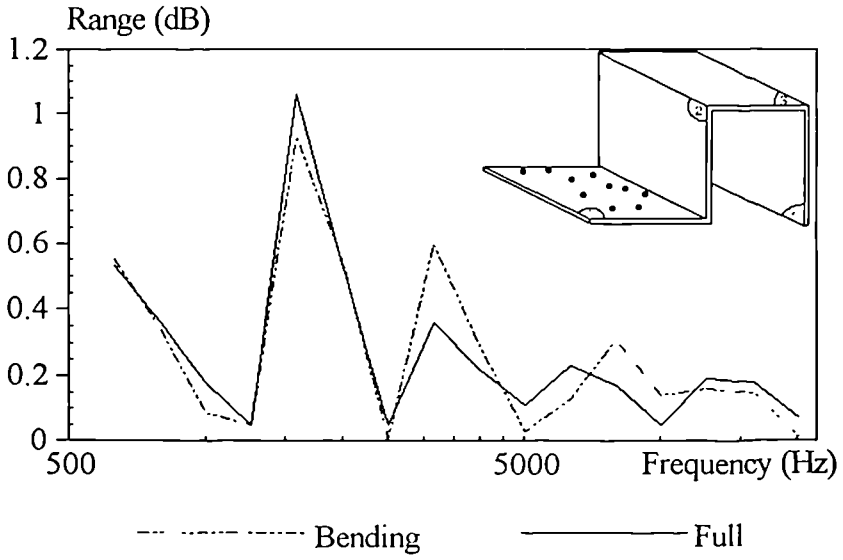

Fig. 5.95

Four Plate Assembly (Case 2)
Relative range in the E_3/E_1 predictions of excitation set 1&2
Average range: Bending=0.35, Full=0.37

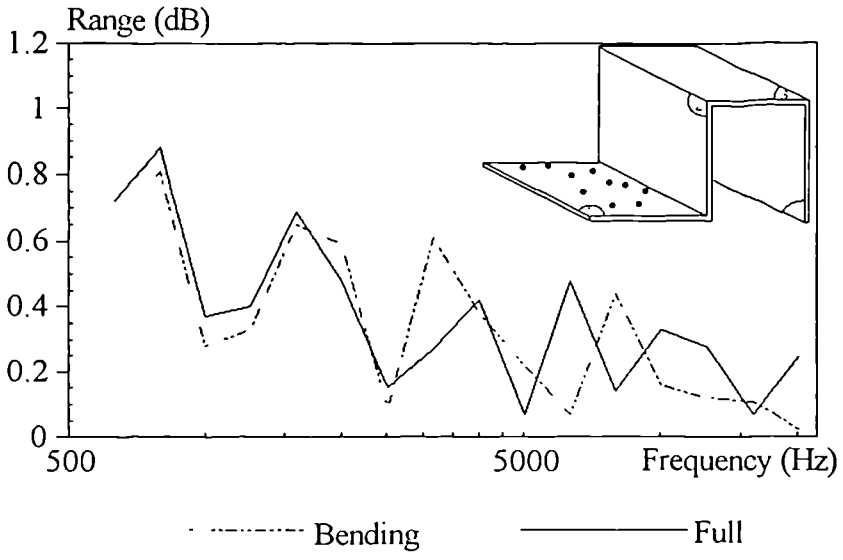

Fig. 5.96

Four Plate Assembly (Case 2)
Relative range in the E_4/E_1 predictions of excitation set 1&2
Average range: Bending=0.41, Full=0.40

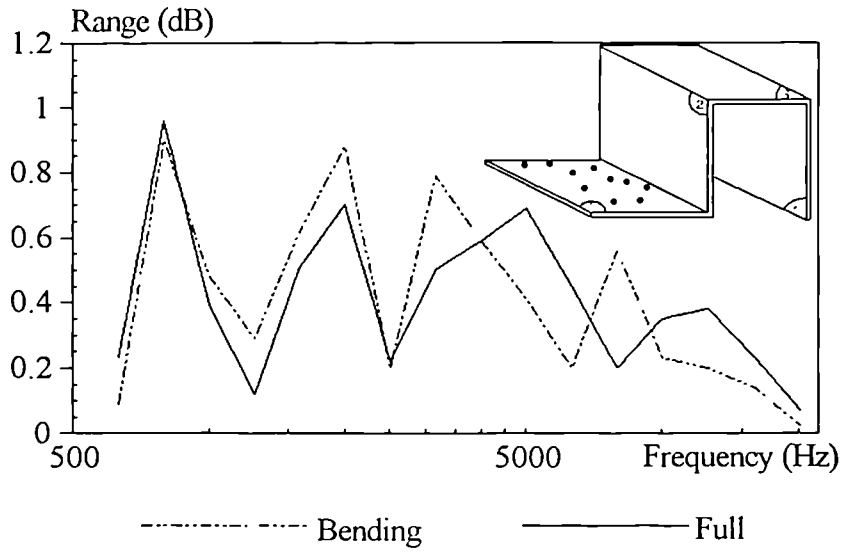

Fig. 5.97

Four Plate Assembly (Case 2)
Scatter in the energy ratio E_2/E_1 over the 9 excitation points

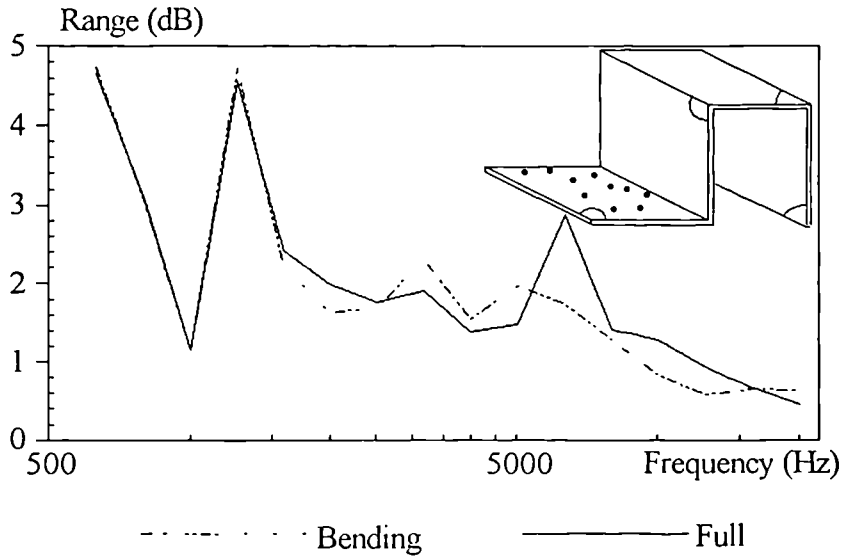

Fig. 5.98

Four Plate Assembly (Case 2)
Scatter in the energy ratio E_3/E_1 over the 9 excitation points

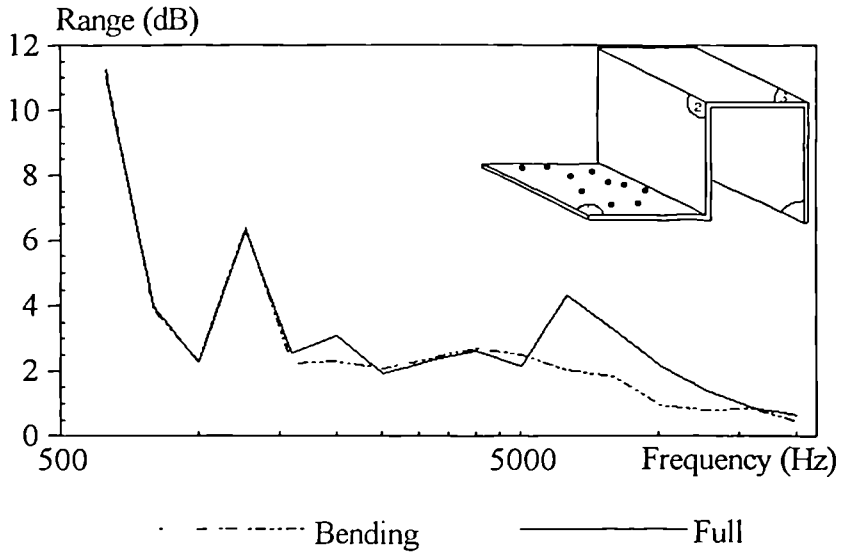

Fig. 5.99

Four Plate Assembly (Case 2)
Scatter in the energy ratio E_4/E_1 over the 9 excitation points

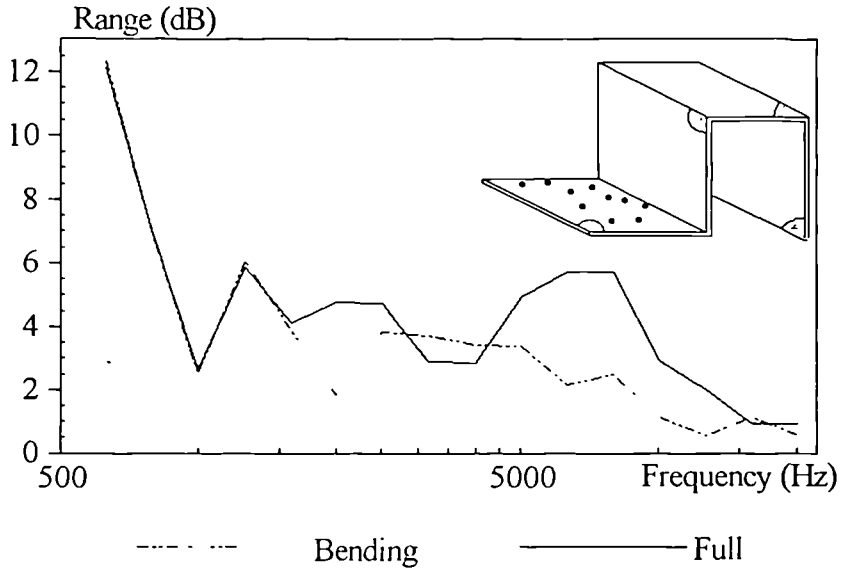

Fig. 5.100

Four Plate Assembly (Case 2)
Influence of point position on the full energy ratio

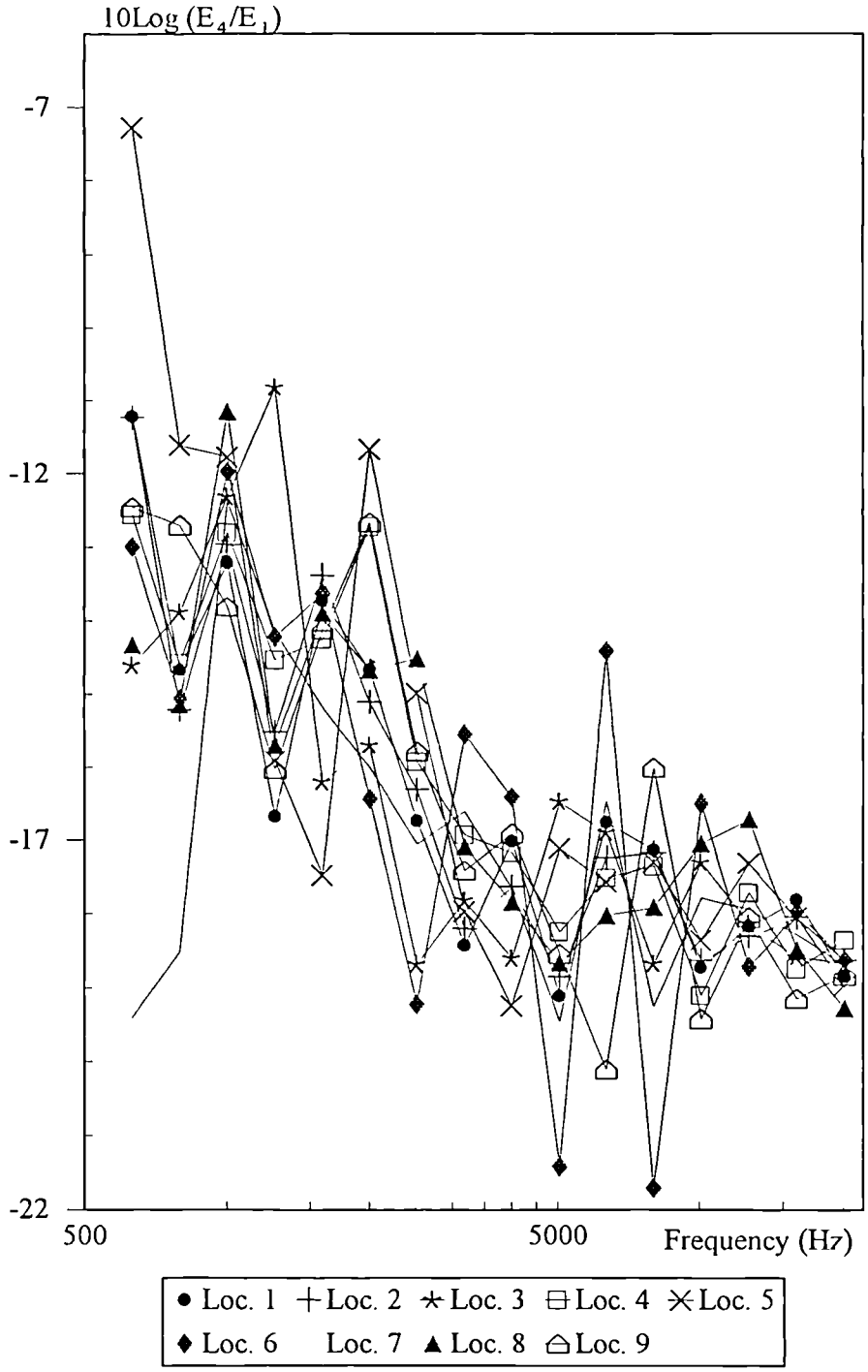

Fig. 5.100.a

Four Plate Assembly In-plane Model (Case 2)
Influence of boundary conditions on the E_2/E_1 ratio

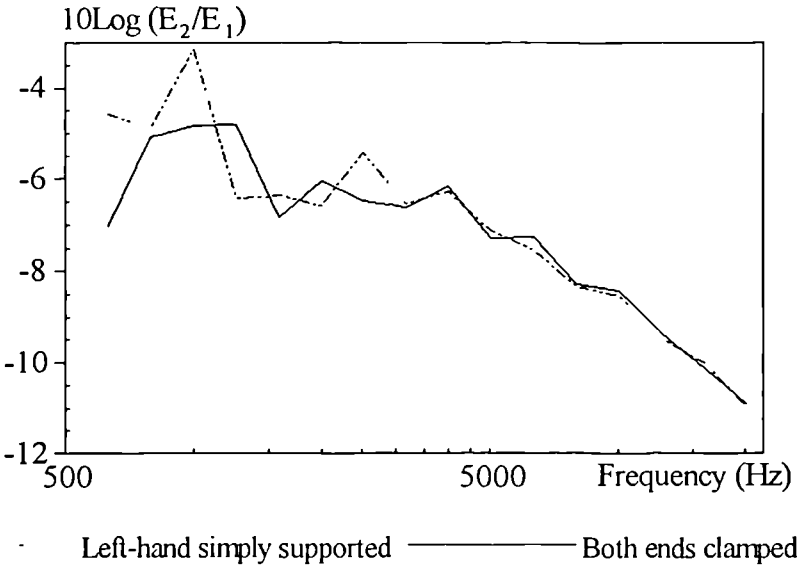

Fig. 5.101

Four Plate Assembly In-plane Model (Case 2)
Influence of boundary conditions on the E_3/E_1 ratio

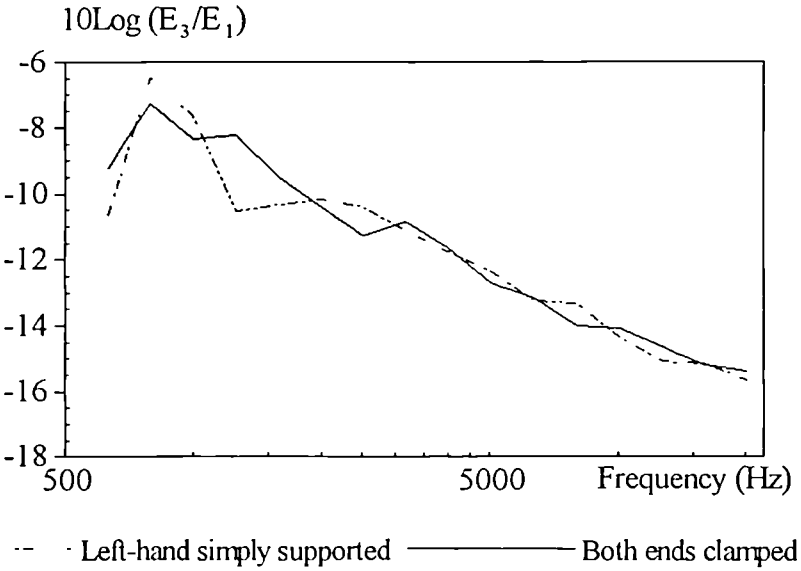

Fig. 5.102

Four Plate Assembly In-plane Model (Case 2)
Influence of boundary conditions on the E_4 /E_1 ratio

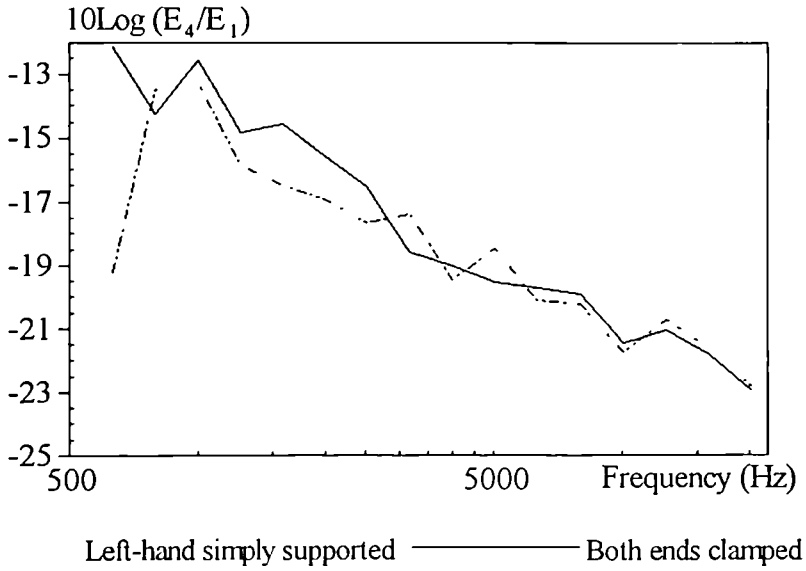

Fig. 5.103

Four Plate Assembly (Case 2)
Effect of number of shape functions on wave energy distribution
Plate 1, centre frequency: 20 kHz.

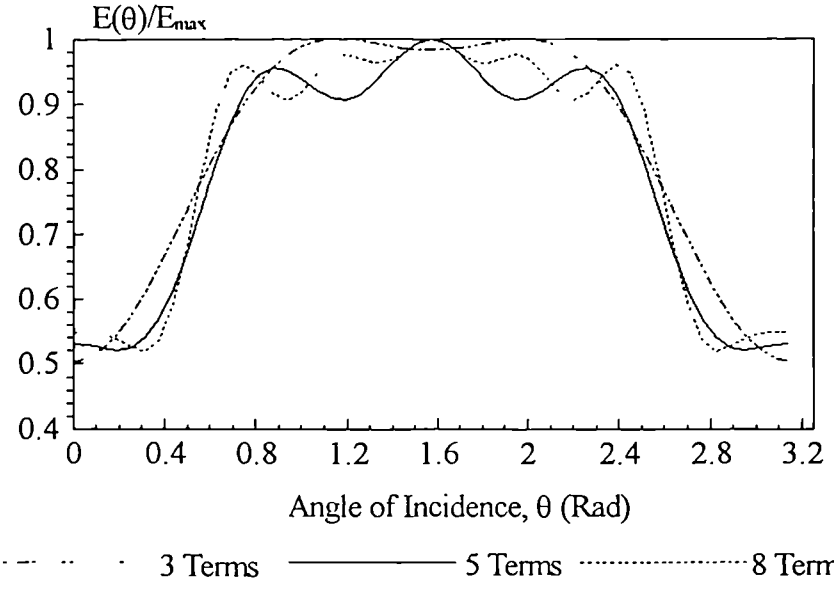

Fig. 5.104

Four Plate Assembly (Case 2)
Effect of number of shape functions on wave energy distribution
Plate 2, centre frequency: 20 kHz

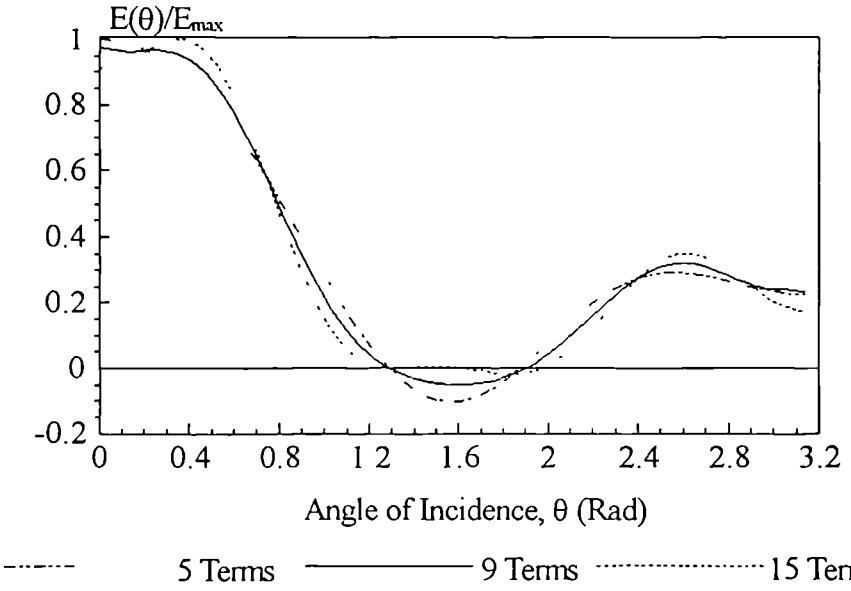

Fig. 5.105

Four Plate Assembly (Case 2)
Effect of number of shape functions on wave energy distribution
Plate 3, centre frequency: 20 kHz

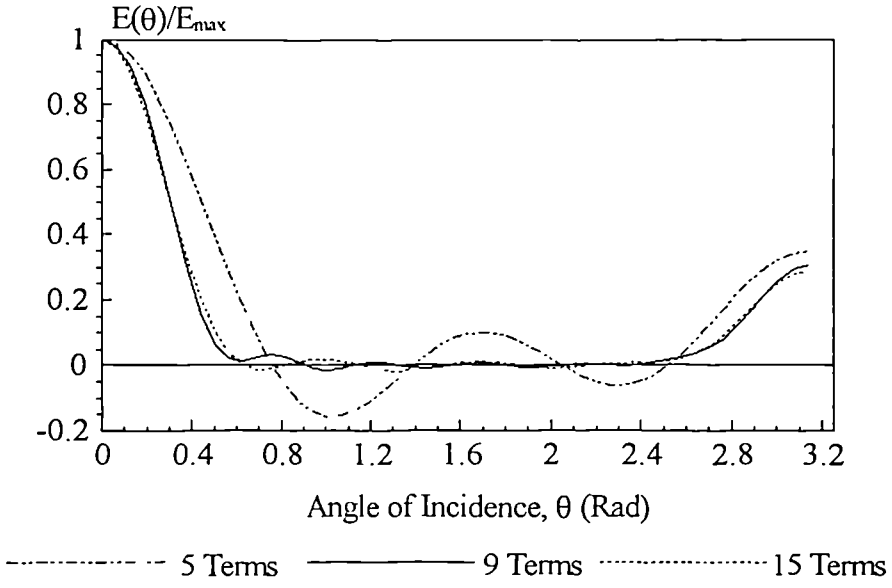

Fig. 5.106

Four Plate Assembly (Case 2)
Effect of number of shape functions on wave energy distribution
Plate 4, centre frequency: 20 kHz

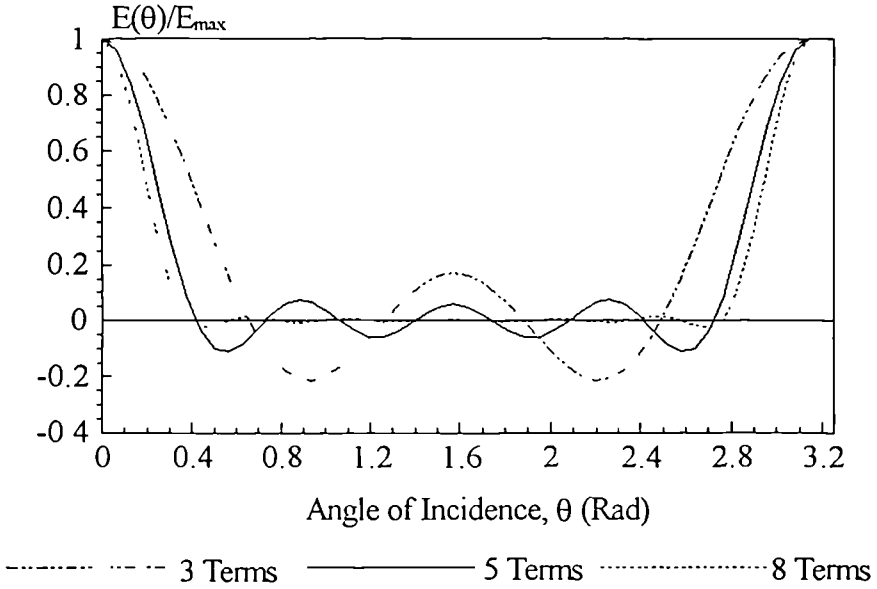

Fig. 5.107

Symmetrically Stiffened Plate Assembly (Case 1)
Effect of number of shape functions on wave energy distribution
Plate 1, centre frequency: 20 kHz

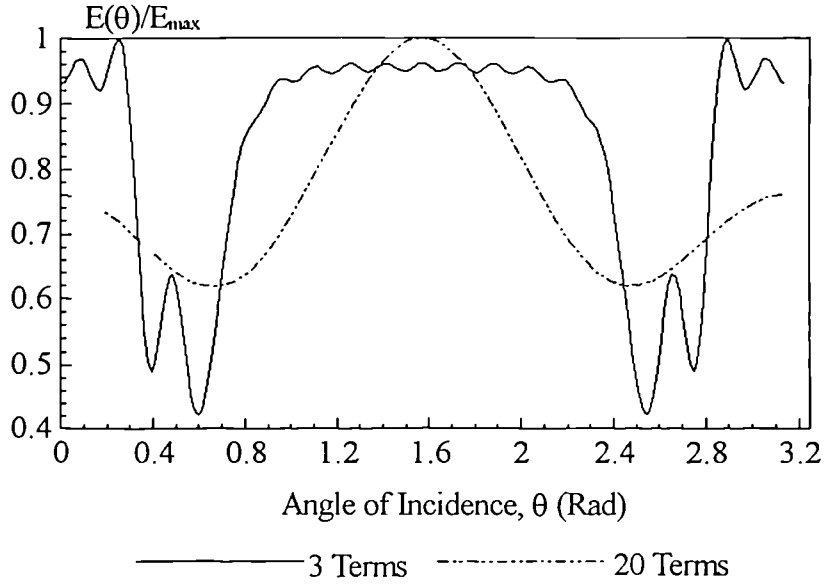

Fig. 5.108

Symmetrically Stiffened Plate Assembly (Case 1)
Effect of number of shape functions on wave energy distribution
Plate 2, centre frequency: 20 kHz

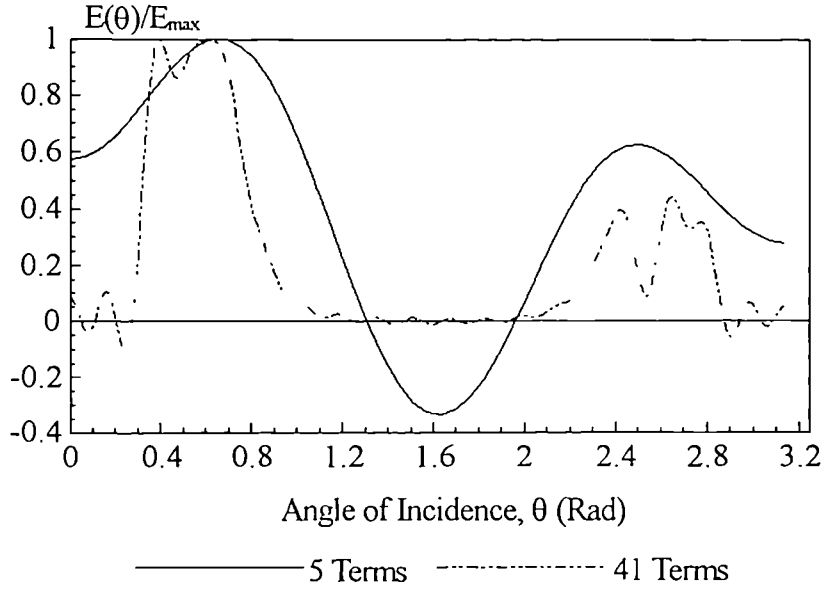

Fig. 5.109

Symmetrically Stiffened Plate Assembly (Case 1)
Effect of number of shape functions on wave energy distribution
Plate 3, centre frequency: 20 kHz

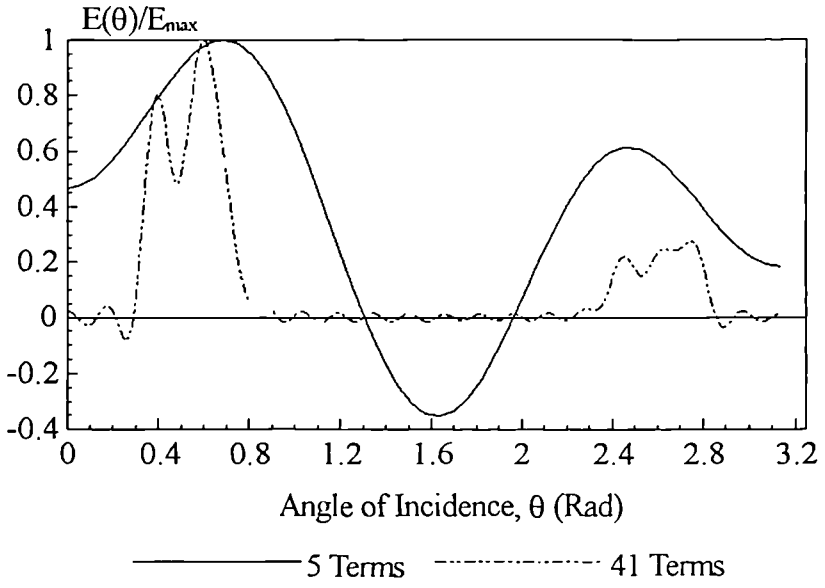

Fig. 5.110

Symmetrically Stiffened Plate Assembly (Case 1)
Effect of number of shape functions on wave energy distribution
Plate 4, centre frequency: 20 kHz

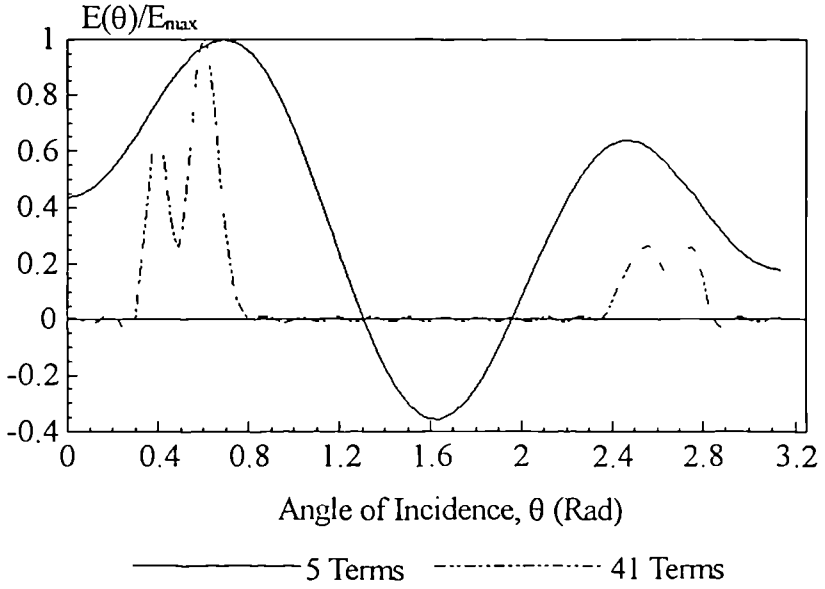

Fig. 5.111

Symmetrically Stiffened Plate Assembly (Case 1)
Effect of number of shape functions on wave energy distribution
Plate 5, centre frequency: 20 kHz

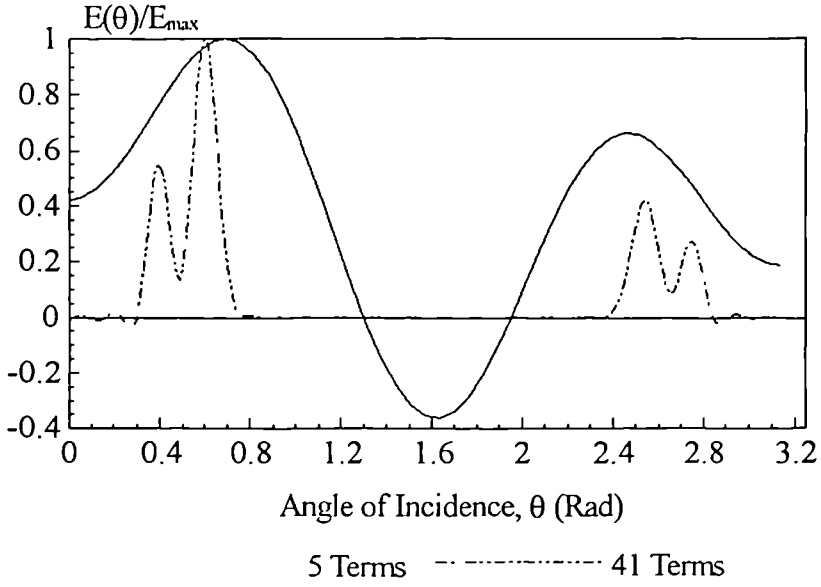

Fig. 5.112

Symmetrically Stiffened Plate Assembly (Case 1)
Effect of number of shape functions on wave energy distribution
Plate 6, centre frequency: 20 kHz

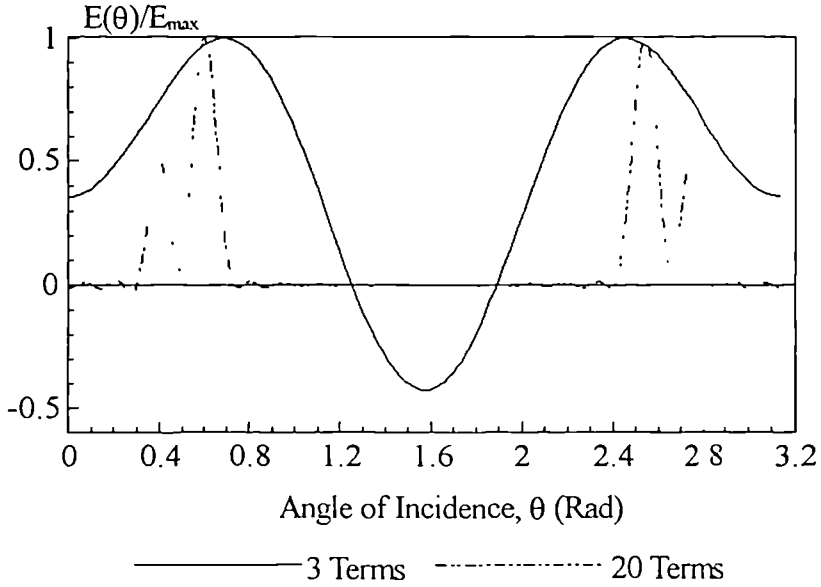

Fig. 5.113

Bending wave transmission coefficients.

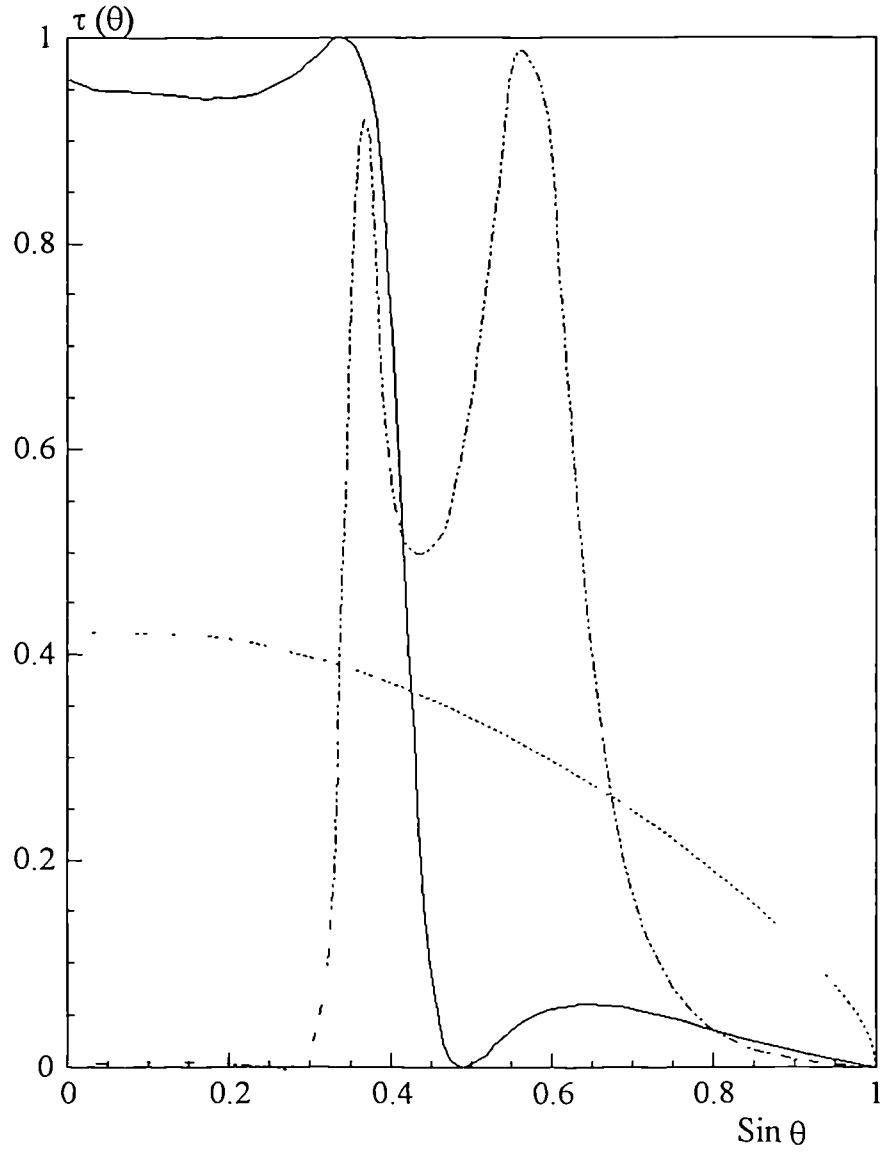

-- Simply-supported

——— Stiffened, ω=1 kHz ----------- Stiffened, ω=20 kHz

Fig. 5.114

Four Plate Assembly
Third Octave Band Energy Ratio
Plate 2, Case 2

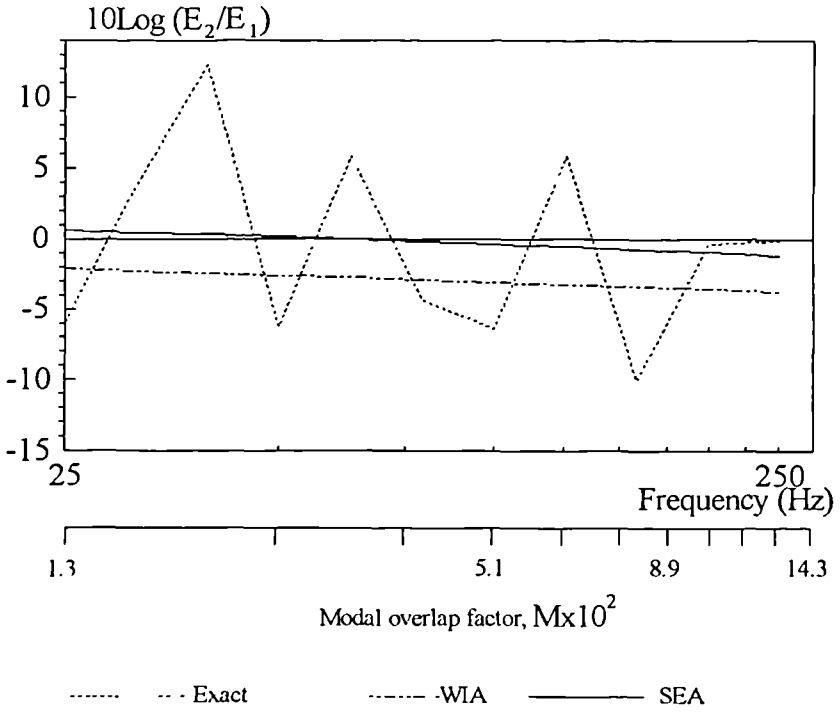

Fig. 5.115.a

Four Plate Assembly
Discrete Frequency Energy Ratio
Plate 2, Case 2

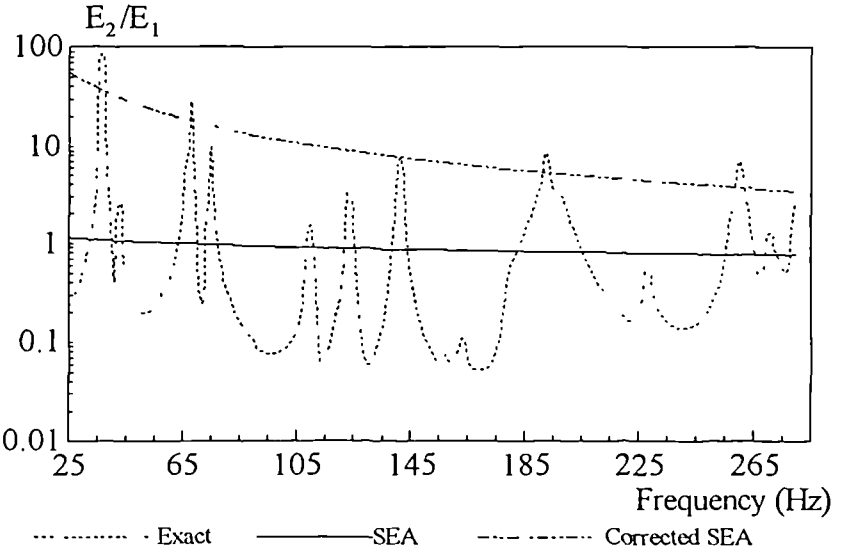

Fig. 5.115.b

Four Plate Assembly
Third Octave Band Energy Ratio
Plate 3, Case 2

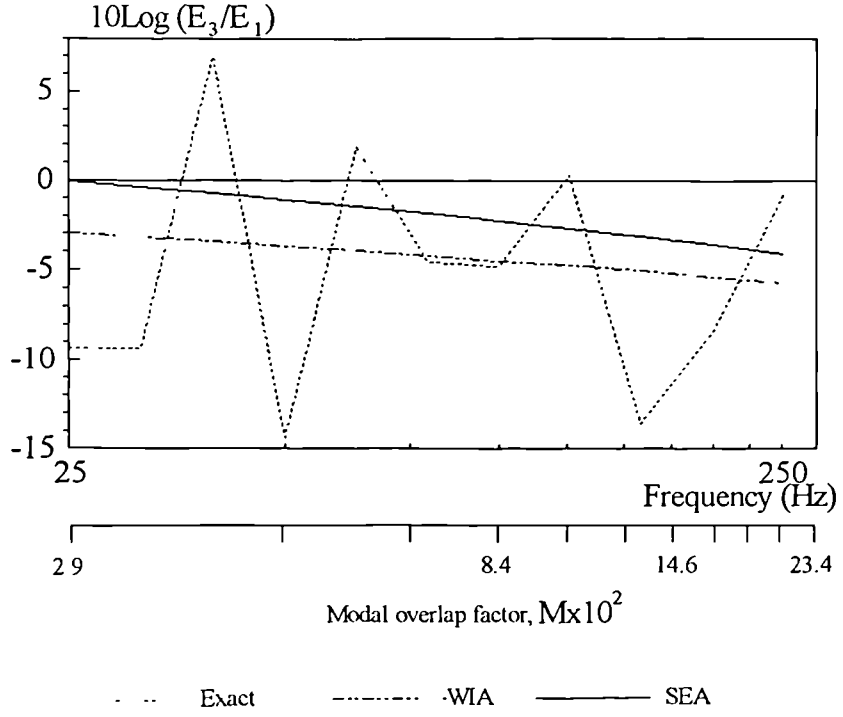

Fig. 5.116.a

Four Plate Assembly
Discrete Frequency Energy Ratio
Plate 3, Case 2

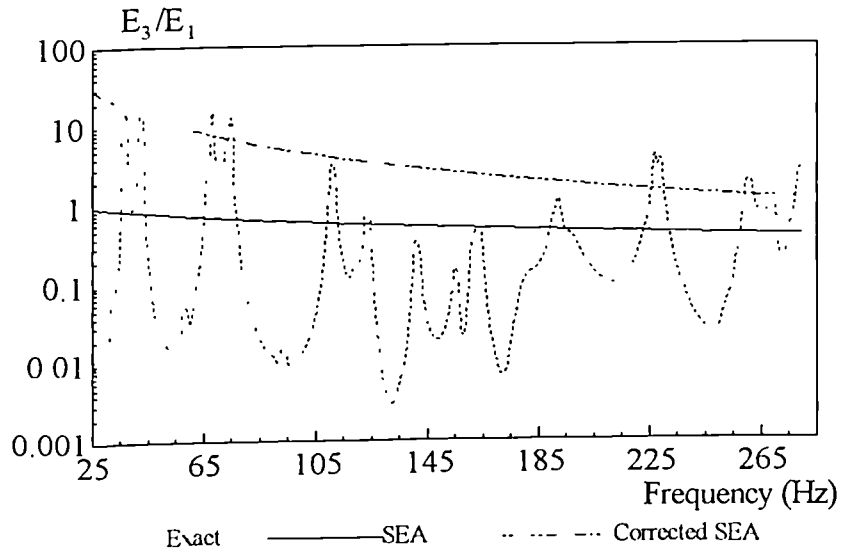

Fig. 5 116.b

Four Plate Assembly
Third Octave Band Energy Ratio
Plate 4, Case 2

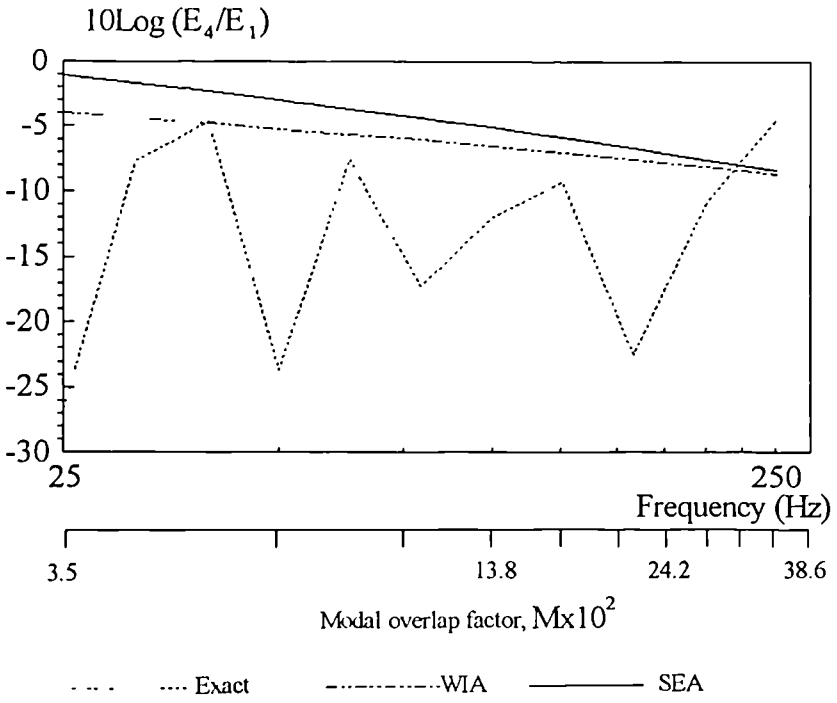

Fig. 5.117.a

Four Plate Assembly
Discrete Frequency Energy Ratio
Plate 4, Case 2

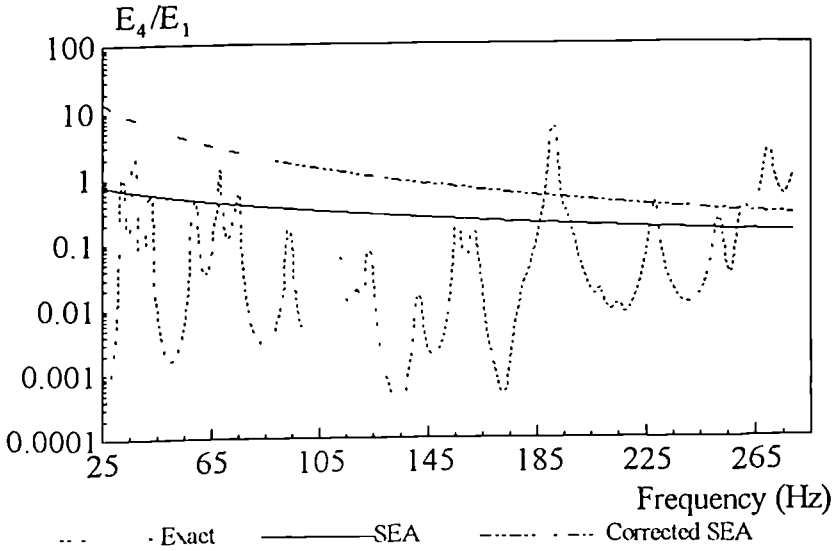

Fig. 5.117.b

Four Plate Assembly
Wave energy distributions of SEA and WIA
Plate 1, Case 2

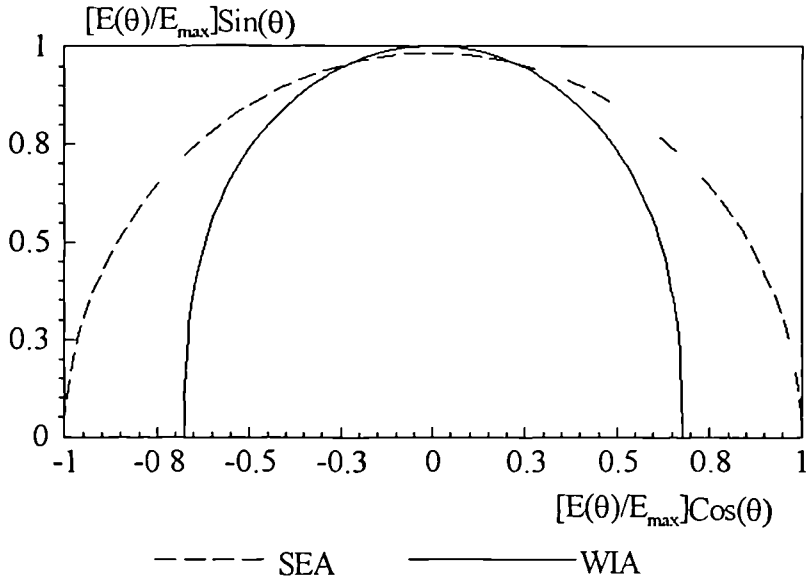

Fig. 5.118

Four Plate Assembly
WIA wave energy distribution at 20 kHz
Plates 2, 3, and 4, Case 2

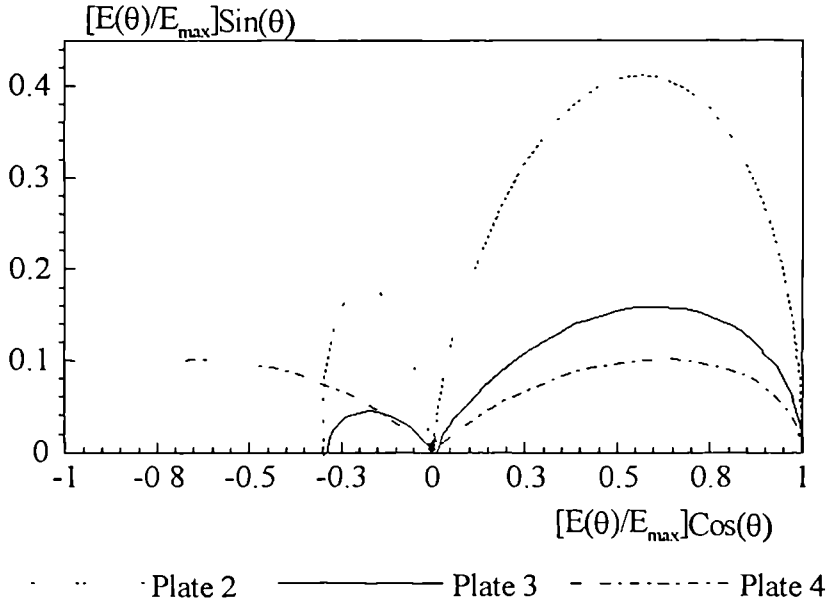

Fig 5 119

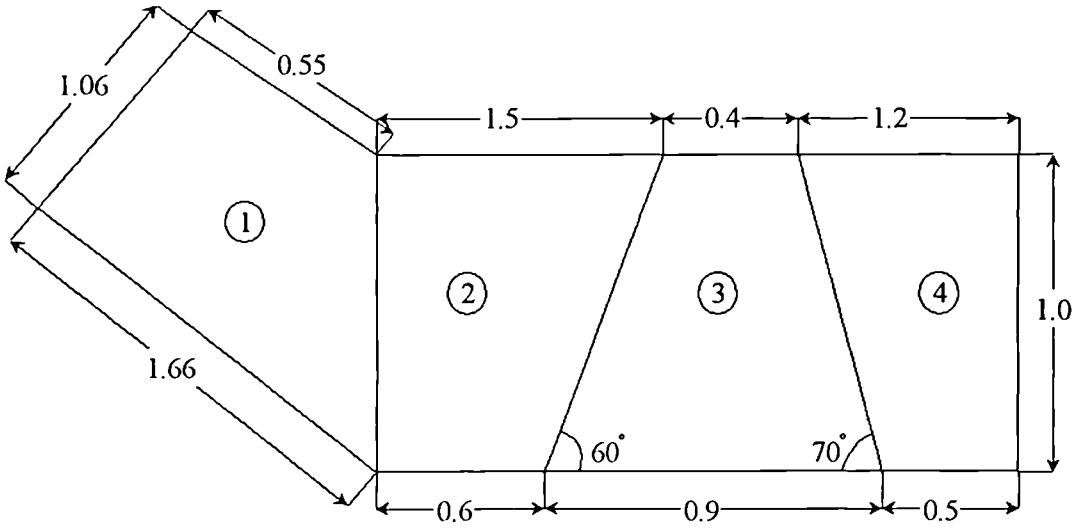

Fig. 5.120 Plan view of simply-supported irregular plate assembly.

Irregular Plate Assembly
Third Octave Band Energy Ratio
Plate 2

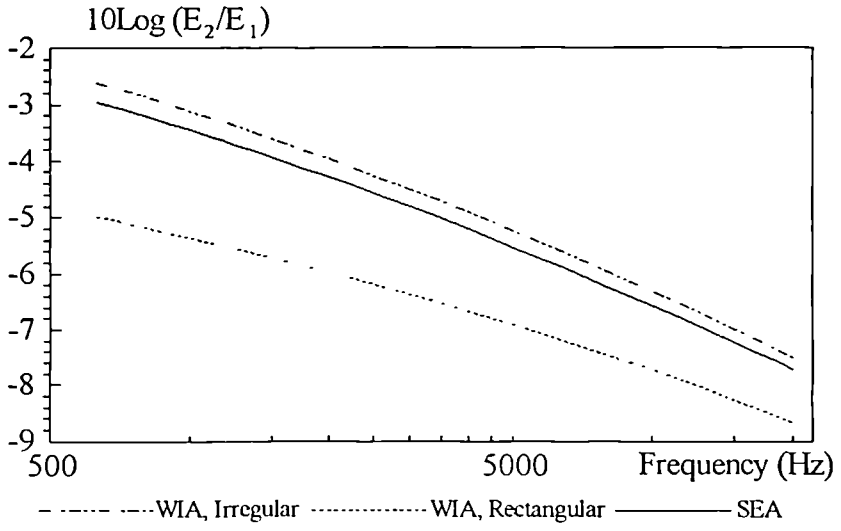

Fig. 5.121

Irregular Plate Assembly
Third Octave Band Energy Ratio
Plate 3

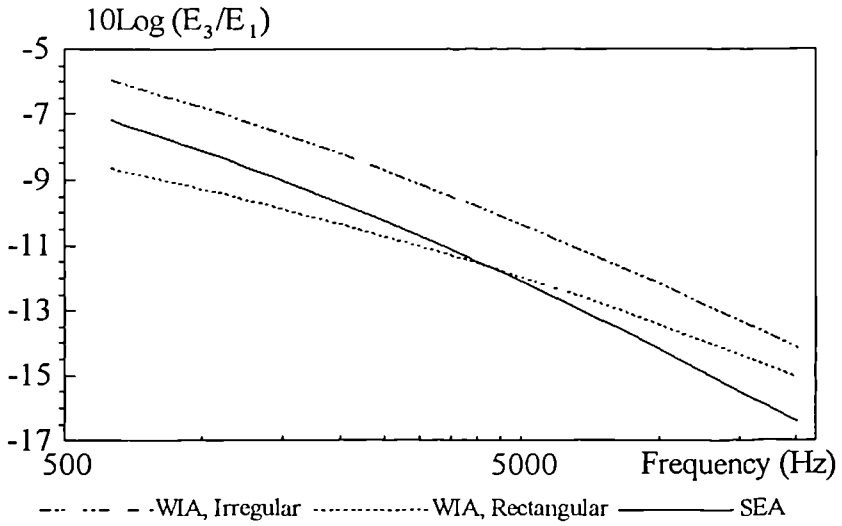

Fig. 5.122

Irregular Plate Assembly
Third Octave Band Energy Ratio
Plate 4

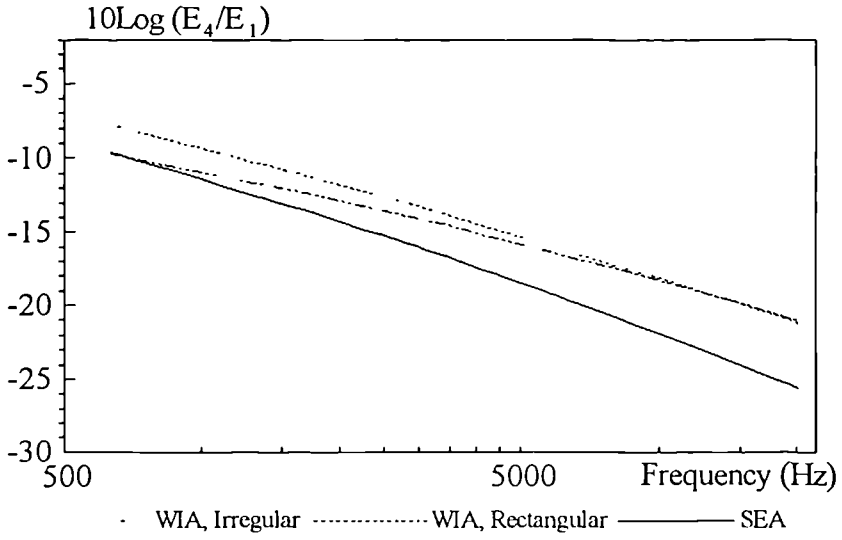

Fig. 5.123

Symmetrically Stiffened Plate Assembly (Case 1)
Energy Distribution in WIA and Exact
Plate 1, centre frequency: 20 kHz

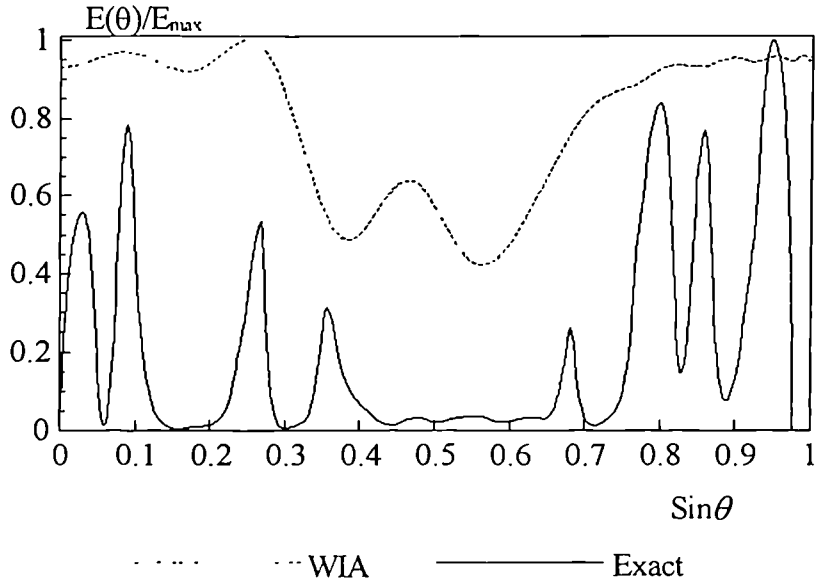

Fig. 5.124

Symmetrically Stiffened Plate Assembly (Case 1)
Energy Distribution in WIA and Exact
Plate 2, centre frequency: 20kHz

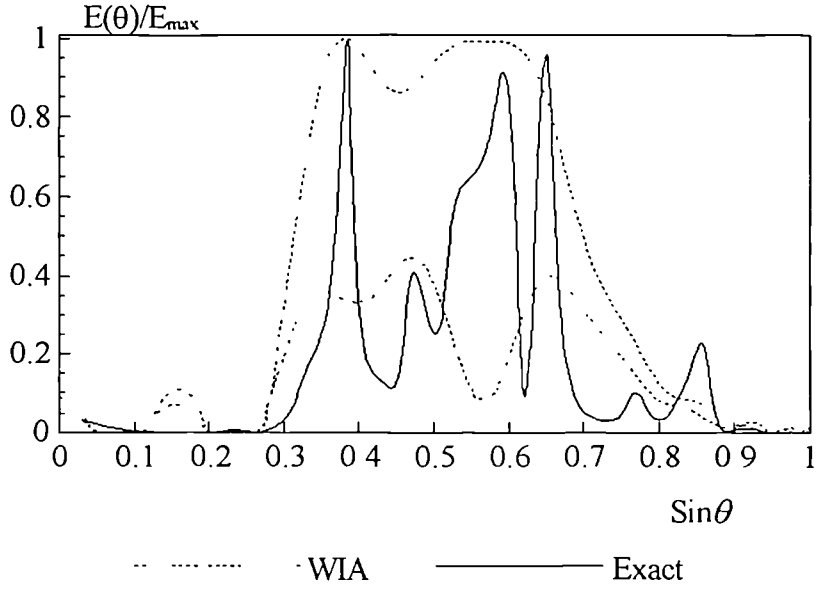

Fig. 5.125

Symmetrically Stiffened Plate Assembly (Case 1)
Energy Distribution in WIA and Exact
Plate 3, centre frequency: 20kHz

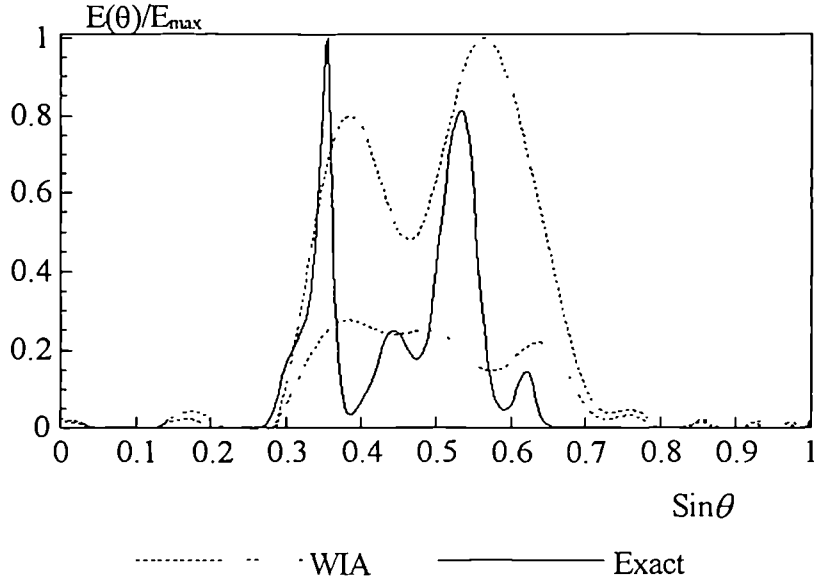

Fig. 5.126

Symmetrically Stiffened Plate Assembly (Case 1)
Energy Distribution in WIA and Exact
Plate 4, centre frequency: 20kHz

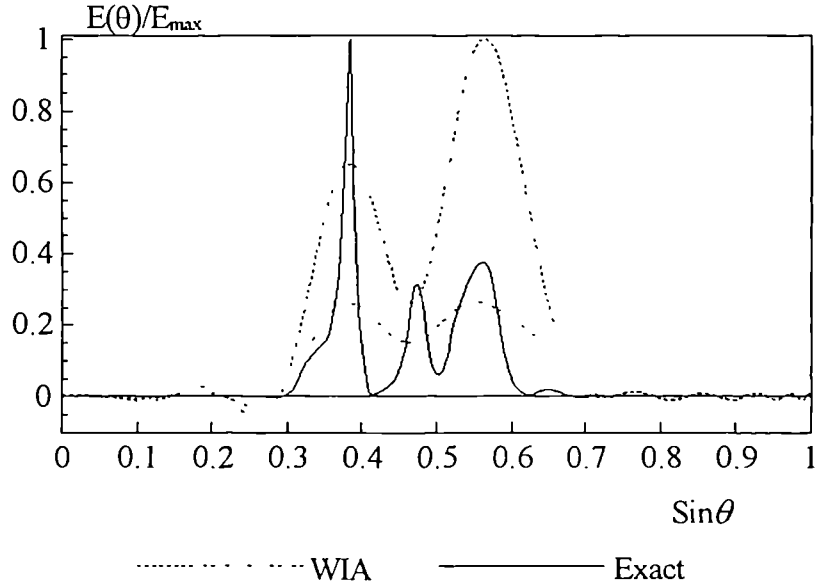

Fig. 5.127

Symmetrically Stiffened Plate Assembly (Case 1)
Energy Distribution in WIA and Exact
Plate 5, centre frequency: 20kHz

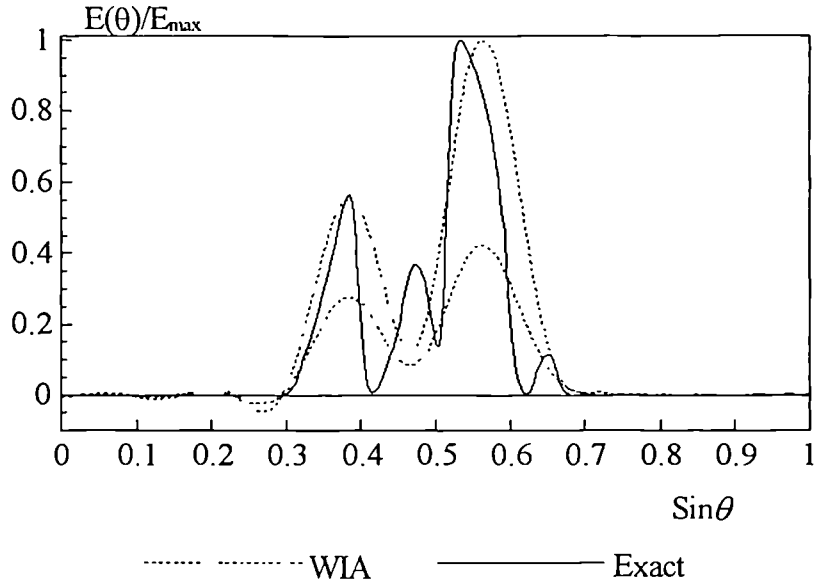

Fig. 5.128

Symmetrically Stiffened Plate Assembly (Case 1)
Energy Distribution in WIA and Exact
Plate 6, centre frequency: 20 kHz

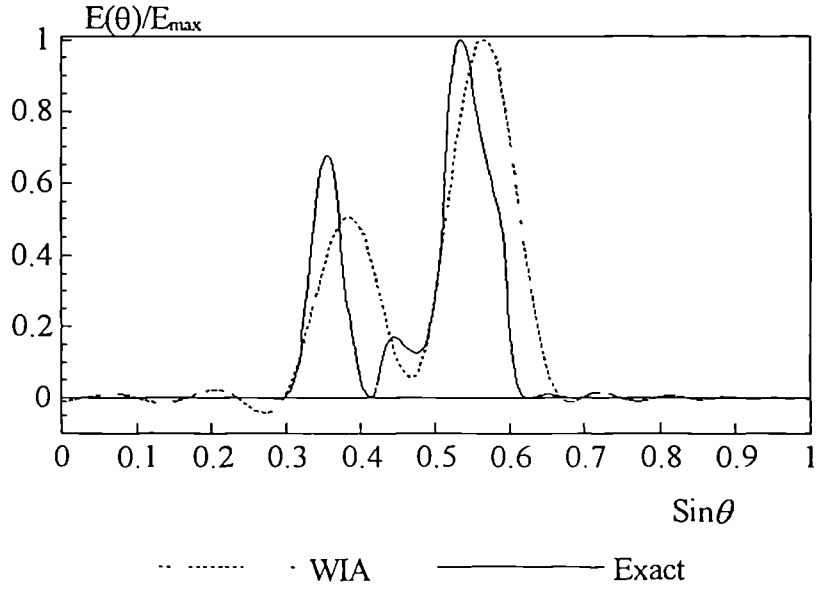

Fig. 5.129

Effect of plate thickness ratio, h_1/h_2, on coupling of bending waves to shear waves

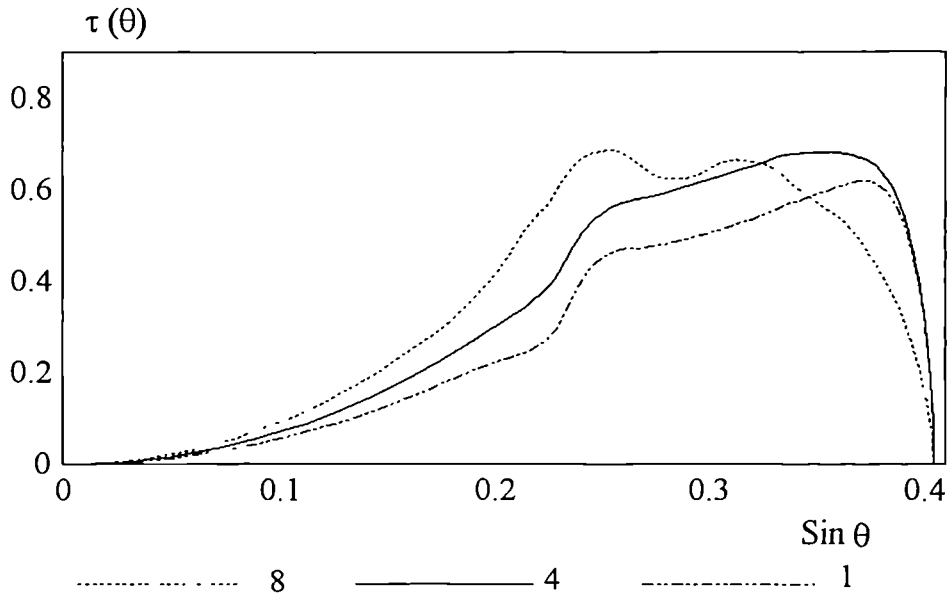

Fig. 5.130.a

Effect of plate thickness ratio, h_1/h_2, on coupling of bending waves to longitudinal waves

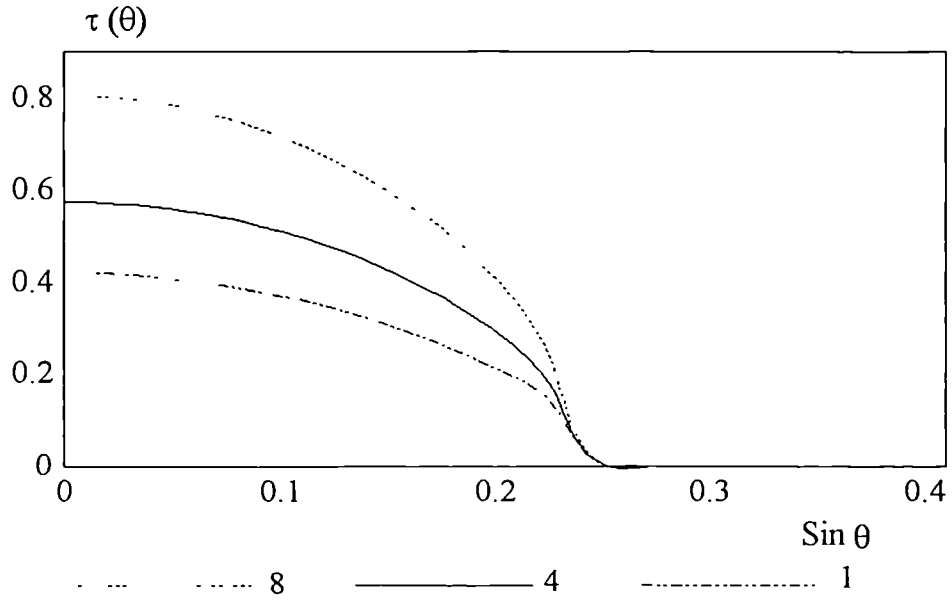

Fig. 5.130.b

Four Plate Assembly (Case 2)
Energy Distribution in WIA and Exact
Plate 1, centre frequency: 20 kHz.

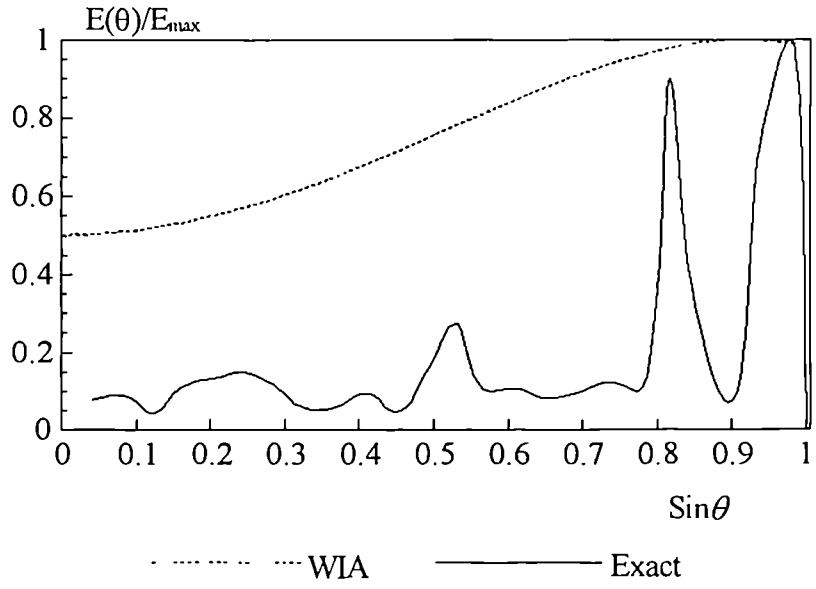

Fig. 5.131

Four Plate Assembly (Case 2)
Energy Distribution in WIA and Exact
Plate 2, centre frequency: 20 kHz

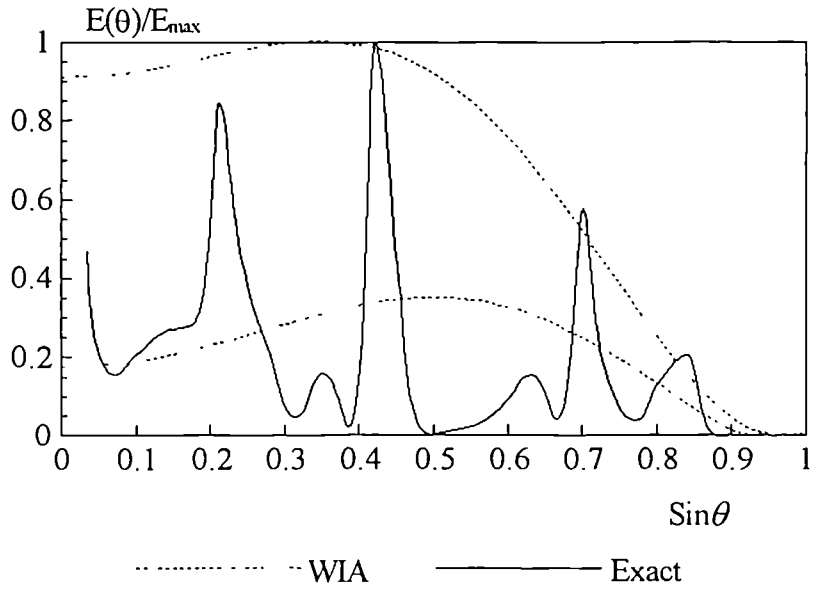

Fig. 5.132

Four Plate Assembly (Case 2)
Energy Distribution in WIA and Exact
Plate 3, centre frequency: 20 kHz

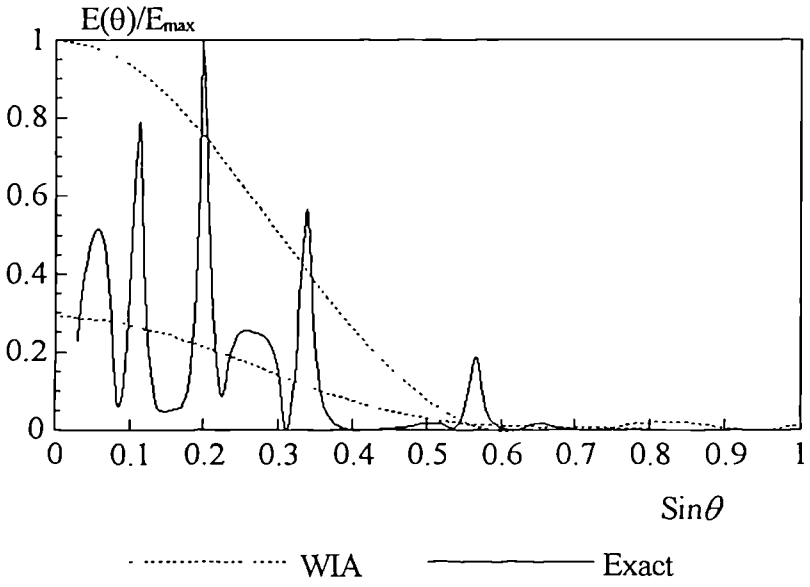

Fig. 5.133

Four Plate Assembly (Case 2)
Energy Distribution in WIA and Exact
Plate 4, centre frequency: 20 kHz

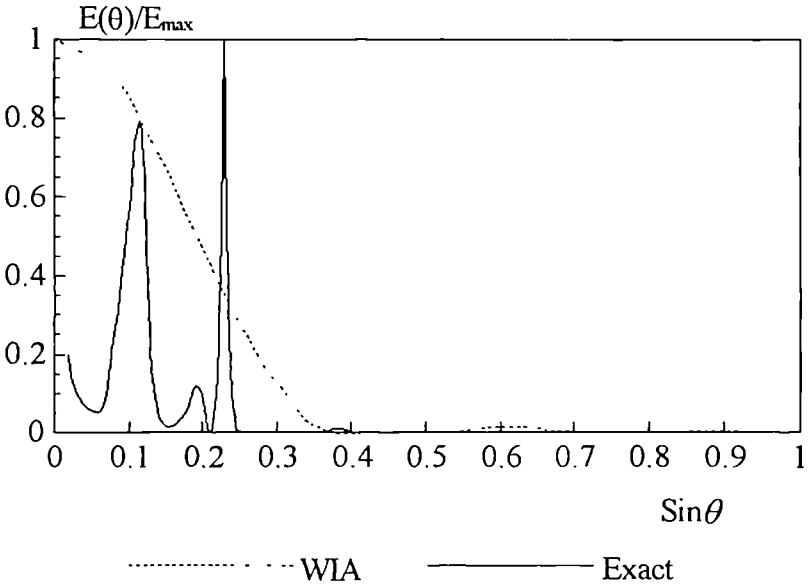

Fig. 5.134

Exact method dB difference
between bending only and full in the last component of plate assemblies.

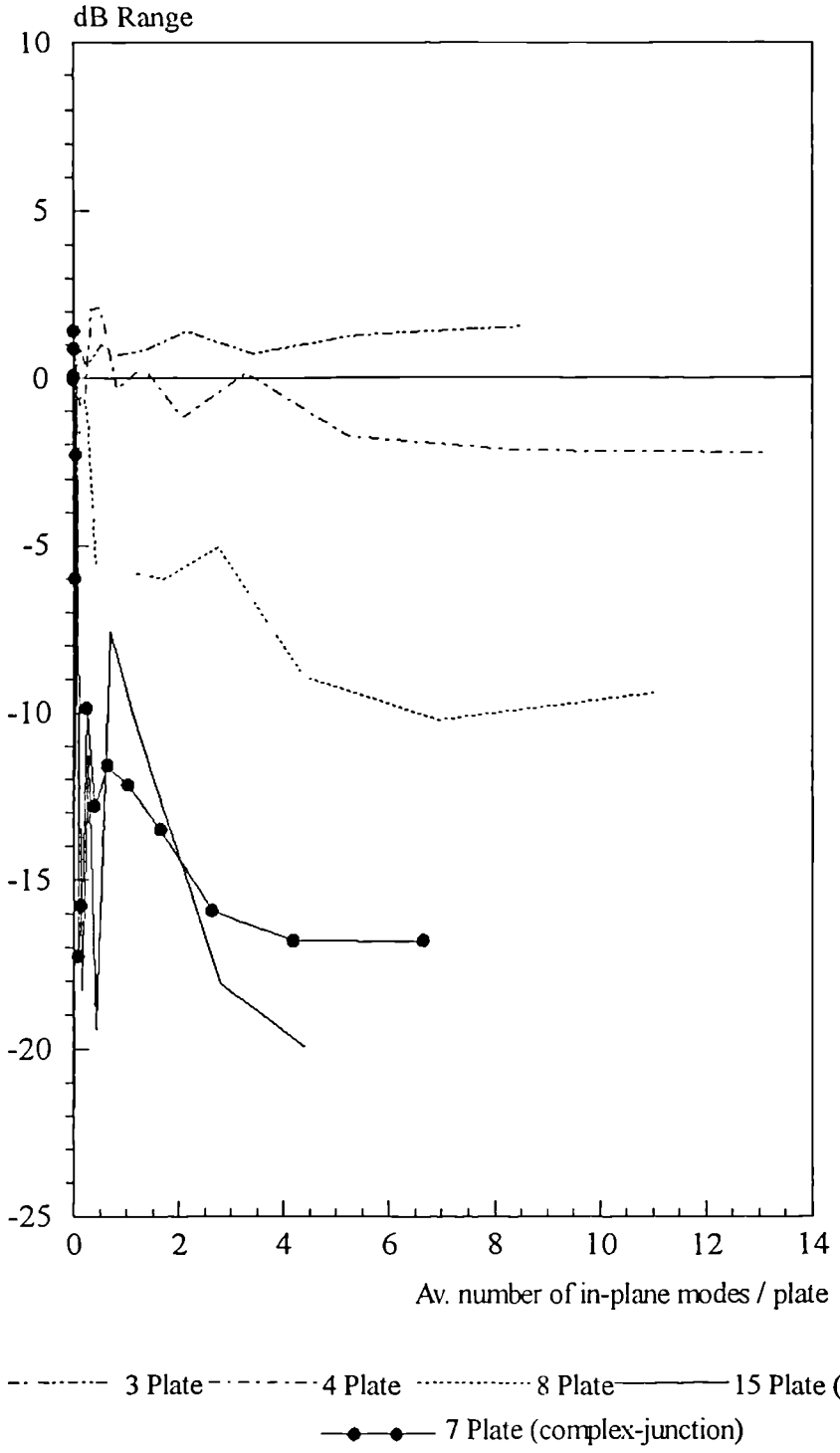

Fig. 5.135

6 SUMMARY AND CONCLUSIONS.

6.1 A BRIEF SUMMARY.

To obtain exact results for the high frequency vibrations of a large class of plate structures, the standard dynamic stiffness method has been extended to deal with the case of in-plane vibrations. This has made it possible to check the results yielded by the Statistical Energy Analysis (SEA) technique which is widely used for high frequency vibration analysis. The Wave Intensity Analysis (WIA) method of reference [50] has also been extended to the case of in-plane vibrations.

All three methods have been applied to a wide range of plate structures and detailed comparisons have been made. Due to the restriction imposed by the dynamic stiffness method, the example cases considered here were extending only in one direction: this in sense a special case which forms wave guide structures. If there are many components extending in every direction the wave field would be expected to be more diffuse, then the wave heading angle will be less critical; thus SEA predictions will improve. However if there is single dominant transmission path in the structure; as in the case of an aircraft fuselage, the conclusions drawn from this study will be more applicable.

It is hoped that the results presented here will serve as a database for prospective users of SEA or WIA.

In what follows a summary of main findings of this work are presented.

6.2 CONCLUSIONS.

(i). Due to the influence of phase effects, the exact results are generally oscillatory at low frequencies, but become smooth as the modal overlap increases. When the in-plane modes are included the scatter due to individual point load locations is higher than in the pure bending case. Even at high frequencies there may be a

5 dB difference in the energy levels arising from different point force locations. However SEA and WIA can not detect this scatter since they are concerned with the "average" response both in terms of phase effects and point load locations.

(ii). Although the results are sensitive to the point load location for a *single* point force, it has been shown (Figs. 5.95-5.97) that the result obtained by averaging over a number of point force locations (nine were considered here) is relatively insensitive to the location of the individual forces, providing a relatively random distribution is used.

(iii). In WIA, it has been observed that while three to five Fourier terms are sufficient to represent the directional dependency of a wave field in the simply-supported and orthogonally coupled plate assemblies, in stiffened plates the required number is higher. Although up to mid-range frequencies three to five Fourier components are sufficient, at higher frequencies as many as forty shape functions may be needed, due largely to the strong dependence of the transmission coefficients on the angle of wave incidence at these frequencies.

(iv). The use of three to five Fourier components in WIA may lead to the prediction of negative energy in the system at certain incidence angles, although this effect disappears as the number of shape functions is increased. Generally the negative energy does not significantly degrade the overall results, providing the main part of the energy distribution curve is accurately predicted. In fact only the first (constant) Fourier component has a non-zero contribution to the total energy in a subsystem, and thus a negative total energy is never predicted.

(v). Although at low frequencies SEA may predict a good average response in some components, in the remote plates SEA overestimates the energy levels due to strong coupling and low modal density. However a fair knowledge of peaks which are found in the exact results may be obtained if the results of SEA or WIA are

multiplied by a correction factor. That might be useful to a design engineer who is seeking the rapid estimation of maximum response.

(vi). Considering the pure bending results: even though the requirements of weak coupling , high modal overlap, many modes excited, and reverberance are satisfied, SEA overestimates the response in the component which is directly connected to the source plate. In the third plate the SEA predictions are higher than the exact results at low frequencies, while at high frequencies an underprediction occurs. An underprediction is always observed in the remaining components of the structure, and the discrepancy is greatest for the furthest plate at the highest frequency. On the other hand the WIA predictions are much closer to the exact results especially at the higher frequencies. The good agreement between WIA with the exact results sheds some light on the poor performance of SEA: it has previously been shown [50] that due to the diffuse wave field assumption, SEA initially overestimates the energy flowing to the neighbouring plate; however in the subsequent plates the energy travelling towards the next component is underestimated by the diffuse field assumption due to the wave filtering effects of the structural junctions. The results presented here confirm these findings.

(vii). As the wave field is more diffuse in box structures, the SEA predictions are in much closer agreement with the exact results. The results for the irregular plate structure, in which the wave field is expected to be more diffuse, indicate that in the limit of a perfectly diffuse wave field WIA will converge to SEA regardless of the number of shape functions used since the higher Fourier terms will tend to zero.

(viii). In stiffened structures the diffuse wave field approximation leads to a significant overestimation of energy flow from the excited to the adjoining plate. In the other components, while SEA may show the general trend, it produces large errors in the energy levels, particularly for the remote plates. In this case it is possible

to obtain very accurate predictions by using WIA providing an adequate number of shape functions are employed.

(ix). It has been shown that the angular distribution of energy predicted by the WIA technique is in close agreement with the exact results (see for example Figs. 5.124-5.129). This indicates that WIA does capture the true physics of the energy transmission process.

(x). When the in-plane modes are included it is found that the bending energy of a plate which is directly connected to the excited plate decreases in comparison to the pure bending case. The reason for this is that some of the bending energy in the excited plate is transmitted to in-plane waves, thus reducing the amount of the energy transmitted in bending waves. This effect becomes more apparent with increasing frequency.

(xi). For greater bending to in-plane transmission the critical angle needs to be larger. This angle approaches to 90° as the frequency of the excitation increases, and also as the relative thickness of the source plate increases. However, for example, in case 1 of the fifteen plate assembly the in-plane effects begin to appear at around 2.5 kHz which corresponds to a small critical angle. Although at this frequency the contribution of in-plane vibrations on the second plate is negligible, on the last component the difference between the pure bending and the full results as predicted by the exact method is as much as 10 dB. This shows that even at moderate frequencies in the remote plates the in-plane effects may be important.

(xii). While in the components near to the source plate the inclusion of in-plane effects may either increase or decrease the bending energy, depending on thickness changes, for remote plates the effect is always to increase the bending energy. This is due to the coupling of the in-plane waves back into bending waves at distant structural locations. There are three main factors that accelerate this increase in the bending energy: **(a)** the number of in-plane

modes excited, which is directly proportional to the frequency and bandwidth, (b) the number of junctions in the structure, (c) the number of plates at each junction.

(xiii). The fact that there are more modes excited, and more transmission paths when the in-plane motion is included, lead to better agreement between SEA and the exact results for this case. However SEA can still severely underestimate the response, especially in larger structures. This is due mainly to the diffuse wave field approximation, as explained in **(vi)**; the WIA results also improve with the inclusion of in-plane effects, and the error yielded by WIA can be as low as 0.5 dB for a case in which SEA yields 40 dB underprediction.

(xiv). When it comes to the question of "how important is in-plane energy transmission in realistic situations?", a generalised answer is difficult to give, as the effect is dependent on both the system under consideration and the frequency of the excitation. Obviously the simplest possible model should be adopted. However, as may be observed from the exact results for the fifteen plate assembly, in the sixth plate there is as much as a 4 dB increase in the energy level even at 5 kHz, and the increment at the same frequency in the last component of the seven plate complex-junction model is as high as 10 dB even though there are just three junctions. On the other hand in the three plate assemblies the difference between bending only and full results does not exceed 2 dB across the whole frequency range. Further the bending energy level decreases in these structures because of the reasons given in **(xii)**, and therefore the contribution of the in-plane vibrations may be neglected if the structure is very simple. The majority of engineering structures consist of many interconnecting elements with a lot of junctions, and in these cases the exclusion of the in-plane modes may result in a severe underprediction unless the concern is with low frequencies only. In such structures due allowance should therefore be made for the presence of in-plane modes.

(xv). In general SEA predictions become unreliable, if **(a)** the frequency of the excitation is high, **(b)** there are many components in the structure. Although in the structures which consist of less than four plates it is possible to obtain reasonable response estimates for any frequency, for structures which are composed of many elements the underprediction in the SEA results may reach unacceptable levels with the increase of frequency.

(xvi). In addition to the four requirements (see section 5.5) which are usually postulated for successful application of SEA, the wave field should also be diffuse to yield better results.

(xvii). Throughout this study the main concern has been with the spatial and frequency averaging, rather than ensemble averaging. In reality, although two structures may be physically similar, they can not be exactly identical due to inevitable small differences in fabrication details. In this case the prediction of the vibrational behaviour of one of the systems is not as meaningful as an average response which is obtained from a group of similar systems. Even though ensemble averaging is not performed here, given that excitation frequencies are quite high, it is expected that frequency averaging will yield similar results to ensemble averaging.

(xviii). Based on the observations in this work, the following suggestions can be made to the practising engineer: the relative thickness ratio of the plates should be kept close to unity, so that there is less bending to in-plane conversion. Having "T" or cross junctions, if possible, should also be avoided to prevent coupling of in-plane waves back to bending waves. As the SEA results indicate there may be as much as 40 dB reduction in the energy levels if the wave field is diffuse. This suggests that the structure should be designed in a way that the resulting wave field becomes more diffuse.

6.3 SUGGESTIONS FOR FUTURE WORK.

It has been shown that WIA provides significant improvements over standard SEA for a certain class of plate structures. It would therefore be of great use to extend the method to other engineering structures such as beams and cylindrical shells. This may be easily accomplished provided that the energy transmission coefficients are known for the specific types of junction under consideration.

REFERENCES

1. Zienkiewicz, O.C.
   The Finite Element Method. London.
   McGraw-Hill, Third Edition. 1977
2. Keane, A.J.
   Statistical Energy Analysis of Engineering Structures.
   Ph.D. Thesis Brunel University Uxbridge. 1988
3. Petrolito, J. and Golley, B.W.
   Finite Panel for Plate Vibration
   Journal of Sound and Vibration 120(3) 473-486 1988
4. Woodhouse, J.
   An Introduction to Statistical Energy Analysis of Structural Vibration.
   Applied Acoustics 14 455-469 1981
5. Hodges, C.H. and Woodhouse, J.
   Theories of Noise and Vibration Transmission in Complex Structures.
   Rep. Prog. Phys. (49) 107-170 1986
6. Simmons, C.
   Structure Borne Sound Transmission Through Plate Junctions and Estimates of SEA coupling Loss Factors Using the Finite Element Method.
   Journal of Sound and Vibration 144(2) 215-227 1991
7. Orth, M.T.
   Vibration Database for Aircraft and its Application.
   59th Shock and Vibration Symposium V.1 89-102 Albuquerque, New Mexico Oct. 18-20 1988 pp 81-86
8. Nilsson, A.C.
   Attenuation of Structure-Borne Sound in Superstructures in Ships.
   Journal of Sound and Vibration 55 71-91 1977
9. Tratch Jr, J.
   Vibration Transmission Through Machinery Foundation and Ship Bottom Structure.
   M.Sc. Thesis, Dept. of Mech. Eng., MIT, 1985

10. Cuschieri, J.M.
Structural Power Flow Analysis Using a Mobility Approach of an L Shaped Plate.
Journal of Acoustical Society of America 87(3) 1159-1165 1990
11. Miller, D.W., and von Flotow, A.
A Travelling Wave Approach to Power Flow in Structural Networks
Journal of Sound and Vibration 128(1) 145-162 1989
12. Cuschieri, J.M. and Cimmerman, B.
Mobility Power Flow Analysis of an L-Shaped Plate Subjected to Distributed Loading.
3rd International Congress on Intensity Techniques
431-440 Senlis-France 1990
13. Szilard, R.
Theory and Analysis of Plates.
Prentice-Hall, Inc. 1974
14. Wittrick, W.H.
General Sinusoidal Stiffness Matrices for Buckling and Vibration Analyses of Thin-Walled Structures.
Int. J. Mech. Sci. V 10, 949-966 1968
15. Williams, F.W and Wittrick, W.H.
Computational Procedures for a Matrix Analysis of the Stability and Vibration of Thin Flat-Walled Structures in Compression.
Int. J. Mech. Sci. V 11, 979-998 1969
16. Wittrick, W.H. and Williams, F.W.
A General Algorithm for Computing Natural Frequencies of Elastic Structures.
Quart. Jour. Mech. and Applied Math. 24(3) 263-284 1971
17. Langley, R.S.
Application of The Dynamic Stiffness Method to the Free and Forced Vibrations of Aircraft Panels.
Journal of Sound and Vibration 135(2), 319-331 1989
18. Kirk, C.L.
Natural Frequencies of Stiffened Rectangular Plates.
Journal of Sound and Vibration 13(4) 375-388 1970

19. McDaniel, T.J. and Henderson, J.P.
Review of Transfer Matrix Vibration Analysis of Skin-Stringer Structure Part 1.
The Shock and Vibration Digest 6 13-19 1974
20. Lin, Y.K.
Free Vibration of Continuous Skin-Stringer Panels.
Journal of Applied Mechanics Trans. ASME 24(4) 669-676 1960
21. Aksu, G. and Ali, R.
Free Vibration Analysis of Stiffened Plates Using Finite Difference Method.
Journal of Sound and Vibration 48(1) 15-25 1976
22. Petyt, M.
Finite Strip Analysis of Flat Skin-Stringer Structures
Journal of Sound and Vibration 54(4) 537-547 1977
23. Lyon, R.H and Maidanik, G.
Power Flow between Linearly Coupled Oscillators.
Journal of Acoustical Society of America 34(5) 623-639 1962
24. Lyon, R.H. and Eichler, E.
Random Vibration of Connected Structures.
Journal of Acoustical Society of America 36 1344-1354 1964
25. Hwang, C. and Pi, W.S.
Investigation of Vibrational Energy Transfer in Connected Structures.
Northrop Corporation NASA-CR-124450 1973
26. Gibbs, B.M. and Gilford, C.L.S.
The Use of Power Flow Methods for the Assessment of Sound Transmission in Building Structures.
Journal of Sound and Vibration 49(2) 267-286 1976
27. Wohle, W., Beckmann, T.H. and Schreckenbach, H.
Coupling Loss Factors for Statistical Energy Analysis of Sound Transmission at Rectangular Structural Slab Joints. Part I
Journal of Sound and Vibration 77(3) 323-334 1981
28. Cremer, L., Heckl, M., and Ungar, E.E.
Structure Borne Sound.
Second Edition, Springer Verlag, Berlin 1988

29. Langley, R.S. and Heron, K.H.
Elastic Wave Transmission Through Plate/Beam Junctions.
Journal of Sound and Vibration 143(2) 241-253 1990
30. Bies, D.A. and Hamid, S.
In Situ Determination of Loss and Coupling Loss Factors by the Power Injection Method.
Journal of Sound and Vibration 70 197-204 1970
31. Keane, A.J., Price, W.G.
Statistical Energy Analysis of Strongly Coupled Systems
Journal of Sound and Vibration 117(2), 363-386 1987
32. Smith, P.W.
Statistical Models of Coupled Dynamical Systems and the Transition from Weak to Strong Coupling.
Journal of Acoustical Society of America 65(3) 695-698 1979
33. Langley, R.S.
A general Derivation of the Statistical Energy Analysis Equations for Coupled Dynamic Systems.
Journal of Sound and Vibration 135(3), 499-508 1989
34. Langley, R.S.
A Derivation of Coupling Loss Factors Used In Statistical Energy Analysis.
Journal of Sound and Vibration 141(2) 201-219 1990
35. Keane, A.J.
Energy Flows Between Arbitrary Configurations of Conservatively Coupled Multi-Modal Elastic Subsystems.
Proc. Royal Soc. London A436, 537-568 1992
36. Dimitriadis, E.K. and Pierce, A.D.
Analytical Solution for the Power Exchange Between Strongly Coupled Plates Under Random Excitation: A Test of Statistical Energy Analysis Concepts.
Journal of Sound and Vibration 123(3) 397-412 1988
37. Mace, B.R.
Power Flow Between Two Continuous One-Dimensional Subsystems.
Journal of Sound and Vibration 154(2) 289-319 1992

38. Keane, A.J. and Price, W.G.
A Note on the Power Flowing Between Two Conservatively Coupled Multi-Modal Subsystems.
Journal of Sound and Vibration 144(2) 185-186 1991
39. Guyader, J.L., Boisson, C,. Lesueur, C. and Millot, P.
Sound Transmission by Coupled Structures: Application to Flanking Transmission in Buildings.
Journal of Sound and Vibration 106(2) 289-310 1986
40. Davies, H.G. and Wahab, M.A.
Ensemble Averages of Power Flow in Randomly Excited Coupled Systems
Journal of Sound and Vibration 77(3) 311-321 1981
41. Fahy, F.J & Mohammed A.D.
A Study of Uncertainty in Applications of SEA to Coupled Beam and Plate Systems, Part I: Computational Experiments.
Journal of Sound and Vibration 158(1) 45-67 1992
42. Mace, B.R.
The Statistics of Power flow Between Two Continuous One-Dimensional Subsystems.
Journal of Sound and Vibration 154(2) 321-341 1992
43. Powell, R.E. and Manning, J.E.
The Importance of In-plane and Non-resonant Energy Transmission in Statistical Energy Analysis.
59th Shock and Vibration Symposium V.1 89-102 Albuquerque, New Mexico Oct. 18-20 1988
44. Craik, R.J.M., Steel, J.A., and Evans, D.I.
Statistical Energy Analysis of Structure-Borne Sound Transmission at Low Frequencies.
Journal of Sound and Vibration 144(1), 95-107 1991
45. Landmann, A.E., Tillema, H.F., and Marshall S.E.
Evaluation of Analysis Techniques for Low Frequency Interior Noise and Vibration of Commercial Aircraft.
Nasa-Cr-181851 Oct. 1989

46. Nilsson, A.C.
Reduction of Structure-Borne Sound in Simple Ship Structures: Results of Model Tests.
Journal of Sound and Vibration 61 45-60 1978
47. Gibbs, B.M. and Craven, P.G.
Sound Transmission and Mode Coupling at junction of Thin Plates, Part II: Parametric Survey.
Journal of Sound and Vibration 77(3) 429-435 1981
48. Lyon, R.H.
In-Plane Contribution to Structural Noise Transmission.
Noise Control Engineering Journal 26(1) 22-27 1986
49. Mead, D.J.
in *Noise And Vibration* (editors R.G. White and J.G. Walker).
Chapter 9: Structural Wave Motion.
Chichester: Ellis Horwood. 1982
50. Langley, R.S.
A Wave Intensity Technique for the Analysis of High Frequency Vibrations.
Journal of Sound and Vibration 159(3) 483-502 1992
51. Langley, R.S.
A Dynamic Stiffness Technique for the Vibration Analysis of Stiffened Shell Structures.
Journal of Sound and Vibration 156(3) 521-540 1992
52. Hodges, C.H, Power, J., and Woodhouse, J.
The Low Frequency Vibration of a Ribbed Cylinder Part 1: Theory
Journal of Sound and Vibration 101(2) 219-235 1985
53. Guyader, J.L., Boisson, C., and Lesueur, C.
Energy Transmission in Finite Coupled Plates Part 1: Theory.
Journal of Sound and Vibration 81(1), 81-92 1982
54. Henderson, J.P., and Nashif, A.D.
The Effect of Stringer Width and Damping on the Response of Skin-Stringer Structures.
Jour. of Engineering for Industry 159-166 Feb. 1972

55. Lyon, R.H.
Statistical Energy Analysis of Dynamical Systems.
Cambridge, Massachusetts: MIT Press 1975
56. Fahy, F.J.
in *Noise And Vibration* (editors R.G. White and J.G. Walker).
Chapter 7: Statistical Energy Analysis.
Chichester: Ellis Horwood. 1982
57. Mace, B.R.
Power Flow Between Two Continuous One-Dimensional Subsystems: A Wave Solution.
Journal of Sound and Vibration 154(2), 289-319 1992
58. Scharton, T.D. and Lyon, R.H.
Power Flow and Energy Sharing in Random Vibrations.
Journal of Acoustical Society of America 43(6) 1332 1968
59. Woodhouse, J.
An approach to the Theoretical Background of Statistical Energy Analysis Applied to Structural Vibration.
Journal of Acoustical Society of America 69(6) 1695-1709 1981
60. Maidanik, G. and Maga, L.J.
Transition From A Non-Reverberant to a Reverberant System.
Journal of Sound and Vibration (3), 397-416 1981
61. Maidanik, G.
Extension and Reformulation of Statistical Energy Analysis with the Use of Room Acoustics Concepts.
Journal of Sound and Vibration (3), 417-423 1981
62. Hodges, C.H., Nash, P. and Woodhouse, J.
Measurement of Coupling Loss Factors by Matrix Fitting: An Investigation of Numerical Procedures.
Applied Acoustics 22 47-69 1987
63. Courant, R. and Hilbert, D.
Methods of Mathematical Physics V.II
Interscience Publishers, London 1962
64. McWilliam, S.
Statistical Energy Analysis of Plate/Beam Assemblies and Cabin

Enclosures.
M.Sc. Thesis, Cranfield Institute of Technology 1990

65. University of Southampton
ISVR Internal Report 1992

66. Keane, A.J. and Price, W.G.
Statistical Energy Analysis of Periodic Structures.
Proc. Royal Soc. London. A 423, 331-360 1989

APPENDIX A

FLOW CHARTS OF EXACT AND WIA PROGRAMS.

The implementations of dynamic stiffness method and Wave Intensity Analysis have involved the writing and development of rather lengthy computer programs, and because of their lengths the programs have not been reproduced in the thesis. The steps taken in the main bodies of the exact and WIA programs are, however, shown in the flow diagrams of Figs. A.1 and A.2 respectively.

Fig. A.1 indicates clearly the exact program makes a "do-loop" over a number of half sine waves, and for the sake of simplicity the flowchart is constructed for a single force and frequency. The WIA program makes do-loops over the number of plates, wave types, and shape functions as depicted in Fig. A.2.

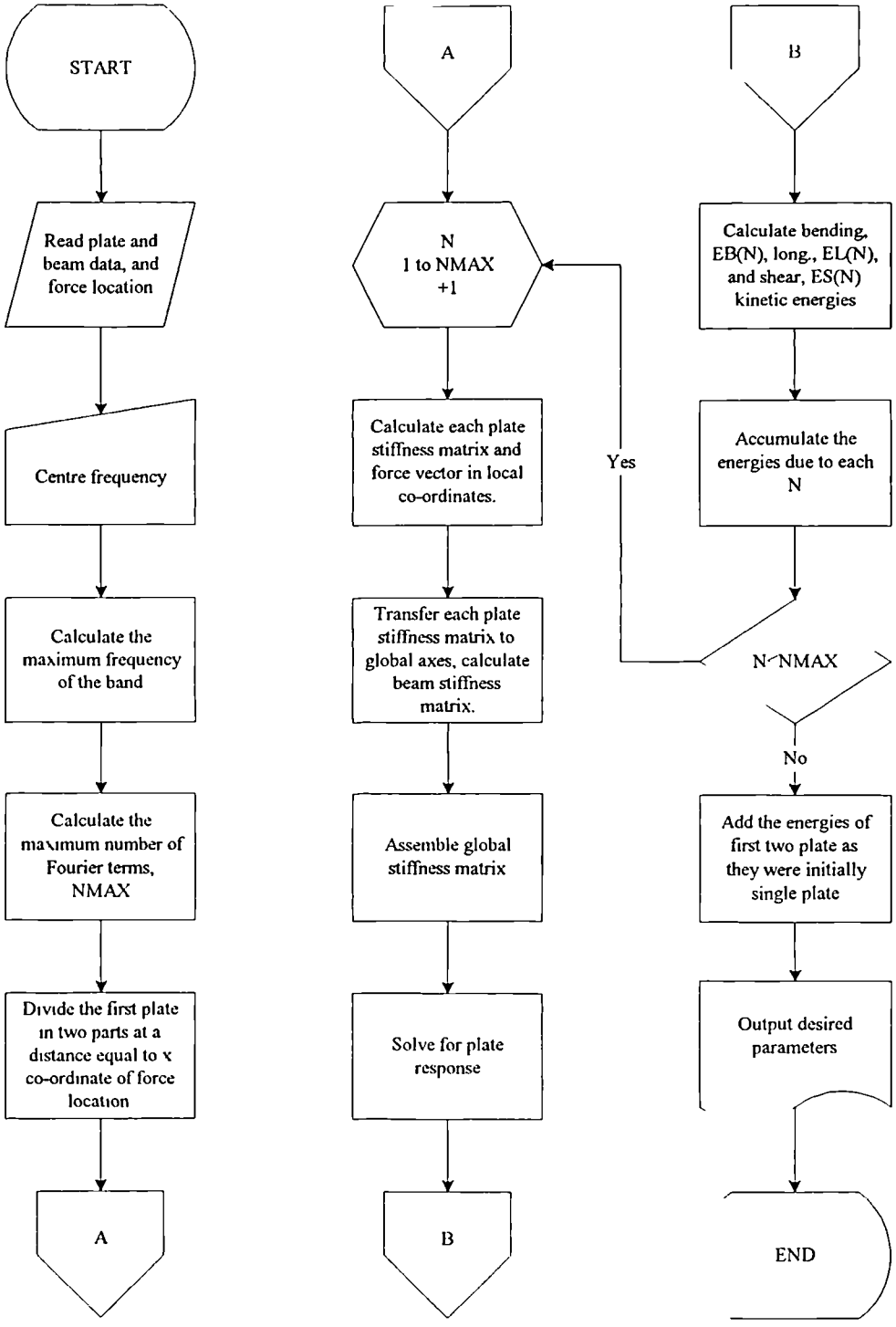

Fig A 1 Dynamic Stiffness Method Main Program Flowchart.

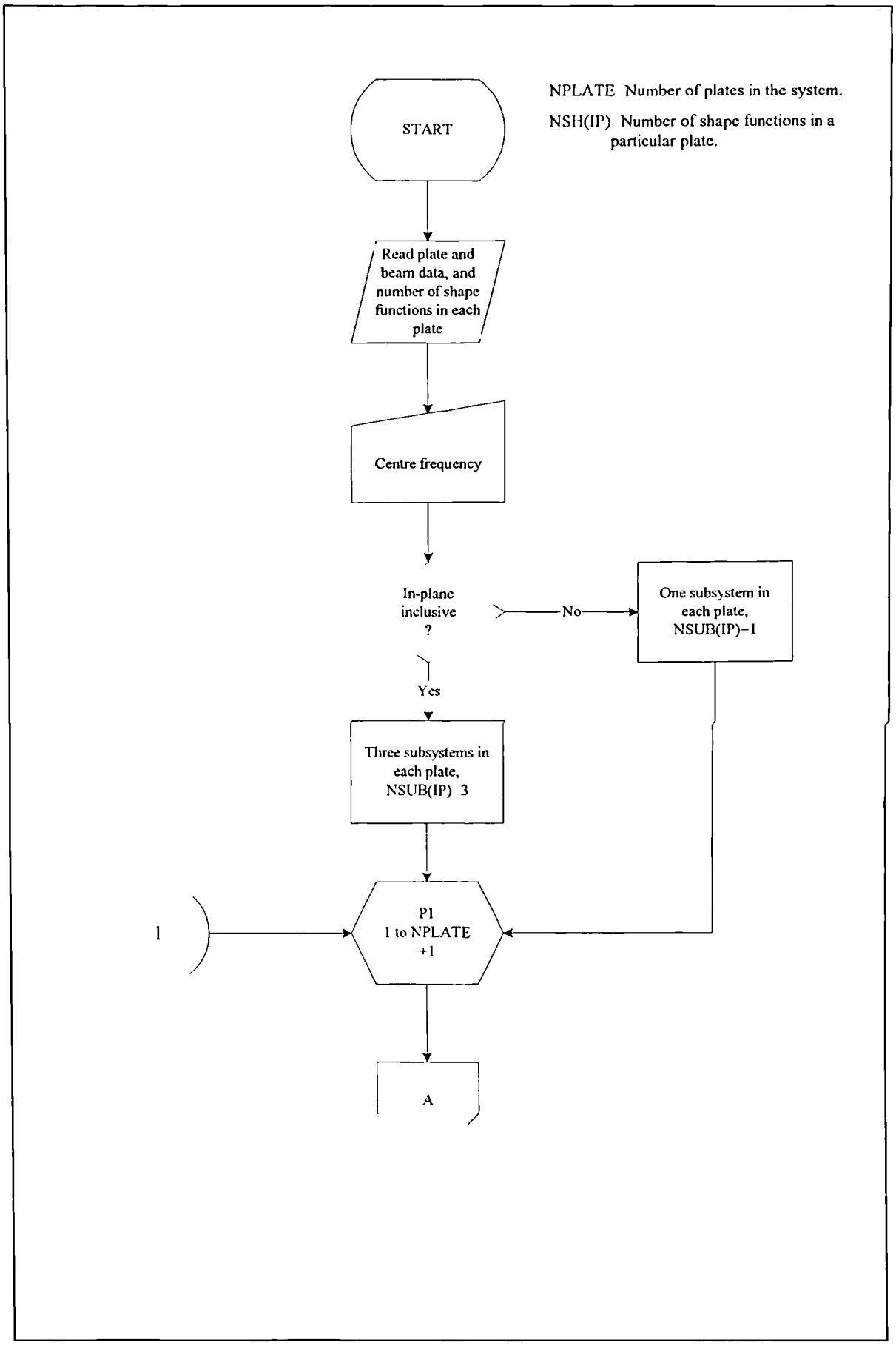
NPLATE Number of plates in the system.
NSH(IP) Number of shape functions in a particular plate.
START
Read plate and beam data, and number of shape functions in each plate
Centre frequency
In-plane inclusive ?
No
One subsystem in each plate, NSUB(IP)=1
Yes
Three subsystems in each plate, NSUB(IP) 3
I
P1
1 to NPLATE
+1
A

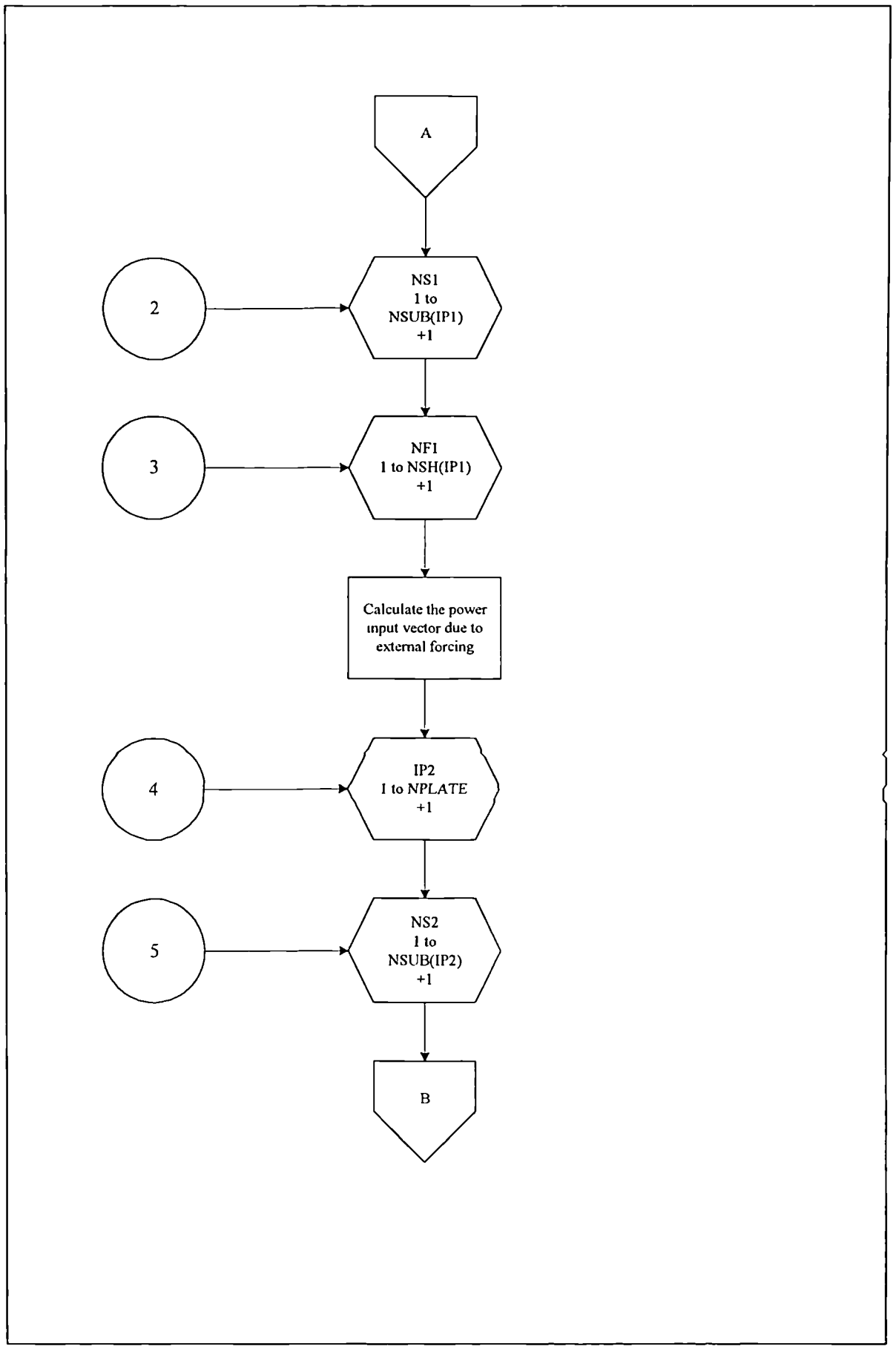
A
2
NS1
1 to
NSUB(IP1)
+1
3
NF1
1 to NSH(IP1)
+1
Calculate the power input vector due to external forcing
4
IP2
1 to NPLATE
+1
5
NS2
1 to
NSUB(IP2)
+1
B

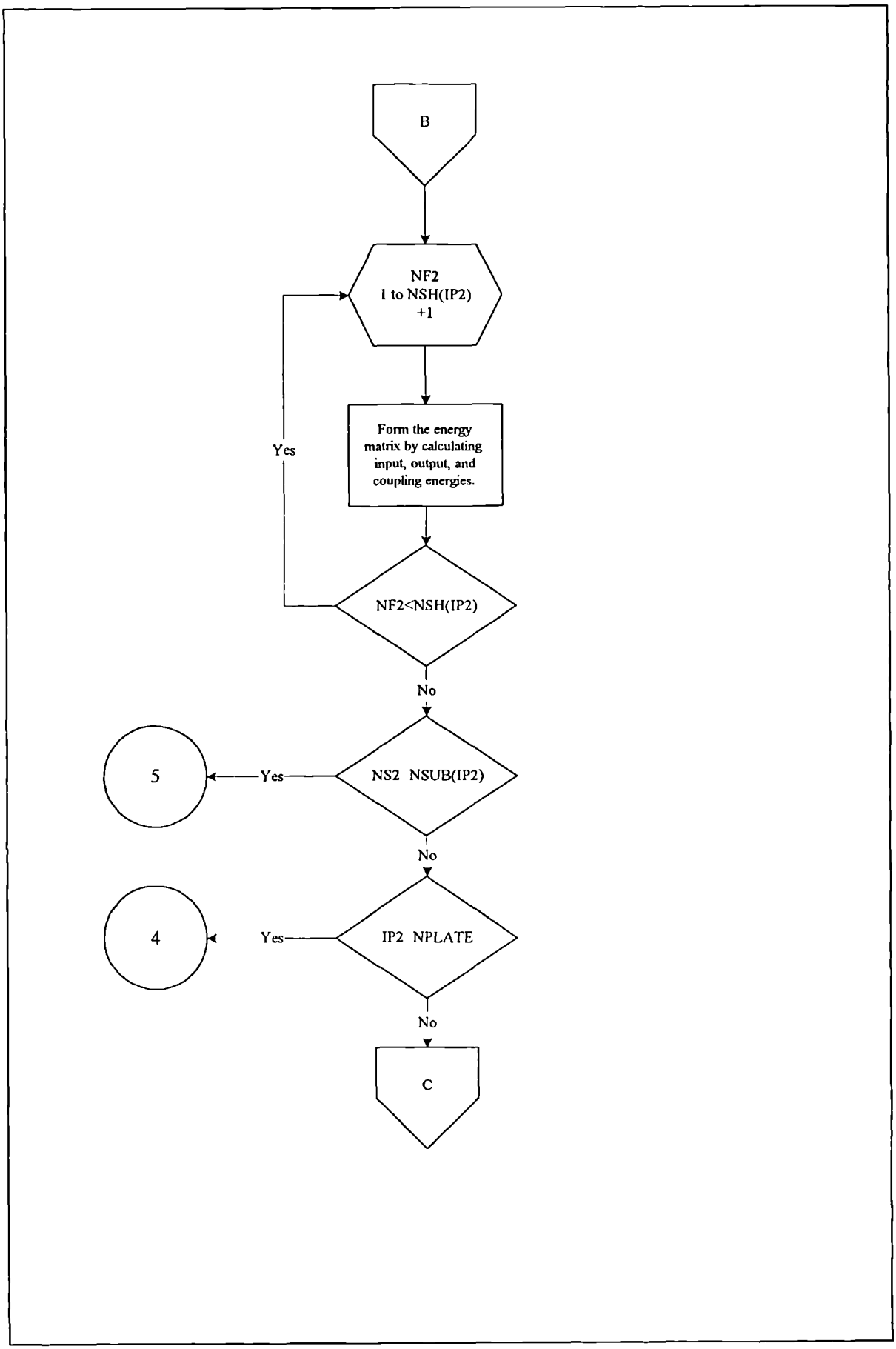
B
NF2
1 to NSH(IP2)
+1
Form the energy matrix by calculating input, output, and coupling energies.
Yes
NF2<NSH(IP2)
No
5
Yes
NS2 NSUB(IP2)
No
4
Yes
IP2 NPLATE
No
C

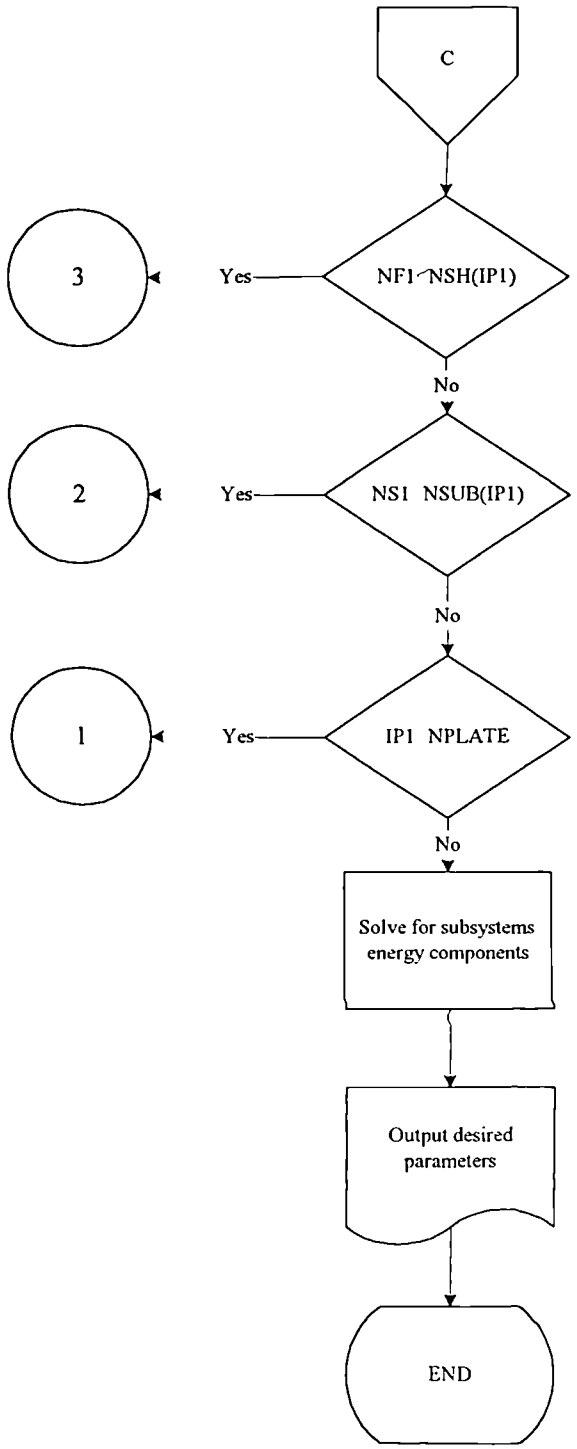

Fig. A.2 Wave Intensity Analysis Method Main Program Flow Chart.